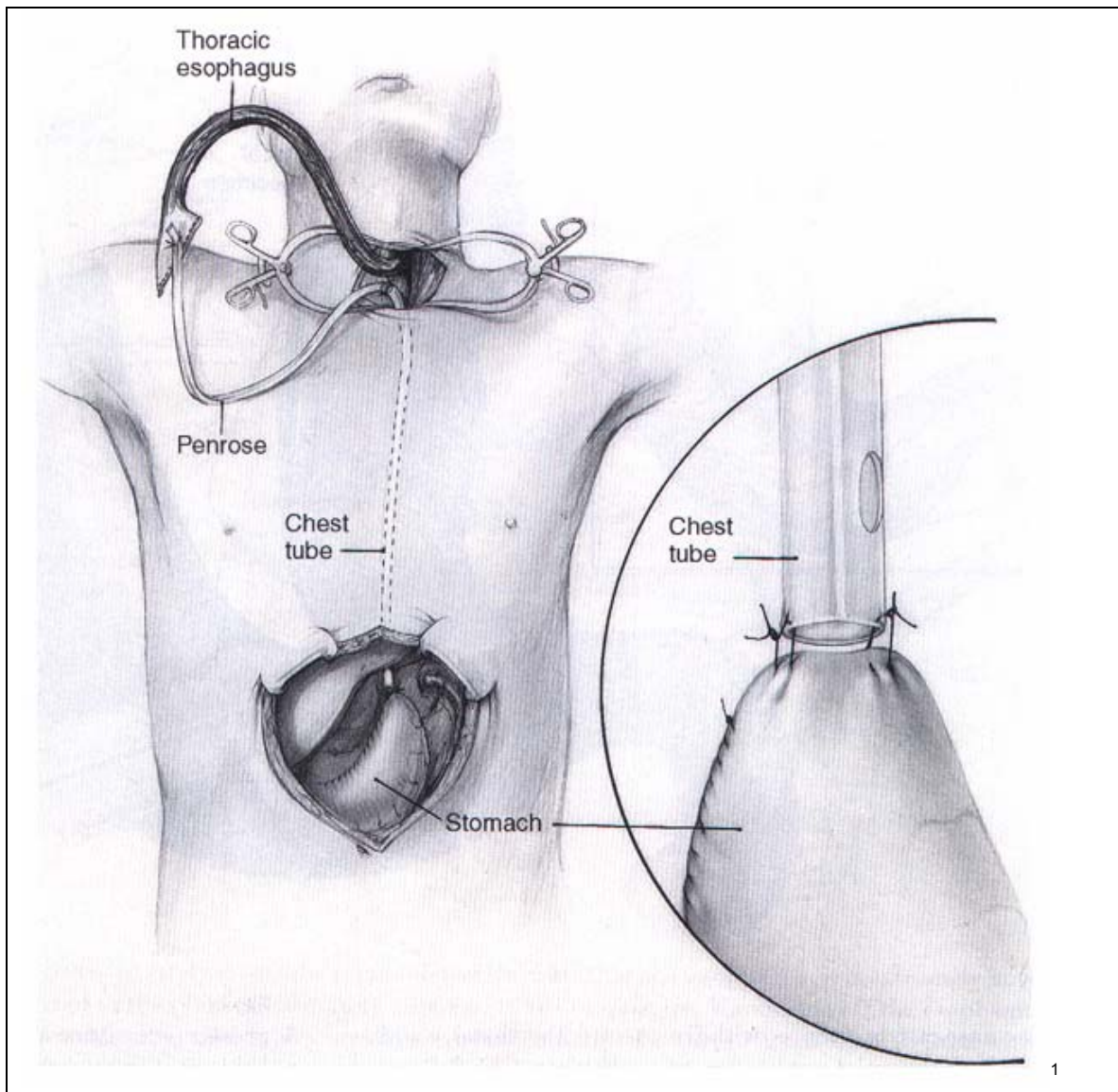


Early detection of anastomotic leakage using oxygen and carbon dioxide sensor



author: **Kar Fee Tang**
1093193

supervisor: prof. dr. Paddy French
ing. P.J. Trimp

Master of Science thesis
Delft University of Technology, March 2011

¹ Picture obtained from: <http://www.ctsnet.org/graphic/passagelarge.jpg>

Table of contents

CHAPTER 1 – INTRODUCTION.....	4
1.1 MOTIVATION.....	4
1.2 OPTICAL SENSOR	5
1.3 CHALLENGES.....	6
1.4 ORGANISATION OF THESIS.....	6
1.5 REFERENCES.....	7
CHAPTER 2 – REALISATION OF THE CO₂ SENSOR.....	8
2.1 INTRODUCTION.....	8
2.1 WORKING PRINCIPLE	8
2.2 CHEMICAL PREPARATION OF THE CO ₂ SENSITIVE COATING.....	11
2.3 SETUP FOR TWO EXCITATION WAVELENGTHS MEASUREMENTS	11
2.3.1 Gas mixer	12
2.3.2 Sample holder	13
2.3.3 T-tube	14
2.3.4 Spectrometer.....	15
2.4 RESULTS OF TWO EXCITATION WAVELENGTHS MEASUREMENTS	16
2.5 SETUP FOR ONE EXCITATION WAVELENGTH MEASUREMENTS	19
2.6 RESULTS OF ONE EXCITATION WAVELENGTH MEASUREMENTS.....	21
2.7 IMPORTANT PARAMETERS FOR THE pCO ₂ SENSITIVE COATING	23
2.8 CONCLUSIONS	25
2.9 REFERENCES.....	26
CHAPTER 3 – O₂ SENSOR.....	27
3.1 INTRODUCTION.....	27
3.2 DETERMINATION OF THE AMOUNT OF O ₂ BASED ON TNO APPROACH	27
3.3 READ-OUT ELECTRONICS BASED ON TNO APPROACH.....	30
3.4 SIMULATION RESULTS OF READ-OUT ELECTRONICS OF TNO	33
3.5 CONCLUSIONS	36
3.6 REFERENCES.....	37
CHAPTER 4 – ALTERNATIVE READ-OUT SYSTEM.....	38
4.1 INTRODUCTION	38
4.2 REALISATION OF THE READOUT ELECTRONICS FOR THE ALTERNATIVE APPROACH	39
4.3 SIMULATION RESULTS OF THE ALTERNATIVE READ-OUT ELECTRONICS.....	41
4.3.1 Simualtion results with the constant current source.....	44
4.3.2 Simulation results with the linear current source	46
4.4 EVALUATION OF THE PERFORMANCE FOR BOTH CURRENT SOURCES.....	48
4.5 CONCLUSIONS	50
CHAPTER 5 – REALISATION OF THE WIRELESS COMMUNICATION	51
5.1 INTRODUCTION	51
5.2 THE WORKING PRINCIPLE AND THE UNITS OF THE EZ430-RF2500	51
5.3 THE FUNCTION OF THE ACCESS POINT.....	52
5.4 THE FUNCTION OF THE END DEVICE.....	54
5.5 TEST RESULTS OF THE WIRELESS COMMUNICATION.....	57
5.5.1 Measurement setup of the END DEVICE	57
5.5.2 Measurement results of the END DEVICE.....	59
5.5.3 Measurement setup of the ACCESS POINT.....	63
5.5.4 Measurement results of the ACCESS POINT	63
5.6 CONCLUSIONS	65

5.7 SUMMARY	65
CHAPTER 6 – MEASUREMENTS BASED ON THE ALTERNATIVE APPROACH.....	66
6.1 INTRODUCTION	66
6.2 SUBSTITUTION OF THE OXYGEN SENSOR	66
6.3 MEASUREMENT SETUP OF THE ALTERNATIVE APPROACH FOR MEASURING THE OXYGEN LEVEL	71
6.4 MEASUREMENT RESULTS OF THE ALTERNATIVE APPROACH.....	72
6.5 CONCLUSIONS	80
CHAPTER 7 – EVALUATION OF BOTH READ-OUT ELECTRONICS.....	81
7.1 INTRODUCTION	81
7.2 THE SIZE AND THE NUMBER OF COMPONENTS	81
7.3 THE MAXIMAL POWER DISSIPATION AND THE COST OF THE READ-OUT ELECTRONICS	82
7.4 THE AVAILABILITY OF COMPONENTS AND THE SPEED OF OBTAINING THE DATA	82
7.5 THE ACCURACY OF BOTH CIRCUITS	83
7.6 CONCLUSIONS	86
CHAPTER 8 – CONCLUSIONS AND RECOMMENDATIONS.....	87
8.1 CONCLUSIONS	87
8.2 RECOMMENDATIONS.....	89
APPENDIX	90
A. SOURCE CODE OF MSP-430, ACCESS POINT	90
B. SOURCE CODE OF MSP-430, END DEVICE	98
C. SOURCE CODE OF AGILENT 33120A.....	107
D. COMPARISON OF DIFFERENT OPAMPS FOR IMPLEMENTING THE READ-OUT ELECTRONICS BASED ON THE ALTERNATIVE APPROACH	111
D.1 REALISATION OF THE READOUT ELECTRONICS FOR THE ALTERNATIVE APPROACH.....	112
D.2 SIMULATION RESULTS OF THE ALTERNATIVE READ-OUT SYSTEM.....	114
D.2.1 Simulation results with the constant current source	117
D.2.2 Evaluation of the performance for the constant current source.....	124
D.2.3 Simulation results with the constant current source	124
D.2.4 Evaluation of the performance for the linear current source	130
D.3 CONCLUSIONS	132

Chapter 1 – Introduction

1.1 Motivation

Anastomosis is defined as the connection of two structures. The connection between blood vessels or the connection of tubular structures, such as loops of intestine is a form of anastomosis. There are many studies on the gastrointestinal (GI) anastomosis. In many research, attentions are paid to study anastomotic cracks, since this phenomena might result in a fatal consequence for the patient.

Based on earlier research [1] which 2842 patients have been examined for all forms of gastrointestinal anastomosis over a period of 12 years, 51 of them show an anastomotic fracture. The forms of gastrointestinal anastomosis are:

1. esophagogastrectomy
2. total gastrectomy
3. partial gastrectomy
4. enterectomy
5. partial colectomy
6. subtotal colectomy

The 51 patients, who suffer of anastomotic crack, is 4.8% of the total investigated patients. 24% of the 51 patients died. Furthermore, these patients need further operations and their hospital stay has to be extended.

In GI surgery, anastomotic disruption is one of the most extensively feared and broadly studied problems. Important factors to this phenomenon are bowel blood supply, tension and accurate approximation of tissue. However, eliminating all these important factors, anastomotic disturbance still can occur. Therefore, anastomotic disruption has been widely feared.

Moreover, anastomotic leakage is the commonly feared complication after the colorectal surgery [2]. Anastomotic leakage (AL) is defined as leaking of the intestinal content into the peritoneal cavity through an anastomotic defect. Due to the AL, colonic bacteria such as *Escherichia coli* and *Enterococcus faecalis* pass through the peritoneal cavity that might lead to peritonitis. Consequently, this may lead to sepsis and mortality.

A potential technique to able to check for the AL is using the existing tool such as CT-scan or conventional X-ray. However, both methods cannot be regularly performed: usually, these methods are applied on day 8 to 13 between operation and the diagnosis of AL. During that period of time, the content of e.g. intestine will leak which results in infection to the patient. Therefore, this technique is inappropriate.

A new concept [2] is introduced for early detection of the AL. They apply the prophylactic drainage to AL. In case of AL, the bacterial load in the drainage fluid will significantly increased over time. The detection in the bacterial variation can be an indication for the AL and thus, the morbidity and mortality rates may be reduced. However, the drawbacks of this new concept are the detection speed, the relative high cost and the detection limit. After the operation, the drain's reservoir was emptied twice daily and transported to the laboratory and used for the analysis. The analysis includes DNA isolation, semi-quantitative Real-Time PCR and making standard curves. The whole analysis takes about two days to complete. Moreover, to be able to perform this analysis, the initial costs (like buying the machines, such as the Real-Time PCR device) are over 50000Euros. Also, an expert is required to perform this analysis: you have to know how to separate DNA from RNA and you also have to know how to operate the Real-Time PCR machine. Using this new concept, it is not able to detect the subclinical anastomotic leakage.

Therefore, a new technique will be invented to study AL. This new technique should be able to detect AL in an early stage, low-cost, ease to use and reliable. Research has been performed on IEEEE and PubMed to look for inspiration for detecting the AL. From the literatures, it seems that an oxygen sensor will be a good alternative upon all conventional methods to determine the AL [3].

This oxygen sensor is based on the optical property of the chemical coating that is sensitive for oxygen variations. The lifetime value is different for various oxygen levels. Therefore, the lifetime value is a measure of the oxygen level.

Subsequently, a carbon dioxide sensor is desired by Erasmus MC. Therefore, this sensor has to be developed. Due to enormous success of the oxygen sensor that is based on the optical principle, we want to build an optical sensor for detecting the carbon dioxide too.

1.2 Optical sensor

Using optical sensor is the best solution for detecting AL. Clinical optical sensor can be classified in two groups: invasive and non-invasive. In clinical applications, the invasive sensors are inserted into the body while the non-invasive sensors are positioned near the surface of the body for non-contact use or adjacent to cell surfaces. To be able to detect AL, we need to build invasive optical sensor. This sensor will be placed at the surroundings of the cut of the anastomosis.

Optical devices prove to be very successful in biomedical fields [4]. For instance, the endoscopy is a very successful optical device that has been used for illumination and for imaging. Subsequently, cavital laser surgery and therapy receive a lot of benefit using fibres. These fibres have a high flexibility and low-attenuation delivery system inside the ancillary channel of endoscopes and inside the natural channels of the human body.

The other advantage of using optical sensor is to reduce the cost. A CT scan machine² that is built in 2008 with the latest technology will cost upwards of \$3.5 million. Compare to the cost of the most advanced and latest endoscope³ that is priced at \$26 500, the price difference is very significant. Therefore, using the optical sensor can save cost.

Generally, other major benefit of using an optical sensor is that it will not suffer from electrical interference. The transmission data is light, while the electronic requires electrical charges. Since light and electrical charges do not interfere, both of them can be integrated into one device. Consequently, this saves device area and miniaturisation of the oxygen is easier.

In this research, a low-cost and low power optical device has to be designed that is able to detect the carbon dioxide and oxygen level. Three main parts are involved to build the optical device, which are:

1. Design of a low-cost carbon dioxide optical sensor
2. Design of a low-cost oxygen optical sensor system
3. Implementing a low power wireless protocol for wireless communication for the sensors

The carbon dioxide optical sensor is a sensor that is able to detect the carbon dioxide level, while the oxygen optical sensor system includes the read-out electronics. Both sensors will be attached to the AL to measure the carbon dioxide and oxygen level. A new research has to be performed to relate the AL to the concentration of the carbon dioxide and the oxygen level, since this is out of the scope of this Master of Science thesis.

We wish to have a wireless communication between the sensors and the computer. Due to the wireless communication, there is no limitation to the patient for his/her daily activities. Moreover, we want to have a real-time measurement of the gasses level. With the help of the wireless communication, we can constant monitoring the patient's health condition.

² source: http://wiki.answers.com/Q/What_is_the_cost_of_a_CT_scanner

³ source: <http://www.miami-med.com/endoscopy.htm>

1.3 Challenges

The optical device must be biocompatible, since it will be used in human tissues. No elicit should be shown when this device gets into contact with the tissues. Therefore, the choice of the materials is very important. Subsequently, the total dimension of the optical device should be as small as possible. Since many optical devices will be left inside and at the surface of the intestine.

The design of the carbon dioxide and oxygen sensor should be optimised for low concentration of these two gasses. The production of carbon dioxide is estimated at less than 20% (volume percentage). The oxygen consumption is estimated at a maximum of 25% (volume percentage). Therefore, a high sensitivity is desired for low concentration of these two gasses.

The chemical reaction of both gas sensors should be stable, reliable and reversible. Choosing the chemical material that can fulfill these requirements is very important. Furthermore, this chemical should not be able to interact with water environment. We want to prevent the gas sensors to fail when they get contact with water / blood plasma.

The ultimate goal is integration of both gas sensors in one single chip. We have to make sure that both sensors do not interact with each other. Therefore, tests have to be performed to check if the carbon dioxide sensor will show a chemical reaction with the oxygen. Earlier tests [5] have been proved that the oxygen sensor is insensitive for carbon dioxide variations. Therefore, there is no extra check required to check for the cross sensitivity.

In previous research [6], a very promising carbon dioxide and oxygen sensor has been introduced for detecting the AL. The gas sensors prove to be very stable, reliable and low-cost. The conventional way to detect the oxygen level is based on the averaging of the intensities of the fluorescence signal [7], [8]. The drawbacks of this method are the complexity of the read-out electronics and the read-out electronics requires a high-end operational amplifier. In this thesis work, an alternative approach will be introduced to measure the oxygen level. This new method will reduce the number of components and the complexity of the read-out electronics can be simplified. It will be proved that this new concept will be a good alternative for the conventional way of determining the oxygen level.

Optical fibre has been used for measuring the carbon dioxide and oxygen level. Using fibre device might be hazardous to patients or it can disrupt the structures or cells into which it is inserted, thereby perhaps invalidating measurements made via the fibres. To prevent this, the design of the optical device should exclude the present of the fibre.

Wireless communication between the sensors and the computer will be introduced. This wireless communication should operate at a frequency that is reserved for scientific or medical purpose. Besides, the power consumption at this frequency should be as low as possible, since the sensors will be left in human body for about 7 days.

1.4 Organisation of thesis

This thesis contains 8 chapters. Each chapter clarifies each part of the complete sensor system. The thesis starts with the implementation of the carbon dioxide sensor from sketch. In this chapter, the working principle of this sensor is discussed. Two setups have been studied in which in each section their results are shown. There are some parameters that one should keep in mind when using this sensor. Therefore, in the last section of this chapter, these parameters are being discussed in detail.

In the next section, attention is focussed on building up the conventional oxygen sensor. This chapter starts also with a short description of its working principle. Subsequently, the complete conventional circuit design has been shown and analysed.

In chapter 4, the alternative approach has been discussed. This chapter starts with explaining the new method for detecting oxygen level. The same chemical sensor has been used, since that sensor has been proved for its proper performance in earlier works.

Wireless communication between the sensor system and the personal computer (PC) has been set up and used for constant monitoring of oxygen variation. This wireless communication has been fully discussed in chapter 5.

In chapter 6, measurements have been performed on the alternative approach. The linearisation of this new approach has been tested with mono-exponential function. Also, the accuracy of the alternative approach has been determined.

The performance of both read-out electronics has been evaluated in chapter 7. The performance has been compared.

This thesis ends with conclusions and recommendations for future work in chapter 8.

1.5 References

- [1] Jack Pickleman, MD, FACS, William Watson, BS, Jennifer Cunningham, BS, Susan G Fisher, PhD, Richard Gamelli, MD, FACS, "The Failed Gastrointestinal Anastomosis: An Inevitable Catastrophe?" *ISSN 1072-7515/99*
- [2] N. Komen, M.C. Morsink, S. Beiboer, A. Miggelbrink, P. Willemsen, E. van der Harst, J.F. Lange, W.B. van Leeuwen, "Detection of colon flora in peritoneal drain fluid after colorectal surgery: Can RT-PCR play a role in diagnosing anastomotic leakage?", *Journal of Microbiological Methods 79 (2009) 67-70*
- [3] Tanase D., French P.J., Komen N., Kleinrensink G.J., Jeekel J., Lange J.F., Draaijer A., "Oxygen-tension measurements – The first step towards prevention and early detection of anastomotic leakage", *proceedings of IEEE Sensors, art. no. 4388337, pp. 68-71*
- [4] Anna Grazia Mignani, Francesco Baldini, "Biomedical sensors using optical fibres", 1996 *rep. prog. Phys. 59 1*
- [5] Jinjun Jiang, Lei Gao, Wei Zhong, Shen Meng, Ben Yong, Yuanlin Song, Xiangdong Wang a, Chunxue Bai, "Development of fiber optic fluorescence oxygen sensor in both in vitro and in vivo systems", www.elsevier.com/locate/resphysiol
- [6] Tanase D., Tang K., French P.J., Komen N., Kleinrensink G.J., Jeekel J., Lange J.F., Draaijer A., "PO₂ and PCO₂ measurements for the prevention and early detection of anastomotic leakage", *2008 Proceedings of the 3rd Frontiers in Biomedical Devices Conference and Exhibition, pp. 41-42*
- [7] Karin Kellner, Gregor Liebsch, Ingo Klimant, Otto S. Wolfbeis, Torsten Blunk, Michaela B. Schulz, Achim Göpferich, "Determination of Oxygen Gradients in Engineered Tissue using a Fluorescent Sensor", *DOI: 10.1002/bit.10352*
- [8] A. Draaijer, J.W. König, J.J.F. van Veen, R.E.G. van Hal, "AN OPTICAL OXYGEN SENSOR" et al, 2nd Inter-Regional Conference on Environment-Water, 1 to 3 Sep. 1999

Chapter 2 – Realisation of the CO₂ sensor

2.1 Introduction

Carbon dioxide (CO₂) sensor has been developed from scratch, because the purpose of starting this biomedical project is building up a sensor that can detect the CO₂ and oxygen (O₂) variations. Oxygen sensor has already been successfully developed and tested to measure the oxygen tension (pO₂). The pO₂ is the partial pressure of oxygen molecules dissolved in blood plasma⁴. The next step is introducing the carbon dioxide (CO₂) sensor that is able to detect the pCO₂.

This chapter is focused on developing the CO₂ sensor only. HPTS-(TOA)₃ has been introduced. This is a chemical material that is sensitive to CO₂ variation. The detection of the CO₂ level is based on the fluorescence property of the HPTS-(TOA)₃. HPTS-(TOA)₃ is a pH-indicator. The amount of the fluorescence corresponds with the amount of CO₂ that interacts with HPTS-(TOA)₃.

HPTS-(TOA)₃ has been selected because of its chemical reaction with CO₂ is reversible, stable and reliable. Moreover, this material dissolves in water environment, which makes it an outstanding matter for biomedical application.

Although HPTS-(TOA)₃ has a lot of advantages, it also shows some drawbacks. One major drawback is its deviated behavior in temperature variations. Therefore, temperature compensation should be applied in each measurement to reduce the error.

This chapter starts with a description of the working principle of HPTS-(TOA)₃ followed by the preparation of this CO₂ sensitive coating.

In the next section, the setup of CO₂ sensor for measuring the CO₂ level will be discussed. Spectrometer has been used to generate two excitation wavelengths, which the HPTS-(TOA)₃ is the most sensitive for. The advantage of using two excitation wavelengths for measuring CO₂ level is that the sensor becomes less sensitive for modifications of the amount of HPTS-(TOA)₃ or adjustments in the system setup.

The results of the measurements of two excitation wavelengths are shown in section 2.4. The fluorescence signal is the most powerful at $\lambda_{\text{emission}} = 520\text{nm}$. The results prove that the more CO₂ involved, the weaker both excitation peaks will be.

However, in able to reduce the number of components of CO₂ sensor and the O₂ sensor, since their excitation light source can be shared, the effect of one excitation light source on the CO₂ sensor has been investigated. The setup of one excitation light source is slightly different from the two excitation wavelengths. Section 2.5 shows this setup.

The next section represents the results of the measurements with one excitation light source. The response time of this measurement is examined. The thickness of the CO₂ coating has also influences on the speed of the response. The thickness is studied and the results can also be found in the same section.

Several aspects should be kept in mind when using HPTS-(TOA)₃. The last section of this chapter deals with these aspects.

2.1 Working principle

HPTS-(TOA)₃ has been used for detecting the small amount (up to 30% of the total content) of CO₂. HPTS is a new lipophilic pH probe and it is a fluorescent dye. Its chemical denomination is known as 1-hydroxy-3,6,8-pyrenetrisulfonie acid trisodium salt or named as pyranine. Figure 2.1.1 shows the chemical structure of this salt.

⁴ According to the definition obtained from <http://medical-dictionary.thefreedictionary.com/oxygen+tension>

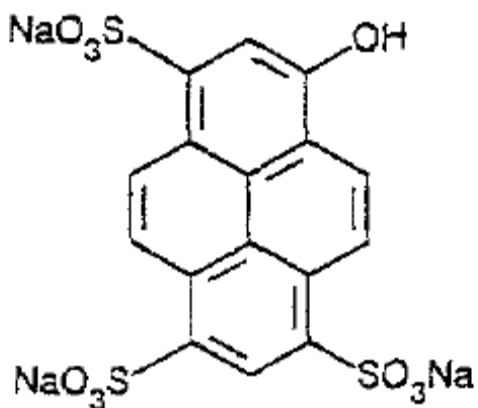


Figure 2.1.1: The chemical structure of HPTS

HPTS-(TOA)₃ has been used for measuring the CO₂ level instead of HPTS, since HPTS-(TOA)₃ shows a higher response level and an improved response time [2]. Therefore, HPTS has to be changed into HPTS-(TOA)₃.

The conversion of HPTS into HPTS-(TOA)₃ is shown in Figure 2.1.2 [1].

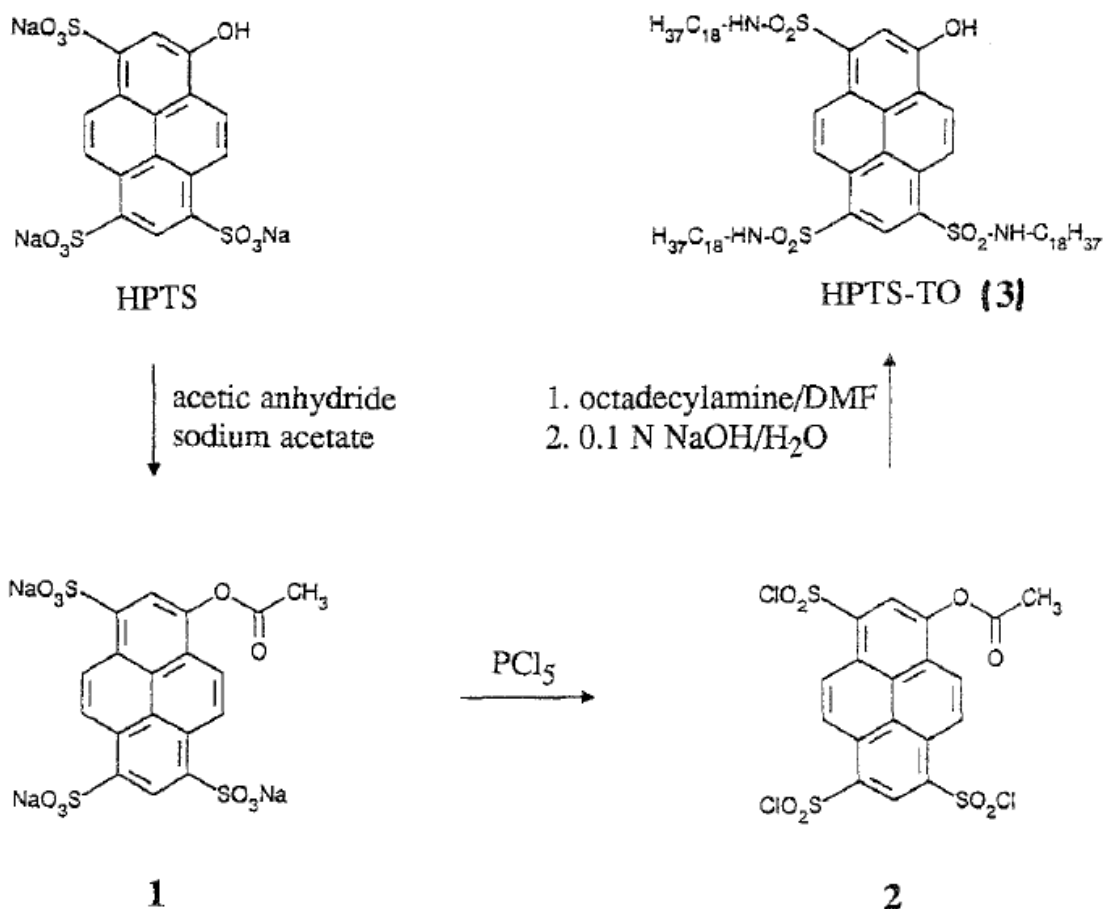
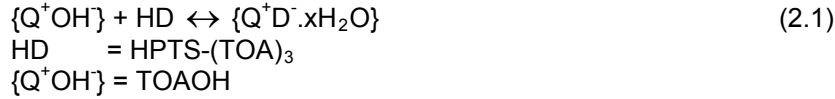


Figure 2.1.2: Conversion of HPTS into HPTS-(TOA)₃

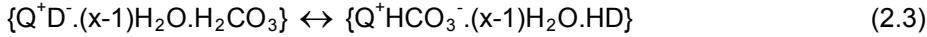
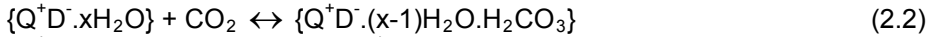
The optical properties in both the excitation and emission are shifted to longer wavelengths due to this conversion. The absorption spectrum that is shown in step 3 in methanol has a longwave at 413nm, which, on addition of 1 M NaOH, shifts to 472nm.

With the help of using HPTS-(TOA)₃, CO₂ can be determined that is in the air or in a dissolved media, such as human body. This fluorescent dye has absorption and emission bands that are separable. Both bands are located in the visible light.

HPTS-(TOA)₃ is an acid. This acid needs to be made neutral in able to detect the CO₂ level, since once CO₂ is solved in water, it becomes H₂CO₃. The conventional base NaOH cannot be used to mix with HPTS-(TOA)₃, since this base will not solve in HPTS-(TOA)₃. Therefore, an alternative material has been looked for. It seems that tetraoctylammonium hydroxide will be able to neutralise the acid. This base is also known as TOAOH, and it is a substitution for NaOH. The chemical reaction is as follows:



When CO₂ is presented, it will react with the product, {Q⁺D⁻.xH₂O}, that is shown in (2.1). The following two chemical reactions are:



The fluorescence signal comes from two compounds. The first ones are the {Q⁺D⁻.xH₂O} and {Q⁺D⁻.(x-1)H₂O.H₂CO₃}. The second one is the {Q⁺HCO₃⁻.(x-1)H₂O.HD}.

When a light source with a wavelength of 395nm is emitting on the {Q⁺HCO₃⁻.(x-1)H₂O.HD}, this compound will give fluorescence. The intensity depends on the involved CO₂. The more CO₂, the stronger the intensity will be.

When a light source with a wavelength of 470nm is used to emit light on the {Q⁺D⁻.xH₂O} or the {Q⁺D⁻.(x-1)H₂O.H₂CO₃}, it will give fluorescence also. The intensity of the fluorescence signal depends on the amount of involved CO₂. Figure 2.1.3 shows the typical absorption spectrum of HPTS-(TOA)₃.

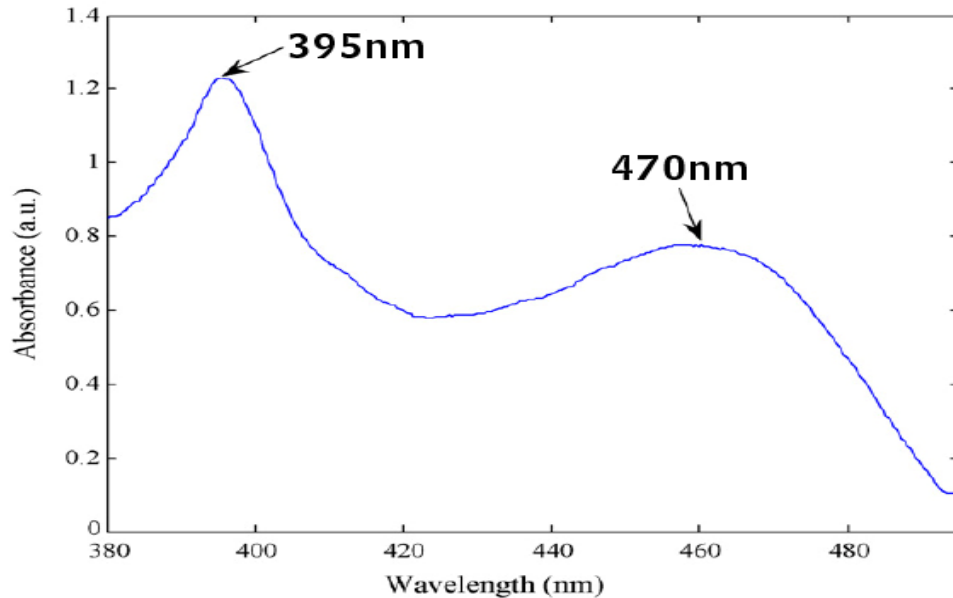


Figure 2.1.3: Typical absorption spectrum of HPTS-(TOA)₃

The strongest emission of the fluorescence signal of both compounds is same, which is located at around 530nm.

In many cases of liquid-phase CO_2 detection, the devices are fit in either a buffered, dye-doped layer of hydrophilic support material such as hydrogel [3] or a moisture-rich sol-gel glass substrate [4] that is located beneath a hydrophobic gas-permeable membrane such as Teflon. The buffer guarantees that the dye is deprotonated⁵ in the initial state, while Teflon prevents any liquid from entering or leaving the dye-doped layer. Using this sensing configuration to gas-phase detection is limited by the requirement to maintain the moisture level of the sensitive membrane at a sufficient level to prevent the sensor layer from drying out. This means that using this sensor in dry gas environment is useless. Mills et al. [5-7] and Weigl and Wolfbeis [8,9] prevailed over this limitation. They use an ion-pair approach to encapsulate highly polar, pH-sensitive fluorescent dyes within the hydrophobic materials such as ethylcellulose and silicone rubber. The authors used a phase transfer reagent to incorporate the polar dye within a lipophilic support matrix in their approach. In the report of Malins and MacCraith, they noticed that this incorporation process resulted in the encapsulation of a significant amount of moisture in water form of crystallisation within the immobilisation matrix [10].

2.2 Chemical preparation of the CO_2 sensitive coating

$\text{HPTS}-(\text{TOA})_3$ is a pH indicator that has a low pH value. This pH indicator should be neutralised before it is exposed to human body. Therefore TOAOH has been added. TOAOH is a base, which will increase the pH.value of $\text{HPTS}-(\text{TOA})_3$. This base is in liquid state at room temperature. After adding TOAOH with $\text{HPTS}-(\text{TOA})_3$, ethyl cellulose (EC) is added. This is required to give the coating a solid structure. The solidarity depends on the amount of ethyl cellulose that is mixed up with toluene and ethanol. The mixing ratio of toluene and ethanol is 8:2. Ethyl cellulose is a solid matter at room temperature. First, toluene is added to the coating which after ethanol will follow. This will fasten the solvability of the mix.

2,5 – 5% mass percentage of ethyl cellulose is highly preferred. A high mass percentage will make the mix too solid. A low mass percentage will turn the mix in aqueous state, which is difficult to work with. Moreover, the fluorescence signal is much weaker due to strong dilution of ethyl cellulose.

The present of ethyl cellulose (2,5 – 5%) makes $\text{HPTS}-(\text{TOA})_3$ much easier to work with. Ethyl cellulose is a polymer which has very small holes in it. Gasses with small molecules can easily pass through, which makes this material an outstanding choice for using it in the CO_2 sensor. Moreover, light can be easily passes through, since this material is transparence. The reflection can be neglected since it is very small.

The next section starts with description of the measurement setup. This measurement setup has been used for two excitation wavelengths to determine the CO_2 level.

2.3 Setup for two excitation wavelengths measurements

This section shows the design of the measurement-setup using two excitation wavelengths. This section is divided into subsections. In each subsections, the part of the measurement-setup design has been discussed. The design of the components involves:

- gas mixer
- sample holder
- T-tube
- spectrometer

⁵ Deprotonation is a chemistry term that refers to the removal of a proton (hydronium cation H_3O^+) from a molecule, forming the conjugate base. Source: <http://en.wikipedia.org/wiki/Deprotonation>

The setup of the complete setup is drawn in Figure 2.3.1.

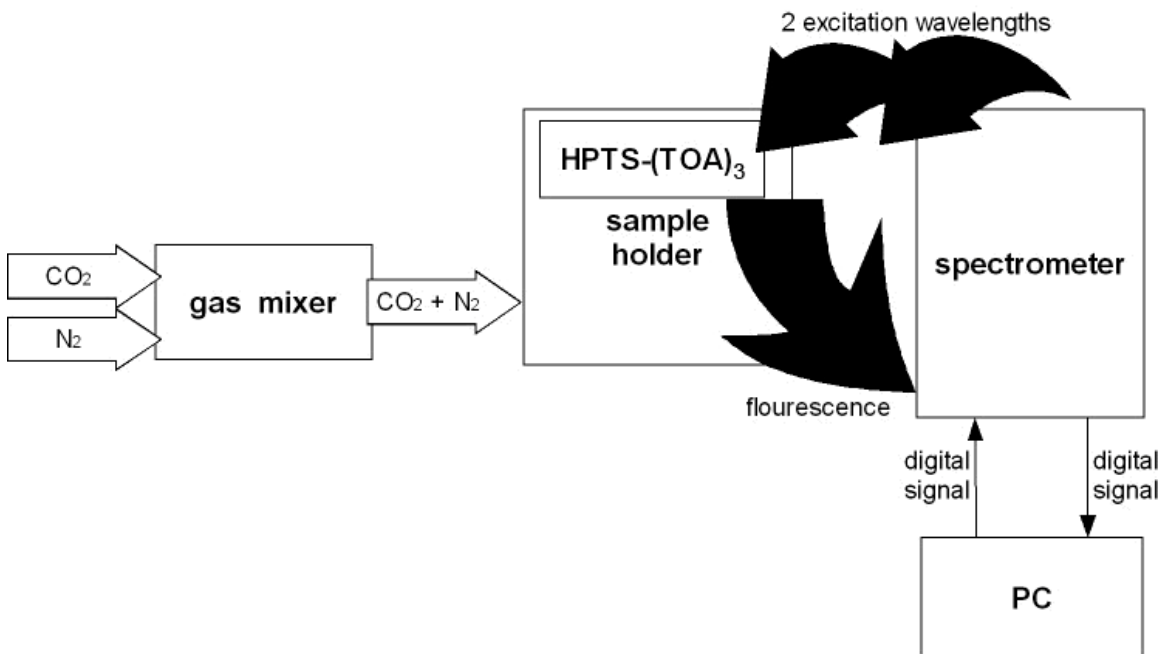


Figure 2.3.1: Setup configuration of two excitation wavelengths

These components are discussed in more detail in separated subsections.

2.3.1 Gas mixer

In able to get a well-defined amount of CO_2 , gas mixer has been used. Two gasses can be flown into this mixer. At the output of the mixer, a well-defined ratio of the two involved gasses is poured out. Figure 2.3.1.1 shows this gas mixer.

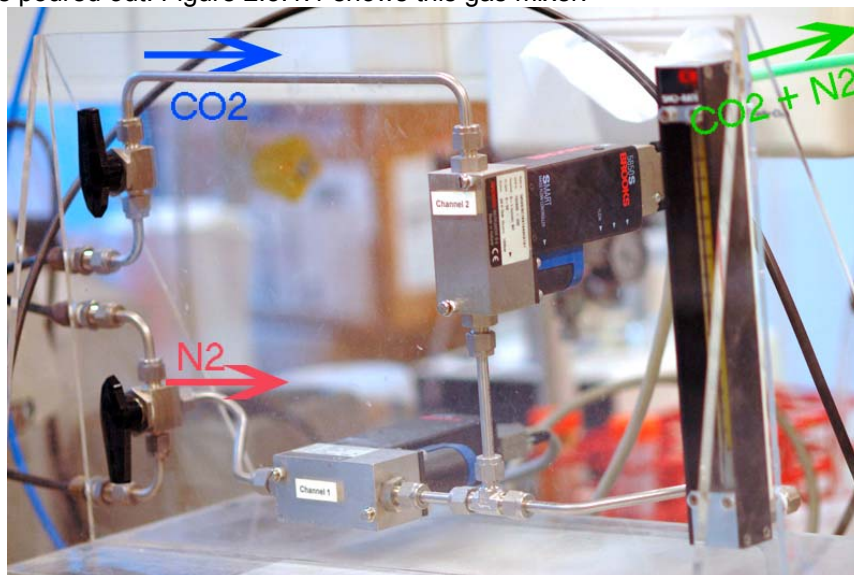


Figure 2.3.1.1: The gas mixer in which CO_2 and N_2 are mixed in a well-defined ratio

Nitrogen (N_2) has been mixed with CO_2 . In the control unit of the gas mixer, three buttons can be found. These buttons are:

- Channel selection: select the channel where gas is flowing in
- up : there are two arrow-buttons. The one on the left, which has two arrows up. This button increases the amount of gas in a large step, while the other button on the right (with just one arrow up), increases the amount by a smaller amount.
- down : there are two arrow-buttons. The one on the left, which has two arrows down. This button decreases the amount of gas in a large step, while the other button on the right (with just one arrow down), decreases the amount by a smaller amount.

2.3.2 Sample holder

Sample holder has been used to hold the mixture of the well-defined ratio of CO_2 and N_2 . In the front side of the holder, a hole has been hollowed out and the prepared HPTS-(TOA)₃ has been added. Figure 2.3.2.1 shows a picture of the sample holder.

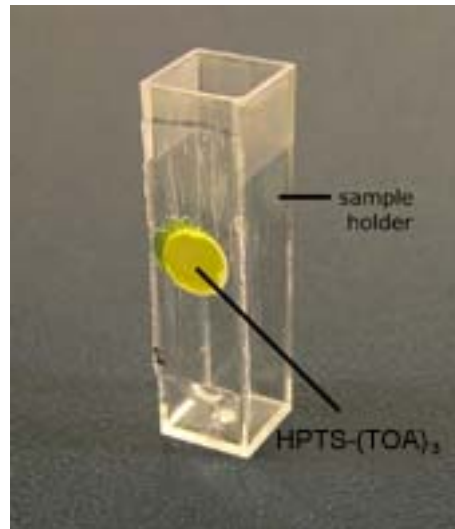


Figure 2.3.2.1: HPTS-(TOA)₃ attaches to the sample holder

The glass is highly reflective. Therefore, a black tape has been used to cover the front side of the sample holder to reduce the reflection. Figure 2.3.2.2 show this configuration.

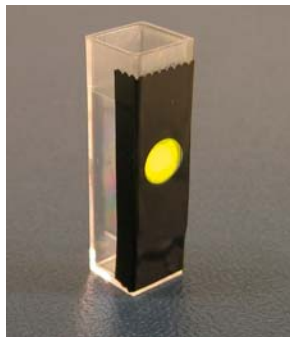


Figure 2.3.2.2: The sample holder with the black tape to reduce the reflections from the glass

2.3.3 T-tube

The sample holder has been closed by the T-tube. This T-tube holds the well-defined gas ratio in the sample holder. Figure 2.3.2.1a and Figure 2.3.2.1b show this T-tube.

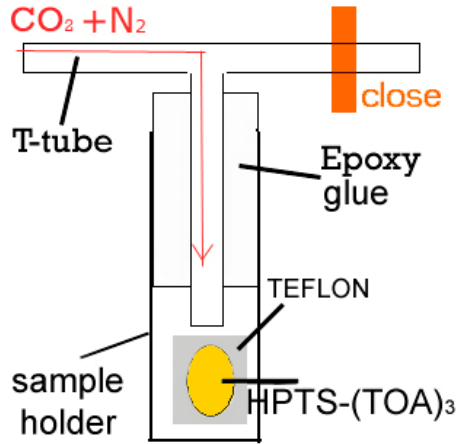


Figure 2.3.3.1a: The schematic drawing of a self designed T-tube with epoxy glue that closes the sample holder

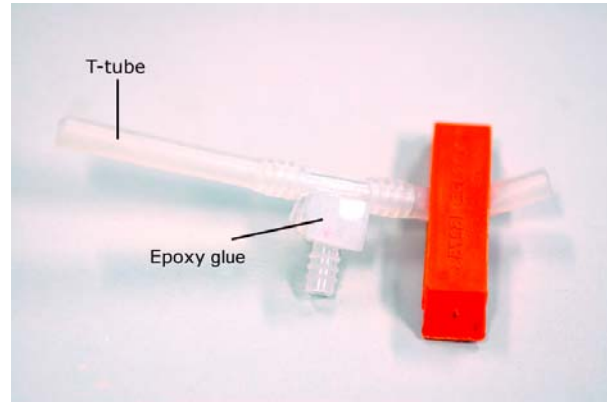


Figure 2.3.3.1b: The self designed T-tube with epoxy glue in real life

One side of the T-tube has been closed by an orange coloured clasp. The well-defined mixture of CO_2 and N_2 is flowing in at the other side of the T-tube.

Ideally, there is no leakage of gas: no gas can pass through the T-tube. However, the T-tube shows leakage. Figure 2.3.3.2 shows the leakage curve of the T-tube.

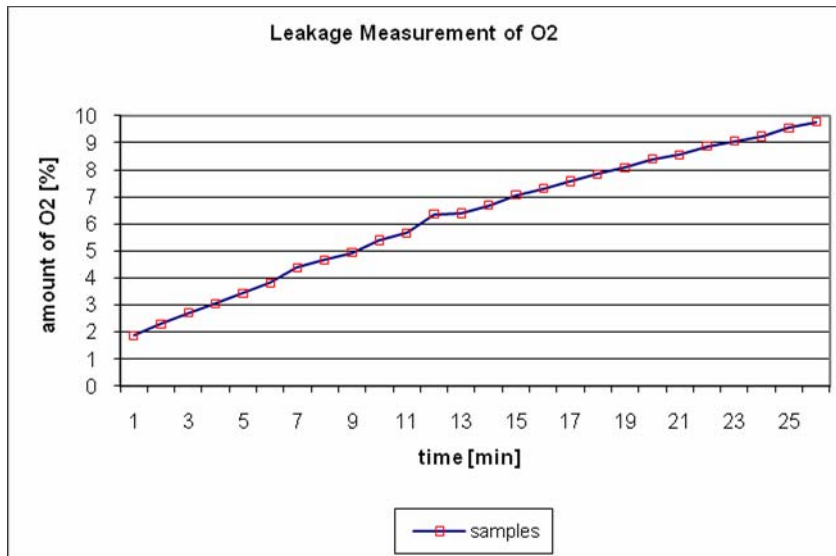


Figure 2.3.3.2: The leakage characteristic of the T-tube

To determine the leakage rate, oxygen sensitive coating has been used. With the help of the oxygen sensor, the oxygen level has been determined, which is related to the leakage rate of the T-tube. First, pure (100%) N_2 has pumped into the gas mixer. Then, the oxygen level has been determined every minute. In case of a perfect T-tube, the oxygen concentration will remain at 0%. However, it is hard to get zero concentration of

oxygen. Therefore, at the beginning of the measurement, the oxygen concentration will not be zero.

Figure 2.3.3.2 shows that this T-tube has a leakage rate that is 0.35% (volume percentage) per minute. Therefore, the measurement of the gas level using this T-tube should be kept as short as possible.

2.3.4 Spectrometer

In the spectrometer, the fluorescence signal which is the response of the amount of CO_2 has been examined. The sample holder with the T-tube is placed in the spectrometer. The gas mixer delivers well-defined ratio of CO_2 and N_2 . Consequently, the level of CO_2 has been determined.

Figure 2.3.3.1a shows how the sample holder that is placed in the spectrometer. The black unit is the inside of the spectrometer. The T-tube is connected with the gas mixer via the white coloured pipe.

Figure 2.3.3.1b shows how the spectrometer works. In the spectrometer, light with a desired range of wavelengths is generated. The green arrow at this figure represents this light source. The blue arrow represents the fluorescence signal that gives the response of the amount of involved CO_2 in the sample holder. This blue light is measured in the spectrometer which after a plot of its intensity over the specific wavelength is shown.

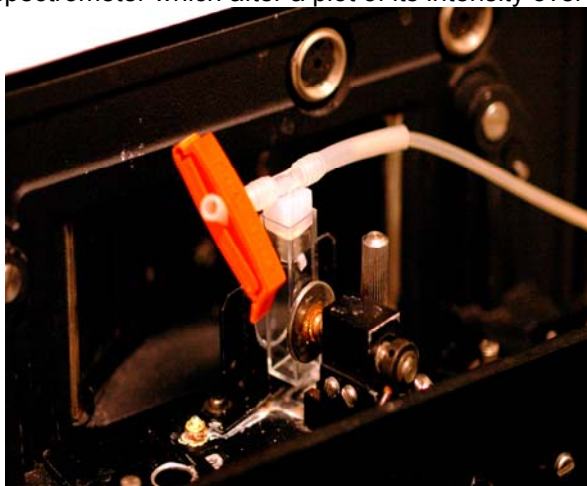


Figure 2.3.4.1a: The sample holder is placed in the spectrometer

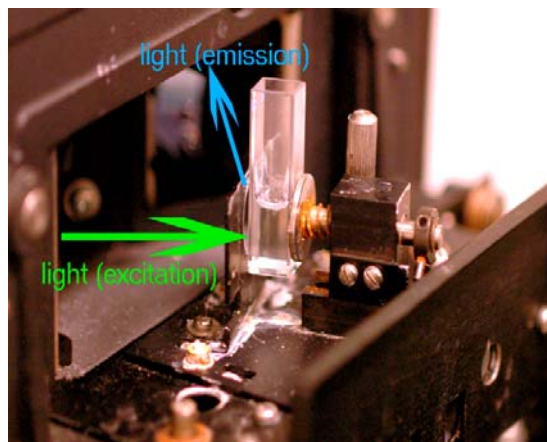


Figure 2.3.4.1b: The way how the fluorescence signal has been measured

The spectrometer is computer controlled. In the software that is included by the manufacture of the spectrometer, you can set the parameters of your interest for doing the measurement. These parameters are:

Start (nm): 350
End (nm): 500
Excitation (nm): 530
Ex. Slit (nm): 10.0
Em. Slit (nm): 2.5
Scan Speed (nm/min): 200
Number of samples : 15
Delay (s): 600

The Start and End parameters indicate the range of light source that has been used to activate the chemical coating. The Excitation parameter is the wavelength that is set to absorb the response (emission wavelength) of the chemical coating. The Ex. Slit is

the value of Excitation split and the Em. Slit is the emission slit. The speed of the scanning process is described by Scan Speed. The number of samples is set by Number of samples. The delay speaks for itself.

In the next section, the results of two excitation light source have been presented. In that section, the optimal values of the emission spectra and the emission spectrum have been determined.

2.4 Results of two excitation wavelengths measurements

This section evaluates the results of the setup that is discussed in the previous section. The working principle of the CO₂ sensitive coating has been discussed in 2.1 in detail. Two excitation light sources have been used to determine the CO₂ level. The CO₂ sensitive coating only shows one emission peak. To locate this peak, one excitation wavelength ($\lambda_{\text{excitation}} = 395\text{nm}$) has been used and a range of emission spectra has been selected to measure the intensity. Figure 2.4.1 shows the results.

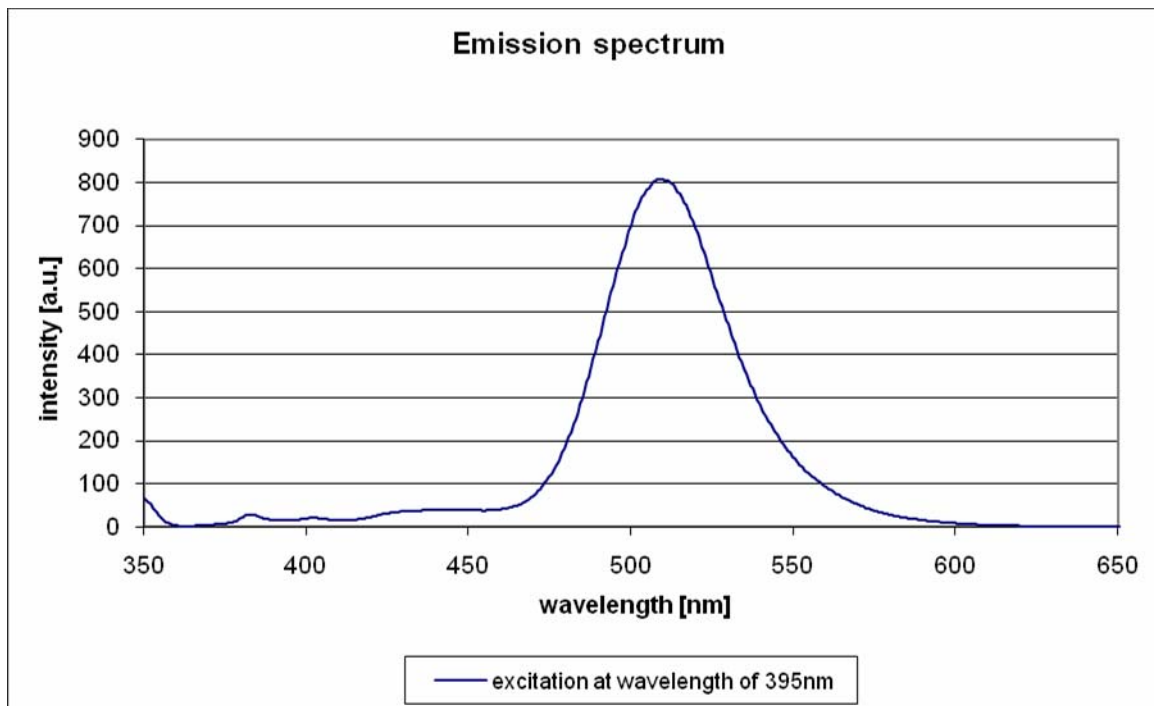


Figure 2.4.1: Emission spectrum at one excitation wavelength of 395nm

One peak can be observed. This peak is located at around $\lambda_{\text{emission}} = 520\text{nm}$. For our CO₂ sensor, we have set the emission wavelength at $\lambda_{\text{emission}} = 530\text{nm}$, since the read-out electronics has been optimised for the intensity that is located at this wavelength. In case of using $\lambda_{\text{emission}} = 520\text{nm}$, the output (voltage) of the read-out electronics will usually show clipping.

Now the excitation wavelength has been examined. We set the emission wavelength at $\lambda_{\text{emission}} = 520\text{nm}$. A range of emission spectra have been used to locate the peaks. Figure 2.4.2 shows the response of the spectrometer.

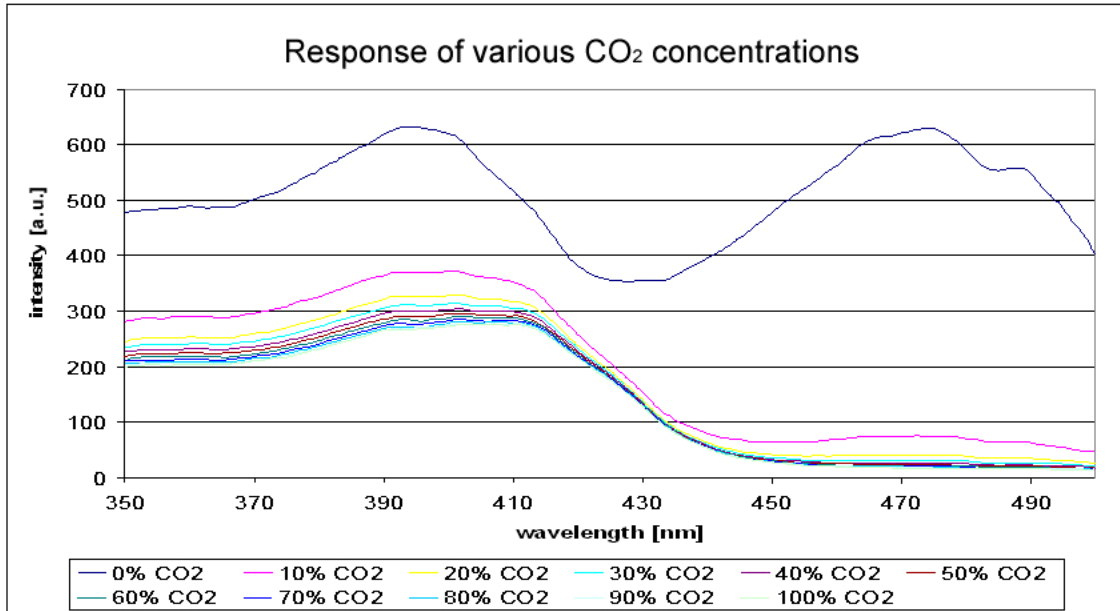


Figure 2.4.2: Excitation spectra for different CO₂ concentrations

Eleven plots have been shown in Figure 2.4.2. Each plot represents the amount of involved CO₂. The measurement starts with 0% CO₂ and it ends at 100% CO₂. The increment is 10%.

Consider the plot of 0% CO₂, which is the top one. Two excitation peaks can be observed. These two peaks are located at around $\lambda_{\text{excitation1}} = 395\text{nm}$ and $\lambda_{\text{excitation2}} = 472\text{nm}$. Thus, in able to get the strongest signal, light sources with wavelength of 395nm and 472nm should be used.

Other plots in Figure 2.4.2 show the responses for higher level of CO₂. Both excitation peaks will decrease in case of increment of CO₂. However, going from 0% CO₂ to 10% CO₂ the decrement of the second excitation peak ($\lambda_{\text{excitation2}} = 472\text{nm}$) is much higher than the first excitation peak. From 10% CO₂ onwards, the decrement of both excitation peaks is much less significant.

The amount of CO₂ is determined by taking the ratios of the second and the first peak ($\lambda_{\text{excitation2}} / \lambda_{\text{excitation1}}$). Figure 2.4.3 shows the ratios of these two peaks that are acquired from Figure 2.4.2.

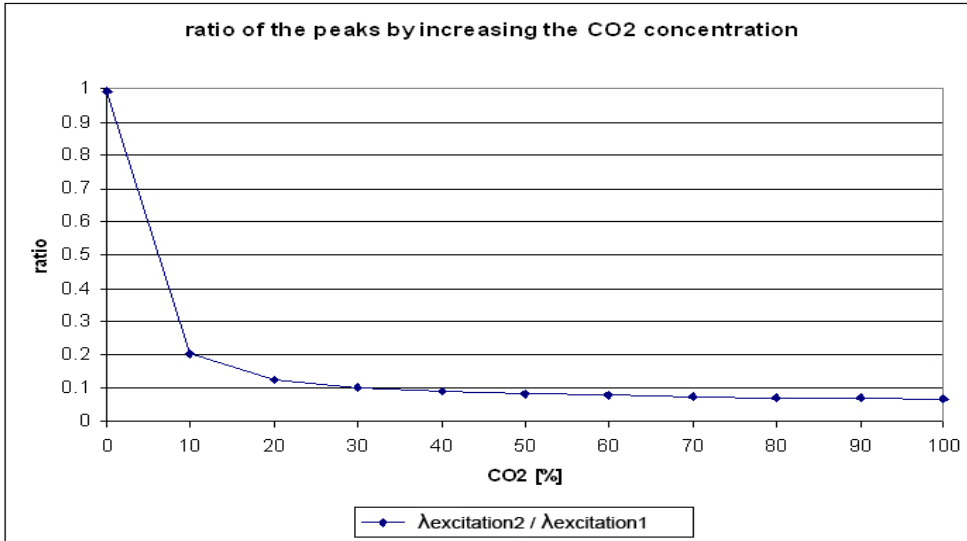


Figure 2.4.3: Response of the CO₂ sensitive coating

To determine the CO₂ level, the intensity of the fluorescence signal of HPTS-(TOA)₃ has been measured. In case of two excitation wavelengths, two light sources with wavelength of 395nm and 470nm have been used to measure the intensity of HPTS-(TOA)₃ at a wavelength of 530nm. The ratio of the intensity values of both light sources ($\lambda_{excitation2} / \lambda_{excitation1}$) is a measure for the CO₂ level.

Figure 2.4.3 shows the characteristic of the ratios of both excitation light sources. The slope of the first 10% CO₂ is very steep compare to the other volume percentages. This means that this chemical coating is very sensitive for a low percentage of CO₂. For a high percentage (from $\pm 15\%$ CO₂ onwards), the sensitivity of HPTS-(TOA)₃ decrease significantly.

The CO₂ sensor will be used for measuring the CO₂ production in human body. We assume that our CO₂ production in our human body will not exceed more than 15%. Therefore, using HPTS-(TOA)₃ is an outstanding choice for measuring low CO₂ concentration.

The linearity of the first 10% CO₂ has been checked. Therefore, new test has been performed. The test starts with 0% CO₂ and with an increment of 2%. Figure 2.4.4 shows the results.

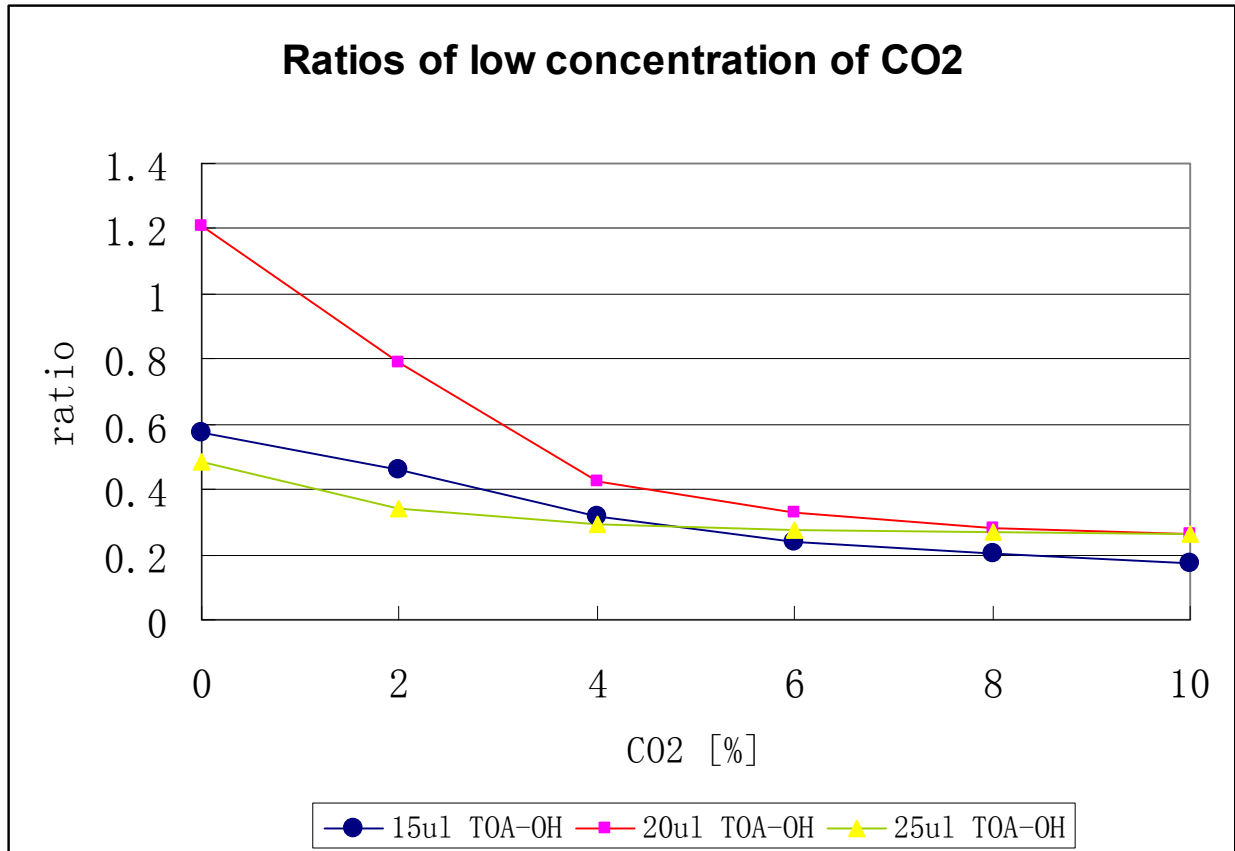


Figure 2.4.4: Response of HPTS-(TOA)₃ till CO₂ 10%.

Figure 2.4.4 shows that there is no linear relationship for the first 10% CO₂ concentration. All ratio values differ from Figure 2.4.3. That is because of using different concentration of TOA-OH. Generally, it can be concluded that increasing of TOA-OH will decrease the ratios of both peaks. However, the ratio of HPTS-(TOA)₃ and TOA-OH should be proportional. 15 μl HPTS-(TOA)₃ has been for all measurements in Figure 2.4.4. The addition of TOA-OH is to neutralise HPTS-(TOA)₃. Adding too much of TOA-OH to HPTS-(TOA)₃ will deviate the expected behaviour of the effect of TOA-OH. To get the highest ratio, the ratio of HPTS-(TOA)₃ and TOA-OH should be set at 3 : 4, respectively.

In the next two sections, the reliability using one excitation light source has been tested. We want to use one excitation light source ($\lambda_{\text{excitation2}} = 472\text{nm}$) to determine the CO₂ level, since we want to integrate the CO₂ sensor and the O₂ sensor in one package using one excitation light that both can share. If the results of HPTS-(TOA)₃ using one excitation wavelength are reliable, no additional light source is required. Thus, the package area can be saved.

2.5 Setup for one excitation wavelength measurements

In the previous section, the results of using two excitation light sources have been discussed in detail. It can be concluded that HPTS-(TOA)₃ is very sensitive for a low concentration of CO₂. To able to integrate the O₂ sensor with the CO₂ sensor in a small package, measurement has been performed for one excitation light source. To activate the chemical coating that is sensitive for oxygen variations, a light source of $\lambda_{\text{excitation_oxygen}} = 470\text{nm}$ has been used. Since the second excitation peak of HPTS-(TOA)₃ is located at $\lambda_{\text{excitation2}} = 472\text{nm}$, one excitation light source with a wavelength at $\lambda_{\text{excitation}} = 470\text{nm}$ can be used to activate both sensors. In the next two sections, reliability test on HPTS-(TOA)₃ has been performed using one excitation light source.

Figure 2.5.1 shows the setup for one excitation light source.

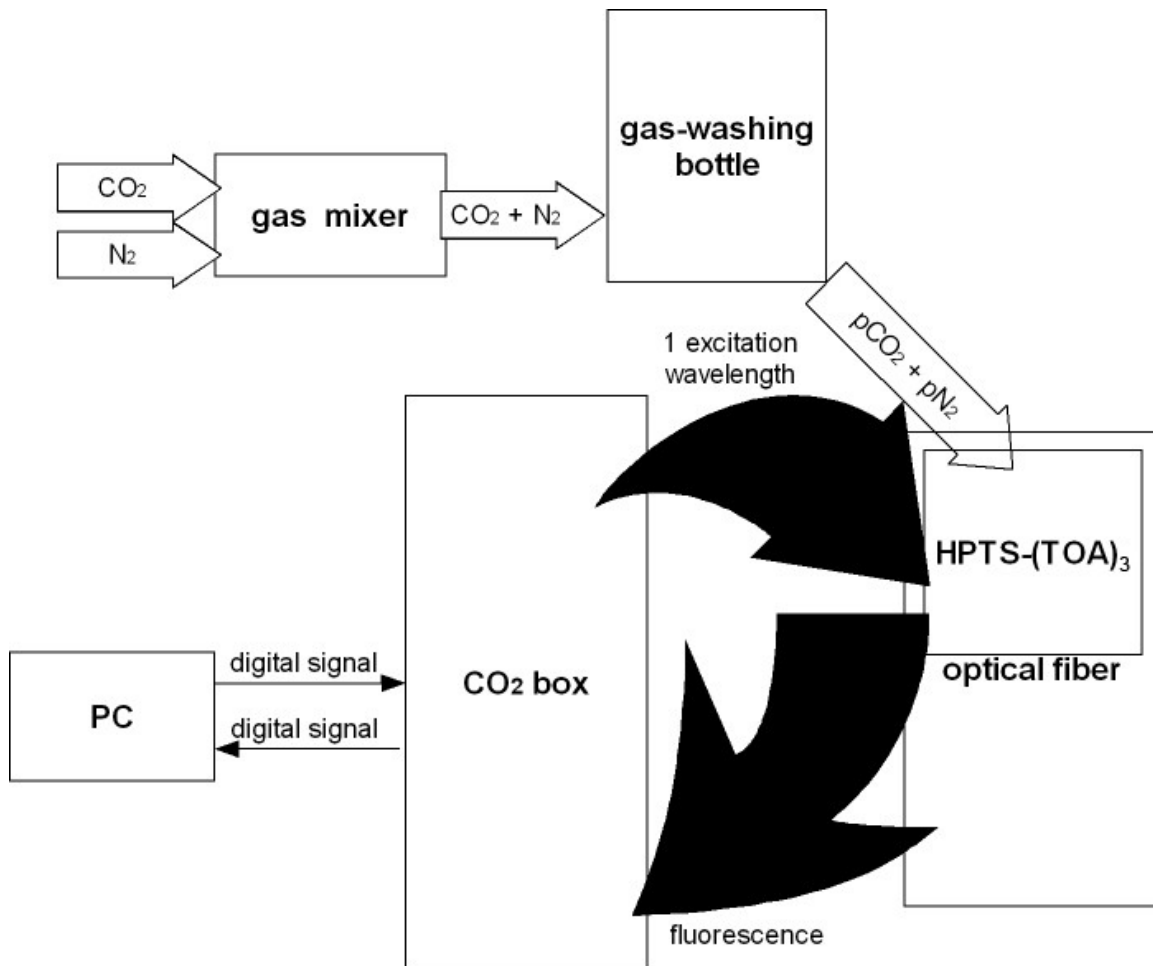


Figure 2.5.1: Setup configuration for one excitation light source

The same gas mixer has been reused. Gas-washing bottle has been added. This unit is introduced to dissolve CO₂ to simulate the condition of CO₂ in our body: CO₂ is dissolved in the blood plasma, which creates a partial tension of CO₂ in the blood (pCO₂). Instead of filling blood in the gas-washing bottle, we fill the bottle with purified water for our experiment. Purified water is preferred because no other solvents are present.

No sample holder has been used. Instead, optical fibre has been introduced. This optical fibre conducts the excitation light source that comes from the CO₂ box. On the tip of the optical fibre, HPTS-(TOA)₃ has been added. The generated fluorescence signal is transmitted to the CO₂ box via the optical fibre. The CO₂ box is connected to the computer for processing and displaying the results of the measurement. The CO₂ box is a substitution for the spectrometer that is discussed in 2.3.4.

This setup originates from the setup of the O₂ sensor. In stead of using HPTS-(TOA)₃, oxygen sensitive coating has been utilised. The CO₂ box can be reused for activating the oxygen sensitive coating, since they share the same excitation light source. However, the emission spectrum of both sensors is different. Therefore, in case of measuring the O₂ level, other photodiode has been used that is sensitive for the emission wavelength of the oxygen sensitive coating.

2.6 Results of one excitation wavelength measurements

The results of the one excitation wavelength are shown in Figure 2.6.1.

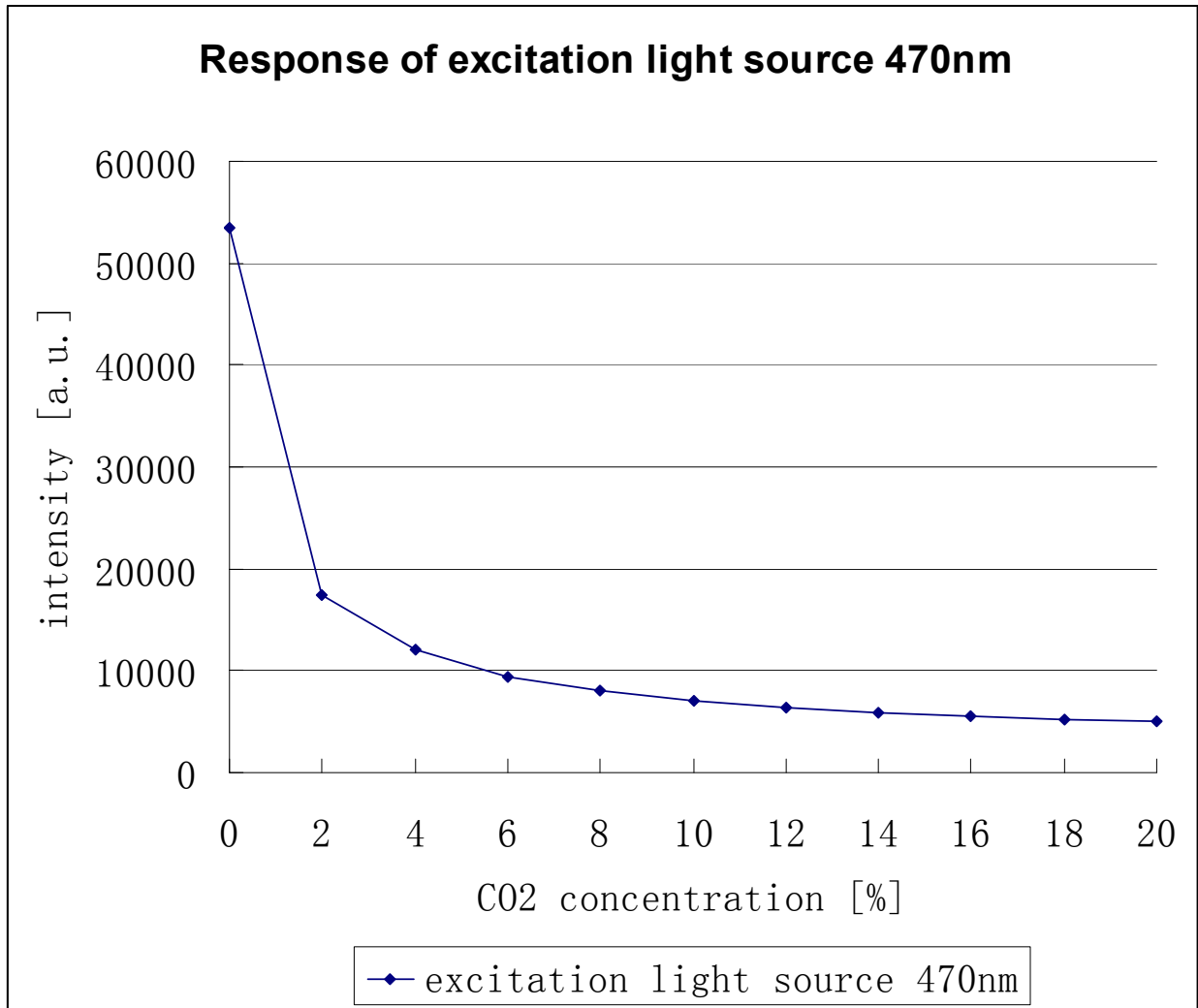


Figure 2.6.1: Response of using one excitation light source for determining the CO₂ level

In case of using one excitation light source, the decrement of pCO₂ level is non-linear. The decrement is very steep for a low concentration of pCO₂. That what it can be expected from previous results (see Figure 2.4.2).

To test the reliability, new measurement has been performed. The new measurement starts with no concentration of pCO₂. The pCO₂ level will be increased with 2% and its intensity will be measured for an instant of time. Subsequently, another 2% pCO₂ will be added and its intensity will be measured. This process repeats till we get 20% pCO₂. Then, the concentration of pCO₂ is reduced to zero and the obtained intensity value of 0% pCO₂ will be compared with the initial state. This should be exactly the same.

The next step of this new measurement will be started. In the next step, 20% of pCO₂ will be added. Its intensity of the fluorescence will be measure for a period of time. Then, the concentration of pCO₂ will be reduced to 18%. The process repeats till we have no pCO₂. Figure 2.6.2 shows the results.

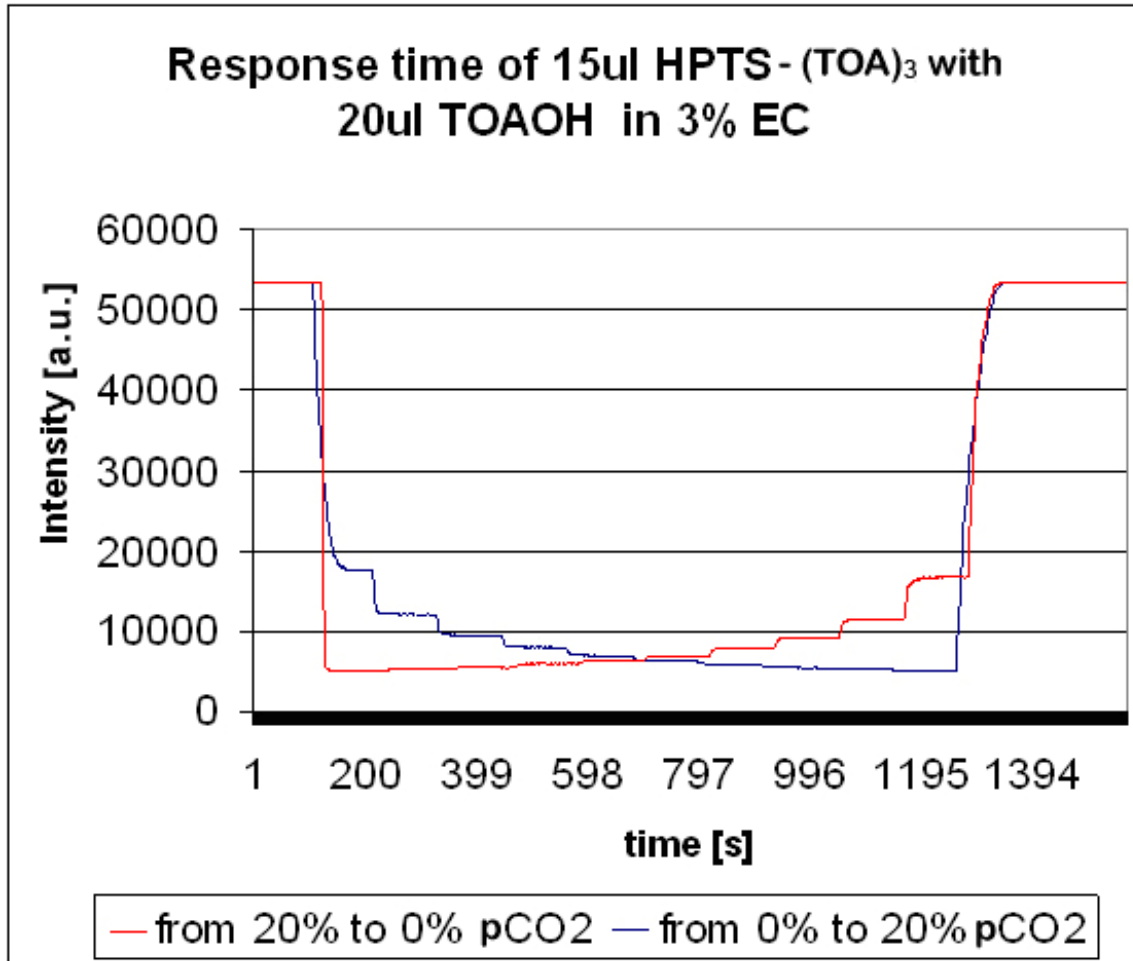


Figure 2.6.2: Reliability test using one excitation wavelength

There are two lines in this figure. The blue one shows the measurement results of the first step: starting from 0% pCO₂ and ends with 20% pCO₂. The red one shows the measurement results of the second step.

Both lines have horizontal lines during the measurements. In these horizontal lines, the mixture of pCO₂ and pN₂ is well-defined and has been kept constant for an instant of time. The intensity of the concentration of pCO₂ is obtained by getting the related value of the horizontal line.

The starting value and the end value of the blue and red lines show the same intensity. For both lines, the concentrations of pCO₂ and pN₂ are the same. Therefore, their intensity is the same. Comparing other mixture ratios of both lines with each other, the intensity values are slightly different. That is because the chemical processes: in case of the red line, pCO₂ is added while in case of the blue line, pCO₂ is reduced. The ratio of pCO₂ and pN₂ in the gas-washing bottle is not well-defined. Therefore, the intensity is slightly different.

The maximum intensity that can be achieved by using the CO₂ box is 60000 approximately. Exceeding this limit, the fluorescence signal can not be fully measured.

Since the pCO₂ sensor will be used during and after the surgical operation for continue monitoring the amount of pCO₂, this sensor must be fast enough. Therefore, the response time of this sensor is determined. The transition time from one intensity to intensity is examined for both lines. The response time in case of increasing pCO₂, thus the blue line, is approximately 163s, while the response time in case of decreasing pCO₂, thus the red line, is approximately 299s. This time is partially due to the property of pCO₂ sensitive coating (ethyl cellulose) and due to the chemical reaction. The thickness of ethyl cellulose depends on its mass percentage. The lower

the mass percentage, the thinner the ethyl cellulose and the faster the response time will be. However, the lower the mass percentage, the weaker the fluorescence signal will be. 3 mass percentage of ethyl cellulose is used for pCO₂ sensor because of the relative fast response and relative strong fluorescence signal.

The pCO₂ level can be determined using one excitation light source. The obtained results are reliable. The drawback of using one excitation light source is that the measurement is sensitive for setup variations: i.e. when the probe is positioned in a different way, the obtained data are slightly different. However, in real life no optical fibre will be used.

Since one excitation light source can be used to determine the pCO₂ level, the CO₂ sensor can be integrated with the O₂ sensor. However, some aspects should be considered. In the next section, these aspects are discussed.

2.7 Important parameters for the pCO₂ sensitive coating

With the help of HPTS-(TOA)₃, pCO₂ concentration can be determined. However, using this pH indicator, several aspects should be considered. In this subsection, these aspects have been presented.

HPTS-(TOA)₃ is a pH indicator. It is important to check whether this pH indicator shows a chemical reaction with an acid or base. Therefore, HPTS-(TOA)₃ with TEFLON tape is immersed in 1M H₃PO₄ with pH value of 3, which after the fluorescence signal is measured in the spectrometer using the setup that is described in 2.3. Before starting with measuring the fluorescence signal in presence of H₃PO₄, HPTS-(TOA)₃ is first put in glass bottle that is filled with purified water. The bottle is sealed to prevent CO₂ flowing in. The ratio of the two excitation wavelengths is being calculated (ratio = 1.4788). This ratio will be compared with the ratio that is obtained when 1M H₃PO₄ has been added.

Figure 2.7.1 shows the results of the measurements when HPTS-(TOA)₃ is immersed in 1M H₃PO₄.

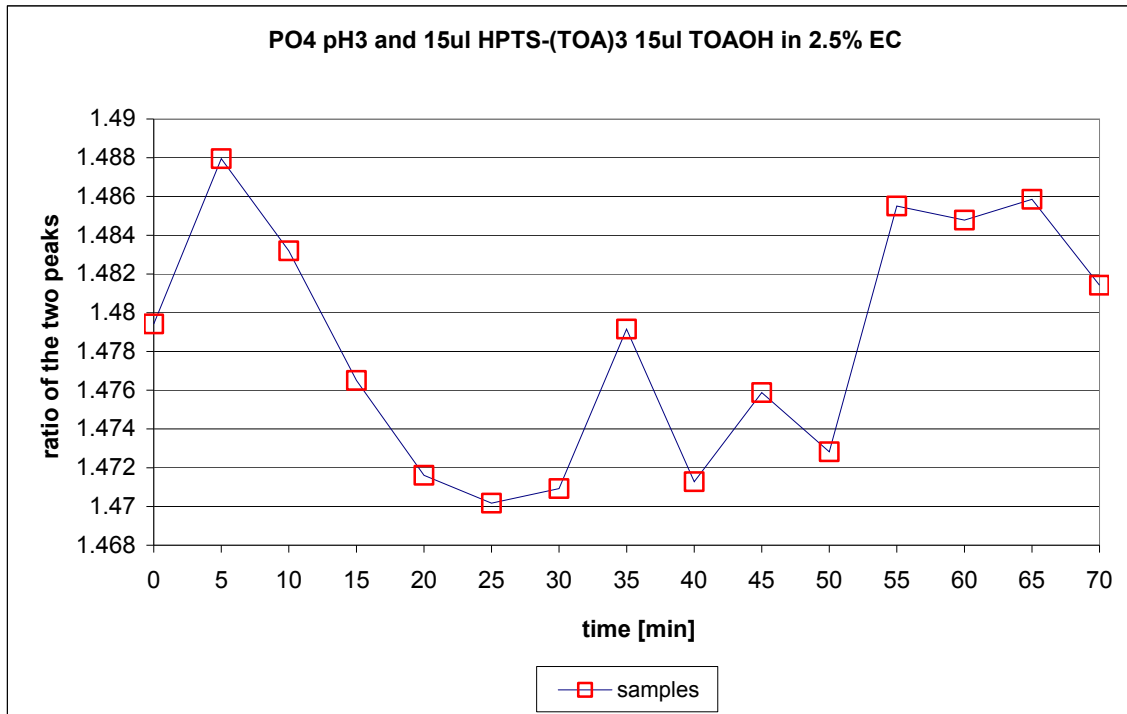


Figure 2.7.1: The response of HPTS-(TOA)₃ that is immersed in H₃PO₄

Figure 2.7.1 shows that the ratios of the two excitation wavelengths are nearly constant. This means that using HPTS-(TOA)₃ in combination with TEFLON tape is insensitive for acid, like H₃PO₄.

Since CO₂ sensor will be integrated with O₂ sensor. It is important to check if HPTS-(TOA)₃ reacts with O₂. The second setup that is described in 2.5 is used to do this experiment. In stead of pumping CO₂ to the gas mixer, O₂ is used. The results are plot in Figure 2.7.2.

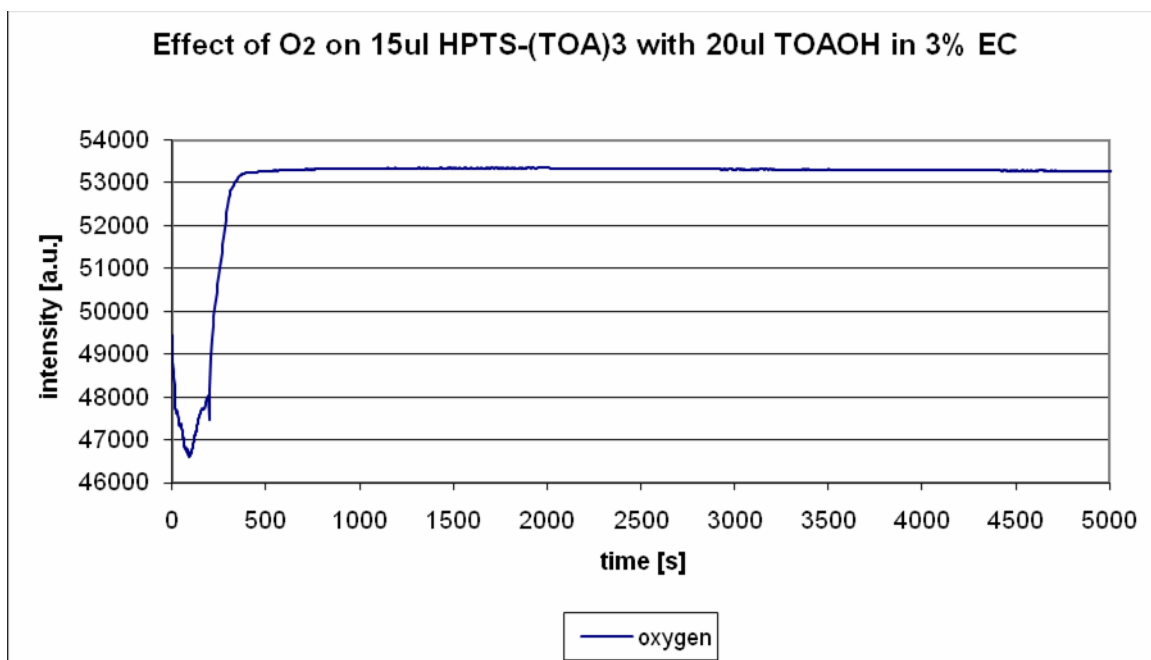


Figure 2.7.2: Effect of O₂ that is touch with HPTS-(TOA)₃

At the beginning of the measurement, the intensity shows a fall. This drop is due to the present of pCO₂ that is present in gas-washing bottle. Once all pCO₂ is flowing out the bottle, the intensity increases. Compare this final value with the final value that is obtained in Figure 2.6.1, in which no pCO₂ is present, both value is the same. Therefore, pO₂ does not react with HPTS-(TOA)₃.

The final parameter that has been studied is the temperature, since many processes are temperature dependent. The temperature effects on three levels of pCO₂ have been studied. Figure 2.7.3 shows the result of intensity variations for different temperature.

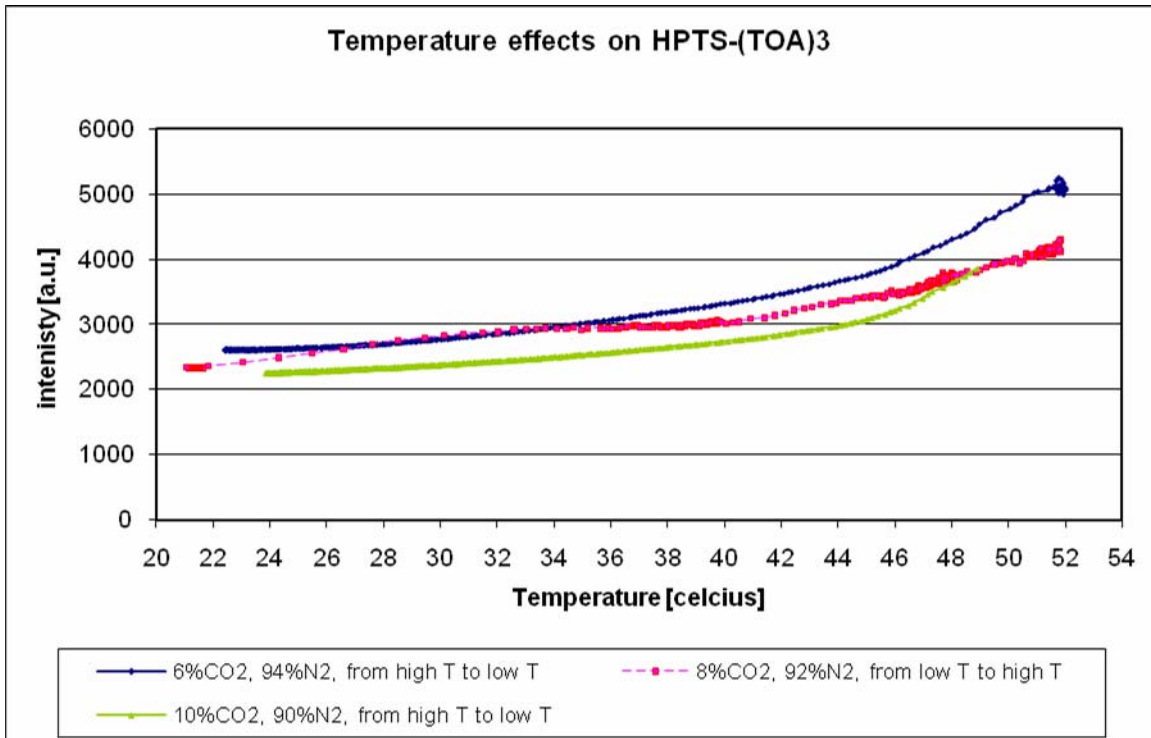


Figure 2.7.3: Temperature effects on HPTS-(TOA)₃ with three different levels of CO₂

Ideally, all lines in Figure 2.7.3 should be flat. A flat line means that the temperature does not have an effect on HPTS-(TOA)₃. However, the practical situation shows that using this chemical sensor, temperature compensation should be taken into account, since the intensity value is different at different temperature.

The intensity of the fluorescence signal of HPTS-(TOA)₃ increases by rising temperature. This increment is approximately linear. To reduce the error in estimating the pCO₂ concentration, temperature compensation must be performed. Thus, a calibration curve has to be created in order to do temperature compensation. The calibration curve can be obtained by plotting all intensities values of different CO₂ levels to estimate a proper function that can be used for compositing the temperature effects. In the attachment of this thesis, all graphs are shown for all mixture of CO₂ concentrations.

Furthermore, make sure that HPTS-(TOA)₃ is not dried out. When this happens, the chemical behavior might not of what it is expected.

2.8 Conclusions

The pH indicator HPTS-(TOA)₃, which does not solve in water, has been used for measuring the pCO₂ (partial pressure of carbon dioxide molecules that are dissolved in blood plasma) and CO₂ (carbon dioxide molecules that are exposed in the air) concentration. In this thesis, measurements on pCO₂ are based on partial pressure of carbon dioxide molecules that are dissolved in water environment. Therefore, we are talking about CO₂ sensor and we are referring pCO₂ to CO₂.

The measurement is based on the fluorescence character of the pH coating. The fluorescence signal is the strongest at two specific excitation peaks, which are located at $\lambda_{excitation1} = 395nm$ and at $\lambda_{excitation2} = 470nm$. Both peaks depend on the involved CO₂ amount. The emission peak that has been used is set at $\lambda_{emission} = 530nm$, because the intensity is the strongest.

In case of low concentration of CO₂, both peaks will have the strongest intensity. The intensity of both peaks will decrease when the CO₂ increase. The ratio of both peaks has been taken to determine the CO₂ level. The big advantage of taking the ratio of both peaks is that the results of the measurements are independent of the setup variations. However, one peak measurement will be used for future analysis, because the CO₂ sensor can be easier integrated with the O₂ sensor.

HPTS-(TOA)₃ is not able to detect a high percentage of CO₂ with a reliable measurement. Up to 20% CO₂, the sensitivity of HPTS-(TOA)₃ is the highest. From 20% CO₂, the intensity difference becomes irrelevant. Figure 2.4.2 and Figure 2.4.3 proof this statement.

The results (Figure 2.6.2) of one peak excitation show that the chemical reaction of HPTS-(TOA)₃ with CO₂ is stable, reliable and reversible. The response time of the CO₂ sensor is studied. The time that is required to react with CO₂ is approximately 3 minutes.

Some aspects should be considered when using HPTS-(TOA)₃ for measuring CO₂. Temperature compensation should be applied and be aware of the setup variation, such as change in the position of the optical in the CO₂ box in case of single excitation wavelength has been used. The HPTS-(TOA)₃ performs its best when it is not dried out. This pH indicator is insensitive to other acid or base and it does not react with the present of O₂. Thus, HPTS-(TOA)₃ is an outstanding material for detecting low level of CO₂.

One excitation light source with wavelength of $\lambda_{\text{excitation}} = 470\text{nm}$ can be used to activate HPTS-(TOA)₃ and oxygen sensitive coating. Since both coating have different emission spectrum, they can be integrated in one single package.

2.9 References

- [1] Gerhard J. Mohr, Tobias Werner, Otto S. Wolfbeis, "Application of a Novel Lipophilized Fluorescent Dye in an Optical Nitrate Sensor", DOI: 10.1007/BF00727530
- [2] Chen-Shane Chu, Yu-Lung Lo, "Fiber-optic carbon dioxide sensor based on fluorinated xerogels doped with HPTS", DOI: 10.1016/j.snb.2007.07.082
- [3] C. Munkholm, D.R. Walt, F.P. Milanovich, A fiber-optic sensor for CO₂ measurement, *Talanta* 35 (1988) 109–112.
- [4] S.C. Kraus, R. Czolk, J. Reichert, H.J. Ache, Optimization of the sol–gel process for the development of optochemical sensors, *Sens. Actuators B: Chem.* 15 (1993) 199–202.
- [5] A. Mills, Q. Chang, N. McMurray, Equilibrium studies on colorimetric plastic film sensors for carbon dioxide, *Anal. Chem.* 64 (1992) 1383–1389.
- [6] A. Mills, Q. Chang, Colorimetric polymer film sensors for dissolved carbon dioxide, *Sens. Actuators B: Chem.* 21 (1994) 83–89.
- [7] A. Mills, A. Lepre, L. Wild, Breath by breath measurement of carbon dioxide using a plastic film optical sensor, *Sens. Actuators B: Chem.* 39 (1997) 419–425.
- [8] B.H. Weigl, O.S. Wolfbeis, Sensitivity studies on optical carbon dioxide sensors based on ion pairing, *Sens. Actuators B: Chem.* 28 (1995) 151–156.
- [9] B.H. Weigl, O.S. Wolfbeis, New hydrophobic materials for optical carbon dioxide sensors based on ion paring, *Anal. Chim. Acta* 302 (1995) 249–254.
- [10] C. Malins, B.D. MacCraith, Dye-doped organically modified silica glass for fluorescence based carbon dioxide gas detection, *Analyst* 123 (1998) 2373–2376.
- [11] Chen-Shane Chu, Yu-Lung Lo, Fiber-optic carbon dioxide sensor based on fluorinated xerogels doped with HPTS, Available online 25 July 2007

Chapter 3 – O₂ sensor

3.1 Introduction

O₂ sensor has been used that is supplied by TNO Quality of Life, located in Zeist. It is a chemical sensor which also has a fluorescence property. The lifetime and the intensity of the fluorescence signal depend on the amount of O₂ and the chemical mixture. The chemical mixture contains of oxygen sensitive coating where ruthenium (Ru) particles are embedded. The pO₂ sensitive coating contains holes where gasses can pass through. When light is on the oxygen sensitive coating, the fluorescence compounds are activated and as a consequence fluorescence occurs.

When a large amount of oxygen is present in the oxygen sensitive coating, the decay of the fluorescence signal will be much faster. That means the lifetime of the fluorescence decreases by increasing amount of oxygen. The decrease in fluorescence signal is due to the collisions of the oxygen molecules with the fluorescent compounds that are embedded in gas permeable polymers. Energy is lost due to collisions.

In this chapter, the technique that TNO has used for determining the O₂ level has been discussed in details. This chapter starts with how the oxygen level has been measured using the conventional method that TNO introduces. For this measurement, some assumptions have been made.

The next section, the readout electronics have been represented. The calculations of output voltages of each operational amplifier have been shown.

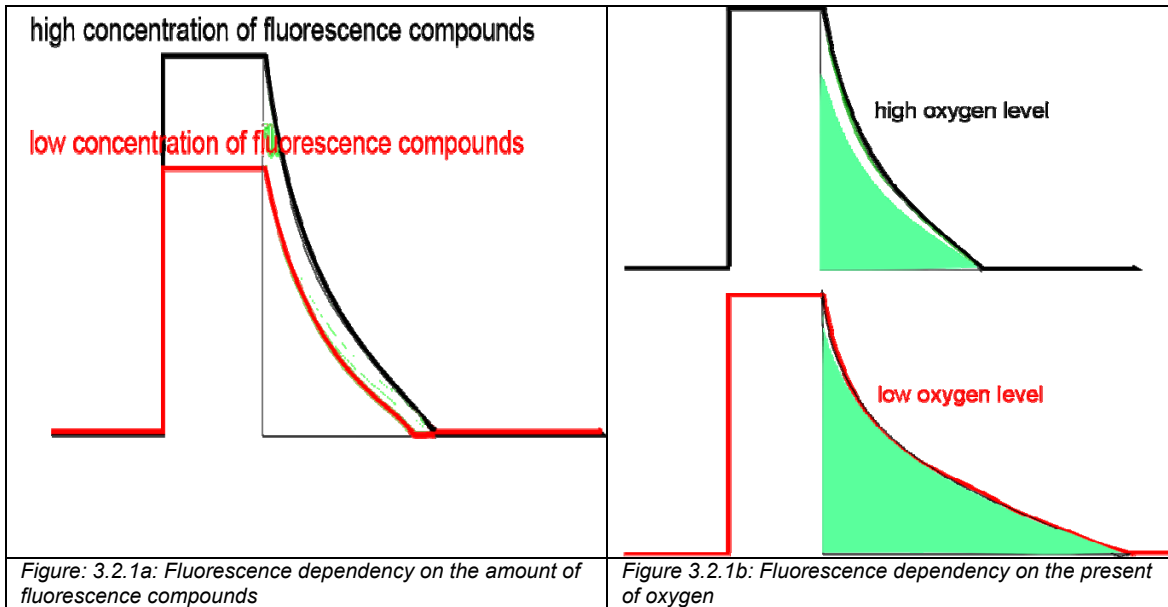
Simulations of this readout electronics have been performed. For the simulations, different operational amplifiers have been used. This chapter ends with conclusion.

3.2 Determination of the amount of O₂ based on TNO approach

The usual way of determining the amount of O₂ has been used by TNO. This approach has been proved for its proper functioning. This section describes how this approach works. This section starts with a description of the working principle of the oxygen sensitive coating.

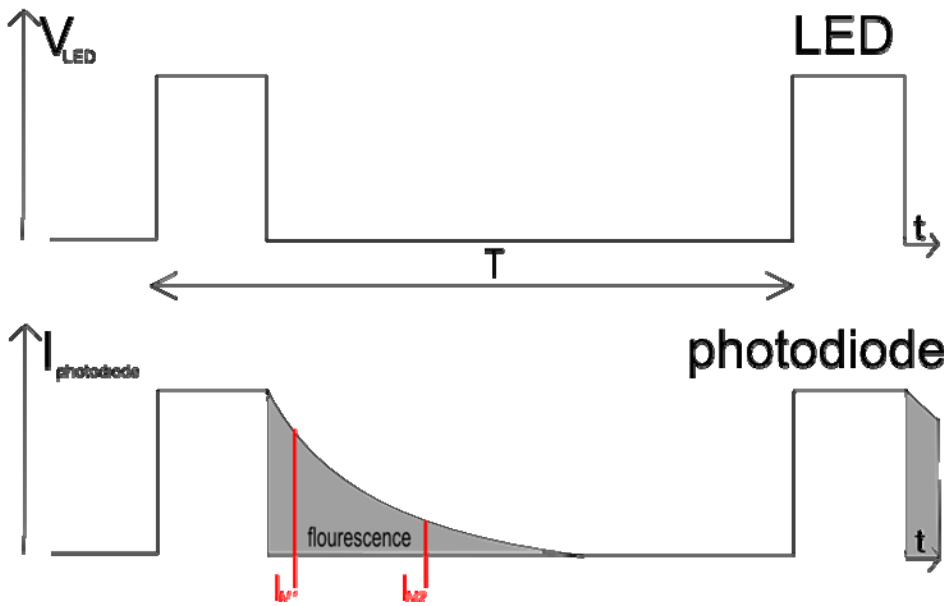
When the O₂ sensitive coating is exposed to light with the wavelength of 480nm, the compounds in the coating are excited. These compounds leave their ground state and they stay in a higher energy level. When they fall back to the ground state, a photon with emission peak of 600nm – 650nm is sent out. The duration of this fluorescence process depends on the amount of the O₂ sensitive coating in the polymer and the involved O₂. The more O₂ sensitive coating, the more intensity of the fluorescence will be, since more fluorescence compounds will be activated simultaneously. The more O₂, the shorter of the fluorescence will be, since due to collisions of the fluorescence compounds in the polymer with the present O₂, more and more energy is lost.

Figure 3.2.1a and Figure 3.2.1b show this principle.



The grey coloured area indicates the fluorescence signal. The intensity depends on the involved fluorescence compounds in the polymer. The lifetime of the fluorescence depends on the present of the oxygen.

To determine the amount of O_2 that is involved, TNO do two measurements at different time frame. Figure 3.2.1c shows this principle.



The graph on top shows the response of the LED (Light Emitted Diode). The duty cycle and the frequency of the LED are fixed. The duty cycle is set at 2% and the period is set at $50\mu s$. The duty cycle must be kept short, since for a big duty cycle the essence of the fluorescence signal is lost for determining the O_2 level.

The photodiode, which represents the O_2 sensor, is shown below. When light is on the photodiode, it will conduct current. A normal diode will not produce current when there is no light. However, since the photodiode is connected with O_2 sensitive coating, this photodiode will show fluorescence which gives photocurrent.

The intensity of the fluorescence signal depends on the amount of the O₂ sensitive compounds and on the involved O₂, which has been discussed earlier. To minimise the fluorescence before the second light pulse is coming, the period is kept long as long as possible.

Two intensity measurements have been performed to determine the amount of O₂. Both measurements are indicated by red vertical lines, I_{M1} and I_{M2}. The fastest decay of the fluorescence is about 1µs, while the lowest decay is about 5µs. Within one microsecond, both measurements should be carried out. So, the width of I_{M1} and I_{M2} are less than 1 µs.

The intensity of the fluorescence I(t) has been assumed as the following function [1]:

$$I(t) = I_o \exp\left(-\frac{t}{\tau}\right) \quad (3.1)$$

I_o = intensity without the quencher (O₂) concentration

t = time (duration)

τ = decay time

It has been assumed [2] that there is one decay time. In reality, we have a set of decay times

Based on the Stern Volmer relationship [3], the oxygen level can be obtained. The Stern-Volmer equation says:

$$\frac{I_0}{I} = 1 + C_{sv} \cdot [O_2] \quad (3.2)$$

C_{sv} = Stern-Volmer constant

[O₂] = oxygen concentration

Thus, the ratio of the intensities is a quantity for the oxygen level. Applying this technique to measure the oxygen level, has some drawbacks. The first one is the sensitivity for the intensity changes. The intensity of the fluorescence might change due to mixture variations in using chemical materials. Besides, the change in sensitivity might also be due to applying a different voltage over the LED.

The other disadvantage of using this technique is the sensitivity of the noise level and offset value of the readout electronics. Due to noise or the offset, the oxygen cannot be obtained

accurately, since $\frac{I_0}{I} \neq \frac{I_0 + a}{I + a}$.

The approach of TNO is based on the lifetime measurements. The lifetime value is obtained by:

$$\tau = \frac{t_2 - t_1}{\ln\left(\frac{A_1}{A_2}\right)} \quad (3.3)$$

It is assumed that the exponential function is monotone decay. The lifetime is calculated by averaging the integral values of I(t) (A₁ and A₂) by recording the intensity I(t) in two different time frames (t = t₁ and t = t₂). (Woods et al., 1984; Ni and Melton, 1993; Liebsch et al., 2001). These two timeframes correspond to I_{M1} and I_{M2} in Figure 3.2.1c.

The advantage of using this lifetime technique is to get rid off the changes in chemical mixture. According to the Stern-Volmer equation, the relationship between the oxygen concentration and the lifetime is given by:

$$\frac{\tau_0}{\tau} = 1 + C_{sv} \cdot [O_2] \quad (3.4)$$

τ = lifetime of the excited state in the absence of the quencher

The next section shows the simulation results of readout electronics for the TNO approach, using operational amplifiers (OpAmps) OPA-355 to evaluate its performance, which will be compared with the new approach that will be discussed later on this thesis.

3.3 Read-out electronics based on TNO approach

The circuit is designed by TNO and this circuit has been mainly used for detecting the oxygen tension (pO_2) level. However, with these circuits, it is also possible to track the oxygen O_2 level. The complete schematic drawing of this circuit is shown on the next page in Figure 3.3.1.

Only one operational amplifier has been used for amplification of the signal purposes. That is the OPA-355. TNO uses OPA-356. Due to unavailability of this component for PSpice simulation, its substitution, OPA-355, has been used. Their difference is in the input offset voltage. The input voltage offset of OPA-355 is lower (8mV versus 2mV).

The photodiode modelled as the pO_2 sensor. The photocurrent as response of the fluorescence is converted into voltage by the first amplifier. The series resistor and the capacitor between the three amplifiers are used as voltage-to-current conversion. As in the second amplifier and as in the third amplifier, the signal is amplified and converted back to voltage again.

Three amplifiers have been used for amplification in stead of one, because the bandwidth product may not be sufficient. Moreover, the amplification factors for obtaining the intensity values at different time frames are different, since the intensity of the fluorescence signal varies at different time frame (see Figure 3.2.1c).

The capacitors that are in series connected with the resistor have been used for filtering out the high frequently components, while the capacitors that are parallel connected with the resistor in the negative feedback configuration of the OpAmps are used for biasing. The values of the resistors in each feedback give the magnification factor of the photocurrent.

The output voltages are denoted as V_{PH_AN0} , V_{PH_AN1} and V_{PH_AN2} for the first, second and the third amplifier. The following formulas show the voltage calculation:

$$\begin{aligned}
 V_{PH_AN0} &= -I_{\text{photodiode}} \cdot \frac{R_{22} \cdot \frac{1}{sC_5}}{R_{22} + \frac{1}{sC_5}} + \frac{\frac{R_{10}}{1 + sR_{10}C_{15}}}{\frac{R_{10}}{1 + sR_{10}C_{15}} + R_{15}} V_{ref} \\
 V_{PH_AN1} &= \frac{\frac{\frac{R_{13}}{1 + sR_{13}C_{22}}}{\frac{R_{13}}{1 + sR_{13}C_{22}} + R_{14}} V_{ref} - V_{PH_AN0}}{R_{24} + \frac{1}{sC_8}} \cdot \frac{R_{40}}{1 + sR_{40}C_{42}} + \frac{\frac{R_{13}}{1 + sR_{13}C_{22}}}{\frac{R_{13}}{1 + sR_{13}C_{22}} + R_{14}} V_{ref} \quad (3.5) \\
 V_{PH_AN2} &= -\frac{\frac{\frac{R_{27}}{1 + sR_{27}C_{47}}}{\frac{R_{27}}{1 + sR_{27}C_{47}} + R_{62}} V_{ref} - V_{PH_AN1}}{R_{74} + \frac{1}{sC_{46}}} \cdot \frac{R_{25}}{1 + sR_{25}C_{45}} + \frac{\frac{R_{27}}{1 + sR_{27}C_{47}}}{\frac{R_{27}}{1 + sR_{27}C_{47}} + R_{62}} V_{ref}
 \end{aligned}$$

The OpAmps that TNO has been used have a large unity bandwidth (350MHz) in able to track the pulse shape that is generated by the ideal current source. In the next section, simulations are performed with this OpAmp. Moreover, to obtain the voltage values at the two different time frames that is mentioned in the previous subsection, the A/D speed must be very high, since the fluorescence is assumed as a mono-exponential decay function. When the A/D speed is slow, the input voltage for the A/D might drop too much which gives unreliable results.

However, the accuracy depends on what kind of A/D converter has been used and how it performance.
Simulation of the A/D is not possible using PSpice. Therefore, the coming section is only focussed on the performance of OPA-355 using TNO approach.

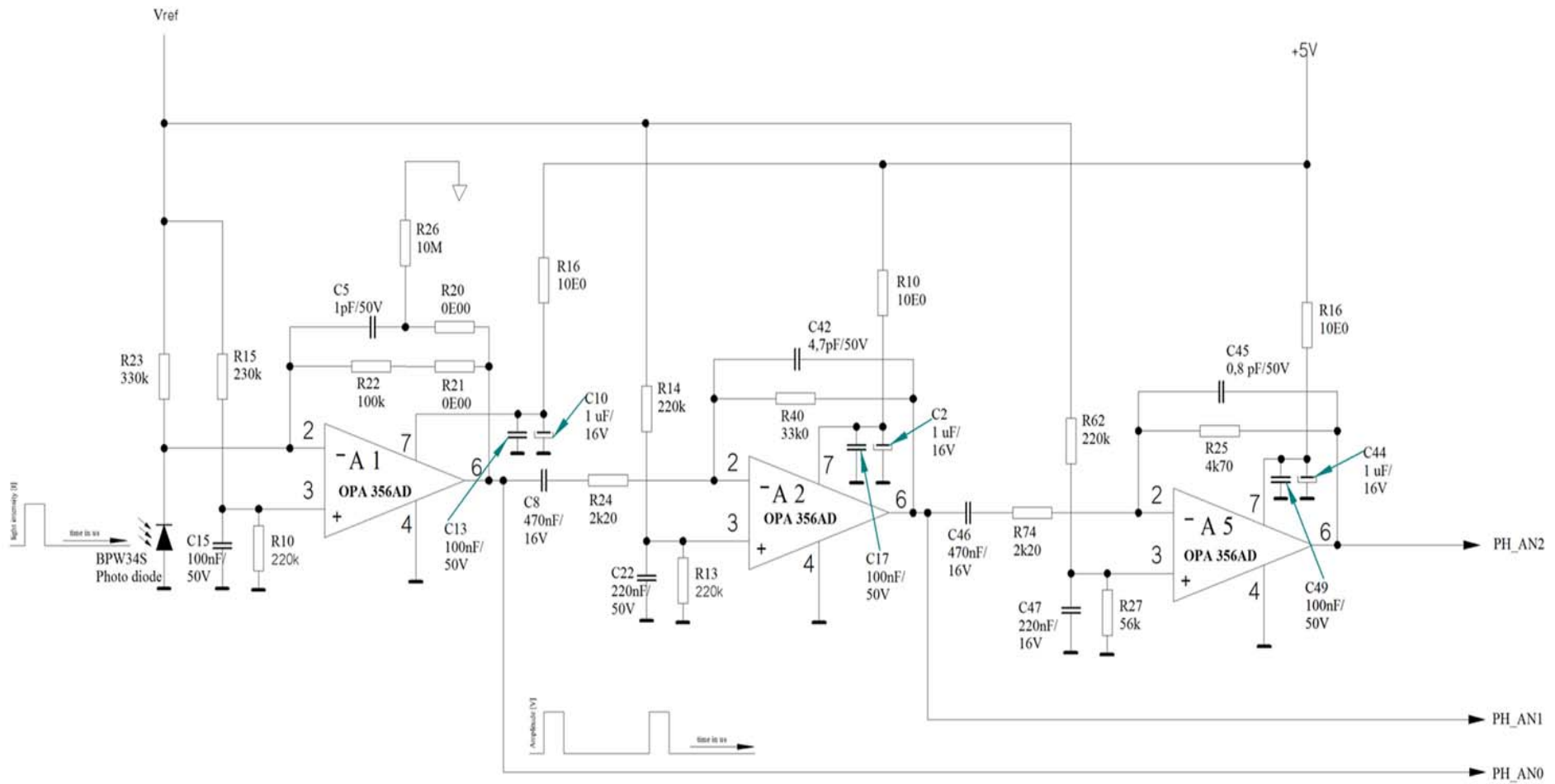


Figure 3.3.1: Readout electronic of the approach of TNO

3.4 Simulation results of read-out electronics of TNO

In this section, the simulation results of the readout electronics will be discussed. All simulation results are performed at $T = 25^{\circ}\text{C}$. Transient analysis has been used. OPA-355 has been used for evaluating the performance of the TNO's concept. The ideal current source represents the O_2 sensor. This current source generates a pulse, which has a period of $50\mu\text{s}$ and a pulse width of $1\mu\text{s}$. The rise time of the pulse is related to the bandwidth requirement of the operational amplifier. Formula 3.6 shows this relationship.

$$BW = \frac{0.35}{t_{rise}} \quad (3.6)$$

Table 3.1 summarises the parameters for the operational amplifiers that might be important for determining the amount of O_2 .

Table 3.1: Important parameters of the operational amplifiers for detecting O_2 level

Type of operational amplifiers	Bandwidth [Mhz]	Typical offset voltage [mV]	Typical bias current [pA]	Typical slew rate [V/ μs]	Noise level [nV/ $\sqrt{\text{Hz}}$]
OPA-355	200	2	3	300	5.8

OPA-356 has been used in the readout electronic of TNO. Since there is no PSpice model available for this device, a substitute has been used. The technical specifications of OPA-356 are very similar to OPA-355. The only difference is in the offset voltage. The input offset voltage of OPA-356 is lower.

Figure 3.4.1 illustrates the first setup for the simulation.

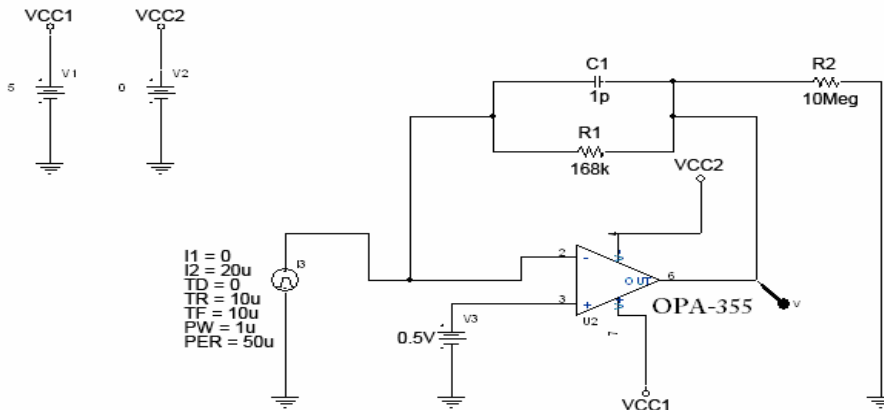


Figure 3.4.1: Simulation setup of the TNO's approach

Only one operational amplifier has been used for simulation, since the essentials of the two other amplifiers can be ignored, because the two excluded amplifiers are used for amplification purpose only.

The amplifier that TNO has been used for the readout circuits is the OPA-356. This is an operational amplifier with a bandwidth of 350MHz, which means that this amplifier is a high bandwidth amplifier. OPA-355 has been used for simulations. Figure 3.4.2 and Figure 3.4.3 show the results of the performance of this amplifier. The simulation is set to stop at 140ns.

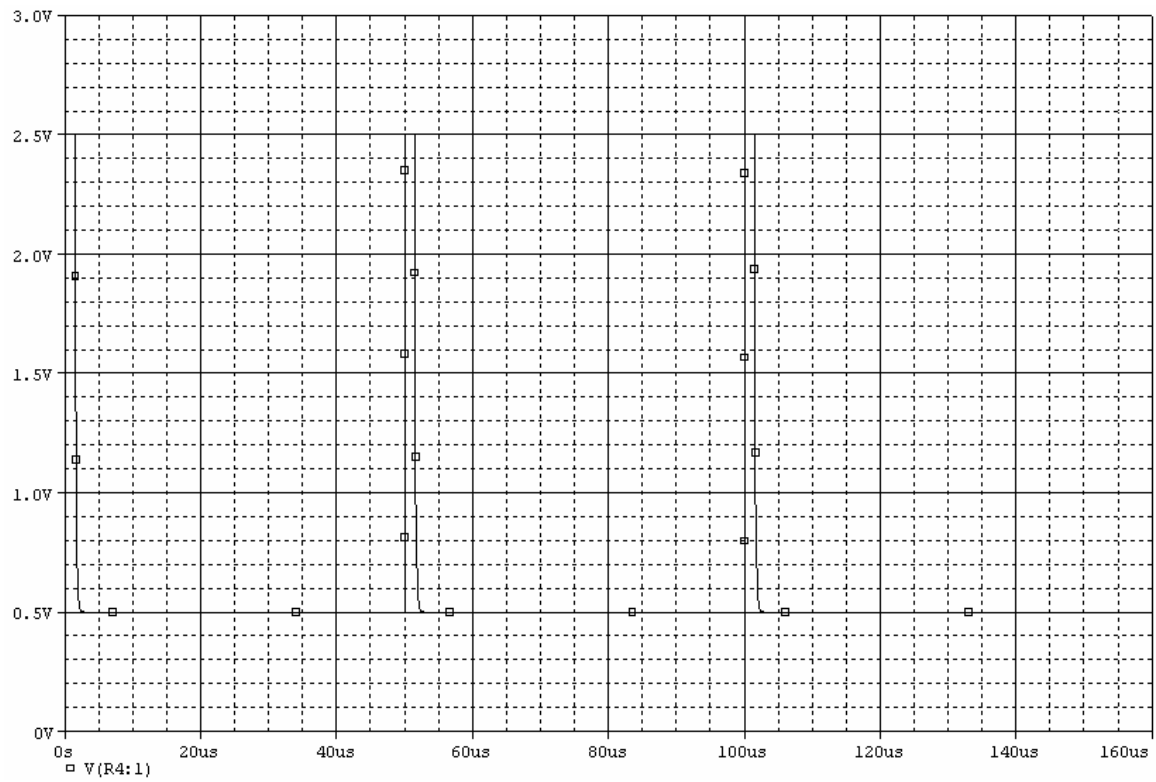


Figure 3.4.2: Results of OPA-355

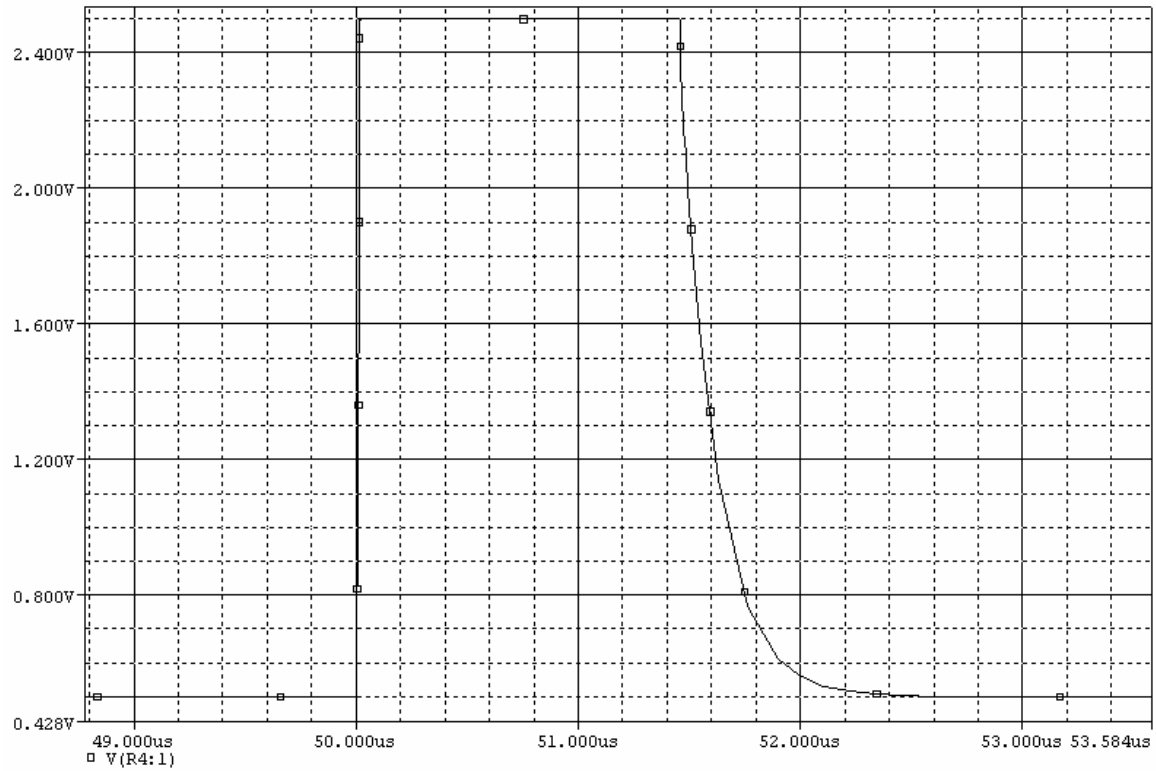


Figure 3.4.3: Results of OPA-355, zoomed in at around $t = 50\mu\text{s}$

The pulse using this OpAmp is well defined. However, the fall time of this operational amplifier is relative much slower compared to its rise time. The ideal current source is turned off right after 51 μ s with a delay of 10ns. Looking at Figure 3.4.3, it shows that the delay is more than expected. The additional delay might be due the operational amplifier itself and due to RC network in the feedback network.

This delay might give trouble for determining the oxygen level. As mentioned before, TNO takes samples at two different time intervals. If one of the samples is taken within the delayed area, the accuracy of determining of the oxygen level is reduced.

To avoid this problem, samples have to be taken after the light pulse is turned off for about 1 μ s. The drawback is that the signal is much weaker, thus the output voltage becomes much lower. If the gain of the system is insufficient, it must be increased.

Bode plot is shown in Figure 3.4.4 to make sure if this OpAmp is able to track the fluorescence signal.

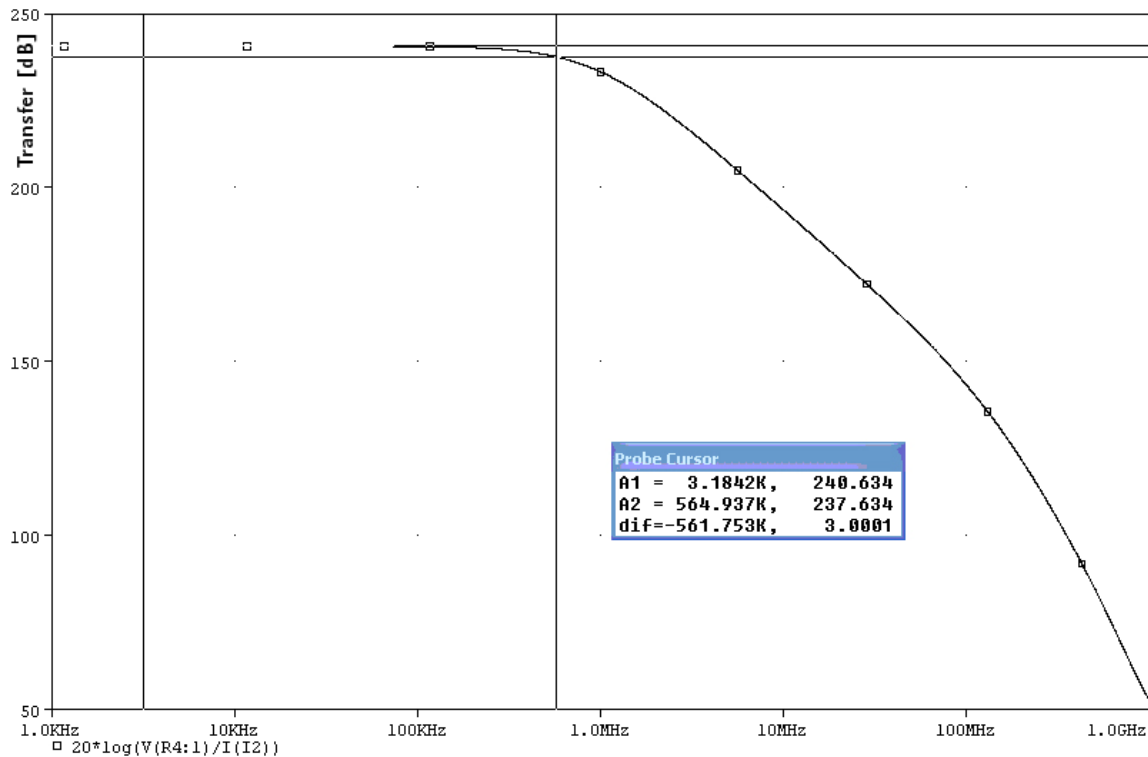


Figure 3.4.7: Bode plot of OPA-355

The -3dB point is located at $f \approx 564.94$ kHz. The minimal fall off time due to fluorescence that has been measured in earlier works [2], [6] is 5 μ s. With this setup using this OpAmp, the bandwidth is sufficient.

The bandwidth of the OpAmp is 200MHz. The bandwidth of the complete circuit (Figure 3.4.1) is ≈ 565 kHz. The difference of the bandwidth is due to position of the poles of the OpAmp and the complete circuit. A pole that is positioned at a low frequency will reduce the bandwidth [5]. A RC combination in Figure 3.4.1 can be found in the feedback network. This RC combination has a RC time of 0.168 μ s. This RC combination introduces a lower pole than what it can get from the OPAMP OPA-355. Therefore, the bandwidth reduction can be expected.

This OPAMP is optimised for voltage-feedback. Using this OPAMP for current-to-voltage conversion, it operates in a not optimised operation.

One note has to be made. To able to do simulation for this operational amplifier, dual supply (± 2.5 V) has been applied. According to the datasheet of this amplifier, single supply is required. However, during the simulation in PSpice, the conversion could not be completed. Using dual supply will solve problem.

The drawback of using this circuit is that it requires an operational amplifier with a high bandwidth and a high slew rate to track rise time. The fall time is the most important parameter to determine the oxygen level. The fastest decay of the fluorescence signal that has been measured is $5 \mu s$. Using an operational amplifier with more than 100MHz is not essential. Therefore, an alternative approach has been examined for the measurement on the oxygen level using a low bandwidth operational amplifier. This new approach is based on the integration of the entire or a part of the fluorescence signal to subtract the lifetime value. This idea will be clarified in the next chapter.

3.5 Conclusions

This chapter describes how the oxygen level has been measured using the chemical material that TNO Quality of life Zeist supplies. The chemical material shows a fluorescence property which the duration of the fluorescence depends on the oxygen level. In case of a high density of oxygen (21%), the duration of the fluorescence signal is the shortest. The duration is about $5\mu s$. In case of a very low level of oxygen (about 0%), the duration of the fluorescence signal is about $25\mu s$.

The duration of the fluorescence can be used as an indication for the oxygen level. This is called the lifetime of the fluorescence signal. To determine the oxygen level via the lifetime measurement, the relationship of Stern-Volmer has been introduced.

TNO measures the output voltage at different time intervals in able to subtract the lifetime value. It is assumed that the fluorescence signal has a mono-exponential decay. If this assumption is wrong, errors in determining the oxygen level will be introduced. In the worst case, the oxygen level cannot be calculated.

The circuit that TNO uses for determining the oxygen level makes use of operational amplifiers with 350MHz. This is a high bandwidth amplifier. Besides, its slew rate is $300V/\mu s$ and its noise level is $5.8nV/\sqrt{Hz}$. This amplifier has a large slew rate and low noise level and it belongs to a "high-end" amplifier.

This high-end amplifier is the OPA-356. There is no PSpice model available for this OpAmp. Therefore, a substitution has been used. The substitution is the OPA-355. The difference of this two OpAmps is the input offset voltage. OPA-355 has a lower input offset voltage.

The simulations are performed in PSpice 9.1. The OPA-355 PSpice model is directly downloaded from its manufacture, Texas Instruments. Other components are the default components that can be found in the default PSpice 9.1 software. During the simulation of OPA-355, the supply voltage must be adjusted to dual supply. According to the datasheet, this operational amplifier should be able to operate with single supply. Using single supply, PSpice is not able to do conversion.

The simulation results show that the TNO circuit is able to track the pulse properly. However, a small delay in the fall off time can be observed. This delay is about 500ns. That is due to the feedback network.

Bode plot has been introduced to check if the bandwidth of the circuit is enough to track the minimum fall off time, which is about $5\mu s$. The Bode plot shows that the bandwidth of the circuit is about $f \approx 564.94kHz$. According to Shannon theorem, this bandwidth is sufficient for a speed of $5\mu s$.

3.6 References

- [1] Karin Kellner, Gregor Liebsch, Ingo Klimant, Otto S. Wolfbeis, Torsten Blunk, Michaela B. Schulz, Achim Göpferich, "Determination of Oxygen Gradients in Engineered Tissue Using a Fluorescent Sensor", DOI: 10.1002/bit.10352
- [2] A. Draaijer, J.W. König, J.J.F. van Veen, R.E.G. van Hal, "AN OPTICAL OXYGEN SENSOR" et al, 2nd Inter-Regional Conference on Environment-Water, 1 to 3 Sep. 1999
- [3] Ocean Optics, "Fiber Optic Oxygen Sensors: Theory of Operation", www.oceanoptics.com/Products/sensorththeory.asp
- [4] PSpice models of Texas Instruments, OPA-355: <http://focus.ti.com/docs/prod/folders/print/opa355.html>
- [5] C.J.M. Verhoeven, A. van Staveren, G.L.E. Monna, M.H.L. Kouwenhoven, E. Yildiz, "Structured Electronic Design Negative-Feedback Amplifiers", Kluwer Academic Publishers
- [6] Tanase D., French P.J., Komen N., Kleinrensink G.J., Jeekel J., Lange J.F., Draaijer A., "Oxygen-tension measurements – The first step towards prevention and early detection of anastomotic leakage", *proceedings of IEEE Sensors*, art. no. 4388337, pp. 68-71

Chapter 4 – Alternative read-out system

4.1 Introduction

In the previous chapter, the oxygen sensor has been fully discussed. TNO uses his circuit to measure the intensity values at two different time frames to subtract the lifetime, τ , from the fluorescence signal. Many passive and active components are involved to build this circuit. Therefore, new read-out electronics has been introduced to reduce the number of components.

The alternative read-out system has another approach to obtain the lifetime. The new method is based on extracting the lifetime with the help of integration. For this alternative approach, no optimisation has been applied. Consequently, there is no temperature compensation applied to the measurement results.

The alternative approach retrieves the lifetime of the fluorescence signal, which can be related to the O_2 level. This relationship of the lifetime with the oxygen level is given by the Stern-Volmer equation:

$$\frac{\tau_0}{\tau} = 1 + C_{SV} \cdot [O_2] \quad (4.1)$$

τ_0 = the fluorescence lifetime at quencher (O_2) concentration zero

τ = the fluorescence lifetime at a specific quencher (O_2) concentration

C_{SV} = Stern-Volmer constant

$[O_2]$ = oxygen concentration

The readout electronic of the new approach uses two integrators to extract the lifetime of the fluorescence signal. The idea is based on the mathematical determination of a constant, which is in this case the lifetime, τ , by integrating the exponential twice and which after a division is done. The following formulas show this concept.

Assume the fluorescence signal is represented by

$$f(t) = a \cdot e^{-\frac{t}{\tau}} \quad (4.2)$$

$f(t)$ = function of the fluorescence signal

a = amplitude of the starting value of the fluorescence signal

t = time

τ = a set of lifetime values

Now, integrating this gives:

$$F_1(t) = \int f(t) \cdot dt = \int a \cdot e^{-\frac{t}{\tau}} \cdot dt = -a \cdot \tau \cdot e^{-\frac{t}{\tau}} + c \quad (4.3)$$

$$F_2(t) = \iint f(t) \cdot dt = \iint \left(a \cdot e^{-\frac{t}{\tau}} \right) \cdot dt = \left[a \cdot \tau^2 \cdot e^{-\frac{t}{\tau}} \right] + c \quad (4.4)$$

$$= a \cdot \tau^2 \cdot e^{-\frac{t}{\tau}} + c$$

$F_1(t)$ and $F_2(t)$ are the first and the second integral over the signal respectively. Assume that both constant values are zero. The ratio of both integrals gives us the lifetime:

$$\frac{F_2}{F_1} = \frac{a \cdot \tau^2 \cdot e^{-\frac{t}{\tau}}}{-a \cdot \tau \cdot e^{-\frac{t}{\tau}}} = -\tau \quad (4.7)$$

It is assumed that the decay of the fluorescence signal is a monoexponential function. In real life, the integration has been realised by using electronic circuits. These circuits will be discussed in the first section. The second section, simulations with the selected operational amplifier. Moreover, two different types of current source have been introduced to test the reliability of this new approach. They are named as the constant and linear current sources that act as the fluorescence signal. After the simulation, evaluation of the performance of this new read-out electronics has been discussed in the next section. This chapter ends with conclusion.

4.2 Realisation of the readout electronics for the alternative approach

The readout electronic should be able to extract the lifetime, τ , to determine the O_2 level. The photodiode is represented by a simple pulse current source. The rise time, the fall time, the duty cycle, delay and the amplitude of the current can be perfectly matched with the real photodiode that has been used. The fluorescence signal is represented by the fall time of the pulse.

The simulation is performed in PSpice9.1. In this simulation program, there is also a current source which can generate an exponential decay. This source has not been used, because the analysis in PSpice will become more complex. When the readout electronic proves its proper working for the simple constant source and the linear source, this new circuit should also work for an exponential source. The constant and the linear sources will be discussed later on to clarify the idea.

To able to do the integration of the current, capacitor has been used. The value of this capacitor depends on the charge and discharge time. The period of the photodiode is about 20kHz and it has a duty cycle of 2%. When the light pulse is on, the capacitor should be fully discharged. After the light pulse is fully turned off, the capacitor has to be charged slowly to prevent exceeding the reference voltage of the A/D converter, V_{ref} . This reference voltage is set at 1.5V. Because the turn-on time of the light pulse is very short (only 1 μ s), discharging the capacitor should be very fast. This means, that the impedance of the turned on MOS transistor should be as low as possible.

MOS transistor is used as the switch. MOS transistor is preferred to bipolar transistor, because ideally no current can flow from the gate to the source terminal of the MOS transistor, which influences the measurement. In the simulation, the ideal switch with a specific resistor is used to characterize the MOS transistor. However, the parameters of the ideal switch can be tweaked to match the MOS transistor that will be used in real life.

The microcontroller is used for controlling the switch. The microcontroller is symbolised as a simple pulse voltage source. The duty cycle and the period are perfectly matched with the photodiode to ensure that the capacitor is charged and discharged correctly.

The last main component is the operational amplifier. Operational amplifier is required to allow the charging and discharging of capacitor. In case of this simulation setup, the integration will work without the presence of the amplifier. In real life, the pulse current source is a photodiode. Without the amplifier, the capacitor will not discharge well, since the built-up voltage across the capacitor will activate the photodiode.

The integration method that has discussed in (4.3) and in (4.4), has been realised by using the integrators that are connected in series. The fluorescence can be modelled as a current source. In able to integrated current, capacitor has been used. The setup of the new approach has been shown in Figure 4.2.1.

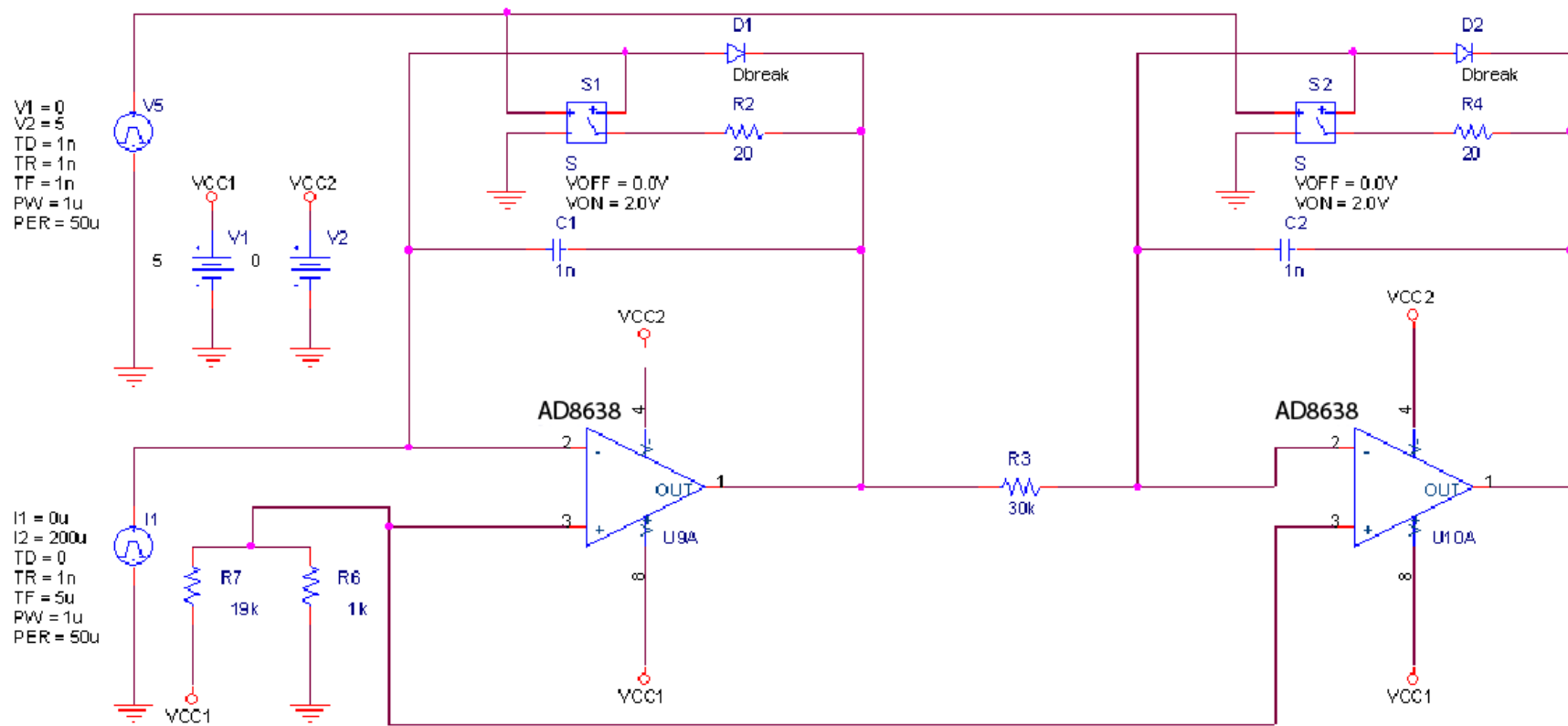


Figure 4.2.1: Measurement setup of the alternative approach

At the inverting input of the Operational Amplifier, the current source has been attached. At the non-inverting input of the OpAmp, a self created offset voltage has been introduced. This offset is introduced because the A/D converter can only accept positive voltage values. The A/D converter is embedded in the microcontroller that will be discussed in chapter 5.

In the negative feedback loop of both amplifiers, a switch and a capacitor in parallel have been added. The switch controls the charge and discharge time of the capacitor. The duration of the charge and discharge time is controlled by the microcontroller.

Both integrators are connected with each other via a resistor. This resistor is used as a voltage-to-current converter which allows the integration in the second integrator (the one that is on the right on Figure 4.2.1).

The output voltage can be calculated as follows:

$$V_1 = \frac{1}{C_1} \int_{t_0}^{t_1} I_{\text{photodiode}} \cdot dt \pm V_{\text{offset}_1} + V_{\text{offset-selfadded}} \approx \frac{1}{C_1} \int_{t_0}^{t_1} I_{\text{photodiode}} \cdot dt + V_{\text{offset-selfadded}} \quad (4.8)$$

$$V_2 = \frac{1}{C_2} \int_{t_0}^{t_1} \frac{V_1}{R_3} \cdot dt \pm V_{\text{offset}_2} + V_{\text{offset-selfadded}} \approx \frac{1}{R_3 C_2} \int_{t_0}^{t_1} V_1 \cdot dt + V_{\text{offset-selfadded}} \quad (4.9)$$

V_1 = output voltage of the first integrator

V_2 = output voltage of the second integrator

V_{offset_1} and V_{offset_2} are the offset values of the OpAmps. If the output voltages are much larger than the offset values, these offset values can be overlooked.

AD8638 have been used to evaluate the performance of the alternative approach. The next section, attention is paid on the simulations of this new approach. All simulations are performed in about room temperature, which is $T = 27^\circ\text{C}$. Two different current pulses are used to test the concept of this new approach, which will be discussed in the next section.

4.3 Simulation results of the alternative read-out electronics

In this section, simulation results are shown for one operational amplifier. This is the AD8638. This operational amplifier will be used for implementing the read-out electronics of the alternative approach. Other operational amplifiers have been considered too. But AD8638 has been selected, because of its availability, low bandwidth compare with the operational amplifier that TNO uses, relative low offset voltage and bias current. Hands-on calculation has been done to verify the results from the simulations. Two types of current sources have used: a linear and a constant one. The focus is on the linear current source, since the actual photodiode shows decay in the fall time which is now very simplified by a linear decreasing amount. The simulation starts with the constant current source which after the linear current source follows.

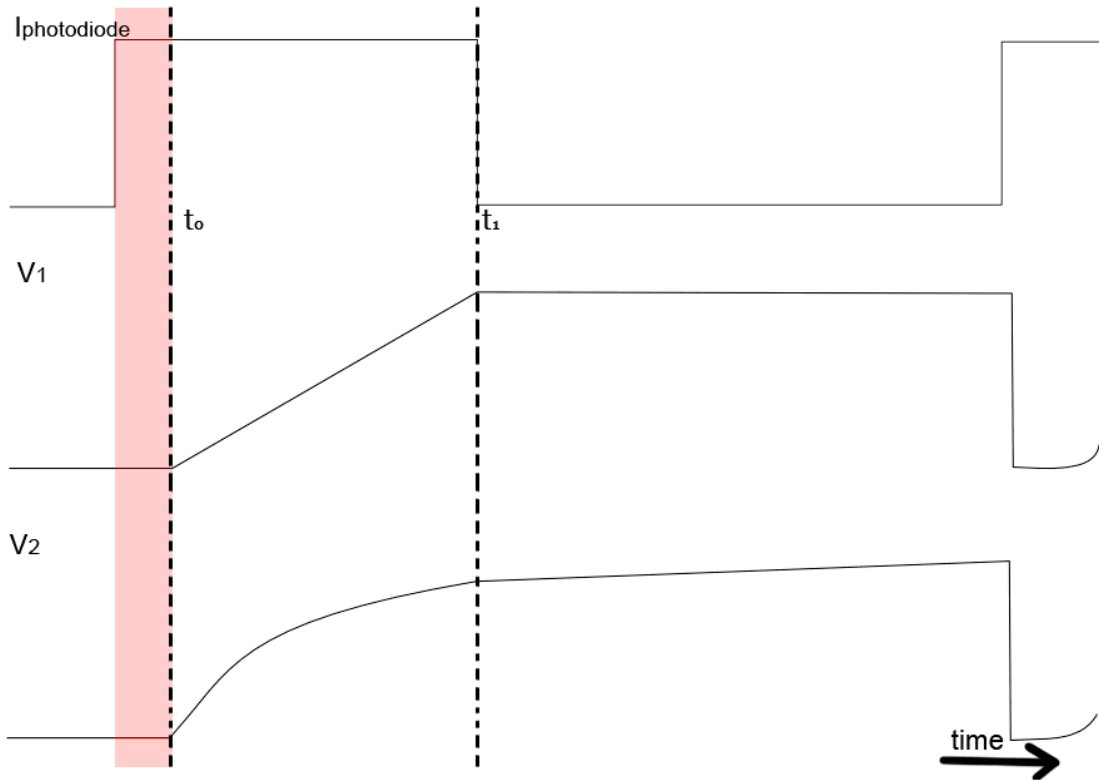


Figure 4.3.1: Constant current source

The constant current means that the pulse width is wider than it supposed to be. Thus, the duty cycle is larger than conventional. Constant current is used to do an easy analysis of this approach. Recall formula (4.8) and assume there is no offset voltage. In case of the constant current source, we have:

$$V_1 = \frac{1}{C_1} \int_{t_0}^{t_1} I_{\text{photodiode}} dt \pm V_{\text{offset}_1} + V_{\text{offset-selfadded}} = \frac{1}{C_1} \int_{t_0}^{t_1} I_{\text{const}} dt + V_{\text{offset-selfadded}} = \frac{1}{C_1} [I_{\text{const}} t]_{t_0}^{t_1} + V_{\text{offset-selfadded}}$$

V_1 is a linear function, since the integration is taken over a constant value.

Now, the output voltage of the second amplifier is:

$$\begin{aligned} V_2 &= -\frac{1}{C_2} \int_{t_0}^{t_1} \frac{V_1}{R_1} dt \pm V_{\text{offset}_2} + V_{\text{offset-selfadded}} \approx -\frac{1}{C_2} \int_{t_0}^{t_1} \frac{V_1}{R_1} dt + V_{\text{offset-selfadded}} = -\frac{1}{C_2} \int_{t_0}^{t_1} \frac{1}{R_1 \cdot C_1} [I_{\text{const}} t]_{t_0}^{t_1} \cdot dt + V_{\text{offset-selfadded}} \\ &= -\frac{1}{R_1} \frac{1}{C_1} \frac{1}{C_2} \int_{t_0}^{t_1} [I_{\text{const}} t]_{t_0}^{t_1} \cdot dt + V_{\text{offset-selfadded}} = -\left[\frac{1}{2} \frac{1}{R_1} \frac{1}{C_1} \frac{1}{C_2} I_{\text{const}} t^2 \right]_{t_0}^{t_1} + V_{\text{offset-selfadded}} \end{aligned}$$

V_2 is a quadratic function. Again, the offset voltage of the operational amplifier is omitted.

There are two very remarkable notes in Figure 4.3.1 and also in Figure 4.3.2. The first one is the pink coloured rectangle window. In this rectangle window, the capacitor has been discharged. Therefore, the two output voltages of both amplifiers are set to $V_{\text{offset-selfadded}}$. Right after the window, the integration starts which is denoted as t_0 in the integrator. t_1 is the time when the integration stops, which is right before the capacitor is being discharged again.

Second, the output voltage of the second amplifier is linear after there is no photocurrent. This is due to the constant voltage of the first amplifier, which produces a linear voltage on the second OpAmp.

Figure 4.2.2 shows the response of the two amplifiers for a linear current source. V_1 is a quadratic function, since the source is a linear function. V_2 is a third order function, since V_1 is a quadratic function.

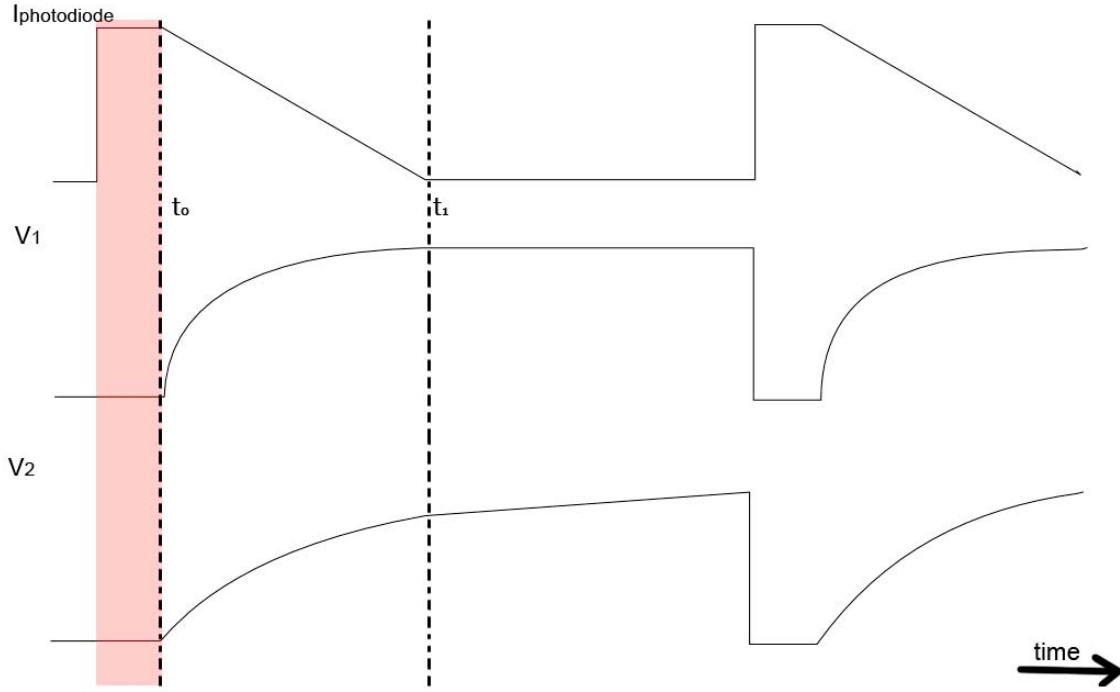


Figure 4.3.2: Linear current source

V_1 and V_2 can be calculated via (4.9):

$$\begin{aligned}
 V_1 &= \frac{1}{C_1} \int_{t_0}^{t_1} I_{\text{photodiode}} \, dt \pm V_{\text{offset}_1} + V_{\text{offset-selffaded}} = \frac{1}{C_1} \int_{t_0}^{t_1} I_{\text{linear}} \, dt + V_{\text{offset-selffaded}} \\
 &= \frac{1}{C_1} \int_{t_0}^{t_1} (200 \cdot 10^{-6} - 40t) \cdot dt + V_{\text{offset-selffaded}} = \frac{1}{C_1} \left[200 \cdot 10^{-6} t - 20t^2 \right]_{t_0}^{t_1} + \text{const} + V_{\text{offset-selffaded}} \\
 &\approx \frac{1}{C_1} \left[200 \cdot 10^{-6} t - 20t^2 \right]_{t_0}^{t_1} + V_{\text{offset-selffaded}} \\
 V_2 &= -\frac{1}{C_2} \int_{t_0}^{t_1} \frac{V_1}{R_1} \, dt \pm V_{\text{offset}_2} + V_{\text{offset-selffaded}} \approx -\frac{1}{C_2} \int_{t_0}^{t_1} \frac{V_1}{R_1} \, dt + V_{\text{offset-selffaded}} = -\frac{1}{C_2} \int_{t_0}^{t_1} \frac{1}{R_1 \cdot C_1} I_{\text{linear}} \cdot dt + V_{\text{offset-selffaded}} \\
 &= -\frac{1}{R_1} \frac{1}{C_1} \frac{1}{C_2} \int_{t_0}^{t_1} (200 \cdot 10^{-6} t - 20t^2 + \text{const}) \cdot dt + V_{\text{offset-selffaded}} = -\frac{1}{R_1} \frac{1}{C_1} \frac{1}{C_2} \left[100 \cdot 10^{-6} t^2 - \frac{20}{3} t^3 \right]_{t_0}^{t_1} + \text{const} + V_{\text{offset-selffaded}} \\
 &\approx -\frac{1}{R_1} \frac{1}{C_1} \frac{1}{C_2} \left[100 \cdot 10^{-6} t^2 - \frac{20}{3} t^3 \right]_{t_0}^{t_1} + V_{\text{offset-selffaded}}
 \end{aligned}$$

The next section shows the simulation results of the setup for both the constant and linear current source with AD8638. The hands-on calculation and the simulation results will be compared.

4.3.1 Simulation results with the constant current source

AD8638 has been used as integrator in the readout electronics of the new approach. The performance of using this operational amplifier has been shown in Figure 4.3.1.1.

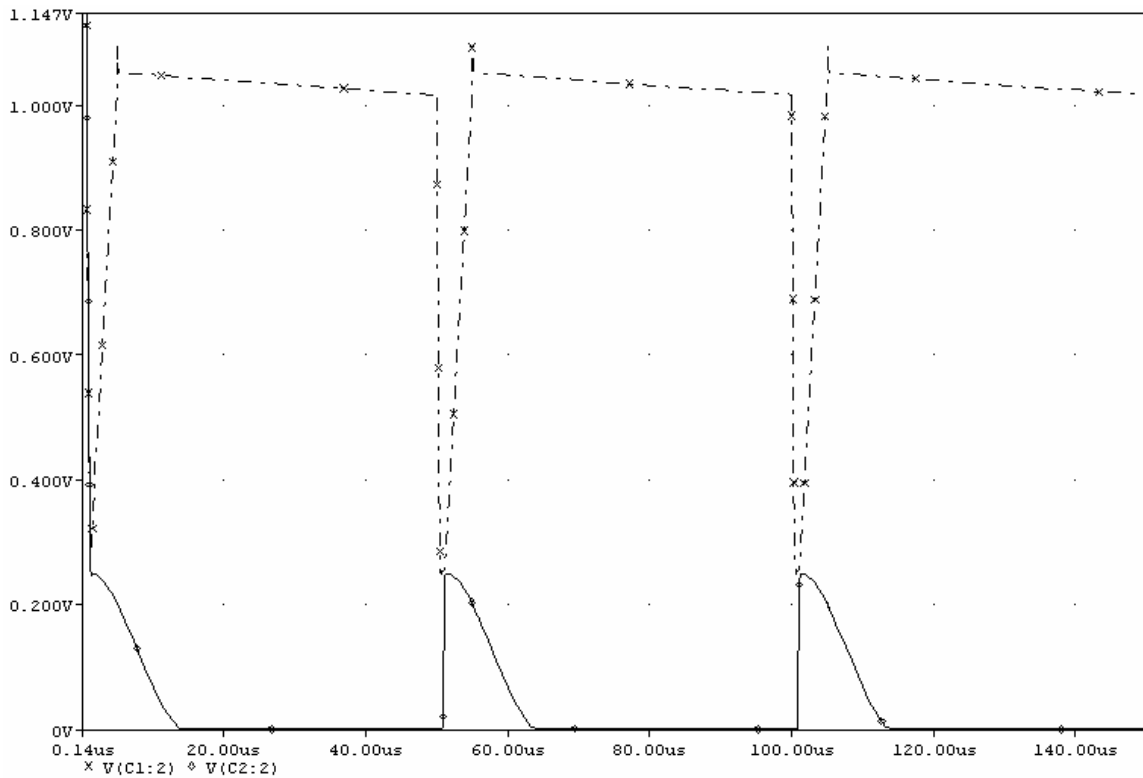


Figure 4.3.1.1: Output voltages of both amplifiers of AD8638 with constant current source

The performance of this operational amplifier looks good. The current can be integrated. The upper (dotted) line is the output voltage of the first integrator, while the lower line is the output voltage of the second integrator.

The output voltage of the first integrator (the dotted line) shows a voltage drop. This is due to capacitor discharge. The voltage difference of the input and output of the amplifier results in this voltage drop.

Figure 4.3.1.2 shows a closer view of the results at t around $54\mu\text{s}$.

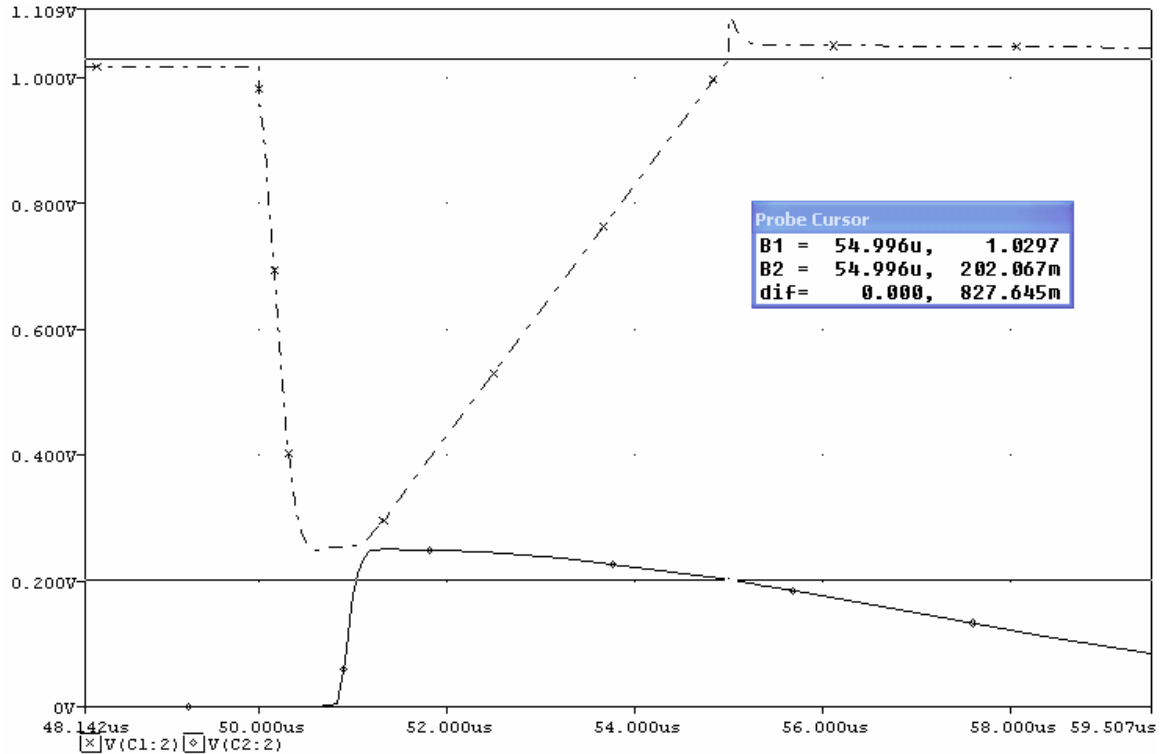


Figure 4.3.1.2: Output voltages of AD8638 with constant current source

Recall the hands-on calculation values of the output voltages.

$$\begin{aligned}
 V_1 &= \frac{1}{C_1} \int_{t_0}^{t_1} I_{\text{photodiode}} dt \pm V_{\text{offset}_1} + V_{\text{offset-self-faded}} = \frac{1}{C_1} \int_{t_0}^{t_1} I_{\text{const}} dt + V_{\text{offset-self-faded}} = \frac{1}{C_1} [I_{\text{const}} t]_{t_0}^{t_1} + V_{\text{offset-self-faded}} \\
 &= \frac{1}{1.0 \cdot 10^{-9}} \left[200 \cdot 10^{-6} t \right]_0^{4 \cdot 10^{-6}} + V_{\text{offset-self-faded}} = 0.8V + 0.25V = 1.05V \\
 V_2 &= -\frac{1}{C_2} \int_{t_0}^{t_1} \frac{V_1}{R_1} dt \pm V_{\text{offset}_2} + V_{\text{offset-self-faded}} \approx -\frac{1}{C_2} \int_{t_0}^{t_1} \frac{V_1}{R_1} dt + V_{\text{offset-self-faded}} = -\frac{1}{C_2} \int_{t_0}^{t_1} \frac{1}{R_1 \cdot C_1} [I_{\text{const}} t]_{t_0}^{t_1} \cdot dt + V_{\text{offset-self-faded}} \\
 &= -\frac{1}{R_1} \frac{1}{C_1} \frac{1}{C_2} \int_{t_0}^{t_1} [I_{\text{const}} t]_{t_0}^{t_1} \cdot dt + V_{\text{offset-self-faded}} = -\left[\frac{1}{2} \frac{1}{R_1} \frac{1}{C_1} \frac{1}{C_2} I_{\text{const}} t^2 \right]_{t_0}^{t_1} + V_{\text{offset-self-faded}} \\
 &= -\left[\frac{1}{2} \frac{1}{30 \cdot 10^3} \frac{1}{1 \cdot 10^{-9}} \frac{1}{1 \cdot 10^{-9}} 200 \cdot 10^{-6} t^2 \right]_0^{4 \cdot 10^{-6}} + 0.25 = -0.053 + 0.25 = 0.197V
 \end{aligned}$$

According to the simulation, the output voltage of the first integrator (B1) is 1.0297V. Compare to the hand calculation, the mismatch is 20.3mV. This mismatch is relative large compare with the signal. If the mismatch is a few mV, then it is acceptable, since the A/D converter has that amount of variation. Therefore, this amount of mismatch also can not be disregarded.

Figure 4.3.1.2 shows the output voltage of the second integrator at $t \approx 55\mu\text{s}$ of 202.067mV. The mismatch is 5.067mV. This error is less than the first integrator. Compare this mismatch value with the previous one, this amount is smaller. To able to get a non-error measurement from the read-out, compensation should be applied.

4.3.2 Simulation results with the linear current source

Simulations of the linear current source have now performed. In the previous section, the simulation results of the constant current source have been presented. The simulation shows that the mismatch with the hands-on calculation is relative large. Therefore, error compensation has to be applied to get an accurate system. In this subsection, the performance of the linear current source has been evaluated. Figure 4.3.2.1 shows the performance of this amplifier for the linear current source.

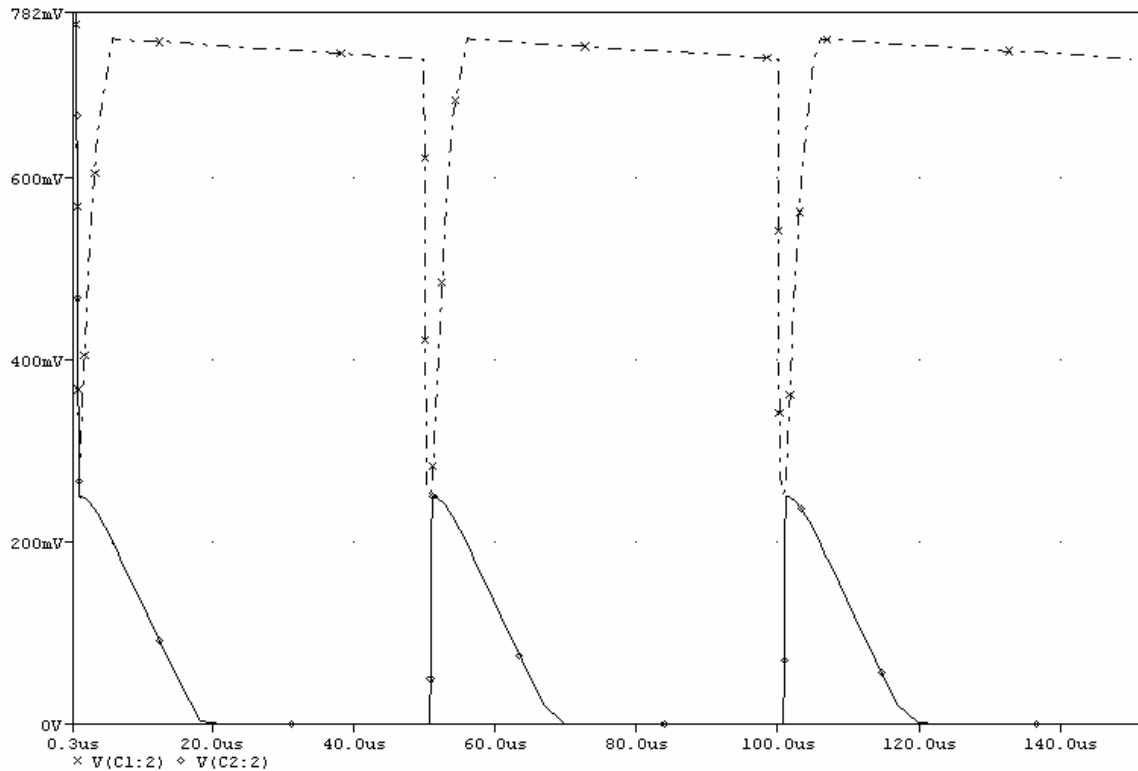


Figure 4.3.2.1: Output voltages of both amplifiers of AD8638 with linear current source

The dotted line that is on top is the output voltage of the first integrator. The straight line that lies on the bottom is the output voltage of the second amplifier. Figure 4.3.2.2 shows a zoomed-in area of the plot.

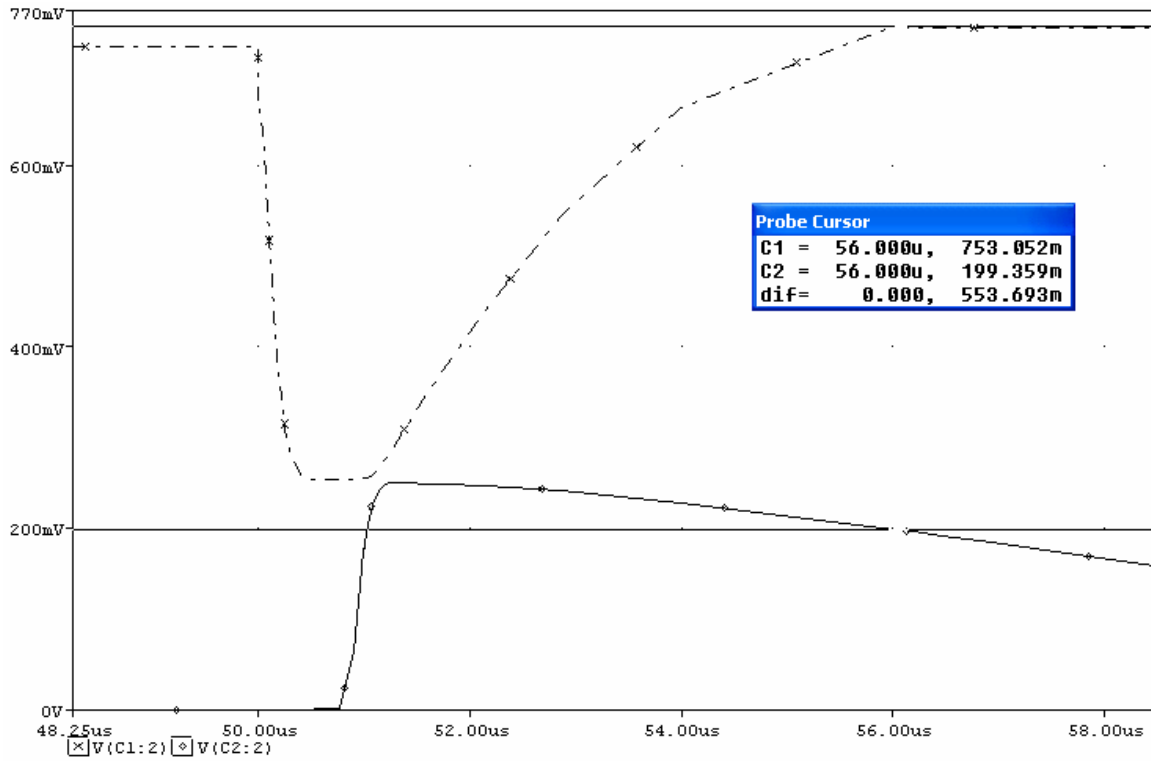


Figure 4.3.2.2: Output voltages of both amplifiers of AD8638 with linear current source zoomed in at t around $54\mu\text{s}$

C1 shows the output voltage of the first integrator, while C2 shows the output voltage of the second integrator. The mismatch values for the first and the second integrator are 3.052mV and 5.359mV , respectively. Both mismatches can not be disregarded, since the mismatches exceed slightly over the error of the A/D converter. Both curves prove that the integrators are able to integrate the linear decay of the current source. The first integrator shows a second order function, while the third integrator shows a third order increment. The evaluation of both current sources is presented in the next section.

4.4 Evaluation of the performance for both current sources

In this section, evaluation of both current sources has been deeply discussed. Table 4.1 summarizes the simulation results.

Table 4.1: Evaluations of the obtained results for both current sources using AD8638

	Constant current source		Linear current source	
	V ₁ [mV]	V ₂ [mV]	V ₁ [mV]	V ₂ [mV]
Hands-on calculation	1.05V	197	750	194
Simulation results	1.029V	202.067	753.052	199.359
Mismatch [mV]	21	5.067	3.052	5.359
Error [%]	2	2.5	0.407	2.76

The error amount using this operational amplifier is less than 3%. The error is defined as:

$$\text{error} = \frac{|(\text{hands-on calculation}) - (\text{simulation result})|}{\text{simulation result}} \times 100\%$$

The relative error is the smallest for the output voltage of the first integrator in case of the linear current source, while the relative error is the largest of the second integrator in case of the linear current source. This might be due to the relative small output voltage compared to the case when constant has been used: the output voltage of the first integrator in case of a constant current source is 40% larger than in case of the linear current source.

Using linear constant current source, the error is generally less, since the output voltage is relative smaller. However, the error of the hands-on calculation with the simulation result does not have a direct relationship with the accuracy of the read-out electronics. Considering the mismatch, the accuracy of the system can be better evaluated.

The mismatch is defined as the absolute difference of the hands-on calculation and the simulation result. Ideally, this mismatch should be zero. However, if the mismatch is within the error range of the A/D converter, then the mismatch can be considered as ideal. The determination of the error range of the A/D converter can be retrieved in its datasheet. According to the datasheet, the A/D converter has an error margin of two bits. Since the reference voltage of the A/D converter is set at $V_{\text{ref}} = 1.5\text{V}$ and 10bit analogue-to-digital conversion has been used, one bit will give a voltage of $\approx 1.5\text{mV}$. Since two bits can be ignored, thus the error of the A/D converter is 2.9mV. This means that all mismatch of the hands-on calculation and the simulation less than 2.9mV is acceptable and can be considered as an ideally non-error system.

Looking at table 4.1, it is clear that none of the mismatch for both kinds of current sources is less than 2.9mV. Therefore, the mismatch should be compensated afterwards. This can be dealt in the data processing part, e.g. cancellation in the software.

The mismatch is relatively smaller in case of a linear current source compared to the constant current source. This might be due to the relative large output voltage. To prove this statement, another simulation has been performed. In this new simulation, the linear decay is reduced to 4 μs .

Recall formula (4.8):

$$\begin{aligned}
V_1 &= \frac{1}{C_1} \int_{t_0}^{t_1} I_{\text{photodiode}} \cdot dt \pm V_{\text{offset}_1} + V_{\text{offset-selfadded}} = \frac{1}{C_1} \int_{t_0}^{t_1} I_{\text{linear}} \cdot dt + V_{\text{offset-selfadded}} \\
&= \frac{1}{C_1} \int_{t_0}^{t_1} (200 \cdot 10^{-6} - 50t) \cdot dt + V_{\text{offset-selfadded}} = \frac{1}{C_1} \left[200 \cdot 10^{-6} t - 25t^2 \right]_{t_0}^{t_1} + \text{const} + V_{\text{offset-selfadded}} \\
&\approx \frac{1}{C_1} \left[200 \cdot 10^{-6} t - 25t^2 \right]_{t_0}^{t_1} + V_{\text{offset-selfadded}} = \frac{1}{1 \cdot 10^{-9}} \left[200 \cdot 10^{-6} t - 25t^2 \right]_0^{4 \cdot 10^{-6}} + 0.25 \\
&= 0.4 + 0.25 = 0.65V
\end{aligned}$$

$$\begin{aligned}
V_2 &= -\frac{1}{C_2} \int_{t_0}^{t_1} \frac{V_1}{R_3} \cdot dt \pm V_{\text{offset}_2} + V_{\text{offset-selfadded}} \approx -\frac{1}{C_2} \int_{t_0}^{t_1} \frac{V_1}{R_3} \cdot dt + V_{\text{offset-selfadded}} = -\frac{1}{C_2} \int_{t_0}^{t_1} \frac{1}{R_3 \cdot C_1} I_{\text{linear}} \cdot dt + V_{\text{offset-selfadded}} \\
&= -\frac{1}{R_3} \frac{1}{C_1} \frac{1}{C_2} \int_{t_0}^{t_1} (200 \cdot 10^{-6} t - 25t^2 + \text{const}) \cdot dt + V_{\text{offset-selfadded}} = -\frac{1}{R_3} \frac{1}{C_1} \frac{1}{C_2} \left[100 \cdot 10^{-6} t^2 - \frac{25}{3} t^3 \right]_{t_0}^{t_1} + \text{const} + V_{\text{offset-selfadded}} \\
&\approx -\frac{1}{R_3} \frac{1}{C_1} \frac{1}{C_2} \left[100 \cdot 10^{-6} t^2 - \frac{25}{3} t^3 \right]_{t_0}^{t_1} + V_{\text{offset-selfadded}} = -\frac{1}{30 \cdot 10^3} \frac{1}{1 \cdot 10^{-9}} \frac{1}{1 \cdot 10^{-9}} \left[100 \cdot 10^{-6} t^2 - \frac{25}{3} t^3 \right]_0^{4 \cdot 10^{-6}} + 0.25 \\
&= -0.0356 + 0.25 = 214.4mV
\end{aligned}$$

The results of the simulations are shown in Figure 4.4.1. A1 is the output voltage of the first integrator (the line on the top) and A2 is the output voltage of the second amplifier (the line on the bottom). The mismatches of the first and the second integrator are 3.831mV and 3.551mV, respectively.

The mismatch at the output voltage of the second integrator is significantly lower ($\approx 1.8mV$ improvement) than in case of a longer integration time while the mismatch of the output voltage of the first amplifier is slightly ($\approx 0.8mV$) larger. This phenomenon cannot be fully understood. It is expected that the mismatch with this linear current source is less. However, with this simulation result, it can be concluded that the duration of the integration time has influence on the accuracy of the system.

AD8638 was chosen from using as integrators, since it has the lowest offset voltage and low bias current. Its bandwidth is much less than OPA-356 that TNO has used for their circuit. The idea of introducing the alternative read-out system is to prove it well functioning of the complete sensor system using a simple circuit with fewer number of components and less high-end performance components.

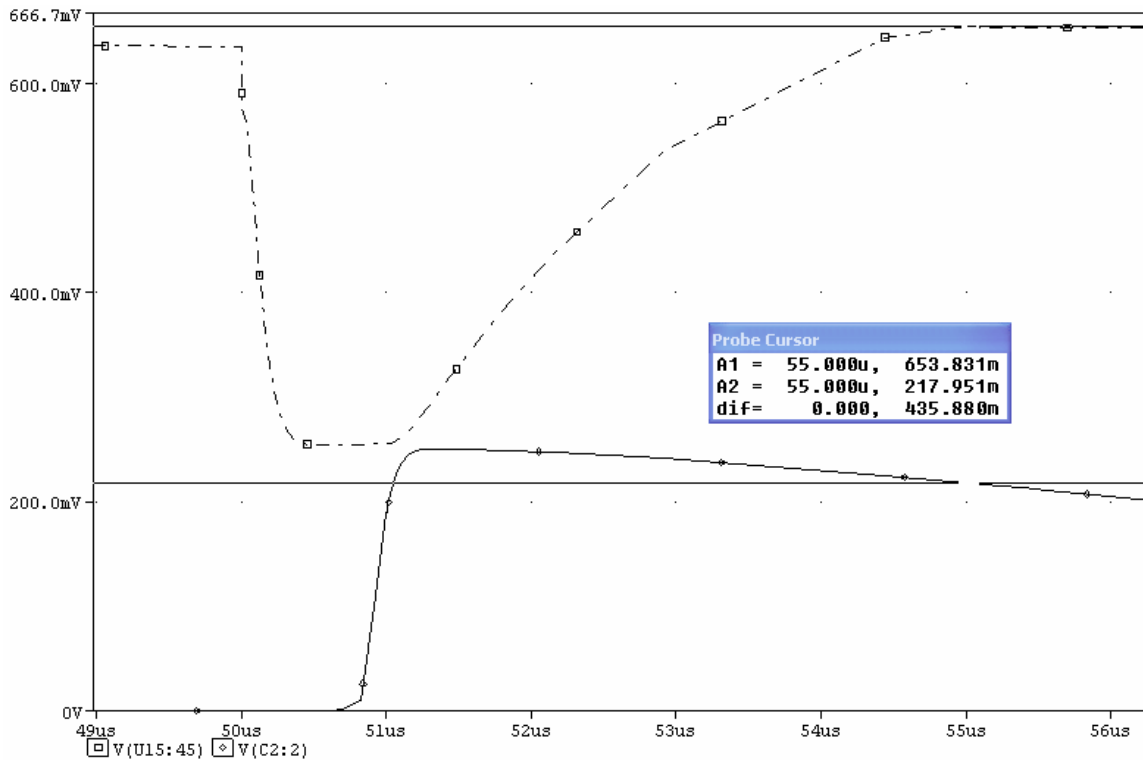


Figure 4.4.1: Simulation results of AD8638 with integration of 4µs with a linear current source

4.5 Conclusions

Two kinds of current source have been used for testing the performances of the operational amplifiers: AD8638. The output voltages of both integrators from the simulations in PSpice have been compared with the output voltages that have been calculated by hand. The results show that there is always a mismatch for both kinds of current sources.

The mismatch should be considered in determining the O_2 level to get an accurate measurement, since the mismatch is larger than the error of the A/D converter. The mismatch is a better determination of the accuracy of the system than the error of the simulation result and the hands-on calculation. Therefore, considering the absolute difference of the simulation result and the hands-on calculation is sufficient. The relative changes for both sources are all less than 3%.

The mismatch depends on the quantity of the output signal. In case of a large output signal, the mismatch is generally larger than for a relative small signal. Compare the output voltage of the first integrator of the linear and constant source, their mismatch difference is very significant.

Overall, this alternative approach can be used for determining the oxygen level. Due to relatively high mismatch that AD8638 produces, one should do compensation during calculation of the oxygen level. This new system proves that it integrates the signal over it's a short period of time (5µs). Thus with a lower and simpler OpAmp, it is able to subtract the lifetime. The number of components can be reduced, which saves the area of the complete system. The cost will also be reduced, since fewer components are required.

During the simulation, temperature variations on the performance of the read-out electronics have not been thoroughly tested. Some simple temperature sweeps have been performed to check the response of the AD8638. The output voltage can be considered as the same. Besides, the temperature variation in human's body is more and less constant. Therefore, there is no much attention paid to test the temperature variations on this new read-out electronics.

Chapter 5 – Realisation of the wireless communication

5.1 Introduction

In this chapter, the realisation of the wireless platform will be discussed in details. This wireless platform has been realised by using two eZ430-RF2500 Target Boards of Texas Instruments. These two boards are the so-called ACCESS POINT and END DEVICE. The ACCESS POINT is directly connected to the personal computer (PC), while the END DEVICE is a unit that can be placed anywhere in the environment. The difference of these devices is their operation. The O₂ sensor includes the read-out electronics are embedded in the END DEVICE, while the ACCESS POINT is a unit that only receives the digital data that come from the END DEVICE and transfer the data to the computer for further processing.

To be able to do constant monitoring the O₂ and temperature, wireless platform is required. The platform should be able to do recording the data during and after the surgical operation. The advantage of using the eZ430-RF2500 is that it is designed for very low-power wireless applications, such as what it is desired. Moreover, using the included source code of this device for temperature measurement has a big benefit because the wireless communication has been proved that it works perfectly. There is no need to find out how this wireless platform is set up and how the initialisation of the wireless protocol has been done in details.

This chapter starts with a very simplified draw of how the two units of eZ430-RF2500 operate. Afterwards each unit are being analysed in details. First, the ACCESS POINT will be discussed, since the modification on this unit is less complicated than the medication for the END DEVICE. Once the functionalities of the ACCESS POINT are clarified, the understanding for how the END DEVICE works is much easier. At the end of this chapter, some simple test results are performed to verify the working of the wireless communication.

5.2 The working principle and the units of the eZ430-RF2500

A microcontroller (MSP430F2274) and a transceiver (CC2500) have been used to form the eZ430-RF2500. To realise the wireless platform, two units of eZ430-RF2500s are required. The one that is directly connected to the computer is named as the ACCESS POINT. This device tries to make a wireless connection with the so-called the END DEVICE. Once the communication is established, the measured digital data of the END DEVICE is transferred to the ACCESS POINT. Before data is transmitted to the computer, some reconstruction of the data has been applied at the side of the END DEVICE. This will be fully discussed in the next section.

The wireless transform of the data has been achieved by using an antenna that has been attached to the transceiver that is placed on the same chip. The circuit is proposed fro the 2400 – 2483.5MHz ISM and SRD frequency band. The ISM stands for Industrial, Scientific and Medical and the SRD stands for Short Range Device. This is a low-cost and low-power RF transceiver which is desired in applications in biomedical areas.

Figure 5.2.1 shows the unit of the eZ430-RF2500. The eZ430-RF2500 can be spilt up into two units. The unit that is displayed on the left-hand side in Figure 5.2.1 is an interface that makes the communication with the personal computer possible via the USB port. With this communication unit, the microcontroller can be programmed and tests can be performed.

The unit on the right-hand side is the heart of the eZ430-RF2500. This heart holds the microcontroller (MSP430F2274), two LEDs, the transceiver unit which is CC2500 and a chip antenna.

However, there is a push button on the eZ430-RF2500 as well. For this project, this button is omitted. Therefore, nothing will happen when the button is being pressed.

An internal diode is embedded in the eZ430-RF2500, which is not clearly visible in Figure 5.2.1. This diode is used for the temperature measurements. There is a demo included of how the temperature measurement is performed. This demo includes the source code (as well in C as in

assembly language) with many predefined initialisation that will be used for realising the wireless communication of O₂ sensor.

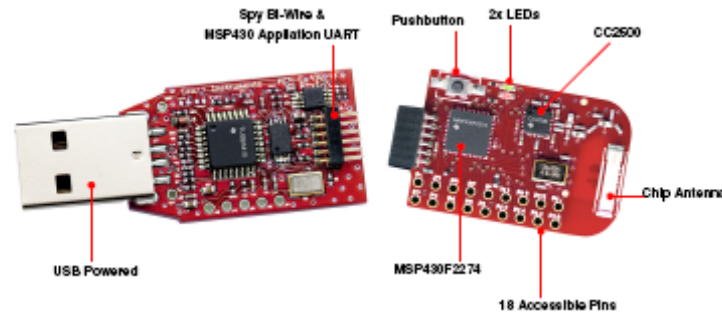


Figure 5.2.1: The two units of the eZ430-RF2500, based on: <http://focus.ti.com/docs/toolsw/folders/print/ez430-rf2500.html>

5.3 The function of the ACCESS POINT

The ACCESS POINT is a name for the eZ430-RF2500 that is directly connected to the computer. Its task is to receive data that have been sent by the END DEVICE. Before the wireless transmission is performed, the ACCESS POINT is looking for an END DEVICE within its detectable range.

In C, there is a predefined method is supplied by Texas Instruments, which is *SMPL_ioctl(IOCTL_OBJ_ADR, IOCTL_ACT_SET, &IAddr)*. The *ioctl* function has been used first before any other initialisations of the ACCESS POINT. This function permits different transceivers settings, e.g. frequency hopping or receiver sensitivity to be configured.

Afterwards, another function is used which called *SMPL_Init(sCB)*. This function allows the transceiver for preparation for sending and receiving messages by configuring the relevant registers and settings in the transceiver.

The wireless communication of ACCESS POINT and END DEVICE is a bi-directional linking. That means that there are two ways of communication. To setup the bi-directional link, a predefined method *SMPL_LinkListen(&sLID[sNumCurrentPeers])* is used. This *LinkListen* function caused the transceiver to listen to a nearby request to connect its network.

Texas Instruments has a predefined method for receiving data that originates from an END DEVICE. This method is the *SMPL_Receive(sLID[i], msg, &len)*. Another predefined method, *SMPL_SUCCESS* has been used to check whether the receiving message is successfully received.

The *sLID[i]* in the *SMPL_Receive()* method is used to identify the END DEVICE. The eZ430-RF2500 allows multiple END DEVICES to connect to the ACCESS POINT. With the help of *sLID[i]*, the sending data of each END DEVICE can be distinguished.

The message contains the digital results of the measurements. To able to use the predefined methods for sending, the sending data should be an 8-bit unsigned integer that all have to be stored in the *msg*. However, the A/D converter is a 10-bit converter. The digital result is stored in a 16-bit register. Therefore, to allow sending the data to the ACCESS POINT, the digital result is cut into 2 pieces of 8-bit unsigned integer by the END DEVICE. The most significant two bits are stored in *msg[0]*, while the other eight bits are stored in *msg[1]*. For each measurement, *msg[2]* is added to distinguish the data to which it belongs to in the ACCESS POINT.

Figure 5.3.1 shows the flowchart of the ACCESS POINT. This flowchart clarifies shortly of how the ACCESS POINT works.

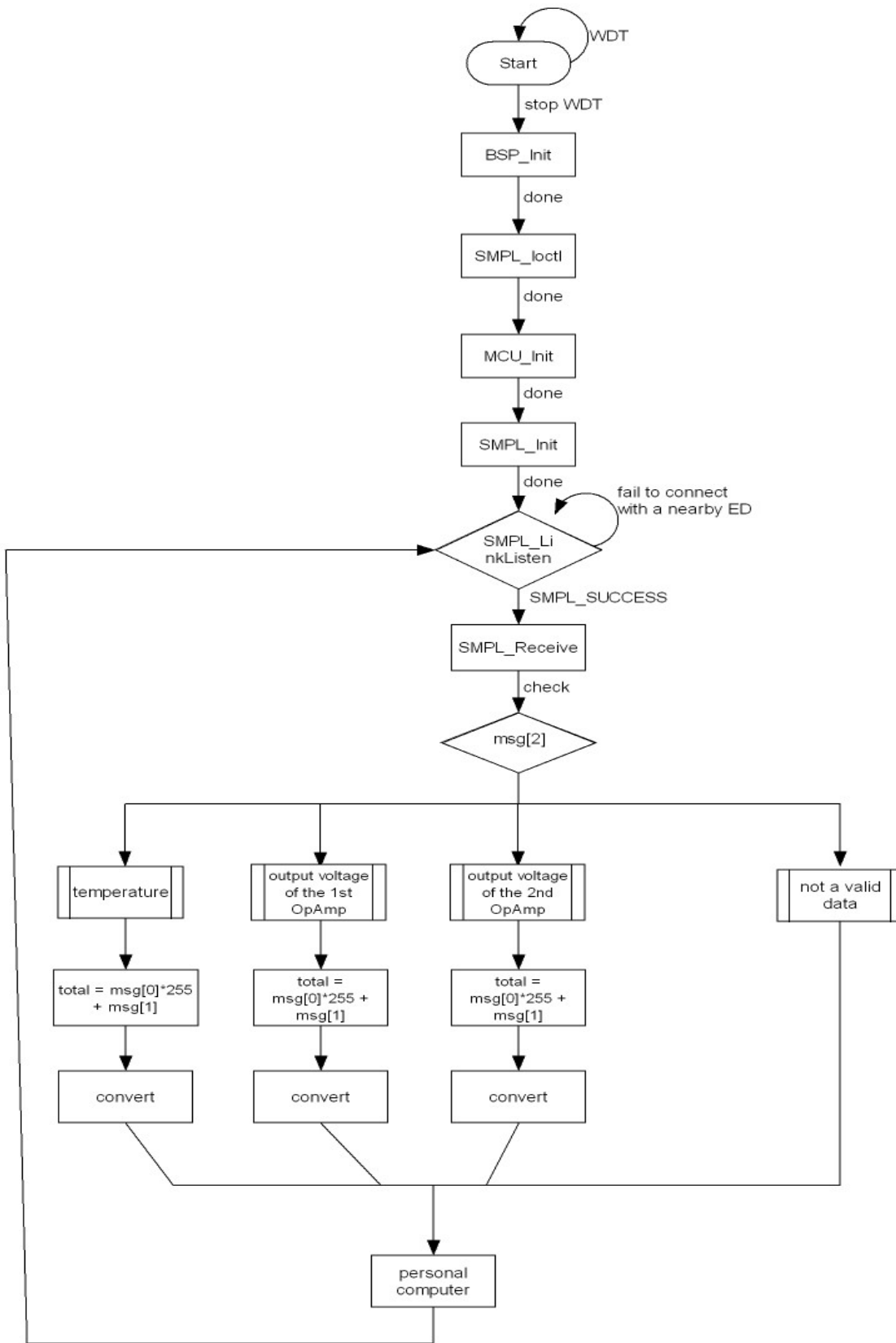


Figure 5.3.1: Simplified flowchart of the ACCESS POINT

When a data is received, the ACCESS POINT identifies from which measurement the data belongs to by checking the value of msg[2]. This message (mg[2]) is assigned to each measured data which gives its identity.

After the sending data is received successfully and checked to which measurement it belongs to, the two messages, msg[0] and msg[1], are combined together to reconstruct the obtained measurement result. The reconstruction is as follows:

msg[0] holds the data of the most significant bits. The value of the msg[0] is multiplication factor that needs to be multiplied by 255, since the sending package is 8-bit ($2^8 - 1$). msg[1] encloses the least significant bits data. To reconstruct the data back from the splitting, the following formula is applied: measured data = msg[0]*255 + msg[1]. The measured data is the same as it is denoted as the total in Figure 5.3.1.

After the measured data has been reconstructed, an integer to a String conversion has to be applied to the data. This is required because the predefined method that prints texts on the computer via HyperTerminal only accepts String. To allow to use this method, the measured data is converted into String. The conversion happens in the so called convert() method. In the section 5.5, more details will be explained about this conversion.

Notice that BSP_Init() and MCU_Init() are not discussed earlier. BSP_Init() is a predefined method that simply initialise the eZ430-RF2500 board and its drivers. This method is supplied by Texas Instruments. Another predefined method is the MCU_Init(). This method simply does the initialisations of the embedded microcontroller (MSP430F2274).

5.4 The function of the END DEVICE

The task of the END DEVICE is performing the O₂ measurements, which after the results are sent to the ACCESS POINT for further processing. The O₂ sensor is attached on the END DEVICE since this unit is supposed to do the O₂ measurements on living tissues. The output of this sensor is fed into the input of the 10-bit A/D converter that is embedded in the microcontroller of the END DEVICE.

The data of the measurements have been written to the ADC10MEM register. This register is 16-bit. A 16-bit temporary register has been used to store the value of ADC10MEM to ensure that the data is not lost due to modification such as a second store operation. The most 4 significant bits in the ADC10MEM as well as in the temporary register are not used and they are both set to 0 by default.

Once the data in ADC10MEM is stored in the temporary register, the data needs to be split up in two 8-bits temporary registers. The splitting is as follow: The value is divided by 255, since the maximum value which a 10-bit A/D can have is 1023 ($2^{10} - 1$). The division factor is stored in the first element of an array of 8-bit register, msg[0]. Afterwards, the rest term is stored in the second element of the array, msg[1].

Assume that the digital value of the O₂ measurement is 788. After the first division factor, the first element of the array is a 3, since $788/255 = 3$. The second element is 13. Both elements are used for sending to the ACCESS POINT.

Before sending the data to the ACCESS POINT, a third element is added, msg[3]. This third element is required to identify which measurement it belongs to. Figure 5.4.1 shows the header format of the sending data.

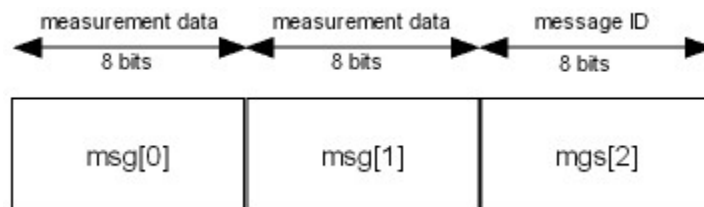


Figure 5.4.1: Header of the sending message

The ACCESS POINT will analyse the third message first, which is msg[2]. This is the identity of which measurements it belongs to. Each msg is sent to the ACCESS POINT one after another.

Apart from the A/D conversion, the port setting needs to be configured first. Four analogue inputs pins are used for performing the measurements. The data for each input is read according to a fixed sequence. After the input data is being read, A/D conversion has been performed. Afterwards, the A/D converter is turned off to save the power consumption, followed by the digital data is sent to the ACCESS POINT. Then, the A/D converter is turned on again. Another port is selected for doing other measurement and this process keeps running.

Figure 5.4.2 shows the flowchart of the END DEVICE. Before the initialisation, the port will be set first. The port setting can be changed anytime. After the port setting is done, other initialisation processes follows. Those initialisation processes are already described in the previous section and thus will not be discussed here again.

There are some new methods in the END DEVICE. The LinkTo is a method that tries to link to the ACCESS POINT. This is an unconditional link to the ACCESS POINT which is listening due to successful join. SMPL_Link is quite similar to the SMPL_LinkListen that is already mentioned in the previous section. Their difference is that that SMPL_Link causes the transceiver to attempt to join the network of a nearby transceiver, while SMPL_LinkListen will cause the transceiver listen to a nearby request to join its network.

A very remarkable thing in the flowchart is about using the two SMPL_Ioctl methods right after each other. The included source code already contains these two methods that are used at this way. Their purpose is to reduce power consumption. Since this method does not affect the O₂ measurements, they are not taken out.

One note should be marked. There is only one 10-bit A/D converter available in eZ430-RF2500. Therefore, A/D conversions cannot be executed simultaneously. They should be performed one by one. The user defines the sequence of which measurement the A/D conversion should apply. The definition is done in C or in Assembly, depends on which programme environment the user prefers and uses.

After each A/D conversion, the digital data is split into two 8-bits as mention earlier in this subsection. The splitter method in the flowchart is the splitting. Afterwards, the data is sent to the ACCESS POINT.

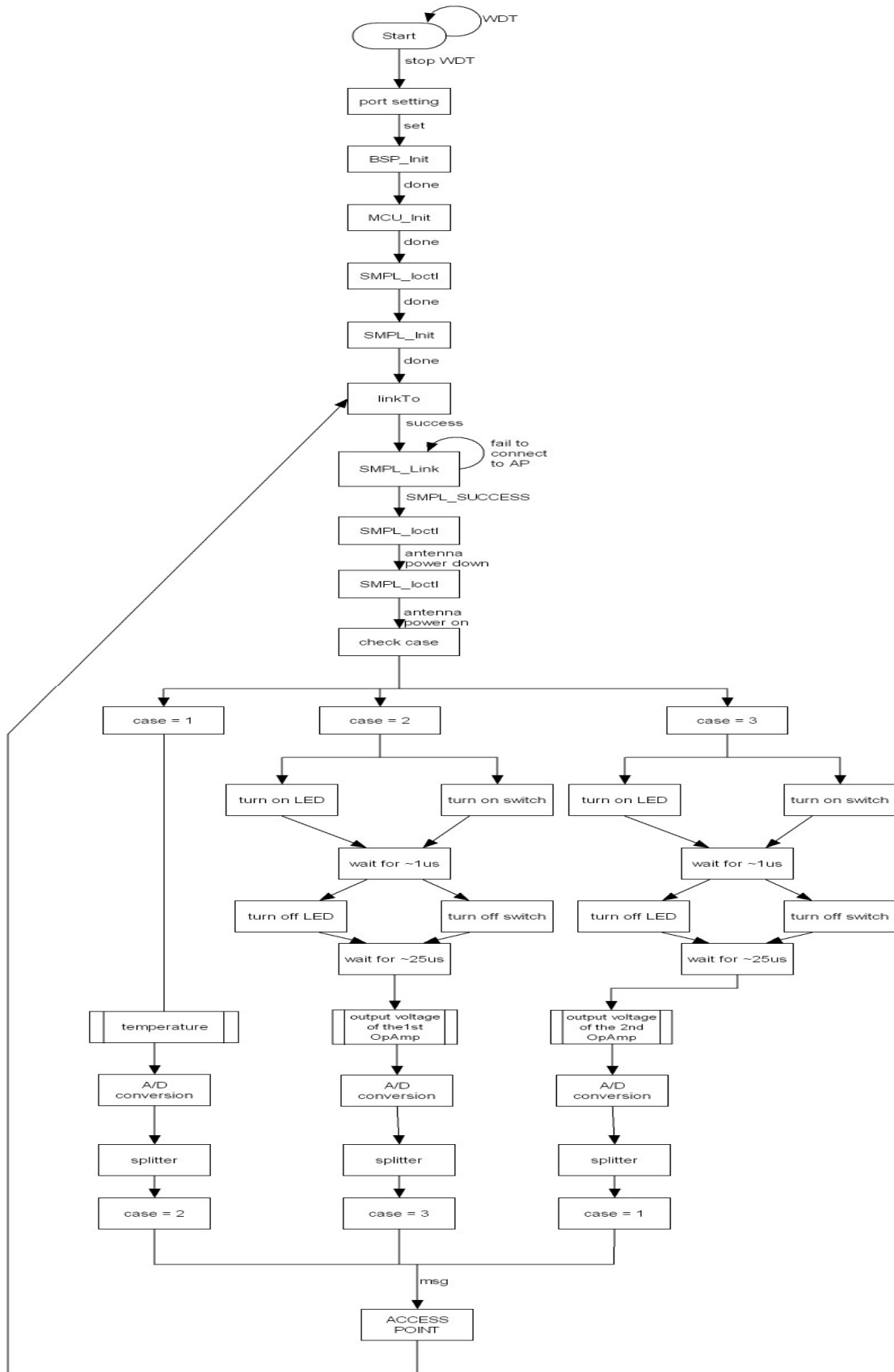


Figure 5.4.2: Simplified flowchart of the END DEVICE

5.5 Test results of the wireless communication

In this section, the test results on the wireless communication are discussed. This section is divided into subsections to distinguish the different measurement setups and their results. First, the setup of the END DEVICE is examined which after the results of the measurements are analysed. In addition, the results are mainly based on the responses of the 10-bit A/D converter at different voltages. The internal reference voltage for the A/D converter is used, which is 1.5V. Thus, the digital representation of the measurement, $output_{digital}$, is:

$$output_{digital} = \frac{V_{measurement}}{2^{10} - 1} \cdot 1.5 \quad (5.1)$$

with

$2^{10} - 1$ = the number of bits of the A/D minus 1
 1.5 = the reference voltage [V]
 $V_{measurement}$ = the voltage at the input of the A/D converter [V]

5.5.1 Measurement setup of the END DEVICE

Figure 5.5.1 shows the schematic drawing of the measurement setup for the END DEVICE.

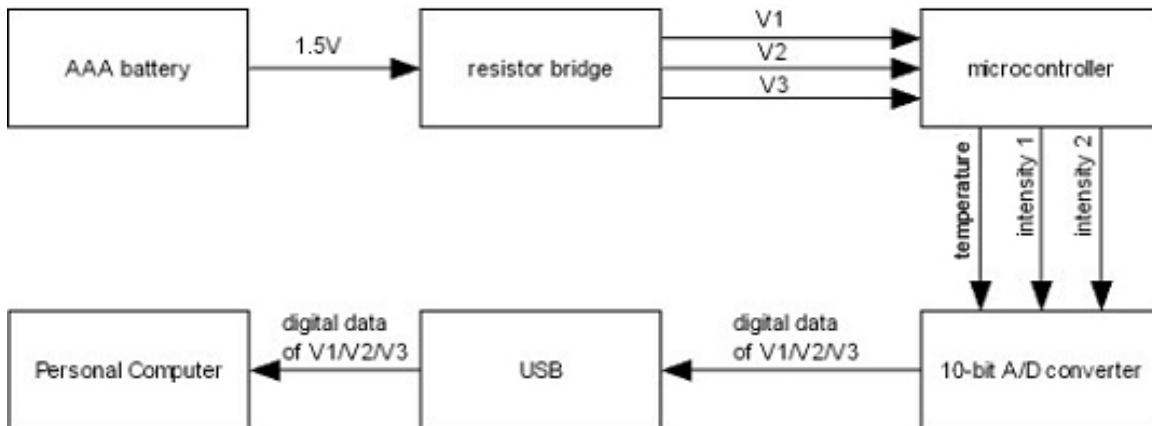
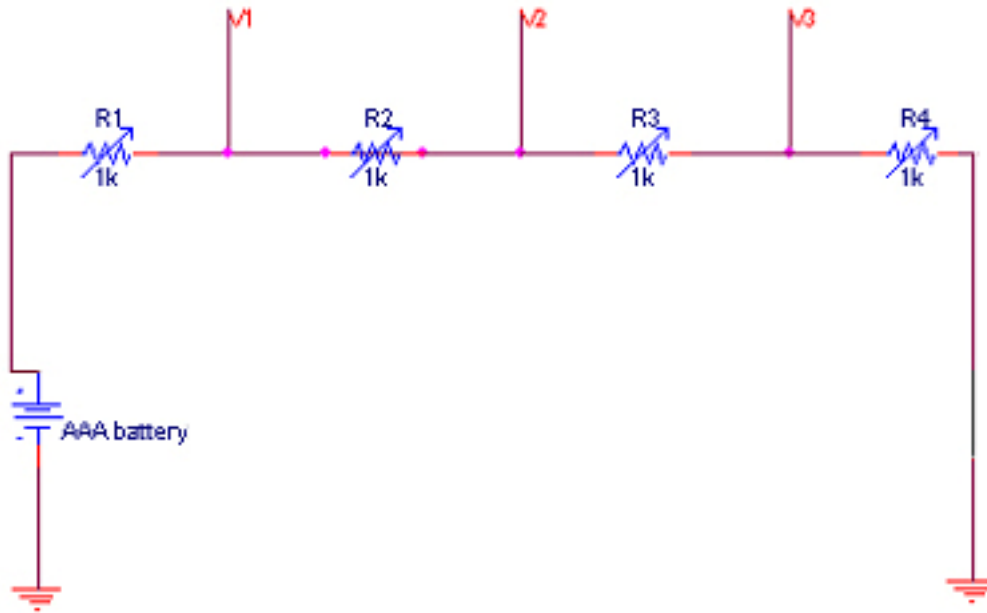


Figure 5.5.1: Schematic drawing of the measurement setup for the END DEVICE

The END DEVICE has been represented by the microcontroller, the 10-bit A/D converter and the USB interface. The O_2 sensor is missing in the setup, since the read-out electronics is not being built for testing yet. Therefore, this unit is substituted by a very simple and common AAA battery. Battery is preferred because of its very steady voltage: its variations are far less compared to the power supply or a function generator. The exact voltage should be measured before using the AAA battery, since that will be not equal to 1.5V.

AAA battery can only produces one fixed voltage. To able to manipulate different voltage, a simple resistor bridge is being built. This simple bridge has four resistors in serial. Three terminals, indicated with V_1 , V_2 and V_3 in Figure 5.5.2, are added to the bridge to acquire the different voltages.



simple resistors bridge

figure 5.5.2: A

The voltage difference has been realised by:

1. the voltage division
2. replacing the resistors manually by different values

The voltages [V] at the terminals are given by the following formulas:

$$V_1 = \frac{R_2 + R_3 + R_4}{R_1 + R_2 + R_3 + R_4} \cdot V_{AAA_batt} \quad (5.2)$$

$$V_2 = \frac{R_3 + R_4}{R_1 + R_2 + R_3 + R_4} \cdot V_{AAA_batt} \quad (5.3)$$

$$V_3 = \frac{R_4}{R_1 + R_2 + R_3 + R_4} \cdot V_{AAA_batt} \quad (5.4)$$

The three terminals are directly connected to the microcontroller. V_1 is used for background measurement, while V_2 is used for the first intensity measurement and V_3 is used for the second intensity measurement. These three voltages are not only calculated by hand, but they are also been measured in real life.

Before this measurement has been tested, a simple test script is written to do a check if the communication performs well. In this simple script test, a self defined value is assigned to msg. For instance, msg[0] = 18, msg[1] = 1 and msg[2] = 0. To check if these self defined values are truly passed to the SMPL_Send(linkID1, msg, sizeof(msg)), these msg has been printed on the computer screen first. HyperTerminal is used to display the print screen results. To allow sending message to the computer screen, those self defined values need to be converted into String first, because the predefined TXString() method requires a String as its input. A very typical integer to a String conversion is the itao() in C. This typical method cannot be used, because of the license of the IAR Assembler for MSP430. Therefore, the integer-to-String conversion has to be realised by yourself. The self-made integer to a String method is called convert(). This method assumes that there are maximal of two bytes. If integer is larger than two bytes, the conversion lost data.

The maximum value that two bytes can have is 65535. Suppose that the value is 65535. The conversion is as follows: the value is divided by 10000. The division factor is stored in a

temporary register, while the rest term is used for further division. The second division is on the rest term. The rest term is divided by 1000. Again, the division factor is stored, but in other temporary register. The rest term is used for third division. This whole process continues till the division factor is 10. Numbers below 10 cannot be divided by 10. These numbers are stored in a temporary register. So, in each temporary register, there the division factor is stored. Before the real job of integer-to-String conversion, all values in msg need to be added with 48 according to the ASCII table⁶. The summing results are stored back in their own temporary register. The last temporary register is used to realise the real conversion. In this last register, '0' value is added and the conversion is done.

After the simple test to confirm that the wired communication works via the USB interface with the personal computer, the A/D conversion has been fully tested. The next subsection shows the results.

5.5.2 Measurement results of the END DEVICE

In the previous subsection, the measurement setup is discussed in details. This subsection describes the results of the setup. The focus is only on the obtained results of the A/D conversion, which the results are directly sent to the personal computer for plotting the results. The results which values are self assigned are not discussed here, since the results of the A/D conversion cover them already.

All the results of the measurements are shown in table 5.1. This table proves that the direct wired communication, via the USB interface, between the END DEVICE and the Personal Computer works, since the data in the END DEVICE can be obtained successfully. These data are displayed on the computer screen via the HyperTerminal.

Different values of the resistors are used to produce different analogue voltages (V_1 , V_2 and V_3) at the resistor bridge, since the source voltage, which AAA battery is used, is unchangeable. Relative low resistor values are preferred, because the relative voltage drop is very low. The cause of the voltage drop is due to using the multi-meter, which is Hewlett Packard 973A. This meter has a typical input impedance of 10M Ω . The analogue voltage values are the values of V_1 , V_2 and V_3 at the resistor bridge measured by the multi-meter. However, these values can be calculated according to the formulas, (5.2), (5.3) and (5.4), as mention at the previous page. Table 5.2 shows the calculated voltages compared to the obtained voltage by the multi-meter.

Table 5.1: Calculated voltages compared to the obtained voltage by the multi-meter

Analogue voltage value [mV]			Calculated analogue voltage value [mV]		
V_1	V_2	V_3	V_1	V_2	V_3
1168	778	389	1169.479	779.7395	389.479
969	646	323	971.133	647.0614	323.4225
1234	646	323	1235.928	647.0614	323.4225
1234	911	323	1235.928	912.2896	323.4225
1234	911	588	1235.928	912.2896	588.867
833	555	278	834.5051	556.2127	278.1064
1279	555	278	1281.708	556.2127	278.1064
1279	1001	278	1281.708	1003.601	278.1064
1279	1001	723	1281.708	1003.601	725.4949
693	462	231	694.5375	462.9218	231.4609
1326	462	231	1328.384	462.9218	231.4609
1326	1094	231	1328.384	1096.923	231.4609

⁶ Source: <http://www.asciitable.com/>

1326	1094	863	1328.384	1096.923	865.4625
621	414	207	622.2799	414.7608	207.3804
1350	414	207	1352.481	414.7608	207.3804
1350	1142	207	1352.481	1145.1	207.3804
1350	1142	935	1352.481	1145.1	937.7201

The difference between the calculated values and the measured results is very small. This very small difference is due to voltage drop by using the multi-meter, which a small amount of voltage is lost. The voltage drop depends on the input impedance of the multi-meter and on the resistor values in the resistor bridge.

Table 5.2: The wired communication of the END DEVICE with the Personal Computer test*

Resistors values in the resistor bridge [Ω]				Analogue voltage value [mV]			Digital representation of the A/D conversion			Analogue representation of the A/D conversion [mV]		
R_1	R_2	R_3	R_4	V_1	V_2	V_3	V_1	V_2	V_3	V_1	V_2	V_3
14990	14960	14980	14950	1168	778	389	809	538	271	1186.217	788.8563	397.3607
27220	14980	14960	14950	969	646	323	671	447	225	983.871	655.4252	329.912
14980	27220	14960	14950	1234	646	323	855	447	225	1253.666	655.4252	329.912
14980	14960	27220	14950	1234	911	323	855	629	225	1253.666	922.2874	329.912
14980	14960	14950	27220	1234	911	588	856	629	409	1255.132	922.2874	599.7067
39000	14960	14950	14950	833	555	278	579	386	193	848.9736	565.9824	282.9912
14960	39000	14950	14950	1279	555	278	886	386	194	1299.12	565.9824	284.4575
14960	14950	39000	14950	1279	1001	278	886	692	194	1299.12	1014.663	284.4575
14960	14950	14950	39000	1279	1001	723	886	692	503	1299.12	1014.663	737.5367
55900	14960	14950	14950	693	462	231	485	322	162	711.1437	472.1408	237.5367
14960	55900	14950	14950	1326	462	231	919	322	161	1347.507	472.1408	236.0704
14960	14950	55900	14950	1326	1094	231	919	757	161	1347.507	1109.971	236.0704
14960	14950	14950	55900	1326	1094	863	919	756	599	1347.507	1108.504	878.2991
67600	14960	14950	14950	621	414	207	437	289	145	640.7625	423.7537	212.61
14960	67600	14950	14950	1350	414	207	936	290	145	1372.434	425.2199	212.61
14960	14950	67600	14950	1350	1142	207	936	790	144	1372.434	1158.358	211.1437
14960	14950	14950	67600	1350	1142	935	935	788	646	1370.968	1155.425	947.2141

*Notes:

- All tests are performed with the source voltage (V_{batt}) of 1.56V.
- The A/D conversion uses an internal reference voltage (V_{ref}) of 1.5V.
- All test results are performed at room temperature.
- The digital values are plotted 10 times on the computer screen. The most frequent value is list in this table.

The columns of the Digital representation of the A/D conversion show the obtained digital values of the columns in the Analogue voltage value. The Analogue voltage values are all converted into digital values to able to do further processing of the data.

Internal reference voltage has been used for the A/D conversion, because it saves one unit, thus the complete sensor system can keep small. The reference voltage has a voltage value of 1.5V. Nothing can be said about the accuracy of this value, since this value cannot be easily measured. Moreover, the accuracy of this internal reference voltage is not discussed in the datasheet that is provided by Texas Instrument.

To able to compare the digital data with the measured analogue values, the column of Analogue representation of the A/D conversion [mV] is added to table 5.2. This column converts the digital values into analogue values according to the formula given by (5.1) at the beginning of this section.

A very remarkable note is that all digital values are somewhat higher than what are measured by the multi-meter. This can be due to the not-well-defined of the internal reference voltage. Another possibility is due to inaccuracy of the A/D converter. The inaccuracy is due to non-ideally A/D converter, which the last 2 bits might be incorrect. However, in the datasheet of the MSP430F2274, no full details about the accuracy of the A/D converter are mentioned.

Table 5.3 shows the difference in percentage (%) of the Analogue representation of the A/D conversion and the Analogue voltage value.

Table 5.3: Error in percentage (%) of the Analogue representation and the A/D conversion and the Analogue voltage value

Analogue voltage value [mV]			Analogue representation of the A/D conversion [mV]			Error [%]		
V_1	V_2	V_3	V_1	V_2	V_3	V_1	V_2	V_3
1168	778	389	1186.217	788.8563	397.3607	1.559675	1.395412	2.149281
969	646	323	983.871	655.4252	329.912	1.534672	1.459012	2.139945
1234	646	323	1253.666	655.4252	329.912	1.593654	1.459012	2.139945
1234	911	323	1253.666	922.2874	329.912	1.593654	1.239011	2.139945
1234	911	588	1255.132	922.2874	599.7067	1.712477	1.239011	1.990943
833	555	278	848.9736	565.9824	282.9912	1.9176	1.978812	1.795397
1279	555	278	1299.12	565.9824	284.4575	1.573122	1.978812	2.322834
1279	1001	278	1299.12	1014.663	284.4575	1.573122	1.364911	2.322834
1279	1001	723	1299.12	1014.663	737.5367	1.573122	1.364911	2.010603
693	462	231	711.1437	472.1408	237.5367	2.618138	2.19497	2.829722
1326	462	231	1347.507	472.1408	236.0704	1.621971	2.19497	2.19497
1326	1094	231	1347.507	1109.971	236.0704	1.621971	1.459842	2.19497
1326	1094	863	1347.507	1108.504	878.2991	1.621971	1.325813	1.772783
621	414	207	640.7625	423.7537	212.61	3.182361	2.355958	2.710131
1350	414	207	1372.434	425.2199	212.61	1.661779	2.710131	2.710131
1350	1142	207	1372.434	1158.358	211.1437	1.661779	1.432379	2.001785
1350	1142	935	1370.968	1155.425	947.2141	1.553166	1.175588	1.306318

The error is calculated as follow:

$$\text{error} = \frac{\text{voltage of Analogue representation of the A/D conversion} - \text{Analogue voltage value}}{\text{Analogue voltage value}} \cdot 100\%$$

The averaged error is roughly around 2%. At this stage, it is hard to say whether this error is acceptable, since the complete O₂ sensor system needs to be built first which after measurements in living tissues can be performed to test if this error amount is acceptable.

The next subsection focuses on the wireless communication. ACCESS POINT will be fully examined in combination of the END DEVICE. Moreover, temperature sensor is activated to test the transfer of the digital value from one device to another via the wireless network.

5.5.3 Measurement setup of the ACCESS POINT

In this subsection, the measurement setup of ACCESS POINT to measure the temperature is discussed. Two eZ430-RF2500 have been used for this setup. One of them is the ACCESS POINT while the other one is the END DEVICE, which the O₂ sensor will be attached on.

Figure 5.5.3 shows the measurement setup the ACCESS POINT.

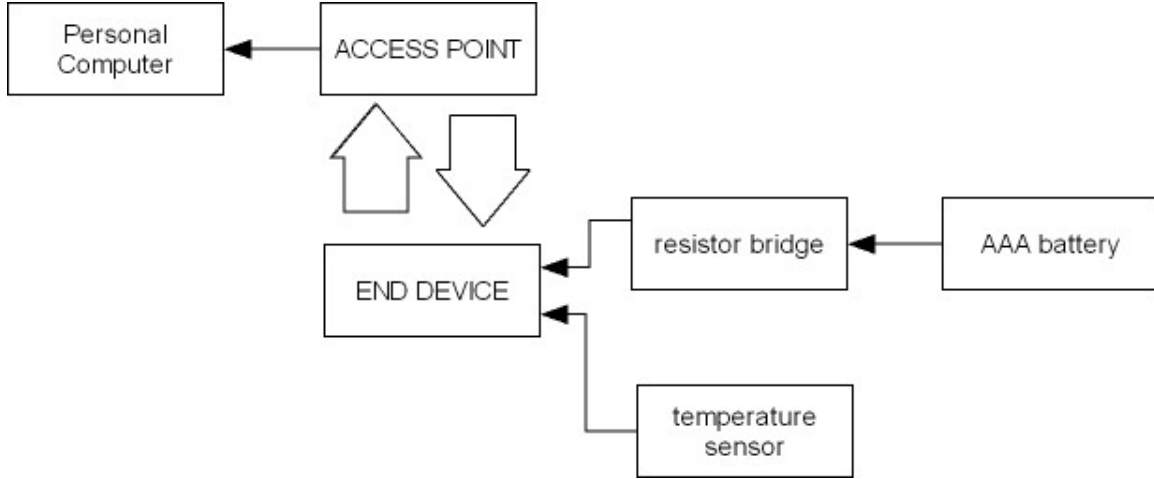


Figure 5.5.3: Measurement setup of the ACCESS POINT

The ACCESS POINT is directly connected to the personal computer. On the END DEVICE, the temperature sensor is now activated and again, the AAA battery and the resistor bridge are used for representing the O₂ sensor.

The distance between the ACCESS POINT and the END DEVICE is kept relatively short. The limitation of the distance is not fully tested. Once the read-out electronics is successfully built and added to the END DEVICE, then this distance will be fully examined.

In the next subsection, the results of this setup are shown. The results are based on a relative short distance between the ACCESS POINT and the END DEVICE. A few measurements are performed on the resistor bridge. This only proves that the wireless communication works. Since the results of the resistor bridge are successfully obtained in the previous subsection, the major focus is the temperature measurements.

5.5.4 Measurement results of the ACCESS POINT

This subsection starts with small testes which the setup is described in Figure 5.5.3 in the previous subsection. For these small testes, the wireless communication has been proved for its well functioning. Table 5.5.4a shows the results of these tests.

Table 5.4: The results of testing the wireless communication

Analogue voltage value [mV]			Digital representation of the A/D conversion			Temperature [°C]	Distance [cm]
V_1	V_2	V_3	V_1	V_2	V_3	T	d
1168	778	389	809	538	271	227	25

969	646	323	671	447	225	227	25
1234	646	323	855	447	225	227	25
1234	911	323	855	629	225	227	25
1234	911	588	856	629	409	227	25

The results of the test show that the wireless communication works perfectly. Signals can be sent from the END DEVICE to the ACCESS POINT successfully. Notice that the values for the temperature sensor are ten times larger than they supposed to be. This is, because the assigned type of variable cannot store decimal values. To make the system less complex, the implementation of the decimal value is left out.

The distance is kept short. The reason for this is because of practical reason: it is easier to work when the END DEVICE and the ACCESS POINT are closed together and when both of them are in room temperature. A very common thermometer⁷ has been used to check the temperature. The temperature on the thermometer shows the same value as what is measured by the temperature sensor.

The next part of the measurement is about testing the performance of the distance on the temperature measurements. The END DEVICE is placed in different distance for measuring the temperature. Table 5.5 shows the results of the measurements.

Table 5.5: The influence of the distance on the temperature measurements

Temperature [°C]	Distance [cm]
T	d
219	25
219	60
219	120
219	240
218	500
218	600
004	400
217	600*

* This measurement is performed when the END DEVICE is packed in a room with the door closed.

The last measurement is to check if the wireless communication allows sending through a barrier. When the END DEVICE is put in a room where it is surrounded by walls and when the door is closed, it is still able to send data to the ACCESS POINT.

So far, nearly all measurements are performed around the room temperature. Only one measurement is difference. For that measurement, the END DEVICE is placed outside the building. The ambient temperature is measured by a very common thermometer to verify the obtained temperature that is measured by the temperature sensor. On the thermometer shows a temperature of $\sim 0.10^{\circ}\text{C}$, while the END DEVCIE measures 0.4°C . This difference is because both sensors are optimal operated in different range of temperature. Once they exceed the range, the accuracy will be lost. In case of the common thermometer which is usually optimized for room temperature, the obtained results for very low temperature (temperature below 10°C), its results might be not reliable. In contrast to the temperature sensor in the END DEVICE, which uses a diode for measuring the temperature, has a much broader range of temperature.

Table 5.5 shows that the distance below 6m does not influence the measurement. It also shows that the data can be sent through walls and door, which may allow sending through living tissues as well.

⁷ It is a simple Hg-filled thermometer.

5.6 Conclusions

The eZ430-RF2500 has been used for processing data before it is sent to the Personal Computer. Two units of eZ430-RF2500 are required to perform the wireless communication. One of the units is directed connected to the computer while the other can be placed anywhere in the environment. However, the maximum distance between the END DEVICE and the ACCESS POINT for the testing purpose is set at about 6m. For this distance, the signal can be still successfully received. The signal also can be received when the END DEVICE is enclosed by walls and door. This is an important issue when this device is left in living tissues for doing measurements.

The error in the A/D conversion is roughly around the 2%. This relative huge error might be due to not-well-defined internal reference voltage that is used. This voltage is embedded in the A/D converter. The performance of the A/D converter is not explained in the supplied datasheet of the eZ430-RF2500 by Texas Instruments.

5.7 Summary

Two eZ430-RF2500 devices have been used to realise the wireless communication. One of the devices acts like a sender which measures the intensity signal of the fluorescence and the ambient temperature. This device is so called the END DEVICE. The other one is attached to the computer that is looking for data of a nearby END DEVICE. This device is so called the ACCESS POINT. The ACCESS POINT is connected to the Personal Computer via the USB interface.

The computer plots the data in the HyperTerminal. The predefined method of Texas Instruments is used for plotting data on the HyperTerminal, which is the TXString(). This method only accepts String in its input. Therefore, the obtained data should be converted into a String. The conversion is self-made because the standard Integer-to-String, which is the itoa(), can not be used because the license issue in the IAR Assembler. The self-made conversion method is names as convert(). The self-made integer-to-String conversion assumes that the data is maximal 2 bytes.

The test of the wireless communication starts with the END DEVICE first, since the wired communication should be proved first for its well functioning. Moreover, it is easier for readers to start understanding the working of the END DEVICE. Any bugs in the END DEVICE can be easier fixed when it is attached to the computer. When the END DEVICE works properly, the ACCESS POINT is added and the wireless communication can be fully test.

The pO₂ sensor and the read out electronics are not added to do the complete test, since the read out electronics are not being built yet. A simple AAA battery and a resistor bridge have been used for replacing the sensor and the electronics. AAA battery is used because the reference voltage in the A/D converter is maximal 1.5V. Moreover, the voltage of the battery is much more stable than a power supply or a function generator. The resistor bridge is used to vary the voltage.

The error in the A/D converter is around 2%. This relative big error might be due to the not well-defined internal voltage reference that is embedded in the A/D converter. Besides, the A/D converter cannot be perfect since the last few bits of the digital results are usually uncertain.

The wireless communication proved for its well functioning. All messages can be successfully distinguished and received within a distance below of 6m. It does not matter if the signals of the END DEVICE are blocked by the walls or door, since the data still can be successfully received.

Chapter 6 – Measurements based on the alternative approach

6.1 introduction

In this chapter, measurements on the oxygen level have been performed and the results have been evaluated. This chapter starts with the setup of the alternative approach to determine the oxygen level. However, the “real” oxygen sensor is excluded since it is not useful anymore: the difference in the duration of the fluorescence signal for different levels of oxygen is almost indistinguishable. Therefore, a substitution has been introduced. The first section is about the substitution of the oxygen sensor. The complete setup of the measurements is discussed in the next section. The results and the evaluation of the measurements have been presented in the third section. This chapter ends with conclusions.

6.2 Substitution of the oxygen sensor

The substitution of the ‘real’ sensor consists of two parts. The first part is the generation of the fluorescence signal. Agilent 33120A has been used to simulate this fluorescence signal. Since the Agilent 33120A can only generate voltage at its output and because the “real” oxygen sensor is a current source, this voltage has to be converted into a current. The second part of the substitution is the conversion of the voltage into a current. This is simply done by using a resistor.

Agilent 33120A is a function generator that can generate any desired waveform. Figure 6.2.1 and Figure 6.2.2 show the front side and the back side of the function generator respectively. The desired waveform that we want to create is not a standard waveform that can directly be generated using the buttons in the Agilent 33120A. Therefore, this waveform has been created in Visual Basic that is embedded in Microsoft Excel.

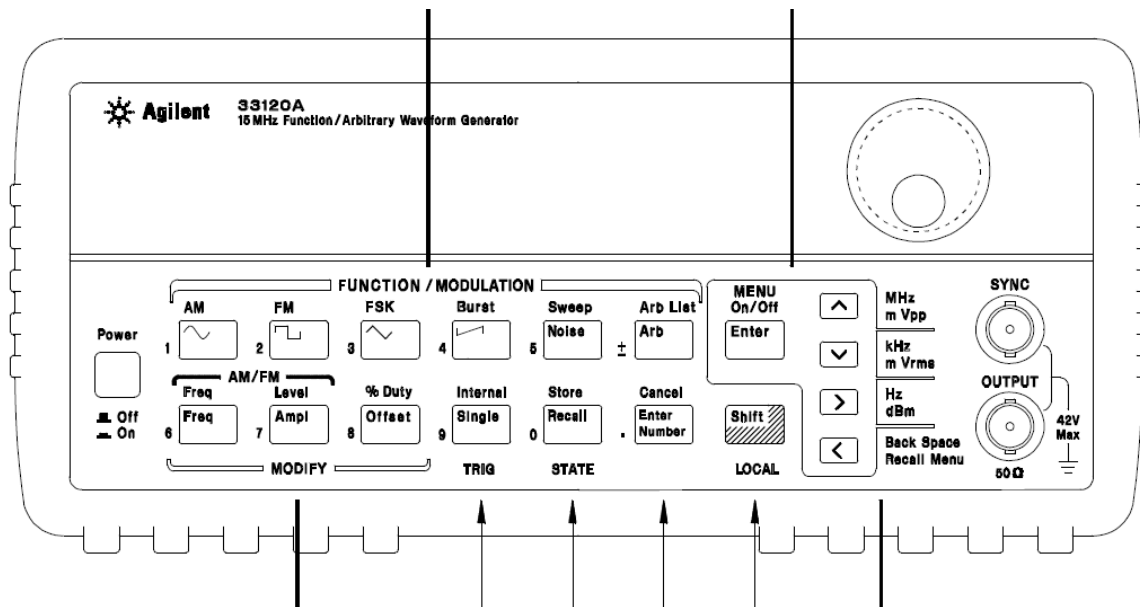


Figure 6.2.1: The front side of the function generator Agilent 33120A, based on <http://mntl.illinois.edu/equipment/docs/agilent33120auserguide.pdf>

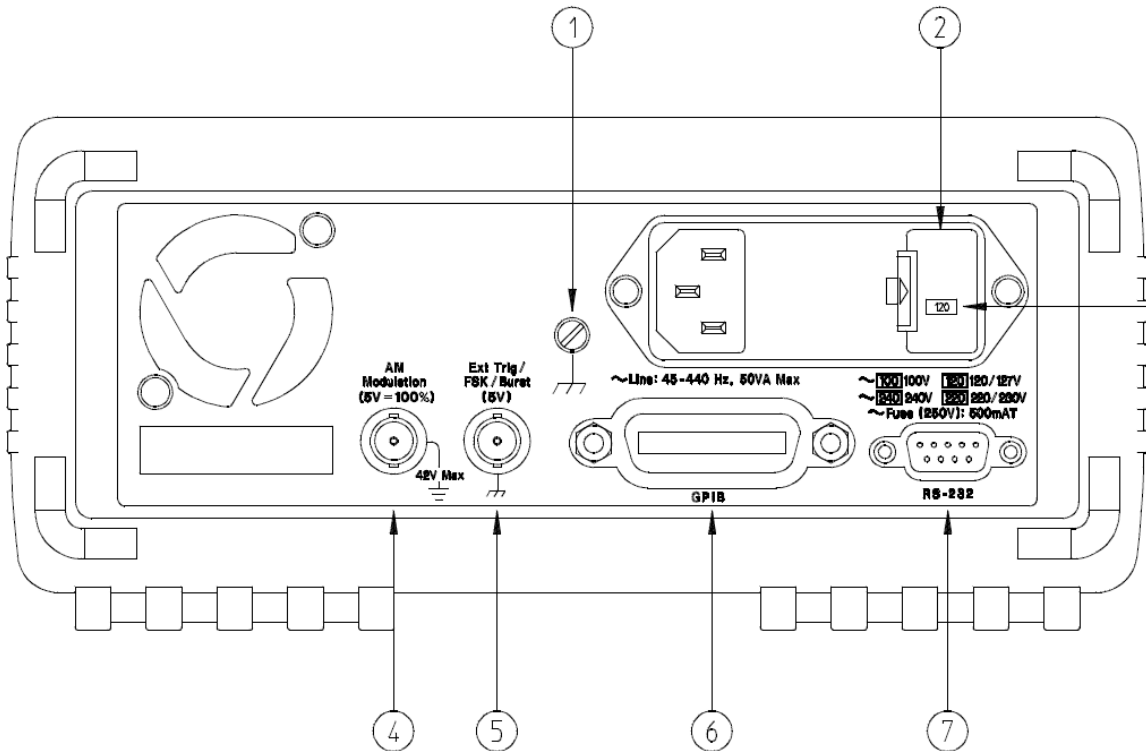


Figure 6.2.2: The back side of the function generator Agilent 33120A, based on <http://mntl.illinois.edu/equipment/docs/agilent33120auserguide.pdf>

When the Excel sheet is opened, you get a screen that is similar to Figure 6.2.3. In this screen, there is a column named as “Point”. The numbers are the number of samples of generating the signal. The more samples you take, the smoother the signal will be.

For each sample a value is assigned to. All the values can be found in the column of “Value”. The generation of these values will be discussed in the programming part of this device.

The desired waveform has a rise and fall time. Therefore, there is a table that is being displayed in columns D and E. The numbers (5 and 100) give the duration of the signal.

The Agilent 33120A is connected to the computer with a GPIB cable. The address can be set. The default value is set at 10.

In able to create data that can be found in “Value” column, the button “Create data” has to be pressed. The generation of the data will be discussed later.

Once the data have been created, they can be sent to the Agilent 33120A. The sending action has been realised by pressing the button “Send to Instrument”. In case that the address of the GPIB is changed, do change the setting by pressing the “SetIO”.

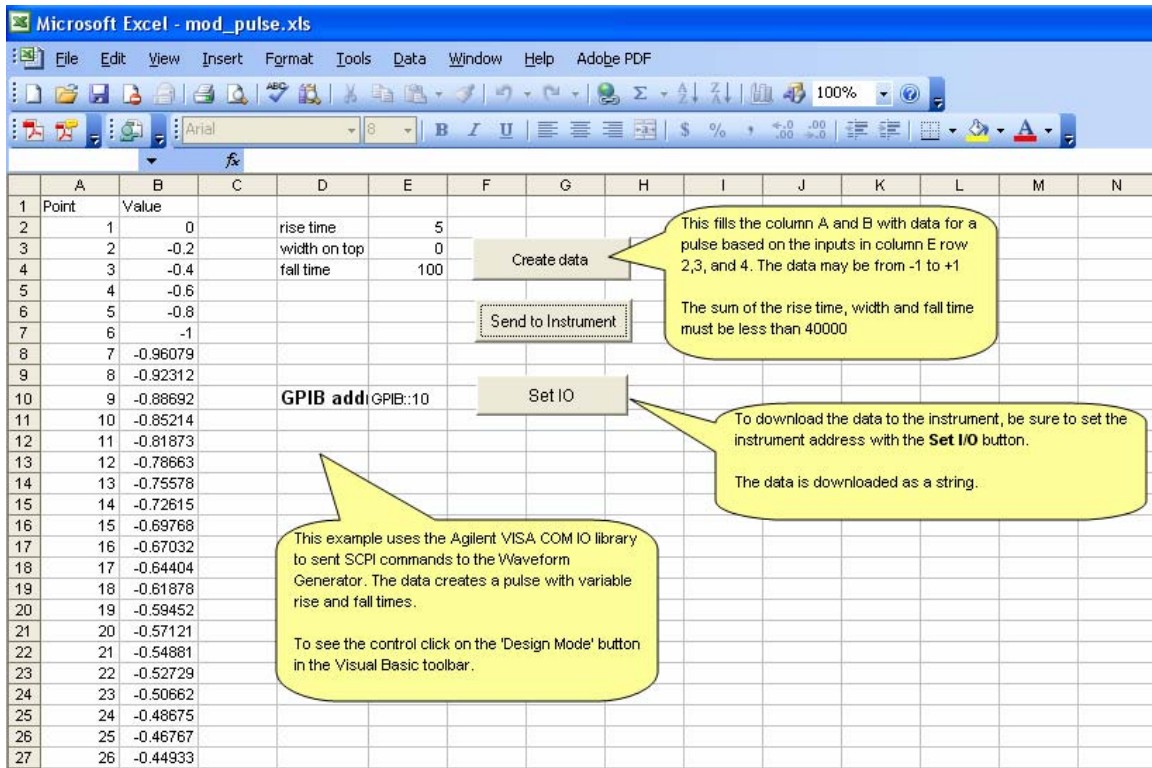


Figure 6.2.3: The screenshot of the Excel sheet that generates the desired waveform

The generation of the data has been taken in Excel. The source code in Excel consists two parts: the setting part and the part of generating the signal. The setting part tells the Agilent 33120A how to set the default setting, like the offset value, the type of waveform etc. This source code is shown below:

```
Public Sub LoadWaveform()
    Dim strData As String

    GetWorksheetData "A2:b500", strData

    ' reset instrument
    With FGen
        .WriteString "*RST"

        ' set timeout large enough to sent all data
        .IO.Timeout = 40000
        ' download data points to volatile memory from array
        .WriteString "Data Volatile, " & strData

        .WriteString "Data:Copy Pulse, Volatile" ' Copy arb to non-volatile memory
        .WriteString "Function:User Pulse" ' Select the active arb waveform
        .WriteString "Function:Shape User" ' output selected arb waveform
        .WriteString "BM:NCYC 1" ' # cycles
        .WriteString "BM:STAT ON" ' enable the burst mode
        .WriteString "TRIG:SOUR EXT" ' TRIGger:SOURce {IMMediate|EXTernal|BUS}
        .WriteString "TRIG:SLOP NEG" ' TRIGger:SLOPe {POSitive|NEGative}
        .WriteString "Output:Load 50" ' Output termination is 50 ohms
        .WriteString "OUTP:SYNC ON" ' synch is activated
        .WriteString "Frequency 1000; Voltage 1.25" ' Ouput frequency is 1kHz @ 2.5 Vpp
    End With
End Sub
```

```
.WriteString "VOLT:OFFS 0.285" ' VOLTage:OFFSet = 570mV
```

End With

The function generator is reset first, and then a time is set to ensure that all data can be successfully sent to the Agilent 33210A. The data have been copied to the non-volatile memory of the function generator. The following steps involve the settings of the signal, e.g.:

1. the type of the waveform
2. the number of cycles
3. enabling the burst mode
4. the trigger type
5. the output load
6. activation of the synchronisation
7. the frequency and its peak to peak voltage
8. the offset value

The second part of the source code is the generation of the waveform. Since the “real” oxygen sensor has a monotone exponential decay, the generated function should be a monotone exponential decay too. The source code below shows how this exponential function is being generated:

```
Sub makePulse(ByVal riseTime As Long, ByVal topWidth As Long, ByVal fallTime As Long)
    Dim Waveform(1 To 4000) As String
    Dim topStart As Long
    Dim topStop As Long
    Dim endPulse As Long
    Dim i As Long

    topStart = riseTime
    topStop = topStart + topWidth
    endPulse = topStop + fallTime

    ' set the heading in worksheet
    Cells(1, 1) = "Point"
    Cells(1, 2) = "Value"

    ' Set rise time
    For i = 1 To riseTime
        Cells(i + 1, 1) = i
        Cells(i + 1, 2) = -(i - 1) / riseTime
    Next i

    ' set pulse width
    For i = riseTime + 1 To topStop
        Cells(i + 1, 1) = i
        Cells(i + 1, 2) = -1
    Next i

    ' set fall time
    For i = topStop + 1 To endPulse
        Cells(i + 1, 1) = i
        ' this is for f = 1kHz
        Cells(i + 1, 2) = -Exp(-(i - topStop - 1) / (5 * topStart)) ' ~ 100us
        Cells(i + 1, 2) = -Exp(-(i - topStop - 1) / (8 * topStart)) ' ~ 200us
        Cells(i + 1, 2) = -Exp(-(i - topStop - 1) / (12 * topStart)) ' ~ 300us
        Cells(i + 1, 2) = -Exp(-(i - topStop - 1) / (16 * topStart)) ' ~ 400us
    Next i
End Sub
```

```
'Cells(i + 1, 2) = -Exp(-(i - topStop - 1) / (25 * topStart)) ' ~ 500us
```

```
Next i
```

```
' set zero level for rest of points
```

```
For i = endPulse + 1 To 4000
```

```
Cells(i + 1, 1) = i
```

```
Cells(i + 1, 2) = 0
```

```
'Cells(i + 1, 2) = -Exp(-(i - topStop) / (fallTime))
```

```
Next i
```

```
End Sub
```

First, the rise time has been created. It is assumed that the rise time is a linear increasing signal. Then the pulse width is defined. Since the fluorescence signal does not have a pulse width, the value for the pulse width is zero. The creation of the mono-exponential function is the final part.

Figure 6.2.4 shows the output of the function generator Agilent 33210A. Two lines are shown. The yellow line, the one on the bottom, gives the representation of the waveform that is generated from Agilent 33210A.

One remark has to be noted. The desired waveform is a monotone-exponential decay that has been shown in Figure 6.2.4. The generated waveform represents its inverted signal. Since this function generator is connected to the inverted input of the amplifier, the waveform will be inverted. Therefore, the generated waveform should be the inversion of the desired waveform.

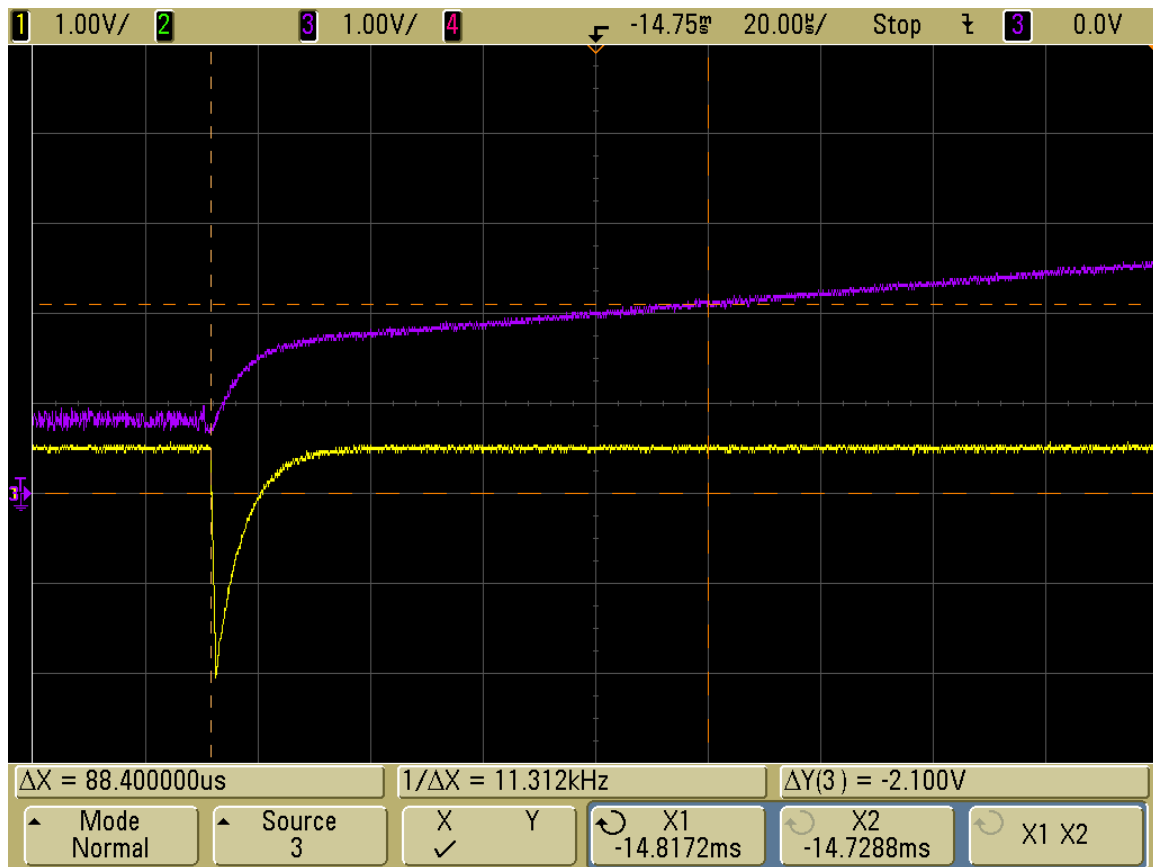


Figure 6.2.4: The waveform at the top is the output of the Agilent 33210A.

6.3 Measurement setup of the alternative approach for measuring the oxygen level

In the previous section, the programming part of the function generator of Agilent 33120A has been discussed in detail. To able to transfer the source code from the computer to the function generator, GPIB cable has been used. Figure 6.3.1 shows the setup of the transfer of the source code from the computer to the “signal generator” that is represented as the function generator.

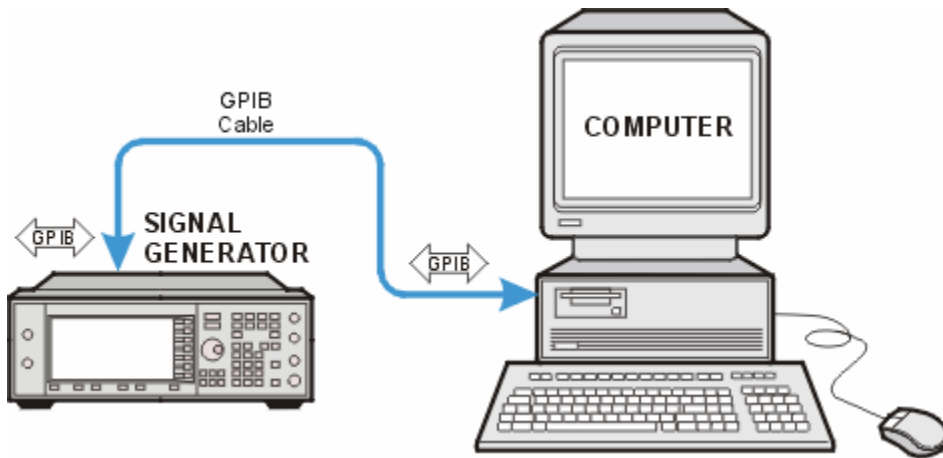


Figure 6.3.1: The setup for code-transfer from the computer to the Agilent 33120A, based on <http://wireless.agilent.com/wireless/helpfiles/n7601b/dk717b.gif>

The generated signal from the signal generator is fed into the input of the read-out electronics via a resistor. The read-out electronics subtracts the lifetime value of the generated signal. This lifetime value has been recorded by the End Device. The recorded value has to be converted into a digital representation, because of the wireless transmission protocol to the Access Point. The results of the measurements will be plotted on the computer screen. Figure 6.3.2 shows the complete setup of oxygen measurement based on the alternative approach.

The signal generator and the read-out electronics represent the sensor for measuring the oxygen level. The wireless platform, which enables the transmission of the data to the computer, is the Access Point and the End Device. The computer has been used to determine the oxygen level.

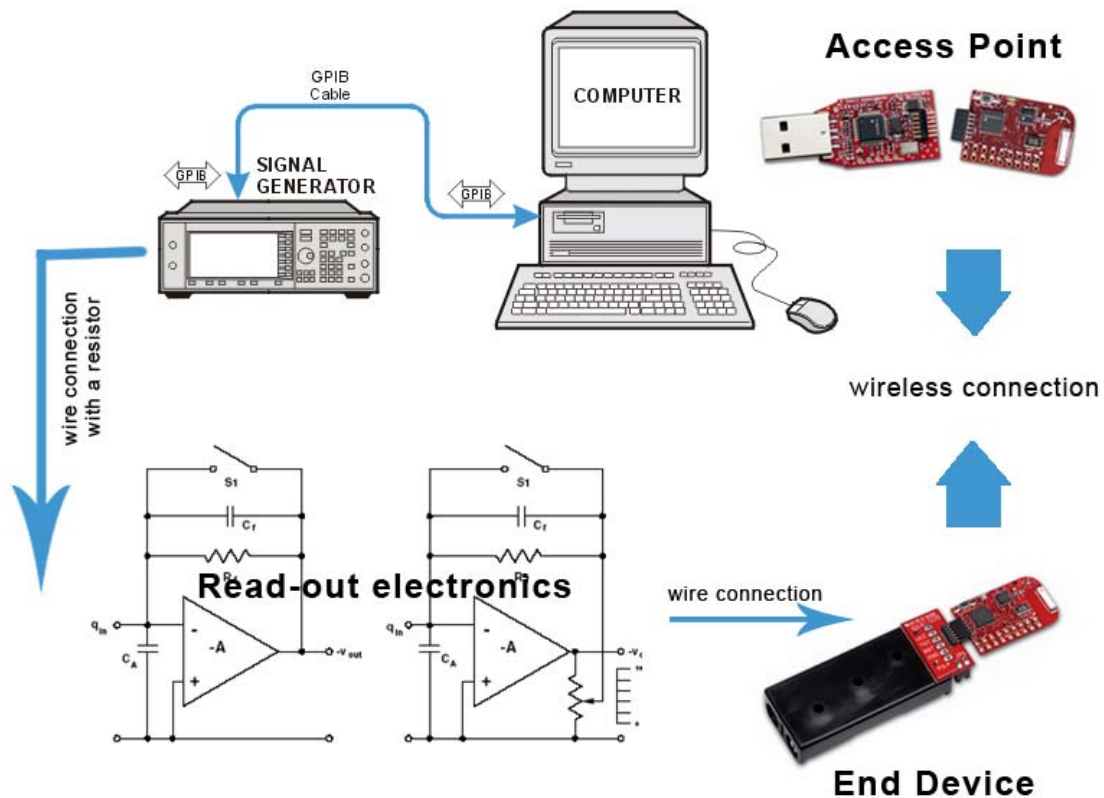


Figure 6.3.2: The complete setup of the alternative approach to measure the oxygen level, based on <http://www.dytran.com/img/tech/a7-fig-3.gif>

6.4 Measurement results of the alternative approach

The output voltages of both integrators have been examined with a Tektronix TDS3034B oscilloscope. Both output voltages have been simultaneously plotted on the screen of the Tektronix TDS3034B oscilloscope. The results are shown in Figure 6.4.1.

Two lines are shown. The line on the top gives the output representation of the second integrator. This is an exponential decreasing line that will not get negative value, because of the single (positive) voltage that the AD converter in the MSP430. This output is an exponential decreasing function, since the double integration over an exponential function is a still an exponential function. The output of the second integrator is a decreasing line, because of the inverse current direction.

The bottom line represents the output of the signal function generator. The decreasing part, which is defined as the rise time in the Excel sheet, is not a perfect straight line, since the limitation of the bandwidth of the function generator. The generated signal has an offset. This generated offset is needed to cancel out the offset voltage of the first integrator to reduce additional current flowing into the read-out circuits no matter what the status of the switches are (turned on or off). Since the additional current will introduce error in subtracting the lifetime measurements.

Both lines show oscillations. The riddles are due to the noise production of the oscilloscope and the probes. The read-out electronics is not shielded from the measurement environment. This can also increase the noise production.

The lifetime of the second integrator is set at the desired value in the programming part of the signal generator. This is clarified by generation of the mono decreasing exponential characteristic that says:

$$Cells(i + 1, 2) = -Exp(-(i - topStop - 1) / (5 * topStart)) \sim 100us \quad (6.1)$$

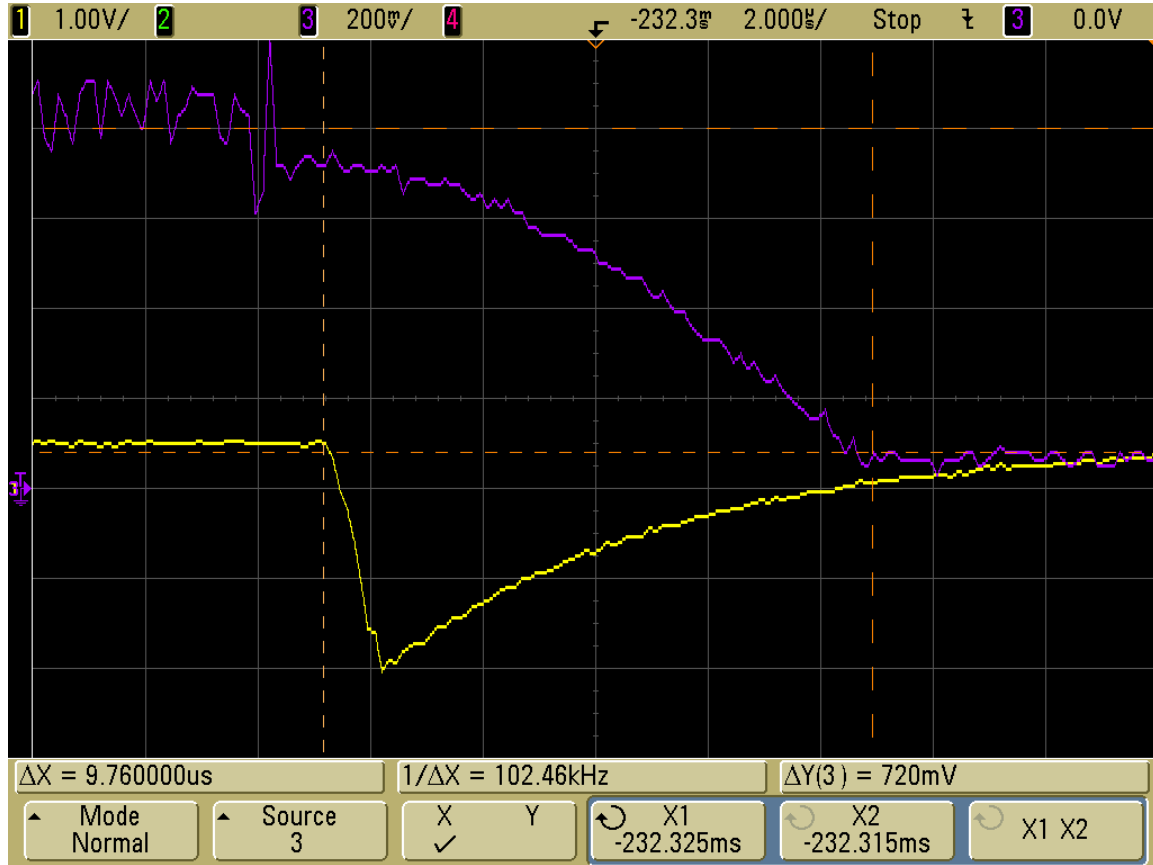


Figure 6.4.1: Output voltage of the second integrator (top) and the signal generator (bottom).

The standard mono exponential function has this expression:

$$f(t) = a \cdot \exp\left(-\frac{t}{T}\right) \quad (6.2)$$

a = amplitude
t = time duration
T = lifetime value

Looking at both expressions, expression (6.1) will be written in the form of (6.2) to ease to see what its lifetime value is:

$$\begin{aligned} cells(i) &= -Exp\left(-\frac{(i - topStop - 1)}{(5 \cdot topStart)}\right) = -Exp\left(-\frac{(t - topStop - 1)}{(5 \cdot topStart)}\right) \quad (6.3) \\ &= -Exp\left(-\frac{t}{(5 \cdot topStart)}\right) \cdot -Exp\left(\frac{topStop}{(5 \cdot topStart)}\right) \cdot -Exp\left(\frac{1}{(5 \cdot topStart)}\right) \end{aligned}$$

Thus,

$$a = \text{Exp}\left(\frac{\text{topStop}}{(5 \cdot \text{topStart})}\right) \cdot \text{Exp}\left(\frac{1}{(5 \cdot \text{topStart})}\right)$$

$$T = 5 \cdot \text{topStart}$$

The value of topStart is 1 μ s. Therefore, the lifetime (T) is set at 5 μ s. Examine Figure 6.4.1, the lifetime of the fluorescence signal corresponds with the set lifetime value.

Next, the output of the first integrator has been examined. Figure 6.4.2 shows the output of the first integrator and the signal generator.

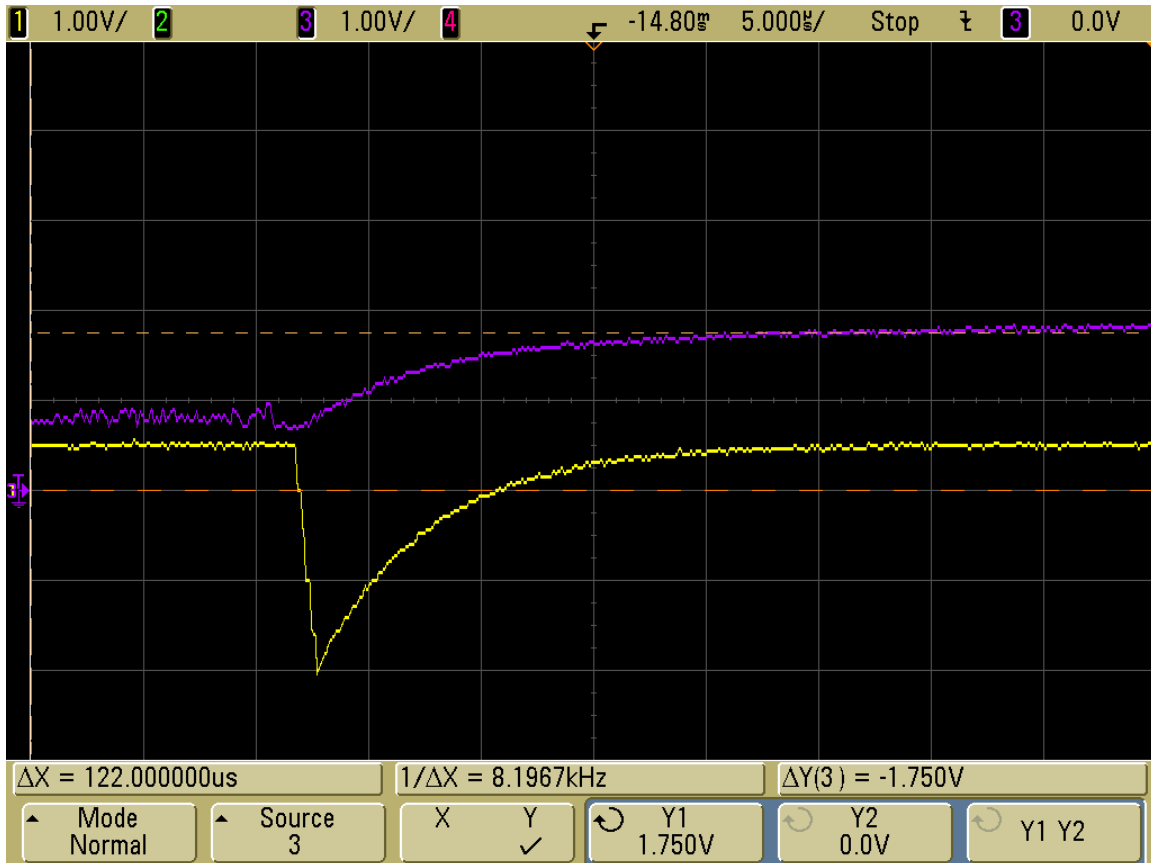


Figure 6.4.2: Outputs of the first integrator (top) and the signal generator (bottom).

The output of the first integrator should be a monotone increasing exponential curve. The first glance on this figure, it seems like that the curve of the output of the first integrator is the expected curve. Later on this section, a proof will be given to test if the integrator takes the integrator to subtract the lifetime value.

The output of the first integrator is an increasing exponential curve, since integrator over an exponential function is still an exponential function. However, the curve is positive, because of the read-out electronics. The first integrator provides the current, which means that the output voltage of the first integrator is positive. The more current is driven, the more positive the curve it becomes.

Notice that there is a difference in offset voltage of the first integrator and the generated signal. This mismatch will cause an error in subtracting the lifetime value. Two methods can be applied to deal with this offset.

The first one is better matching with the offset voltage of the first integrator by tweaking on the pre-set offset value of the signal generator. This method is relative simpler than the second one and the first method is also highly recommended.

The second way to deal with is keep this difference and cancel out the difference in the data processing part. In the data processing, which means the measured data have been converted into a digital representation. This offset value can be cancelled out, since the offset value of the first integrator and the signal generator are known. To do a perfect compensation, thus the error is zero in the offset difference, the integration time must be known accurately.

Using the second method to do the error compensation has some drawbacks. The first one is that the error at the first stage of integrator will enlarge the error in the second stage of integration. Therefore, the error compensation should be applied to the first and the second integrator to minimize the error in subtracting the lifetime value.

Secondly, if the difference is too large, the generated fluorescence signal will be 'covered' by the difference. Therefore the read-out electronics will not be able to subtract the lifetime value.

Thirdly, in the read-out electronics, the current is flowing no matter what the condition of the switch is. This "leaky" current might affect the proper functioning of other components that are attached to the read-out electronics.

Setting the duration of the integration time is uttermost important. If the duration is set too long, more error will introduce into subtracting the lifetime value. Figure 6.4.3 shows this.

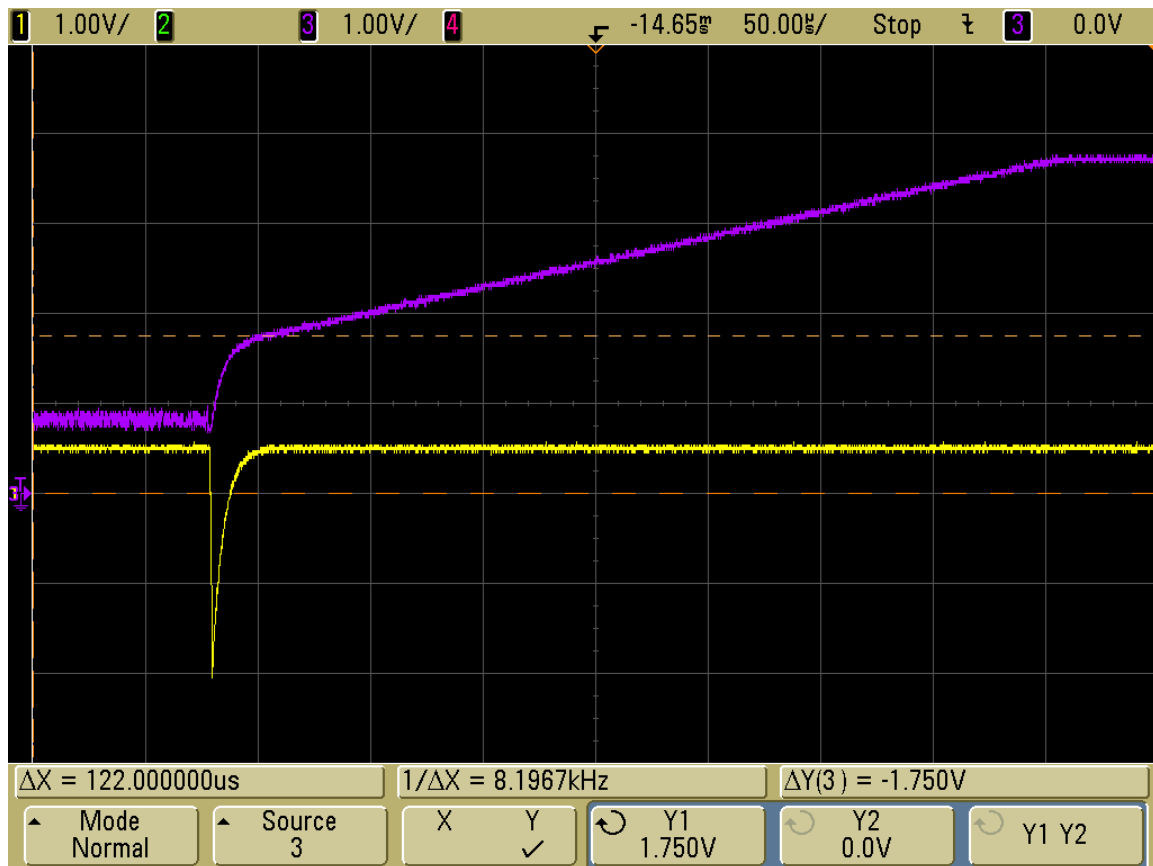


Figure 6.4.3: The turn off time of the switch of the first integrator. Output of the first integrator (top) and the output of the signal generator (bottom).

The generated fluorescence signal is just a small fraction of the period of the turn off time of the switches. The turn off time of the switches is set at about 3.88ms while the period of the generated fluorescence signal is set at 200μs.

In the ideal case, the turn off time and the time frame of the generated fluorescence signal should be perfectly matched, thus both time frame is the same. However, in real life, these two time frames are different. The switch off time cannot be further reduced, since the limited clock speed in the ultra low power mode of MSP430. The generated fluorescence signal can be

extended to match up with the turn off time of the switches, but that is not recommended for three main reasons.

First, if the generated fluorescence signal is extended, all the values of the passive components in the read-out electronics should be adjusted too. A lot of new hand-on calculations should be performed to ensure that the integrators do not saturate.

Second, the difference in the offset becomes more a serious, since the time is extended. To adjust the time, you have to solve the offset first, which means that it takes time.

Third, the saturation point might become more serious issue. Examining Figure 6.4.3 carefully, you notice that the output of the integrator stops doing integration. The value of this saturation is not what we have expected. The saturation value is at 3.2V approximately, while the power supply is fed with 5V. The used integrators are rail-to-rail amplifier. Therefore, these amplifiers should be able to clip close to 5V. Extending time means that the integrator might have faster clipping. Thus, the read-out electronics is not able to subtract the lifetime value successfully.

This saturation point is a very serious issue that we have no idea what the real main cause of this phenomenon is. It might be of the active feedback network that is introduced by using the switches. This active network reduces the loopgain of the integrator, which means that there is clipping. Positive feedback network is not covered in the whole course of the Master of electrical engineering. Therefore, I am not able to prove this clarification.

The saturation point is present. No matter if the time is reduced or extended. To be able to do oxygen measurement, the integration time which is controlled by the MSP430, should be carefully set: the integration time should be set before the integrators start clipping.

The integration time is chosen based on the speed of the MSP430 and the duration of the fluorescence signal. The clock speed of MSP430 in ultra low power mode is 32kHz. Thus, working in a very fast environment (from a few megahertz) to obtain the lifetime value is very a tough job. To increase the speed, the MSP430 should be operated in ultra low power. However, a complete new wireless protocol should be written for non-low power mode. Thus rewriting the source code to increase the speed for current situation is not practical due the limited time of this M.Sc. project.

The duration of fluorescence signal is chosen from 100 μ s to 500 μ s. To prevent integration of the offset difference and clipping, the integration time should be less than 100 μ s. Thus, the integration time is set at 90 μ s.

Since the integration time is set, measurement can be started. However, the frequency of the signal generator should be adjusted, since with 1kHz, the fluorescence does not operate well for a long fall off time. Therefore, clock speed and the source code are slightly adjusted. Now, the clock speed is set at 5kHz and in the source code, the lifetime value is extended by 20 times. Table 6.1 shows the measurement results.

Table 6.1: Measurement results of the output voltages of both integrators

<i>Time [μs]</i>	<i>Output voltage of the first integrator [digital]</i>	<i>Output voltage of the second integrator [digital]</i>	<i>Ratio of both output voltage</i>
100	334	266	398
200	354	263	371
300	372	262	352
400	383	261	340
500	399	259	324

Time is defined as the period which the fluorescence signal occurs. In real life, this period is about 5 – 25 μ s. For the simulation purpose, the period is extended because of the limited speed of the MSP430 in low power mode. Moreover, the speed of the embedded ADC converter is also limited.

The ratio of both output voltage is defined as the ratio of the output voltage of the second integrator over the first one. Ideally, this should give the lifetime value only. However, since electronics has been used, an additional factor is added. This has been clarified in earlier chapters.

The lifetime value is linear increased. That means, that each time, the lifetime amount is added with the same amount. Ideally, the measured ratios should a linear curve as well. Figure 6.4.4 shows the ratios over time.

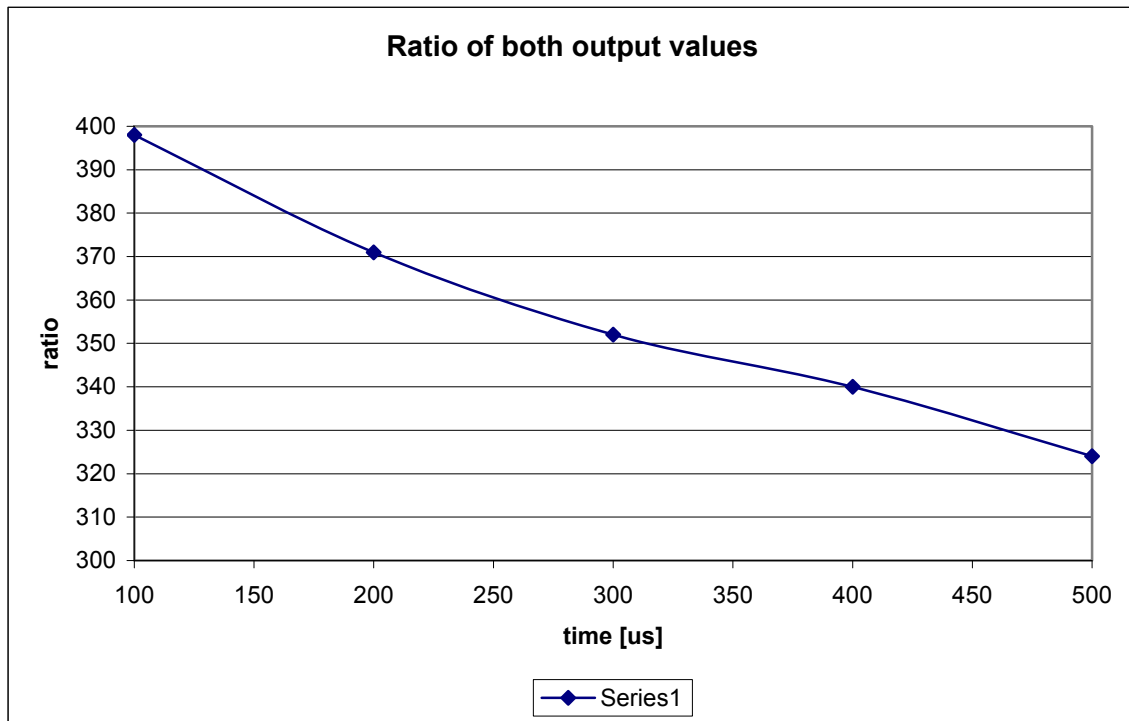


Figure 6.4.4: The obtained ratios for different lifetime values.

The drawn line is approximately linear. It is not ideally linear, because we have a rise pulse that is $5\mu\text{s}$ long. That is at least 1% of the entire fluorescence signal that is generated.

A check has been performed to check the obtained result of the output voltage of both integrators. The output voltage of the first integrator is:

$$\begin{aligned}
V_1 &= \frac{1}{C_1} \int_{t_0}^{t_1} I_{\text{signalGenerator}} dt \pm V_{\text{offset}_1} = \frac{1}{C_1} \int_{t_0}^{t_1} \frac{V_{\text{offset}_1} - V_{\text{gen}}}{R_{\text{gen}}} dt \pm V_{\text{offset}_1} \\
&= \frac{1}{C_1} \frac{V_{\text{off}}}{R_{\text{gen}}} t - \frac{1}{C_1} \int_{t_0}^{t_1} \frac{a \exp(-\frac{t}{T})}{R_{\text{gen}}} dt + V_{\text{off}} \\
&= \frac{1}{C_1} \frac{V_{\text{off}}}{R_{\text{gen}}} t - \frac{a}{R_{\text{gen}} C_1} \int_{t_0}^{t_1} \exp(-\frac{t}{T}) dt + V_{\text{off}} \\
&= \frac{1}{C_1} \frac{V_{\text{off}}}{R_{\text{gen}}} t + \frac{aT}{R_{\text{gen}} C_1} \left[\exp(-\frac{t}{T}) \right]_{t_0}^{t_1} + V_{\text{off}} \\
&= \frac{1}{C_1} \frac{V_{\text{off}}}{R_{\text{gen}}} t + \frac{aT}{R_{\text{gen}} C_1} \left(\exp(-\frac{t_1}{T}) - \exp(-\frac{t_0}{T}) \right) + V_{\text{off}} \\
&= \frac{1}{C_1} \frac{V_{\text{off}}}{R_{\text{gen}}} t + \frac{aT}{R_{\text{gen}} C_1} \left(\exp(-\frac{t_1}{T}) - 1 \right) + V_{\text{off}} \\
&= \frac{1}{C_1} \frac{V_{\text{off}}}{R_{\text{gen}}} t + \frac{aT}{R_{\text{gen}} C_1} \exp(-\frac{t_1}{T}) - \frac{aT}{R_{\text{gen}} C_1} + V_{\text{off}}
\end{aligned}$$

The output of the second integrator can be calculated as:

$$\begin{aligned}
V_2 &= \frac{1}{C_2} \int -I_2 dt + V_{\text{off}} = -\frac{1}{C_2} \int \frac{V_{\text{off}} - V_1}{R} dt + V_{\text{off}} \\
&= -\frac{1}{C_2} \frac{V_{\text{off}}}{R} t + \frac{1}{RC_2} \int V_1 dt + V_{\text{off}} = -\frac{1}{C_2} \frac{V_{\text{off}}}{R} t + \frac{1}{RC_1 C_2} \int \frac{a \exp(-\frac{t}{T})}{R_{\text{gen}}} dt + V_{\text{off}} \\
&= -\frac{1}{C_2} \frac{V_{\text{off}}}{R} t + \frac{aT^2}{RR_{\text{gen}} C_1 C_2} \left[\exp(-\frac{t}{T}) \right]_{t_0}^{t_1} + V_{\text{off}} = -\frac{1}{C_2} \frac{V_{\text{off}}}{R} t + \frac{aT^2}{RR_{\text{gen}} C_1 C_2} \left(\exp(-\frac{t_1}{T}) - \exp(-\frac{t_0}{T}) \right) + V_{\text{off}} \\
&= -\frac{1}{C_2} \frac{V_{\text{off}}}{R} t + \frac{aT^2}{RR_{\text{gen}} C_1 C_2} \left(\exp(-\frac{t_1}{T}) - 1 \right) + V_{\text{off}} = -\frac{1}{C_2} \frac{V_{\text{off}}}{R} t + \frac{aT^2}{RR_{\text{gen}} C_1 C_2} \exp(-\frac{t_1}{T}) - \frac{aT^2}{RR_{\text{gen}} C_1 C_2} + V_{\text{off}}
\end{aligned}$$

The ratio is thus,

$$ratio = \frac{V_2}{V_1} = \frac{-\frac{1}{C_2} \frac{V_{off}}{R} t + \frac{aT^2}{RR_{gen} C_1 C_2} \exp\left(-\frac{t_1}{T}\right) - \frac{aT^2}{RR_{gen} C_1 C_2} + V_{off}}{\frac{1}{C_1} \frac{V_{off}}{R_{gen}} t + \frac{aT}{R_{gen} C_1} \exp\left(-\frac{t_1}{T}\right) - \frac{aT}{R_{gen} C_1} + V_{off}}$$

Assume, $\frac{aT^2}{RR_{gen} C_1 C_2} \exp\left(-\frac{t_1}{T}\right) \ll \frac{aT^2}{RR_{gen} C_1 C_2}$ and $\frac{aT}{R_{gen} C_1} \exp\left(-\frac{t_1}{T}\right) \ll \frac{aT}{R_{gen} C_1}$

$$ratio \approx \frac{-\frac{1}{C_2} \frac{V_{off}}{R} t - \frac{aT^2}{RR_{gen} C_1 C_2} + V_{off}}{\frac{1}{C_1} \frac{V_{off}}{R_{gen}} t - \frac{aT}{R_{gen} C_1} + V_{off}}$$

$$a = Exp\left(\frac{topStop}{(5 \cdot topStart)}\right) \cdot Exp\left(\frac{1}{(5 \cdot topStart)}\right)$$

topStop = topStart + topWidth

topStart = riseTime = 5

topWidth = 0

R_1 = the resistor between both integrators

R_{gen} = the resistor between the signal generator and the read-out electronics

C_2 = the capacitor in the feedback network of the first integrator

C_2 = the capacitor in the feedback network of the second integrator

V_{offset} = the self created offset value of the integrator

V_{rise} = the rise time value that is defined in the source code in Excel

a = a constant value that is defined in (6.3)

T = lifetime value

To able to check the result, the obtained ratios need to convert into an analogue representation. Let's assume, we take Time of 300 μ s. For this time value, we obtain 352 as digital representation of the lifetime value. The conversion, which is described earlier, is as follows:

$$analogue = \frac{digital}{2^n} V_{ref} = \frac{digital}{2^{10}} V_{ref} = \frac{digital}{1024} V_{ref} = \frac{digital}{1024} 2.5$$

n = number of bits

V_{ref} = reference voltage of the ADC converter

Thus, the analogue representation of 352 is:

$$analogue = \frac{352}{1024} 2.5 \approx 0.859$$

Solving this analogue representation in the ratio formula, we get a lifetime value that is equal to 1.6732 $\cdot 10^{-4}$ s. Ideally, this should be 150 μ s. The difference is because of the assumption. The assumption is made to ease to solve the equation. The error is about 10%. This error is acceptable if the lifetime value for each desired detectable oxygen level is significant. In case that this error is too large, the assumption is not valid. Then the non linear equation should be solved. To make this assumption valid, the integration can be extended.

6.5 Conclusions

The Agilent 33210A is the substitution of the oxygen sensor, since the real oxygen sensor does not show a significant difference in the fluorescence for different levels of oxygen. Agilent 33120A is a function generator that can generate many kinds of custom-made waveforms. Therefore, this device is the ideal substitution.

The fluorescence signal has been successfully integrated over the defined time period. However, there is an offset difference of the function generator and the read-out electronics. This offset difference gives an error in obtaining the lifetime. Therefore, to minimize the effect of this offset difference, the integration time is set before the complete fluorescence dies off.

For the testing purpose, the lifetime values are 20 times larger than the actual case. This is because the limited speed of the MSP430 that operates in the low-power-mode. To increase the speed of MSP430, we should exit the low-power-mode. However, the whole wireless protocol operates in this mode. To exit this mode, a complete new wireless protocol should be rewritten. Due to the limited time of this project, the fluorescence signal is increased by 20 times.

There is one phenomenon that is not well-understood. That is the clipping point of the integrators. According to the specification of the devices, both should be able to handle of the supply voltage, which is $\pm 5V$. The reality shows that both integrators clip at $\pm 3.2V$ which is beyond from the 5V. There is no clear clarification for this. There is no way to prevent this clipping phenomenon, since there is no clear cause. However, the clipping can be minimised by reducing the offset difference and keep the (peak) signal small.

Five measurements have been performed for different lifetime levels. The lifetime is increased by a fixed amount. The obtained results from the measurements, shows a linear relationship too. It is not perfect linear, because of the offset difference and the rise time period has taken into account. In real life, the offset difference can be omitted. The rise time of the fluorescence signal might be still an issue. But that depends on the response time of the photodiode that has been used.

To able to subtract the lifetime value, approximation has been used to calculate the value. For this approximation, it is assumed that the integration time is long enough to make this assumption valid. With the current integration period, the error is slightly more than 10%. If the lifetime value for different oxygen level is significant, this error is acceptable. To check this, this read-out electronics should be tested in real life, with the real oxygen sensor.

Chapter 7 – Evaluation of both read-out electronics

7.1 Introduction

In this chapter, the performance of the TNO's read-out electronics and the read-out electronics of the alternative approach is compared. The performance is based on the following criteria:

1. the size
2. the number of components
3. the power dissipation
4. the cost
5. the availability
6. the speed of measuring the oxygen
7. the accuracy of the circuit

7.2 The size and the number of components

The size is defined as the area that all components (in SMD mounting) of the read-out electronics will consume on a chip. Ideally, this should be as small as possible, since the electronics will be left in human body for a couple of days.

Looking at the circuits of both read-out electronics, the TNO circuit uses a lot more passive components than the alternative approach. However, these passive components can be very small. Summing up all the passive components of both circuits, we have 30 passive components (14 capacitors and 16 resistors) for the TNO circuit while we have 6 passive components (4 capacitors and 2 resistors) for the alternative approach. Based on the number of components only, the alternative circuit is a better choice. Even decoupling capacitors have been added. In both read-out electronics, we have passive component: the operational amplifier. TNO circuit has 3 of them while the alternative approach has 2 operational amplifiers. Table 7.2.1 shows the number of components and the minimal required chip area for both approaches.

Table 7.2.1: The number of components and the minimal required chip area for both approaches

	The number of components		The minimal required chip area [mm ³]	
	TNO	Alternative Approach	TNO	Alternative Approach
Capacitors	14	4	56.925819	8.054
Resistors	16	2	6.126125	0.325
Operational amplifiers	3	2	3865545.99	3.12256
Total	33	8	≈3865609	≈11.4

From this table, it can be concluded that the total size of all required components for the alternative approach is a few ten thousands smaller than all the required components of TNO's read-out electronics. This is due to the amount of components and the size of the operational amplifiers.

7.3 The maximal power dissipation and the cost of the read-out electronics

In this section, the power dissipation and the cost of both approaches have been evaluated. Table 7.3.1 shows the maximal power dissipation of each components and their commercial price that is based on the website of Farnell (The Netherlands country).

Table 7.3.1: The maximal power dissipation and the costs

	The maximal power dissipation [mW]		The cost [€] checked 15 th January 2011	
	TNO	Alternative Approach	TNO	Alternative Approach
Capacitors	1.51896319	0.007932521	3.674	0.306
Resistors	1303.5	126	0.618	0.387
Operational amplifiers	231	13	8.79	7.88
Total	≈1535.5	≈139	≈13	≈8.5

The maximal power dissipation of the TNO read-out electronics is about ten times larger than the read-out electronics of the alternative approach. This is also due to the amount of components. Also, TNO uses a “relative high power consuming” operational amplifier. One OPA355 consumes more power than all three AD8638 collectively.

Looking at the cost, again, the read-out electronics of TNO overpower the alternative approach. The TNO circuit uses a lot of capacitors which will dissipate a lot of power and cost more money.

One remarkable thing is the cost of OPA355. Three OPA355 is roughly as expensive as two AD8638. However, the total cost of all components of the alternative approach is almost twice lower.

7.4 The availability of components and the speed of obtaining the data

The stock of the required electronic components has been checked according to the store of the webshop of Farnell (The Netherlands as country base) on the 15th of January 2011. Table 7.4.1 gives an overview of the components and their stock.

General, it can be concluded that all components are largely in stock. The least amount of stock is the operational amplifier. The amount of stock of as well as OPA355 and the AD8638 is the lowest of all components. Their amount is a few hundreds, while other components exceed over a few thousands and some of them even exceed a few ten thousands.

The speed of obtaining the data (lifetime values) depends on the speed of the A/D converter. The speed of the A/D converter of the alternative approach uses a 200kHz oscillator. This converter operates in low-power mode which means, the operating frequency is slower. To able to finish one set of data, it took almost 90ms. The A/D converter of TNO is much faster. It can finish one set of data in a few microseconds. Thus, we can conclude that TNO can obtain data faster than the alternative approach.

Table 7.4.1: The availability of the components

Components	Required amount	Types	The stock, checked 15 th January 2011
	5	220k	28806
	2	2k20	3704
	1	330k	15274

TNO read-out electronics	<i>Resistors</i>	1	230k	9150
		1	10M	26497
		1	100k	24544
		1	33k	4551
		1	4k70	24349
		3	10	6028
	<i>Capacitors</i>	4	100nF	12329
		1	1pF	10240
		2	470nF	19243
		2	220nF	3206
		1	4.7pF	11364
		1	0.8pF	8815
		3	1uF	17250
<i>OpAmp</i>	3	OPA355	703	
The alternative approach	<i>Resistors</i>	1	19k	2293
		1	1k	17716
	<i>Capacitors</i>	2	100nF	12329
		2	1nF	53446
	<i>OpAmp</i>	2	AD8638	411

7.5 The accuracy of both circuits

In this section, the accuracy of both read-out electronics has been evaluated. The accuracy is based on the error that is made by both read-out electronics in order to subtract the lifetime values.

In chapter 6.4, the error of the alternative approach has been determined. The error is about 10%. This error is due to the approximation that is made to be able to calculate the lifetime in a simplified mathematics. In this section, the error of the alternative approach and the TNO method has been compared in a theoretical way.

Three kinds of errors will be present. These are:

1. The error at the beginning of the generation of the fluorescence signal. This error will not be taken into account of evaluating the performance of both read-out electronics, since it is not the error that is produced due or by the circuits.
2. Equivalent noise at input of the A/D converter. This noise is due to mismatch in the components. Since the read-out electronics of the alternative approach consists of much less (active) components, the equivalent noise source will be less. Hence, using the same power, the read-out electronics of the alternative approach will have a better signal to noise ratio.
3. The error at the input of the A/D converter, which is the quantisation error. The resolution in case of the alternative approach will be better, since the equivalent noise is less. However, this section examines the effect of the error contribution keeping at the same quantisation.

We have

$$I = I_0 \cdot e^{\left(\frac{-t}{T}\right)} + \Delta$$

as current source for both read-out electronics, since there some uncertainty about the current source due to the starting time of taking sample. The delta Δ denotes the uncertainty.

The effect of this uncertainty affects the accuracy of both read-out electronics in obtaining the life time value of the fluorescence signal, which will be discussed now.

Accuracy of the alternative approach

In chapter 4, the principle of obtaining the life time value using the alternative approach has been fully discussed. This alternative approach shows:

$$T = -\frac{I_2}{I_1} = -\frac{T^2 I_0 \cdot e^{\left(\frac{-t_2}{T}\right)}}{T I_0 \cdot e^{\left(\frac{-t_1}{T}\right)}} = -\frac{T^2 I_0 \cdot e^{\left(\frac{-t_1}{T}\right)}}{T I_0 \cdot e^{\left(\frac{-t_1}{T}\right)}}$$

t_1 and t_2 are the times of integration. These two time frames are the same, t_1 and t_2 . Quantisation error, Δ , can be found in obtaining the life time value, which results:

$$T = -\frac{I_2 + \Delta_2}{I_1 + \Delta_1}$$

This quantisation error introduces an error of:

$$T = -\frac{I_2 + \Delta_2}{I_1 + \Delta_1} = -\frac{(I_2 + \Delta_2)(I_1 - \Delta_1)}{(I_1 + \Delta_1)(I_1 - \Delta_1)} = -\frac{I_1 I_2 + \Delta_2 I_1 - \Delta_1 I_2 - \Delta_1 \Delta_2}{I_1^2 - \Delta_1^2}$$

Since the contribution of Δ is very small, its quadratic value and the product of them become even smaller. Therefore, we can approximate the life time value by:

$$T \approx -\frac{I_1 I_2 + \Delta_2 I_1 - \Delta_1 I_2}{I_1^2}$$

Developing this equation in more details, we have:

$$T \approx -\frac{I_1 I_2 + \Delta_2 I_1 - \Delta_1 I_2}{I_1^2} = -\frac{I_2}{I_1} - \frac{\Delta_2}{I_1} + \Delta_1 \frac{I_2}{I_1^2} = -\frac{I_2}{I_1} \left(1 + \frac{\Delta_2}{I_2} - \frac{\Delta_1}{I_1}\right) \quad (7.5.1)$$

Considering the worst case, the maximum quantisation error is:

$$\Delta_1 = \frac{I_{1,\max}}{2^N} = -\frac{I_0 T}{2^N} \text{ with } I_{1,\max} = \max(I_1(t)) = \max\left(\int I_0 e^{\frac{-t}{T}} dt\right) = -I_0 T$$

$$\Delta_2 = \frac{I_{2,\max}}{2^N} = \frac{I_0 T^2}{2^N} \text{ with } I_{2,\max} = \max(I_2(t)) = \max\left(\iint I_0 e^{\frac{-t}{T}} dt\right) = I_0 T^2$$

Substituting the quantisation errors in (7.5.1):

$$T = -\frac{I_2}{I_1} \left(1 + \frac{\frac{I_0 T^2}{2^N}}{I_2} - \frac{\frac{I_0 T}{2^N}}{I_1}\right) = -\frac{I_2}{I_1} \left(1 + \frac{\frac{I_0 T^2}{2^N}}{T^2 I_0 \cdot e^{\left(\frac{-t_2}{T}\right)}} - \frac{\frac{I_0 T}{2^N}}{T I_0 \cdot e^{\left(\frac{-t_1}{T}\right)}}\right)$$

$$\xrightarrow{\text{worstcase}} -\frac{I_2}{I_1} \left(1 + \frac{e^{\left(\frac{t_2}{T}\right)} + e^{\left(\frac{t_1}{T}\right)}}{2^N}\right) = -\frac{I_2}{I_1} \left(1 + \frac{2}{2^N}\right) = -\frac{I_2}{I_1} (1 + 2^{1-N}) \quad (7.5.2)$$

with $t_1 = t_2$ and $t_{1,2} = 0s$

Some important conclusions can be concluded from formula (7.5.2). This formula shows that the quantisation error is linear with $\frac{I_2}{I_1}$. Thus, the error has a linear relationship with T_{ideal} .

The additional term $(1 + 2^{1-N})$ is present due to integration principle.

Accuracy of TNO system

The principle of subtracting the life time has been in chapter 3. Ideally, we have:

$$\frac{I_1}{I_2} = \frac{I_0 \cdot e^{\left(\frac{-t_1}{T}\right)}}{I_0 \cdot e^{\left(\frac{-t_2}{T}\right)}} = e^{\left(\frac{-(t_1-t_2)}{T}\right)} \rightarrow T = -\frac{t_1-t_2}{\ln\left(\frac{I_1}{I_2}\right)}$$

The uncertainty is in obtaining the current values (I_1 and I_2). Hence, the ratio of the currents introduces an error of:

$$\begin{aligned} T &= -\frac{t_1-t_2}{\ln\left(\frac{I_1}{I_2}\right)} = -\frac{t_1-t_2}{\ln\left(\left(\frac{I_1}{I_2}\right)\left(1+\frac{\Delta_2}{I_2}-\frac{\Delta_1}{I_1}\right)\right)} = -\frac{t_1-t_2}{\ln\left(\frac{I_1}{I_2}\right)+\ln\left(1+\frac{\Delta_2}{I_2}-\frac{\Delta_1}{I_1}\right)} \\ &= -\frac{(t_1-t_2)\left(\ln\left(\frac{I_1}{I_2}\right)-\ln\left(1+\frac{\Delta_2}{I_2}-\frac{\Delta_1}{I_1}\right)\right)}{\ln^2\left(\frac{I_1}{I_2}\right)-\ln^2\left(1+\frac{\Delta_2}{I_2}-\frac{\Delta_1}{I_1}\right)} \approx -\frac{(t_1-t_2)\left(\frac{1}{\ln\left(\frac{I_1}{I_2}\right)}-\frac{\ln\left(1+\frac{\Delta_2}{I_2}-\frac{\Delta_1}{I_1}\right)}{\ln^2\left(\frac{I_1}{I_2}\right)}\right)}{\ln^2\left(\frac{I_1}{I_2}\right)} \end{aligned}$$

This approximation holds, since $\ln^2\left(\frac{I_1}{I_2}\right) \gg \ln^2\left(1+\frac{\Delta_2}{I_2}-\frac{\Delta_1}{I_1}\right)$ and $\ln^2\left(1+\frac{\Delta_2}{I_2}-\frac{\Delta_1}{I_1}\right)$ is close to zero.

Call $T_{ideal} = -\frac{t_1-t_2}{\ln\left(\frac{I_1}{I_2}\right)}$, hence we have:

$$T = T_{ideal} - T_{ideal} \cdot \frac{\ln\left(1+\frac{\Delta_2}{I_2}-\frac{\Delta_1}{I_1}\right)}{\ln\left(\frac{I_1}{I_2}\right)} \quad (7.5.3)$$

The maximum quantization error is:

$$\Delta_{1,2} = \frac{\max\left(I_0 \cdot e^{\left(\frac{-t_{1,2}}{T}\right)}\right)}{2^N} = \frac{I_0}{2^N}$$

Substituting the maximum quantization error in (7.5.3), results:

$$\begin{aligned} T &= T_{ideal} - T_{ideal} \cdot \frac{\ln\left(1+\frac{I_0}{2^N I_2}-\frac{I_0}{2^N I_1}\right)}{\ln\left(\frac{I_1}{I_2}\right)} = T_{ideal} - T_{ideal} \cdot \frac{\ln\left(1+\frac{I_0}{2^N I_0 \cdot e^{\left(\frac{-t_2}{T}\right)}}-\frac{I_0}{2^N I_0 \cdot e^{\left(\frac{-t_1}{T}\right)}}\right)}{\ln\left(\frac{I_0 \cdot e^{\left(\frac{-t_1}{T}\right)}}{I_0 \cdot e^{\left(\frac{-t_2}{T}\right)}}\right)} \\ &= T_{ideal} - T_{ideal} \cdot \frac{\ln\left(1+\frac{e^{\left(\frac{t_2}{T}\right)}}{2^N}-\frac{e^{\left(\frac{t_1}{T}\right)}}{2^N}\right)}{\ln\left(\frac{e^{\left(\frac{-t_1}{T}\right)}}{e^{\left(\frac{-t_2}{T}\right)}}\right)} \xrightarrow{\text{worstcase}} T_{ideal} - T_{ideal} \cdot \frac{\ln\left(1-\frac{e^{\left(\frac{t_2}{T}\right)} \pm e^{\left(\frac{t_1}{T}\right)}}{2^N}\right)}{\frac{-t_1+t_2}{T}} \end{aligned}$$

$$=Tideal -Tideal \cdot \frac{\ln(1-\frac{2}{2^N})}{\frac{-t_1+t_2}{T}} =Tideal -Tideal \cdot \frac{\ln(1-2^{1-N})}{\frac{-t_1+t_2}{T}} \quad (7.5.4)$$

From (7.5.4) we can conclude that the error has a not linear relationship with the lifetime value. The error in worst case is an exponential function, which is much larger than the alternative approach.

Using the alternative approach has another advantage. The t_1 and t_2 are the same, since both integrators have the same starting and ending time. This means that this read-out electronics is insensitive for introduction of delays in the circuits, while time t_1 and t_2 are crucial to be accurate to get an accurate value of life time. Any delay in time will affect the accuracy of the TNO circuits significantly.

7.6 Conclusions

In this chapter, the performances of the read-out electronics of TNO and the alternative approach have been compared. The performance is based on the seven criteria that are mentioned in the introduction of this chapter. A “good” performer is a circuit that requires the minimum total area that the components need when they are put on a PCB board. Comparing the total area of both read-out electronics, the circuits of the alternative requires area that is 3,5 times less compare to the TNO circuit. This is due to the large number components and the operational amplifiers that consume a lot of space.

The maximum power dissipation of the read-out electronics of TNO is more than 10 times larger. The main reason is the operational amplifier that has a higher maximum dissipation power. Also, due to the relatively large amount of components, the dissipation power is relatively higher.

Looking at the cost, the read-out electronics of TNO is almost twice as expensive. Although, the cost of building the TNO circuit is twice as expensive, the operational amplifier is cheaper than the one that the alternative approach uses.

The stock of all required components of both read-out electronics have been checked at the webshop of Farnell (The Netherlands) on the 15th of January 2011. All components are largely in stock. Therefore, we can say that both read-out electronics can be built without any limitation.

The speed of obtaining the lifetime value from the measurement depends on the speed of the A/D converter. Both read-out electronics are not able to retrieve the lifetime value within one period of time. In case of TNO circuit, the speed of the A/D converter is limited. In case of the alternative approach, there is no second A/D converter available. Although both read-out electronics are not able to finish the measurement within one period, the speed of TNO is faster.

In terms of the accuracy, the alternative approach has many advantages over the TNO circuits. The TNO circuit is very sensitive for delay in the signal. Based on the worst case scenario, the error of both systems is significant. The error of the alternative approach shows a linear relationship with the life time value, while the TNO circuit has an exponential relationship. Therefore, the quantisation error of the alternative approach is lower.

Chapter 8 – Conclusions and recommendations

8.1 Conclusions

For this Master of Science thesis, a research has been performed on creating a sensor system that is able to track the oxygen tension and carbon dioxide variations in real life. The temperature deviations have to be measured to be able to do temperature compensation for determining the oxygen and the carbon dioxide level. This sensor system will be used in human's body for detecting anastomotic leakage in the early stage to reduce the serious complications and death from a surgical operation on e.g. dissection on the colon.

HPTS-(TOA)₃ has been for detecting the carbon dioxide level. HPTS-(TOA)₃ is a pH indicator that does not solve in water and it is able to measure the carbon dioxide as well as in the air as in dissolved water. Two "protection" layers have been used for the so-called CO₂-sensor to keep HPTS-(TOA)₃ away from water environment and to make it a better sensor. These two layers are: 1. ethyl cellulose and 2. TEFLON.

Ethyl cellulose is essential to make the HPTS-(TOA)₃ a solid substance and to prevent that HPTS-(TOA)₃ is being taken away by liquid. The required amount of ethyl cellulose is 2.5 – 5% mass percentage. Since HPTS-(TOA)₃ does not solve in water, ethyl cellulose is mixed with a defined ratio of ethanol and toluene, 2 : 8. To increase the speed of solvability ethanol is first mixed with ethyl cellulose which after the whole substance toluene is added.

TEFLON is used for preventing that HPTS-(TOA)₃ will get mixed with liquid. This extra precaution is highly recommended.

The measurement of the carbon dioxide level is based on the duration of the fluorescence character of HPTS-(TOA)₃. In the fluorescence spectrum two specific excitation peaks can be obtained. They are located at $\lambda_{\text{excitation1}} = 395\text{nm}$ and at $\lambda_{\text{excitation2}} = 470\text{nm}$. The intensities of both peaks depend on the involved CO₂ amount. The emission peak that has been used is set at $\lambda_{\text{emission}} = 530\text{nm}$, because at this wavelength the intensity is the strongest.

In case of low concentration of CO₂, both peaks will have the strongest intensity. The intensity of both peaks will decrease when the CO₂ increases. The two excitation wavelengths use the ratio of both peaks to determine the CO₂ level. The big advantage of taking the ratio of both peaks is that the results of the measurements are independent of the setup variations. One excitation wavelength can also be used to measure the CO₂ level. This single wave measurement is very sensitive to the changes in the setup. However, one excitation wavelength has been used for developing the CO₂ sensor, since it can be easier integrated with the O₂ sensor.

HPTS-(TOA)₃ is not able to detect the complete range of CO₂. Since for a high level of CO₂, from 20% volume percentage, there is no significant difference in the intensity. Therefore, HPTS-(TOA)₃ can only be used for detecting CO₂ lower than 20%.

From the measurement results, it is proved that the chemical reaction of HPTS-(TOA)₃ with CO₂ is stable, reliable and reversible. The response time, time that is required for the chemical reaction with the CO₂, is approximately 3 minutes, which might be fast enough in the biomedical applications.

HPTS-(TOA)₃ is insensitive to other acid or base and it does not react with the present of O₂. Therefore, HPTS-(TOA)₃ is an outstanding material for detecting "low level" of CO₂.

The other focus of this Master thesis is on developing the oxygen sensor. TNO has a working oxygen sensor. However, this sensor requires three OpAmps with high bandwidth, 350MHz. TNO's circuit measures the average intensity values at different time frame to obtain the lifetime of the fluorescence signal. The oxygen level has been calculated via the Stern-Volmer formula.

Alternative approach of measuring the oxygen has been presented in this Master work. This new approach reduces the number of components, which also means the area can be saved. Moreover, this new method uses a very low bandwidth, relatively high bias current, low slew rate

and relatively large noise level OpAmp, AD8638. With this alternative approach, I want to show that it is still possible to obtain the lifetime value using relatively simple and a fewer components. Only two OpAmps are required to obtain the lifetime value, which means that the power consumption and cost can be reduced.

This alternative approach is based on the integration of the fluorescence signal. Similar assumption has been made as for TNO, that the decay of the fluorescence signal is a mono-exponential decay. Integration of an exponential function will return its original function plus its argument, which is the lifetime value. A division of a double integration and mono integration will give you lifetime value solely.

Simulations in PSpice have been performed to evaluate the performance of this alternative approach with hand-on calculations. Two kinds of current source, the so-called linear current source and the constant current source, have been used for evaluating the performances. There is always a mismatch in simulations and hand-on calculation for both current sources. This mismatch should be considered when the oxygen level has been determined, because the mismatch is larger than the error of the A/D converter.

The simulations show that this alternative approach is able to acquire the lifetime value using relative simple and fewer circuit components. Therefore, the cost can be reduced.

The obtained lifetime should be sent to the computer via a wireless platform. To save time, a commercial wireless device has been used. This wireless device contains two parts. The part that is attached to the computer that is so-called the Access Point, AP. The other part is the part that is attached to the read-out electronics that sends measured data to the AP. This part is called the End Device, ED.

Using this commercial device has two major disadvantages:

1. there is only one A/D converter
2. the limitation in the speed due to low-power mode

Since there is only one A/D converter, lifetime value cannot be obtained within one clock cycle. Only one measured result can be fed into an A/D converter. Since the A/D converter is embedded in the microcontroller, it is not possible to add another one.

To allow using the predefined wireless protocol, the wireless device should be operated in low power mode. This mode slows down the A/D converter. It takes about 90 μ s to finish the A/D conversion. The TNO system measures the oxygen level every 50 μ s (20kHz with 2% duty cycle). This means, that the speed to obtain the oxygen level of the alternative approach is slower, because of the limited speed of the A/D converter in the low power mode.

Agilent 33210A has been used as the substitution for the oxygen sensor. Different kinds of exponential functions have been generated to test the performance of the alternative approach. The generated waveforms are 20 times larger compare to the case of what TNO has been used. This is because of the limitation of the speed of the A/D converter that operates in low power mode.

Five different lifetime levels have been generated to test the performance of the alternative approach. The results have been presented in a graph (Figure 6.3.4). The graph shows a linear relationship of the obtained results. This is beyond of expectation, since the lifetime of the generated mono-exponential function is linear increased.

To obtain the lifetime value, an approximation has been applied to ease the calculation. This approximation introduces 10% error in retrieving of lifetime values. If the lifetime values of different levels of oxygen differ significant from each other, this approximation can be used.

There is one phenomenon that is not well-understood. That is the clipping point of the integrators. According to the specification of the devices, both should be able to handle of the supply voltage, which is $\pm 5V$. The reality shows that both integrators clip at $\pm 3.2V$ which is beyond from the 5V. There is no clear clarification for this. There is no way to prevent this clipping phenomenon, since there is no clear cause. However, the clipping can be minimised by reducing the offset difference and keep the (peak) signal small.

Comparing the performance of both read-out electronics, the alternative approach is a better choice, since the number of components is significantly less, the power consumption can be saved, the cost can be almost reduced twice and the area can be saved. The accuracy of the alternative is also better in terms of the contribution of the quantisation error.

8.2 Recommendations

HPTS-(TOA)₃ itself does not solve in water. But to make this acid able to determine the carbon dioxide level in real life, ethyl cellulose is added. Ethyl cellulose is a polymer that contains many holes in its molecule structure. Only small molecules can pass through this polymer which means that water molecules are prohibited to enter. Therefore, water molecules that are present in the HPTS-(TOA)₃ will remain at its place. Thus dry-out is prevented. Besides, water molecules that want to the polymer are excluded.

For extra precaution, TEFLON can be added to HPTS-(TOA)₃ and the ethyl cellulose. TEFLON is a reflective material that has pores which gasses with small molecule can pass through and it dissolve in water.

Some aspects should be kept in mind when using HPTS-(TOA)₃ for measuring CO₂ level. Temperature compensation should be applied and be aware of the setup variation, such as change in the position of the optical in the CO₂ box in case of single excitation wavelength. The HPTS-(TOA)₃ performs its best when it is not dried out. Therefore, make sure that this chemical substance is not dried out.

Compare the TNO system with the alternative approach, the speed of the measurements on determining the oxygen level is different. TNO system has a faster system than the alternative approach, because the microcontroller that has been used in the alternative approach operates in low power mode, which its speed is reduced. To fasten the speed, low power mode should not be used and a new WiFi protocol in C should be written.

The alternative approach uses an approximation to obtain the lifetime values for different levels of oxygen. This approximation can only be used if the lifetime values have a significant difference. If that is not the case, a new approximation has to be found to obtain a better accuracy, thus with less error.

Appendix

A. Source code of MSP-430, ACCESS POINT

```

//*****
// eZ430-RF2500 Temperature Sensor End Point
//
// Description: This is the Access Point software for the eZ430-2500RF
//             Temperature Sensing and Oxygen tension (pO2) measurement
//
//
// K.F. Tang
// Version 1.00
// TU Delft
// September 2009
// Built with IAR Embedded Workbench Version: 4.09A
//*****
//Change Log:
//*****
//Version: 2.00
//Version: 2.00
//Comments: Initial Release Version
//      pO2 is based on integrations of the whole fluorescence signal
//*****

#include "bsp.h"
#include "mrfi.h"
#include "bsp_leds.h"
#include "bsp_buttons.h"
#include "nwk_types.h"
#include "nwk_api.h"
#include "nwk_frame.h"
#include "nwk.h"

#include "msp430x22x4.h"
#include "vlo_rand.h"

#define MESSAGE_LENGTH 3
void TXString( char* string, int length );
void MCU_Init(void);
void transmitData(int addr, signed char rssi, char msg[MESSAGE_LENGTH] );
void transmitDataString(char addr[4],char rssi[3], char msg[MESSAGE_LENGTH]);
void createRandomAddress();
void USART_init();

__no_init volatile int tempOffset @ 0x10F4; // Temperature offset set at production
__no_init volatile char Flash_Addr[4] @ 0x10F0; // Flash address set randomly

// reserve space for the maximum possible peer Link IDs
static linkID_t sLID[NUM_CONNECTIONS];
static uint8_t sNumCurrentPeers;

// callback handler
static uint8_t sCB(linkID_t);
```

```

// work loop semaphores
static uint8_t sPeerFrameSem;
static uint8_t sJoinSem;
static uint8_t sSelfMeasureSem;

// mode data verbose = default, deg F = default
char verboseMode = 1;
char degCMode = 0;
int m = 0;
int upper, lower, header;

void main (void)
{
    addr_t IAddr;
    bspiState_t intState;

    WDTCTL = WDTPW + WDTHOLD; // Stop WDT
    {
        // delay loop to ensure proper startup before SimpliciTI increases DCO
        // This is typically tailored to the power supply used, and in this case
        // is overkill for safety due to wide distribution.
        volatile int i;
        for(i = 0; i < 0xFFFF; i++){}
    }
    if( CALBC1_8MHZ == 0xFF ) // Do not run if cal values are erased
    {
        volatile int i;
        P1DIR |= 0x03;
        BSP_TURN_ON_LED1();
        BSP_TURN_OFF_LED2();
        while(1)
        {
            for(i = 0; i < 0x5FFF; i++){}
            BSP_TOGGLE_LED2();
            BSP_TOGGLE_LED1();
        }
    }

    BSP_Init();

    if( Flash_Addr[0] == 0xFF &&
        Flash_Addr[1] == 0xFF &&
        Flash_Addr[2] == 0xFF &&
        Flash_Addr[3] == 0xFF )
    {
        createRandomAddress(); // set Random device address at initial startup
    }
    IAddr.addr[0]=Flash_Addr[0];
    IAddr.addr[1]=Flash_Addr[1];
    IAddr.addr[2]=Flash_Addr[2];
    IAddr.addr[3]=Flash_Addr[3];
    SMPL_ioctl(IOCTL_OBJ_ADDR, IOCTL_ACT_SET, &IAddr);

    MCU_Init();
    //Transmit splash screen and network init notification

```

```

//TXString( (char*)splash, sizeof splash);
// TXString( "\r\nInitializing Network...", 26 );
BSP_TOGGLE_LED2(); // turn on LED2 after MCU is initialised

SMPL_Init(sCB);
BSP_TOGGLE_LED1(); // turn on LED1

// USART_init();
// BSP_TOGGLE_LED2();

// network initialized
// TXString( "Done\r\n", 6);

// main work loop
while (1)
{
// Wait for the Join semaphore to be set by the receipt of a Join frame from a
// device that supports and End Device.

if (sJoinSem && (sNumCurrentPeers < NUM_CONNECTIONS))
{
// listen for a new connection
SMPL_LinkListen(&sLID[sNumCurrentPeers]);
sNumCurrentPeers++;
BSP_ENTER_CRITICAL_SECTION(intState);
if (sJoinSem)
{
sJoinSem--;
}
BSP_EXIT_CRITICAL_SECTION(intState);
}

// Have we received a frame on one of the ED connections?
// No critical section -- it doesn't really matter much if we miss a poll
if (sPeerFrameSem)
{
uint8_t msg[MAX_APP_PAYLOAD], len, i;
// process all frames waiting
for (i=0; i<sNumCurrentPeers; ++i)
{
if (SMPL_Receive(sLID[i], msg, &len) == SMPL_SUCCESS)
{
switch (msg[2]){
case 1:
header = 97;
upper = msg[0];
lower = msg[1];
// upper = 0;
// lower = 2;
while (!(IFG2&UCA0TXIFG)); // USCI_A0 TX buffer ready?
UCA0TXBUF = header;
while (!(IFG2&UCA0TXIFG));
UCA0TXBUF = upper;
while (!(IFG2&UCA0TXIFG));
UCA0TXBUF = lower;
while (!(IFG2&UCA0TXIFG));
}
}
}
}

```



```

BCSCTL1 = CALBC1_1MHZ;           // Set DCO to 1MHz
DCOCTL = CALDCO_1MHZ;
FCTL2 = FWKEY + FSSEL0 + FN1;    // MCLK/3 for Flash Timing Generator
FCTL3 = FWKEY + LOCKA;          // Clear LOCK & LOCKA bits
FCTL1 = FWKEY + WRT;            // Set WRT bit for write operation

Flash_Addr[0]=(rand>>8) & 0xFF;
Flash_Addr[1]=rand & 0xFF;
Flash_Addr[2]=(rand2>>8) & 0xFF;
Flash_Addr[3]=rand2 & 0xFF;

FCTL1 = FWKEY;                  // Clear WRT bit
FCTL3 = FWKEY + LOCKA + LOCK;   // Set LOCK & LOCKA bit
}

/*-----
*
-----*/
void transmitData(int addr, signed char rssi, char msg[MESSAGE_LENGTH] )
{
    char addrString[4];
    char rssiString[3];
    volatile signed int rssi_int;

    addrString[0] = '0';
    addrString[1] = '0';
    addrString[2] = '0'+(((addr+1)/10)%10);
    addrString[3] = '0'+((addr+1)%10);
    rssi_int = (signed int) rssi;
    rssi_int = rssi_int+128;
    rssi_int = (rssi_int*100)/256;
    rssiString[0] = '0'+(rssi_int%10);
    rssiString[1] = '0'+((rssi_int/10)%10);
    rssiString[2] = '0'+((rssi_int/100)%10);

    transmitDataString( addrString, rssiString, msg );
}

/*-----
*
-----*/
void transmitDataString(char addr[4],char rssi[3], char msg[MESSAGE_LENGTH] )
{
    char temp_string[] = {" XX.XC"};
    int temp = msg[0] + (msg[1]<<8);

    if( !degCMode )
    {
        temp = (((float)temp)*1.8)+320;
        temp_string[5] = 'F';
    }
    if( temp < 0 )
    {
        temp_string[0] = '-';
        temp = temp * -1;
    }
}

```

```

}
else if( ((temp/1000)%10) != 0 )
{
temp_string[0] = '0'+((temp/1000)%10);
}
temp_string[4] = '0'+(temp%10);
temp_string[2] = '0'+((temp/10)%10);
temp_string[1] = '0'+((temp/100)%10);

if( verboseMode )
{
char output_verbose[] = {"\r\nNode:XXXX,Temp:-XX.XC,Battery:X.XV,Strength:XXX%,RE:no "};

output_verbose[46] = rssi[2];
output_verbose[47] = rssi[1];
output_verbose[48] = rssi[0];

output_verbose[17] = temp_string[0];
output_verbose[18] = temp_string[1];
output_verbose[19] = temp_string[2];
output_verbose[20] = temp_string[3];
output_verbose[21] = temp_string[4];
output_verbose[22] = temp_string[5];

output_verbose[32] = '0'+(msg[2]/10)%10;
output_verbose[34] = '0'+(msg[2]%10);
output_verbose[7] = addr[0];
output_verbose[8] = addr[1];
output_verbose[9] = addr[2];
output_verbose[10] = addr[3];
TXString(output_verbose, sizeof output_verbose );
}
else
{
char output_short[] = {"\r\n$ADDR,-XX.XC,V.C,RSI,N#"};

output_short[19] = rssi[2];
output_short[20] = rssi[1];
output_short[21] = rssi[0];

output_short[8] = temp_string[0];
output_short[9] = temp_string[1];
output_short[10] = temp_string[2];
output_short[11] = temp_string[3];
output_short[12] = temp_string[4];
output_short[13] = temp_string[5];

output_short[15] = '0'+(msg[2]/10)%10;
output_short[17] = '0'+(msg[2]%10);
output_short[3] = addr[0];
output_short[4] = addr[1];
output_short[5] = addr[2];
output_short[6] = addr[3];
TXString(output_short, sizeof output_short );
}
}

```

```

}

/*-----
*
-----*/
void TXString( char* string, int length )
{
    int pointer;
    for( pointer = 0; pointer < length; pointer++)
    {
        volatile int i;
        UCA0TXBUF = string[pointer];
        while (!(IFG2&UCA0TXIFG));          // USCI_A0 TX buffer ready?
    }
}

/*-----
*
-----*/
void MCU_Init()
{
    BCSCTL1 = CALBC1_8MHZ;                // Set DCO
    DCOCTL = CALDCO_8MHZ;

    BCSCTL3 |= LFXT1S_2;                  // LFXT1 = VLO
    TACCTL0 = CCIE;                       // TACCR0 interrupt enabled
    TACCR0 = 12000;                       // ~1 second
    TACTL = TASSEL_1 + MC_1;              // ACLK, upmode

    P3SEL |= 0x30;                        // P3.4,5 = USCI_A0 TXD/RXD
    UCA0CTL1 = UCSSEL_2;                   // SMCLK
    UCA0BR0 = 0x41;                        // 9600 from 8Mhz
    UCA0BR1 = 0x3;                         // 8MHz 9600
    UCA0MCTL = UCBRS_2;                    // Modulation UCBRSx = 1
    UCA0CTL1 &= ~UCSWRST;                  // **Initialize USCI state machine**
    IE2 |= UCA0RXIE;                       // Enable USCI_A0 RX interrupt
    __enable_interrupt();
}

/*-----
*
-----*/
void USART_init(void){
    BCSCTL1 = CALBC1_8MHZ;                // Set DCO
    DCOCTL = CALDCO_8MHZ;

    P3SEL = 0x30;                        // P3.4,5 = USCI_A0 TXD/RXD
    UCA0CTL1 |= UCSSEL_2;                  // SMCLK
    UCA0BR0 = 0x41;                        // 9600 from 8Mhz
    UCA0BR1 = 0x3;                         // 8MHz 9600
    UCA0MCTL = UCBRS0;                     // Modulation UCBRSx = 1
    UCA0CTL1 &= ~UCSWRST;                  // **Initialize USCI state machine**
}

/*-----
*
-----*/
* Runs in ISR context. Reading the frame should be done in the
* application thread not in the ISR thread.

```

```

-----*/
static uint8_t sCB(linkID_t lid)
{
    if (lid)
    {
        sPeerFrameSem++;
    }
    else
    {
        sJoinSem++;
    }
    // leave frame to be read by application.
    return 0;
}

/*-----
* ADC10 interrupt service routine
-----*/
#pragma vector=ADC10_VECTOR
__interrupt void ADC10_ISR(void)
{
    __bic_SR_register_on_exit(CPUOFF);    // Clear CPUOFF bit from 0(SR)
}

/*-----
* Timer A0 interrupt service routine
-----*/
#pragma vector=TIMER_A0_VECTOR
__interrupt void Timer_A (void)
{
    sSelfMeasureSem = 1;
}

```

B. Source code of MSP-430, END DEVICE

```

/*****
// eZ430-RF2500 Temperature Sensor End Point
//
// Description: This is the Access Point software for the eZ430-2500RF
//              Temperature Sensing and Oxygen tension (pO2) measurement
//
//              MSP430F22x4
//              -----
//              ||      XIN|-
//              ||      |
//              --|RST   XOUT|-
//              |      |
//              |      P2.0|-->LED
//              |      P2.1|<--V1
//              |      P2.2|<--V2
//
// LED = controls the LED for turn on and off period
// V1 = output voltage of the first integrator
// V2 = output voltage of the second integrator
//
// K.F. Tang
// Version 2.00
// TU Delft
// August 2009
// Built with IAR Embedded Workbench Version: 4.09A
/*****
//Change Log:
/*****
//Version: 2.00
//Version: 2.00
//Comments: Initial Release Version
//          pO2 is based on integrations of the whole fluorescence signal
/*****

#include "bsp.h"
#include "mrfl.h"
#include "nwk_types.h"
#include "nwk_api.h"
#include "bsp_leds.h"
#include "bsp_buttons.h"
#include "vlo_rand.h"

void linkTo(void);
void MCU_Init(void);
void TXString( char* string, int length );
void MCU_Init();
void delay(int us);
void nop();

__no_init volatile int tempOffset @ 0x10F4; // Temperature offset set at production
__no_init volatile char Flash_Addr[4] @ 0x10F0; // Flash address set randomly

static char number[6];

```

```

/* integer to a String conversion, assuming the receiving data is 2 bytes */
void convert(int num){
    //I assume there are only two bytes.. so max 65535
    number[0] = num / 10000;
    num -= number[0]*10000;
    number[1] = num / 1000;
    num -= number[1]*1000;
    number[2] = num / 100;
    num -= number[2]*100;
    number[3] = num / 10;
    num -= number[3] * 10;
    number[4] = num;

    number[0] += 48;
    number[1] += 48;
    number[2] += 48;
    number[3] += 48;
    number[4] += 48;
    number[5] = '\0';
}

static char getal[4];
void shortc(uint8_t num){
    getal[0] = num / 100;
    num -= getal[0]*100;
    getal[1] = num / 10;
    num -= getal[1] * 10;
    getal[2] = num;

    getal[0] += 48;
    getal[1] += 48;
    getal[2] += 48;
    getal[3] = '\0';
}

/*
input  : result of the ADC with the voltage shift
output : ADC result without voltage shift
function: cancelling out the voltage shift due to the fixed voltage at the
         + terminal on the OpAmp, because the ADC only accepts positive values
NOTE   : offset is the voltage shift
         offset = ((^n)*(Voffset/Vref)
                 (2^n)*((R1/R2)*Vcc)/Vref)
                 (2^10)*((1.02/7.8)*5)/1.5
                 = 446

int offset = 446;
static uint8_t adcNew; // new register for storing the ADC result w/o voltage shift
void cancel(int adc){
    adcNew = adc - offset;
}
*/

//static uint8_t ad[2];
/*
ad[0] = the divider factor

```

```

ad[1] = the rest term
ad[2] = my header, objective: to distinguish the measurements
*/
static uint8_t ad[3];
/* the storage of the ADC, splitting the results in two registers */
/*
void splitter(int adcNew){
    ad[0] = adcNew / 255;
    adcNew -= ad[0]*255;
    ad[1] = adcNew;
}
*/

void splitter(store){
    ad[0] = store / 255;
    store -= ad[0]*255;
    ad[1] = store;
}

void createRandomAddress();

void main (void)
{
    addr_t lAddr;
    WDTCTL = WDTPW + WDTHOLD;           // Stop WDT
    {
        // delay loop to ensure proper startup before SimpliciTI increases DCO
        // This is typically tailored to the power supply used, and in this case
        // is overkill for safety due to wide distribution.
        volatile int i;
        for(i = 0; i < 0xFFFF; i++){}
    }
    if( CALBC1_8MHZ == 0xFF )           // Do not run if cal values are erased
    {
        volatile int i;
        P1DIR |= 0x03;
        BSP_TURN_ON_LED1();
        BSP_TURN_OFF_LED2();
        while(1)
        {
            for(i = 0; i < 0x5FFF; i++){}
            BSP_TOGGLE_LED2();
            BSP_TOGGLE_LED1();
        }
    }
}

// SimpliciTI will change port pin settings as well
P1DIR = 0xFF;
P1OUT = 0x00;
//P2DIR = 0x27;
P2DIR = 0x21; // self added
P2DIR = 0x10;
P2OUT = 0x00;
P3DIR = 0xC0;
P3OUT = 0x00;
P4DIR = 0x0F;

```

```

// P4DIR = 0x10;// the constant current, make Pin4.4 as the output direction
// P4DIR = 0x20;// the constant current, make Pin4.5 as the output direction
// P4DIR = 0x40;
P4OUT = 0x00;

BSP_Init();
MCU_Init();
TXString( "\n\nTestje.....", 15 );

if( Flash_Addr[0] == 0xFF &&
    Flash_Addr[1] == 0xFF &&
    Flash_Addr[2] == 0xFF &&
    Flash_Addr[3] == 0xFF )
{
    createRandomAddress();          // set Random device address at initial startup
}
IAddr.addr[0]=Flash_Addr[0];
IAddr.addr[1]=Flash_Addr[1];
IAddr.addr[2]=Flash_Addr[2];
IAddr.addr[3]=Flash_Addr[3];
SMPL_ioctl(IOCTL_OBJ_ADDR, IOCTL_ACT_SET, &IAddr);
BCSCTL1 = CALBC1_8MHZ;             // Set DCO after random function
DCOCTL = CALDCO_8MHZ;

BCSCTL3 |= LFXT1S_2;              // LFXT1 = VLO
TACCTL0 = CCIE;                   // TACCR0 interrupt enabled
TACCR0 = 12000;                   // ~ 1 sec
TACTL = TASSEL_1 + MC_1;          // ACLK, upmode
// keep trying to join until successful. toggle LEDS to indicate that
// joining has not occurred. LED3 is red but labeled LED 4 on the EXP
// board silkscreen. LED1 is green.
while (SMPL_NO_JOIN == SMPL_Init((uint8_t (*)(linkID_t))0))
{
    BSP_TOGGLE_LED1();
    BSP_TOGGLE_LED2();
    __bis_SR_register(LPM3_bits + GIE); // LPM3 with interrupts enabled
}
// unconditional link to AP which is listening due to successful join.
linkTo();
}

void createRandomAddress()
{
    unsigned int rand, rand2;
    do
    {
        rand = TI_getRandomIntegerFromVLO(); // first byte can not be 0x00 or 0xFF
    }
    while( (rand & 0xFF00)==0xFF00 || (rand & 0xFF00)==0x0000 );
    rand2 = TI_getRandomIntegerFromVLO();

    BCSCTL1 = CALBC1_1MHZ;          // Set DCO to 1MHz
    DCOCTL = CALDCO_1MHZ;
    FCTL2 = FWKEY + FSSEL0 + FN1;   // MCLK/3 for Flash Timing Generator
    FCTL3 = FWKEY + LOCKA;         // Clear LOCK & LOCKA bits
    FCTL1 = FWKEY + WRT;           // Set WRT bit for write operation
}

```

```

Flash_Addr[0]=(rand>>8) & 0xFF;
Flash_Addr[1]=rand & 0xFF;
Flash_Addr[2]=(rand2>>8) & 0xFF;
Flash_Addr[3]=rand2 & 0xFF;

FCTL1 = FWKEY;           // Clear WRT bit
FCTL3 = FWKEY + LOCKA + LOCK; // Set LOCK & LOCKA bit
}

void linkTo()
{
    linkID_t linkID1;

    int stage = 1; // stage of sending sequence
    int store;     // temp. register for AD storage
    // keep trying to link...
    while (SMPL_SUCCESS != SMPL_Link(&linkID1))
    {
        __bis_SR_register(LPM3_bits + GIE); // LPM3 with interrupts enabled
        BSP_TOGGLE_LED1();
        BSP_TOGGLE_LED2();
    }
    // Turn off all LEDs
    if (BSP_LED1_IS_ON())
    {
        BSP_TOGGLE_LED1();
    }
    if (BSP_LED2_IS_ON())
    {
        BSP_TOGGLE_LED2();
    }
}

while (1)
{
    volatile long temp;
    uint8_t degC;
    //Power down of the radio is done through the SMPL_ioctl() call
    SMPL_ioctl( IOCTL_OBJ_RADIO, IOCTL_ACT_RADIO_SLEEP, "" );
    __bis_SR_register(LPM3_bits+GIE); // LPM3 with interrupts enabled
    SMPL_ioctl( IOCTL_OBJ_RADIO, IOCTL_ACT_RADIO_AWAKE, "" );

    switch (stage){
        case 1:
            /* A/D for A10 temperature measurement*/
            BSP_TOGGLE_LED2();
            P2DIR = 0x01; // set P2.0 as the output
            ADC10CTL1 = INCH_10 + ADC10DIV_4; // Temp Sensor ADC10CLK/5
            ADC10CTL0 = SREF_1 + ADC10SHT_3 + REFON + ADC10ON + ADC10IE + ADC10SR;
            for( degC = 240; degC > 0; degC-- ); // delay to allow reference to settle
            ADC10CTL0 |= ENC + ADC10SC; // Sampling and conversion start
            __bis_SR_register(CPUOFF + GIE); // LPM0 with interrupts enabled
            store = ADC10MEM;
            ADC10CTL0 &= ~ENC;
            ADC10CTL0 &= ~(REFON + ADC10ON); // turn off A/D to save power
            /*

```

```

oC = ((A10/1024)*1500mV)-986mV)*1/3.55mV = A10*423/1024 - 278
the temperature is transmitted as an integer where 32.1 = 321
hence 4230 instead of 423
*/
// degC = ((store - 673) * 4230) / 1024;
degC = ((store*423)/1023) - 278;
if( tempOffset != 0xFFFF ){
degC += tempOffset;
}
splitter(degC);
ad[2] = 1;
/*Send the digital data of the output voltage of the first OpAmp*/
if (SMPL_SUCCESS == SMPL_Send(linkID1, ad, sizeof(ad))){
    BSP_TOGGLE_LED2();
    P2OUT |= 0x01; // turn on the LED
}
else{
    BSP_TOGGLE_LED2();
    BSP_TOGGLE_LED1();
}
stage = 2;
break;

case 2:
/* A/D for A1 to measure the output voltage of the first OpAmp*/
// discharge the capacitor for ~1us first, before integration
// while discharging the capacitor, the LED should be turned on
// delay(1); // wait ~52us to capture the entire fluorescence signal
/*
TBCCTL0 = CCIE; // TBCCR0 interrupt enabled
TBCCR0 = 20000;
TBCTL = TBSSEL_2 + MC_1; // SMCLK, upmode
*/
P2OUT |= 0x01;// turn on the LED again
delay(5);
P2OUT ^= 0x01; // XOR the Pin2.0 to turn off the switch
// P2OUT |= 0x10; // OR Pin2.5, activate the current
ADC10AE0 |= 0x02; // A1, convert A1 into input
delay(10);
ADC10CTL1 = INCH_1; // P2.1 = output voltage of the 1st OpAmp
ADC10CTL0 = SREF_1 + ADC10SHT_2 + REFON + ADC10ON + ADC10IE; // Sampling
for( degC = 240; degC > 0; degC-- ); // delay to allow reference to settle
ADC10CTL0 |= ENC + ADC10SC; // conversion start
// P4OUT ^= 0x20; // XOR Pin4.5, deactivate the current
P2OUT ^= 0x10; // XOR Pin2.5, activate the current
__bis_SR_register(CPUOFF + GIE); // LPM0, ADC10_ISR will force exit
store = ADC10MEM;
splitter(store);
ad[2] = 2;
ADC10CTL0 &= ~ENC;
ADC10CTL0 &= ~(REFON + ADC10ON);
/*Send the digital data of the first OpAmp to the AP*/
if (SMPL_SUCCESS == SMPL_Send(linkID1, ad, sizeof(ad))){
    BSP_TOGGLE_LED2();
// P2OUT |= 0x01;// turn on the LED again
}
}

```

```

else{
    BSP_TOGGLE_LED2();
    BSP_TOGGLE_LED1();
}
stage = 3;
break;

case 3:
/* A/D for A2 to measure the output voltage of the second OpAmp*/
P2OUT |= 0x01;
delay(5);
P2OUT ^= 0x01; // XOR the Pin2.0 to turn off the switch
// P2OUT |= 0x10;
ADC10AE0 |= 0x04; // A2, convert A2 into input
delay(10);
ADC10CTL1 = INCH_2; // P2.2 = output voltage of the 2nd OpAmp
ADC10CTL0 = SREF_1 + ADC10SHT_2 + REFON + ADC10ON + ADC10IE;
for( degC = 240; degC > 0; degC-- ); // delay to allow reference to settle
ADC10CTL0 |= ENC + ADC10SC;
// P4OUT ^= 0x20;
P2OUT ^= 0x10;
__bis_SR_register(CPUOFF + GIE);
store = ADC10MEM;
splitter(store);
ad[2] = 3;
ADC10CTL0 &= ~ENC;
ADC10CTL0 &= ~(REFON + ADC10ON);
/*Send the digital data of the second voltage to the AP*/
if (SMPL_SUCCESS == SMPL_Send(linkID1, ad, sizeof(ad))){
    BSP_TOGGLE_LED2();
// P2OUT |= 0x01;
}
else{
    BSP_TOGGLE_LED2();
    BSP_TOGGLE_LED1();
}
stage = 4;
break;
/*
case 4:
    ad[2] = 4;
    if (SMPL_SUCCESS == SMPL_Send(linkID1, ad, sizeof(ad))){
        BSP_TOGGLE_LED2();
    }
    else{
        BSP_TOGGLE_LED2();
        BSP_TOGGLE_LED1();
    }
stage = 1;
*/
default:
stage = 1;
break;
}
}
}

```

```

/*-----
* ADC10 interrupt service routine
-----*/
#pragma vector=ADC10_VECTOR
__interrupt void ADC10_ISR(void)
{
    __bic_SR_register_on_exit(CPUOFF);    // Clear CPUOFF bit from 0(SR)
}

/*-----
* Timer A0 interrupt service routine
-----*/
#pragma vector=TIMER_A0_VECTOR
__interrupt void Timer_A (void)
{
    __bic_SR_register_on_exit(LPM3_bits);    // Clear LPM3 bit from 0(SR)
}

/*-----
*
-----*/
void TXString( char* string, int length )
{
    int pointer;
    for( pointer = 0; pointer < length; pointer++)
    {
        volatile int i;
        UCA0TXBUF = string[pointer];
        while (!(IFG2&UCA0TXIFG));    // USCI_A0 TX buffer ready?
    }
}

/*-----
*
-----*/
void MCU_Init()
{
    BCSCCTL1 = CALBC1_8MHZ;    // Set DCO
    DCOCTL = CALDCO_8MHZ;

    BCSCCTL3 |= LFXT1S_2;    // LFXT1 = VLO
    TACCTL0 = CCIE;    // TACCR0 interrupt enabled
    TACCR0 = 12000;    // ~1 second
    TACTL = TASSEL_1 + MC_1;    // ACLK, upmode

    P3SEL |= 0x30;    // P3.4,5 = USCI_A0 TXD/RXD
    UCA0CTL1 = UCSSEL_2;    // SMCLK
    UCA0BR0 = 0x41;    // 9600 from 8Mhz
    UCA0BR1 = 0x3;
    UCA0MCTL = UCBRS_2;
    UCA0CTL1 &= ~UCSWRST;    // **Initialize USCI state machine**
    IE2 |= UCA0RXIE;    // Enable USCI_A0 RX interrupt
    __enable_interrupt();
}

/*-----
*
-----*/

```

```
void delay(int us){
  int count = 2;
  count = us * count;
  while(count){
    count--;
  }
}

void nop(){
}
```

C. Source code of Agilent 33120A

Option Explicit

```
.....
' Copyright © 2001 Agilent Technologies Inc. All rights
' reserved.
'
' You have a royalty-free right to use, modify, reproduce and distribute
' the Sample Application Files (and/or any modified version) in any way
' you find useful, provided that you agree that Agilent has no
' warranty, obligations or liability for any Sample Application Files.
'
' Agilent Technologies provides programming examples for illustration only,
' This sample program assumes that you are familiar with the programming
' language being demonstrated and the tools used to create and debug
' procedures. Agilent support engineers can help explain the
' functionality of Agilent software components and associated
' commands, but they will not modify these samples to provide added
' functionality or construct procedures to meet your specific needs.
.....

' This program uses the arbitrary waveform function to
' download and output a square wave pulse with calculated
' rise and fall times. The waveform consists of 4000
' points downloaded to the function generator as ASCII data.
Dim FGen As VisaComLib.FormattedIO488

Public Sub LoadWaveform()
    Dim strData As String

    GetWorksheetData "A2:b500", strData

    ' reset instrument
    With FGen
        .WriteString "*RST"

        ' set timeout large enough to sent all data
        .IO.Timeout = 40000
        ' download data points to volatile memory from array
        .WriteString "Data Volatile, " & strData

        .WriteString "Data:Copy Pulse, Volatile" ' Copy arb to non-volatile memory
        .WriteString "Function:User Pulse" ' Select the active arb waveform
        .WriteString "Function:Shape User" ' output selected arb waveform
        .WriteString "BM:NCYC 1" ' # cyles
        .WriteString "BM:STAT ON" ' enable the burst mode
        .WriteString "TRIG:SOUR EXT" ' TRIGger:SOURce {IMMediate|EXTernal|BUS}
        .WriteString "TRIG:SLOP NEG" ' TRIGger:SLOPe {POSitive|NEGative}
        .WriteString "Output:Load 50" ' Output termination is 50 ohms
        .WriteString "OUTP:SYNC ON" ' synch is activated
        .WriteString "Frequency 5000; Voltage 1.2" ' Ouput frequency is 5kHz @ 2.5 Vpp
        .WriteString "Frequency 1000; Voltage 1.25" ' Ouput frequency is 1kHz @ 2.5 Vpp
        .WriteString "VOLT:OFFS 0.50" ' VOLTage:OFFSet = 800mV
        .WriteString "VOLT:OFFS 0.285" ' VOLTage:OFFSet = 570mV
    End With
End Sub
```

End With

' the arb will require some time to set everything up at this point

End Sub

Sub makePulse(ByVal riseTime As Long, ByVal topWidth As Long, ByVal fallTime As Long)

Dim Waveform(1 To 4000) As String

Dim topStart As Long

Dim topStop As Long

Dim endPulse As Long

Dim i As Long

topStart = riseTime

topStop = topStart + topWidth

endPulse = topStop + fallTime

' set the heading in worksheet

Cells(1, 1) = "Point"

Cells(1, 2) = "Value"

' Set rise time

For i = 1 To riseTime

Cells(i + 1, 1) = i

Cells(i + 1, 2) = -(i - 1) / riseTime

Next i

' set pulse width

For i = riseTime + 1 To topStop

Cells(i + 1, 1) = i

Cells(i + 1, 2) = -1

Next i

' set fall time

For i = topStop + 1 To endPulse

Cells(i + 1, 1) = i

'Cells(i + 1, 2) = -Exp(-(i - topStop) / (topStart)) ' ~ 5us

'Cells(i + 1, 2) = -Exp(-(i - topStop) / (2 * topStart)) ' ~ 10us

'Cells(i + 1, 2) = -Exp(-(i - topStop) / (3 * topStart)) ' ~ 15us

'Cells(i + 1, 2) = -Exp(-(i - topStop) / (4 * topStart)) ' ~ 20us

'Cells(i + 1, 2) = -Exp(-(i - topStop) / (5 * topStart)) ' ~ 25us

'Cells(i + 1, 2) = -Exp(-(i - topStop - 1) / (topStart)) ' ~ 5us

'Cells(i + 1, 2) = -Exp(-(i - topStop - 1) / (2 * topStart)) ' ~ 10us

'Cells(i + 1, 2) = -Exp(-(i - topStop - 1) / (3 * topStart)) ' ~ 15us

'Cells(i + 1, 2) = -Exp(-(i - topStop - 1) / (4 * topStart)) ' ~ 20us

'Cells(i + 1, 2) = -Exp(-(i - topStop - 1) / (5 * topStart)) ' ~ 25us

'Cells(i + 1, 2) = -Exp(-(i - topStop - 1) / (4 * topStart)) ' ~ 100us

'Cells(i + 1, 2) = -Exp(-(i - topStop - 1) / (8 * topStart)) ' ~ 200us

Cells(i + 1, 2) = -Exp(-(i - topStop - 1) / (12 * topStart)) ' ~ 300us

'Cells(i + 1, 2) = -Exp(-(i - topStop - 1) / (16 * topStart)) ' ~ 400us

'Cells(i + 1, 2) = -Exp(-(i - topStop - 1) / (20 * topStart)) ' ~ 500us

Next i

```

' set zero level for rest of points
For i = endPulse + 1 To 4000
    Cells(i + 1, 1) = i
    Cells(i + 1, 2) = 0
    'Cells(i + 1, 2) = -Exp(-(i - topStop) / (fallTime))
Next i

End Sub

Public Sub GetWorksheetData(ByVal rangeAddress As String, strRecord As String)
' gets the data from the worksheet and puts it into very long string
Dim rng As Range
Dim dblTemp As Double
Dim strTemp As String
Dim rowCount As Long
Dim i As Long

Set rng = Range("b2:B1000")

rowCount = rng.Rows.Count

For i = 1 To rowCount - 1
    dblTemp = rng.Cells(i, 1)
    ' reduce the number of digits to make it faster
    strTemp = ConvertToString(dblTemp)
    strRecord = strRecord & strTemp & ","
Next i

dblTemp = rng.Cells(i, 1)
strTemp = ConvertToString(dblTemp)
' there is no comma on the last one
strRecord = strRecord & strTemp

End Sub

Private Function ConvertToString(number As Double) As String
' Converts the number to a string without using too many digits
' accounts for the number having a comma ',' instead of a decimal
' on the spread sheet in some locales
Dim strTemp As String

' reduce the number of digits to make it faster
strTemp = Format$(number, "0.000E+0")

' This is required only for locales that use ',' as a radix
' changes the comma to a decimal that the instrument requires
' in European locales
If InStr(1, strTemp, ",") Then
    Mid(strTemp, InStr(1, strTemp, ",")) = "."
End If

ConvertToString = strTemp

End Function
Sub SetIO()

```

```

' set the I/O address to the text box in case the
' user changed it.
' bring up the input dialog and save any changes to the
' text box
Dim mgr As AgilentRMLib.SRMClS
Dim ioaddress As String

On Error GoTo ioError

ioaddress = Cells(10, 5)
ioaddress = InputBox("Enter the IO address of the DMM", "Set IO address", ioaddress)

If Len(ioaddress) > 5 Then
    Set mgr = New AgilentRMLib.SRMClS
    Set FGen = New VisaComLib.FormattedIO488
    Set FGen.IO = mgr.Open(ioaddress)
    Cells(10, 5) = ioaddress
End If

Exit Sub

ioError:
    MsgBox "Set IO error:" & vbCrLf & Err.Description
End Sub

```

D. Comparison of different OpAmps for implementing the read-out electronics based on the alternative approach

The alternative read-out system is based on extracting of the lifetime, τ , with the help of integration method. For this method new readout electronics has been developed. This new readout electronics requires less bandwidth of the operational amplifier and the number of components can be reduced. The disadvantage of this new circuit is, that is not fully proved for its perfect functioning yet. Therefore, the real-life performances of both approaches cannot be compared directly. Also, this new sensor is not being calibrated to operate perfectly in all kind of conditions.

The new approach takes out the lifetime of the fluorescence signal, which can be related to the O_2 level. This relationship of the lifetime with the oxygen level is given by the Stern-Volmer equation:

$$\frac{\tau_0}{\tau} = 1 + C_{SV} \cdot [O_2] \quad (D.1)$$

τ_0 = the fluorescence lifetime at quencher (O_2) concentration zero

τ = the fluorescence lifetime at a specific quencher (O_2) concentration

C_{SV} = Stern-Volmer constant

$[O_2]$ = oxygen concentration

The readout electronic of the new approach uses two integrators to extract the lifetime of the fluorescence signal. The idea is based on the mathematical determination of a constant, which is in this case the lifetime, τ , by integrating the exponential twice and which after a division is done. The following formulas show this concept.

Assume the fluorescence signal is represented by

$$f(t) = a \cdot e^{-\frac{t}{\tau}} \quad (D.2)$$

$f(t)$ = function of the fluorescence signal

a = amplitude of the starting value of the fluorescence signal

t = time

τ = lifetime

Now, integrating this gives:

$$F_1(t) = \int f(t) \cdot dt = \int a \cdot e^{-\frac{t}{\tau}} \cdot dt = -a \cdot \tau \cdot e^{-\frac{t}{\tau}} \quad (D.3)$$

$$F_2(t) = \iint f(t) \cdot dt = \iint \left(a \cdot e^{-\frac{t}{\tau}} \right) \cdot dt = \left[a \cdot \tau^2 \cdot e^{-\frac{t}{\tau}} \right] \quad (D.4)$$

$$= a \cdot \tau^2 \cdot e^{-\frac{t}{\tau}}$$

$F_1(t)$ and $F_2(t)$ are the first and the second integral over the signal respectively. The ratio of both integrals gives us the lifetime:

$$\frac{F_2}{F_1} = \frac{a \cdot \tau^2 \cdot e^{-\frac{t}{\tau}}}{-a \cdot \tau \cdot e^{-\frac{t}{\tau}}} = -\tau \quad (D.7)$$

It is assumed that the decay of the fluorescence signal is a monoexponential function. In real life, the integration has been realised by using electronic circuits. These circuits will be discussed in the first section. The second section, simulations with the three operational amplifiers that are described in the previous chapter will be performed. Moreover, two different types of current source have been introduced to test the reliability of this new approach. They are named as the constant and linear current sources that act as the fluorescence signal. This chapter ends with conclusion.

D.1 Realisation of the readout electronics for the alternative approach

The readout electronic should be able to extract the lifetime, τ , to determine the O_2 level. The photodiode is represented by a simple pulse current source. The rise time, the fall time, the duty cycle, delay and the amplitude of the current can be perfectly matched with the real photodiode that has been used. The fluorescence signal is represented by the fall time of the pulse.

The simulation is performed in PSpice9.1. In this simulation program, there is also a current source which can generate an exponential decay. This source has not been used, because the analysis in PSpice will become more complex. When the readout electronic proves its proper working for the simple constant source and the linear source, this new circuit should also work for an exponential source. The constant and the linear sources will be discussed later on to clarify the idea.

To able to do the integration of the current, capacitor has been used. The value of this capacitor depends on the charge and discharge time. The period of the photodiode is about 20kHz and it has a duty cycle of 2%. When the light pulse is on, the capacitor should be fully discharged. After the light pulse is fully turned off, the capacitor has to be charged slowly to prevent exceeding the reference voltage of the A/D converter, V_{ref} . This reference voltage is set at 1.5V. Because the turn-on time of the light pulse is very short (only 1 μ s), discharging the capacitor should be very fast. This means, that the impedance of the turned on MOS transistor should be as low as possible.

MOS transistor is used as the switch. MOS transistor is preferred to bipolar transistor, because no current can flow from the gate to the source terminal of the MOS transistor, which influences the measurement. In the simulation, the ideal switch with a specific resistor is used to characterize the MOS transistor. However, the parameters of the ideal switch can be tweaked to match the MOS transistor that will be used in real life.

The microcontroller is used for controlling the switch. The microcontroller is symbolised as a simple pulse voltage source. The duty cycle and the period are perfectly matched with the photodiode to ensure that the capacitor is charged and discharged correctly.

The last main component is the operational amplifier. Operational amplifier is required to allow the charging and discharging of capacitor. In case of this simulation setup, the integration will work without the presence of the amplifier. In real life, the pulse current source is a photodiode. Without the amplifier, the capacitor will not discharge well, since the built-up voltage across the capacitor will activate the photodiode.

The integration methods that have been shown in (D.3) and in (D.4), have been realised by using the integrators that are connected in series. The fluorescence can be modelled as a current source. In able to integrated current, capacitor has been used. The setup of the new approach has been shown in Figure A.1.1.

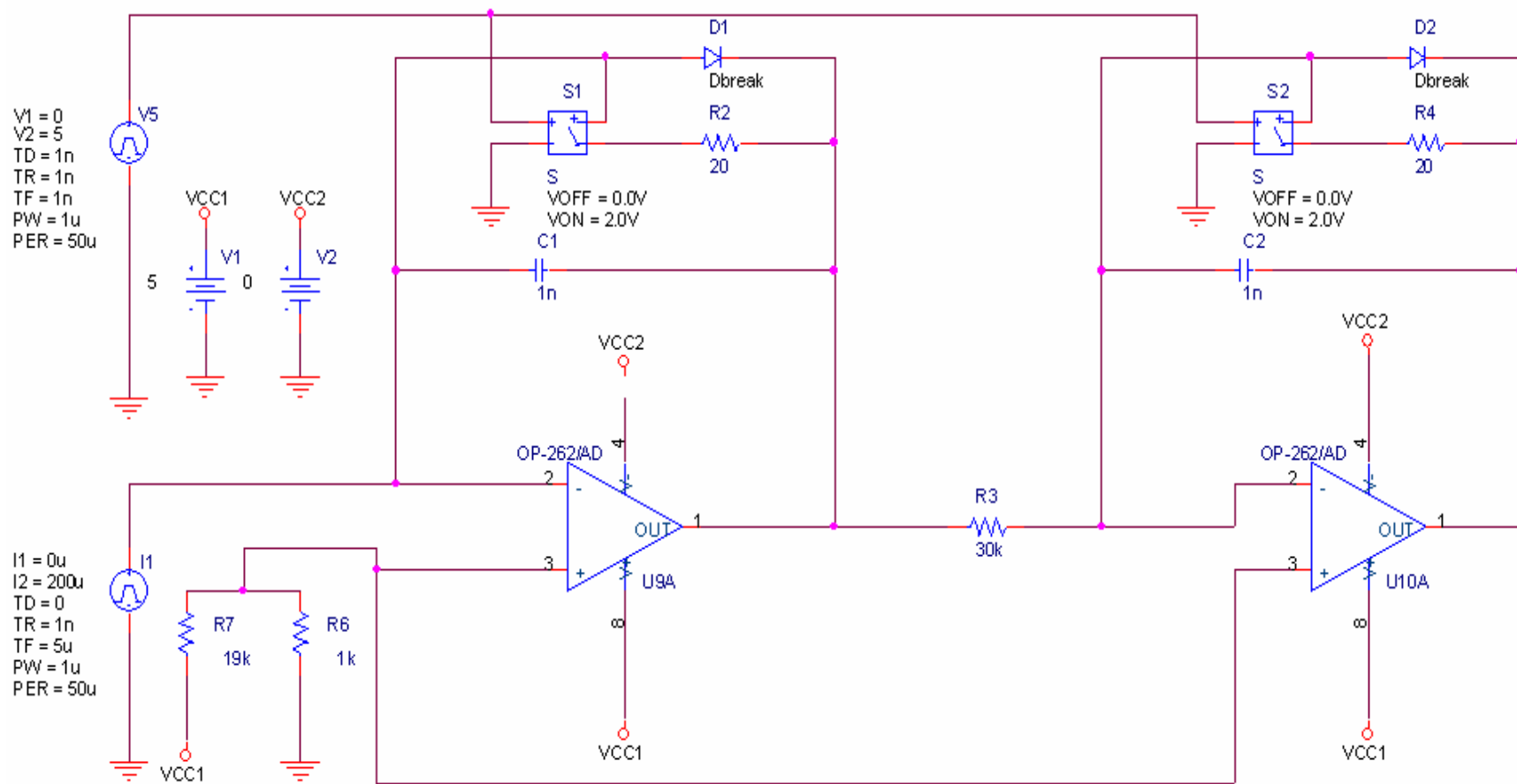


Figure D.1.1: Measurement setup of the alternative approach

At the inverting input of the Operational Amplifier, the current source has been attached. At the non-inverting input of the OpAmp, a self created offset voltage has been introduced. This offset is introduced because the A/D converter can only accept positive voltage values. The A/D converter is embedded in the microcontroller that will be discussed in chapter 5.

In the negative feedback loop of both amplifiers, a switch and a capacitor in parallel have been added. The switch controls the charge and discharge time of the capacitor. The duration of the charge and discharge time is controlled by the microcontroller.

Both integrators are connected with each other via a resistor. This resistor is used as a voltage-to-current converter which allows the integration in the second integrator (the one that is on the right on Figure D.1.1).

The output voltage can be calculated as follows:

$$V_1 = \frac{1}{C_1} \int_{t_0}^{t_1} I_{\text{photodiode}} dt \pm V_{\text{offset}_1} + V_{\text{offset-selfadded}} \approx \frac{1}{C_1} \int_{t_0}^{t_1} I_{\text{photodiode}} dt + V_{\text{offset-selfadded}} \quad (\text{D.8})$$

$$V_2 = \frac{1}{C_2} \int_{t_0}^{t_1} \frac{V_1}{R_1} dt \pm V_{\text{offset}_2} + V_{\text{offset-selfadded}} \approx \frac{1}{R_1 C_2} \int_{t_0}^{t_1} V_1 dt + V_{\text{offset-selfadded}} \quad (\text{4.9})$$

V_1 = output voltage of the first integrator

V_2 = output voltage of the second integrator

V_{offset_1} and V_{offset_2} are the offset values of the OpAmps. If the output voltages are much larger than the offset values, these offset values can be overlooked.

Different operational amplifiers have been used to evaluate their performance. The next section, attention is paid on the simulations of the new approach. All simulations are performed in about room temperature, which is $T = 27^\circ\text{C}$. Two different current pulses are used to test the concept of this new approach, which will be discussed in the next section.

D.2 Simulation results of the alternative read-out system

In this section, simulation results are shown for three different amplifiers. They are: OP-262, OPA-355 and AD8638 which have been evaluated in the previous chapter. Besides, hands-on calculation has been done to verify the results from the simulations. Two types of current sources have used: a linear and a constant one. The focus is on the linear current source, since the actual photodiode shows decay in the fall time. The simulation starts with the constant current source which after the linear current source follows

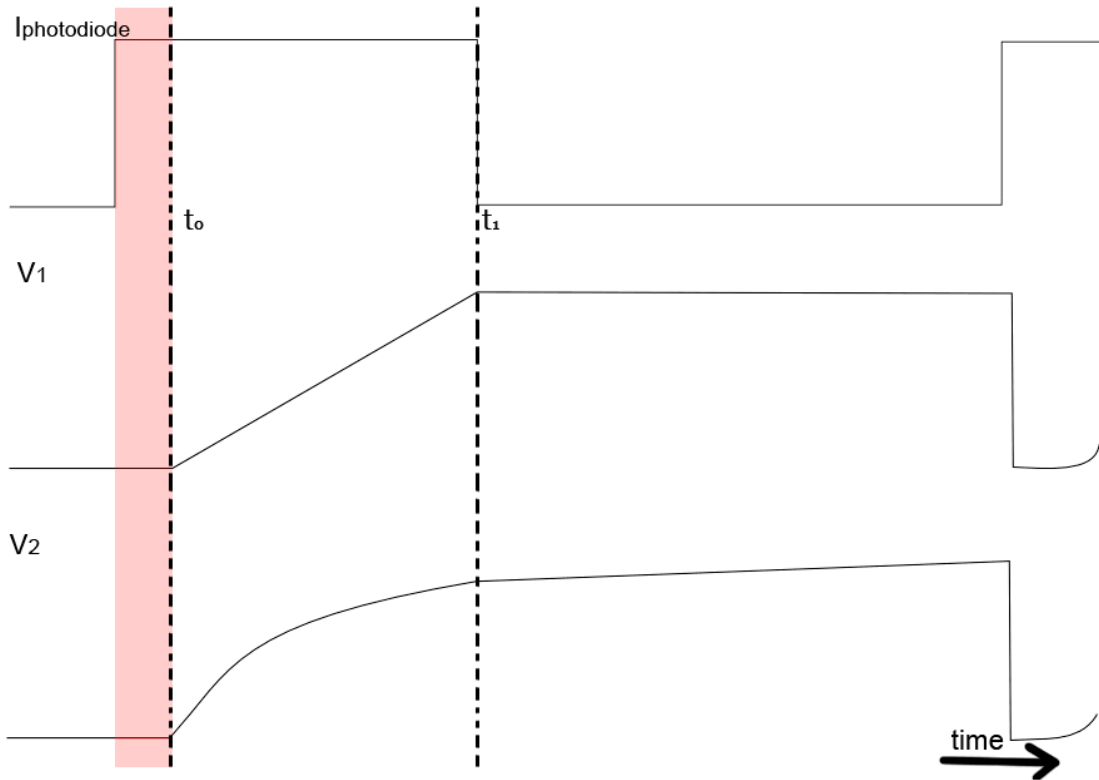


Figure D.2.1: Constant current source

The constant current means that the pulse width is wider than it supposed to be. Thus, the duty cycle is larger than conventional. Constant current is used to do an easy analysis of this approach. Recall formula (D.8) and assume there is no offset voltage. In case of the constant current source, we have:

$$V_1 = \frac{1}{C_1} \int_{t_0}^{t_1} I_{\text{photodiode}} \cdot dt \pm V_{\text{offset}_1} + V_{\text{offset-selfadded}} = \frac{1}{C_1} \int_{t_0}^{t_1} I_{\text{const}} \cdot dt + V_{\text{offset-selfadded}} = \frac{1}{C_1} [I_{\text{const}} t]_{t_0}^{t_1} + V_{\text{offset-selfadded}}$$

V_1 is a linear function, since the integration is taken over a constant value.

Now, the output voltage of the second amplifier is:

$$\begin{aligned} V_2 &= -\frac{1}{C_2} \int_{t_0}^{t_1} \frac{V_1}{R_1} \cdot dt \pm V_{\text{offset}_2} + V_{\text{offset-selfadded}} \approx -\frac{1}{C_2} \int_{t_0}^{t_1} \frac{V_1}{R_1} \cdot dt + V_{\text{offset-selfadded}} = -\frac{1}{C_2} \int_{t_0}^{t_1} \frac{1}{R_1 \cdot C_1} [I_{\text{const}} t]_{t_0}^{t_1} \cdot dt + V_{\text{offset-selfadded}} \\ &= -\frac{1}{R_1} \frac{1}{C_1} \frac{1}{C_2} \int_{t_0}^{t_1} [I_{\text{const}} t]_{t_0}^{t_1} \cdot dt + V_{\text{offset-selfadded}} = -\left[\frac{1}{2} \frac{1}{R_1} \frac{1}{C_1} \frac{1}{C_2} I_{\text{const}} t^2 \right]_{t_0}^{t_1} + V_{\text{offset-selfadded}} \end{aligned}$$

V_2 is a quadratic function. Again, the offset voltage of the operational amplifier is omitted.

There are two very remarkable notes in Figure D.2.1 and also in Figure D.2.2. The first one is the pink coloured rectangle window. In this rectangle window, the capacitor has been discharged. Therefore, the two output voltages of both amplifiers are zero. Right after the window, the integration starts which is denoted as t_0 in the integrator. t_1 is the time when the integration stops, which is right before the capacitor is being discharged again.

Second, the output voltage of the second amplifier is linear after there is no photocurrent. This is due to the constant voltage of the first amplifier, which produces a linear voltage on the second OpAmp.

Figure D.2.2 shows the response of the two amplifiers for a linear current source. V_1 is a quadratic function, since the source is a linear function. V_2 is a third order function, since V_1 is a quadratic function.

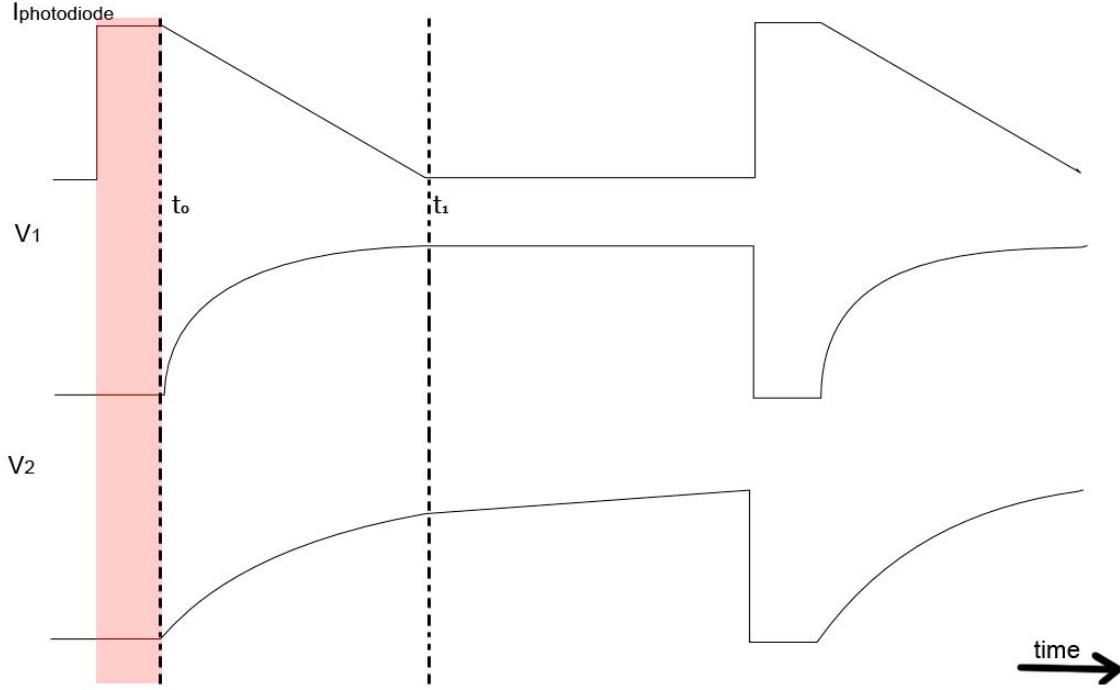


Figure D.2.2: Linear current source

V_1 and V_2 can be calculated via:

$$\begin{aligned}
 V_1 &= \frac{1}{C_1} \int_{t_0}^{t_1} I_{\text{photodiode}} \cdot dt \pm V_{\text{offset}_1} + V_{\text{offset-selffaded}} = \frac{1}{C_1} \int_{t_0}^{t_1} I_{\text{linear}} \cdot dt + V_{\text{offset-selffaded}} \\
 &= \frac{1}{C_1} \int_{t_0}^{t_1} (200 \cdot 10^{-6} - 40t) \cdot dt + V_{\text{offset-selffaded}} = \frac{1}{C_1} \left[200 \cdot 10^{-6} t - 20t^2 \right]_{t_0}^{t_1} + \text{const} + V_{\text{offset-selffaded}} \\
 &\approx \frac{1}{C_1} \left[200 \cdot 10^{-6} t - 20t^2 \right]_{t_0}^{t_1} + V_{\text{offset-selffaded}}
 \end{aligned} \tag{D.9}$$

$$\begin{aligned}
 V_2 &= -\frac{1}{C_2} \int_{t_0}^{t_1} \frac{V_1}{R_1} \cdot dt \pm V_{\text{offset}_2} + V_{\text{offset-selffaded}} \approx -\frac{1}{C_2} \int_{t_0}^{t_1} \frac{V_1}{R_1} \cdot dt + V_{\text{offset-selffaded}} = -\frac{1}{C_2} \int_{t_0}^{t_1} \frac{1}{R_1 \cdot C_1} I_{\text{linear}} \cdot dt + V_{\text{offset-selffaded}} \\
 &= -\frac{1}{R_1} \frac{1}{C_1} \frac{1}{C_2} \int_{t_0}^{t_1} (200 \cdot 10^{-6} t - 20t^2 + \text{const}) \cdot dt + V_{\text{offset-selffaded}} = -\frac{1}{R_1} \frac{1}{C_1} \frac{1}{C_2} \left[100 \cdot 10^{-6} t^2 - \frac{20}{3} t^3 \right]_{t_0}^{t_1} + \text{const} + V_{\text{offset-selffaded}} \\
 &\approx -\frac{1}{R_1} \frac{1}{C_1} \frac{1}{C_2} \left[100 \cdot 10^{-6} t^2 - \frac{20}{3} t^3 \right]_{t_0}^{t_1} + V_{\text{offset-selffaded}}
 \end{aligned}$$

The next section shows the simulation results of the setup for both the constant and linear current source with different OpAmps. The hands-on calculation and the simulation results will be compared.

D.2.1 Simulation results with the constant current source

Constant Current Source with OP-262

The output voltages of the two amplifiers, V_1 and V_2 , have been plotted in Figure D.2.3.

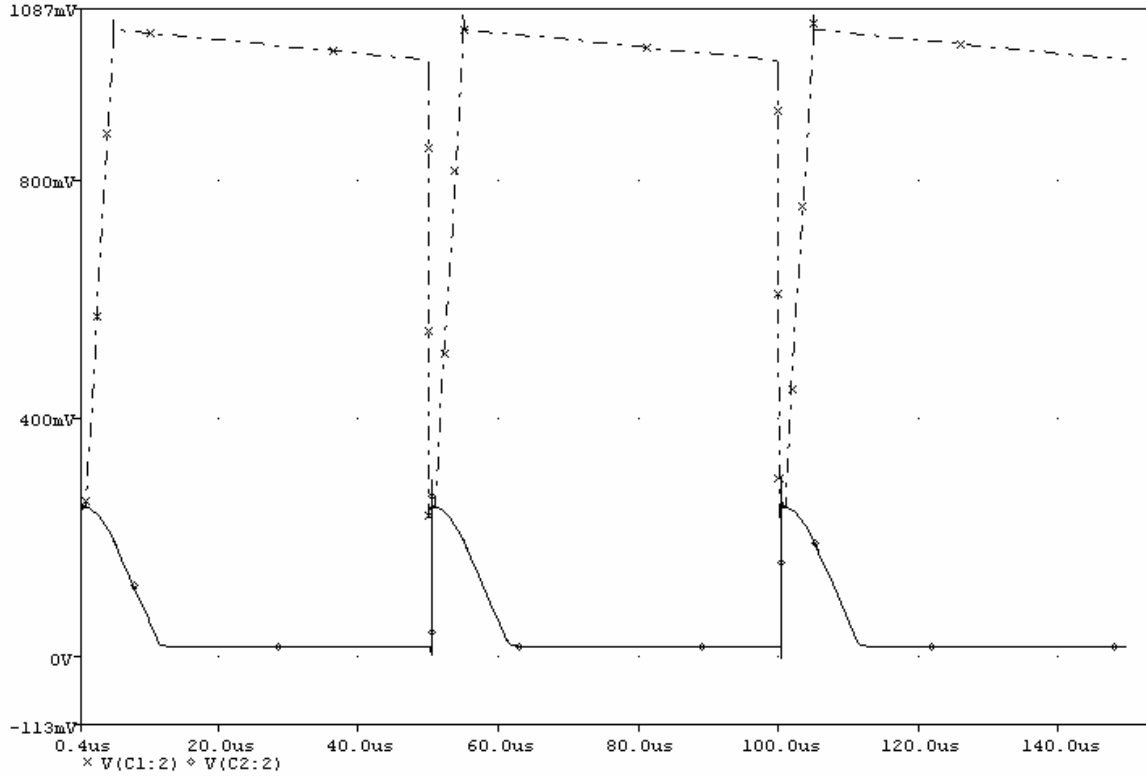


Figure D.2.3: Output voltages of both amplifiers of OP-262 with constant current source

The dotted line in Figure D.2.3 is the output voltage of the first integrator (V_1), while the lined graph is the output voltage of the second integrator (V_2).

According to formula (D.8), the output voltage of the first amplifier, V_1 , should be:

$$\begin{aligned}
 V_1 &= \frac{1}{C_1} \int_{t_0}^{t_1} I_{\text{photodiode}} dt \pm V_{\text{offset}_1} + V_{\text{offset-selfadded}} = \frac{1}{C_1} \int_{t_0}^{t_1} I_{\text{const}} dt + V_{\text{offset-selfadded}} = \frac{1}{C_1} [I_{\text{const}} t]_{t_0}^{t_1} + V_{\text{offset-selfadded}} \\
 &= \frac{1}{1.0 \cdot 10^{-9}} [200 \cdot 10^{-6} t]_0^{4 \cdot 10^{-6}} + V_{\text{offset-selfadded}} = 0.8V + 0.25V = 1.05V
 \end{aligned}$$

Figure D.2.4 shows a zoomed area at t around $54\mu\text{s}$.

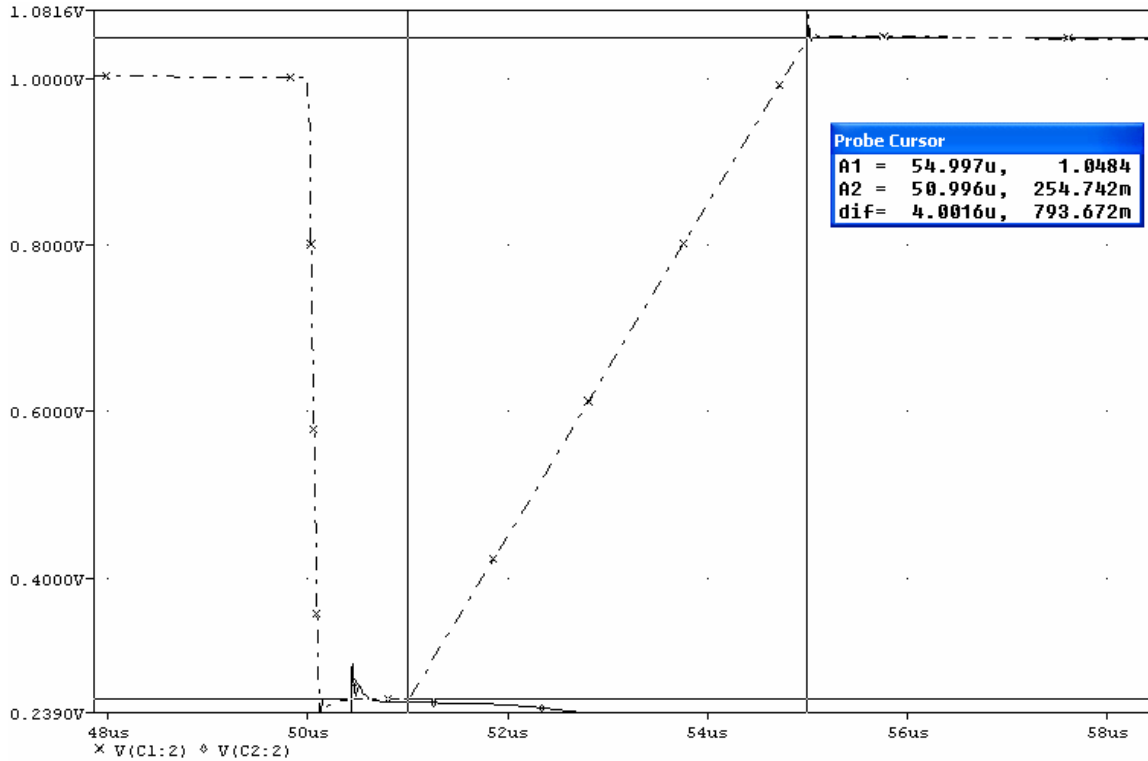


Figure D.2.4: Output voltage, V_1 , of OP-262 with constant current source

The obtained V_1 from the simulation is 1.0484V. The difference with the hand-on calculation is $1.05 - 1.0484 = 1.6\text{mV}$. Therefore the error is:

$$error_1 = \left| \frac{1.0484 - 1.05}{1.05} \right| \times 100\% \approx 0.15\%$$

The small difference will be detected by the A/D converter, since its resolution is $1.5/1024 \approx 1.46\text{mV}$. However, the last two bits of the A/D converter are inaccurate. Therefore, the 1.6mV can be omitted.

Figure D.2.5 represents the simulation result of V_2 of OP-262.

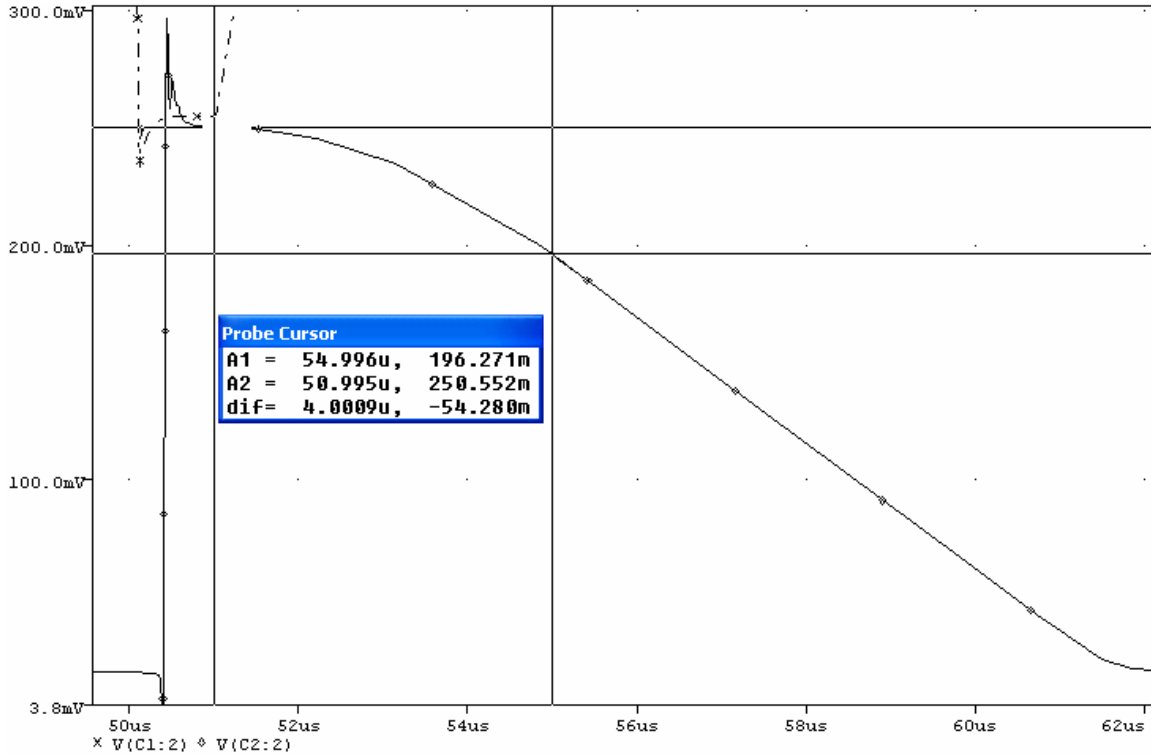


Figure D.2.5: Output voltage, V_2 , of OP-262 with constant current source

Recall the hands-on calculation for V_2 , we have

$$\begin{aligned}
 V_2 &= -\frac{1}{C_2} \int_{t_0}^{t_1} \frac{V_1}{R_1} dt \pm V_{\text{offset}_2} + V_{\text{offset-selfadded}} \approx -\frac{1}{C_2} \int_{t_0}^{t_1} \frac{V_1}{R_1} dt + V_{\text{offset-selfadded}} = -\frac{1}{C_2} \int_{t_0}^{t_1} \frac{1}{R_1 \cdot C_1} [I_{\text{const}} t]_{t_0}^{t_1} \cdot dt + V_{\text{offset-selfadded}} \\
 &= -\frac{1}{R_1} \frac{1}{C_1} \frac{1}{C_2} \int_{t_0}^{t_1} [I_{\text{const}} t]_{t_0}^{t_1} \cdot dt + V_{\text{offset-selfadded}} = -\left[\frac{1}{2} \frac{1}{R_1} \frac{1}{C_1} \frac{1}{C_2} I_{\text{const}} t^2 \right]_{t_0}^{t_1} + V_{\text{offset-selfadded}} \\
 &= -\left[\frac{1}{2} \frac{1}{30 \cdot 10^3} \frac{1}{1 \cdot 10^{-9}} \frac{1}{1 \cdot 10^{-9}} 200 \cdot 10^{-6} t^2 \right]_0^{4 \cdot 10^{-6}} + 0.25 = -0.053 + 0.25 = 0.197V
 \end{aligned}$$

The simulation shows $V_2 = 196.271\text{mV}$, while the calculated V_2 is 197mV . The absolute difference is $|196.271 - 197| = 0.729\text{mV}$ and with an error of:

$$\text{error}_2 = \left| \frac{196.271 - 197}{197} \right| \times 100\% \approx 0.3\%$$

The small difference has no influence for accuracy of the A/D converter, since it is smaller than the resolution of the A/D converter.

The new approach has a high degree of accuracy. The introduced ignorable error might be due to the bias current of the OpAmp and its offset voltage. However, this error has not a serious effect on the measurement. The next test is performed on using the OPA-355.

Constant Current Source with OPA-355

TNO uses this operational amplifier for their readout electronics. Using this amplifier for the new approach will get the results that are shown in Figure D.2.6.

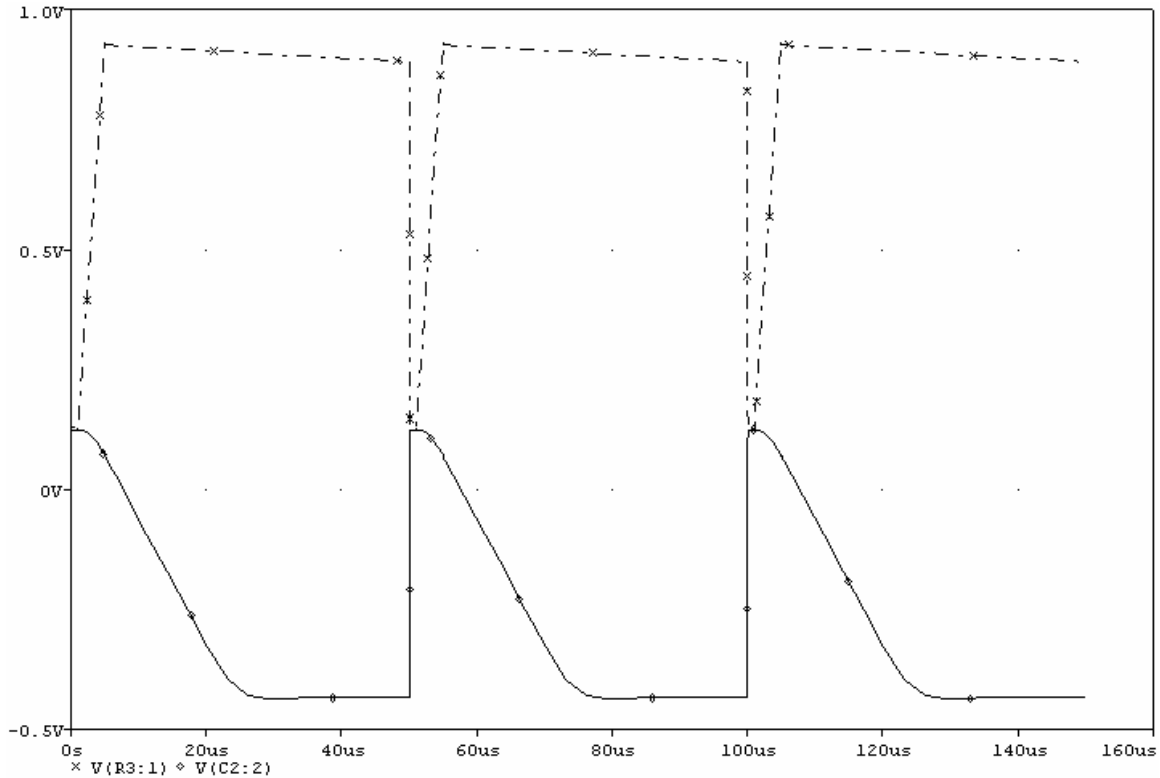


Figure D.2.6: Output voltages of both amplifiers of OPA-355 with constant current source

The dotted, the top one, is the output voltage of the first integrator. The striped line, the bottom one, represents the output voltage of the second integrator.

Compare this figure with Figure D.2.3, one very remarkable thing can be noticed. The second integrator shows negative voltage. In real life, this causes problem for further processing of the data, since the A/D converter can only accept positive values. However, during the simulations when a single supply voltage has been used, errors occur. PSpice said that it is not able to do conversion. To solve this problem, dual supply has been used. This results a negative voltage value at the output of the second integrator.

The dual supply voltage that is set in PSpice, is $\pm 2.5V$. The threshold voltages of the switches are also modified. They are both set to 0.5V to ensure that the switches are on at a gate voltage of 2.5V.

Figure D.2.7 shows the results of the simulation that is zoomed in at t around 52 μs .

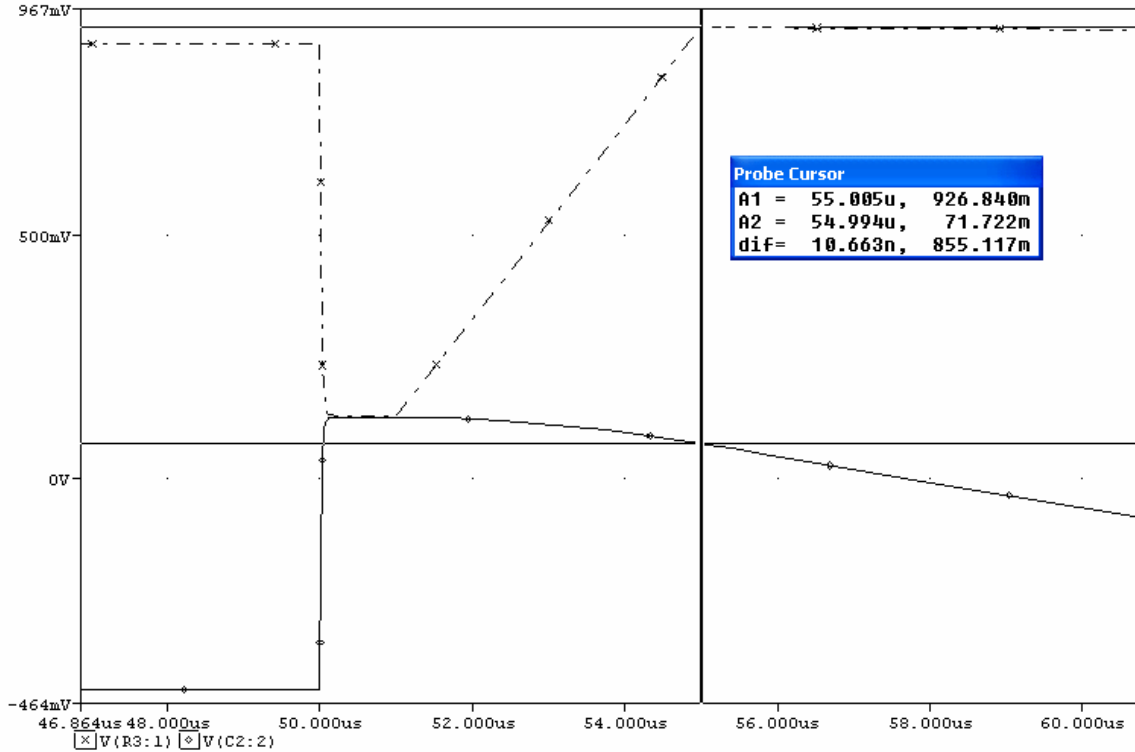


Figure D.2.7: Output voltages of OPA-355 with constant current source

According to PSpice model of OPA-355, the output voltage of the first integrator (that is indicated by A1) is 926.8mV. The hands-on calculation is estimated at:

$$V_1 = \frac{1}{C_1} \int_{t_0}^{t_1} I_{\text{photodiode}} \cdot dt \pm V_{\text{offset}_1} + V_{\text{offset-selfadded}} = \frac{1}{C_1} \int_{t_0}^{t_1} I_{\text{const}} \cdot dt + V_{\text{offset-selfadded}} = \frac{1}{C_1} [I_{\text{const}} t]_{t_0}^{t_1} + V_{\text{offset-selfadded}}$$

$$= \frac{1}{1.0 \cdot 10^{-9}} [200 \cdot 10^{-6} t]_0^{4 \cdot 10^{-6}} + V_{\text{offset-selfadded}} = 0.8V + 0.125V = 0.925V$$

The mismatch of the hand calculation and the simulation is 1.84mV. This is less than 1% error and it does not seriously affect the accuracy of the system.

Recall the hands-on calculation of the output voltage of the second integrator:

$$V_2 = -\frac{1}{C_2} \int_{t_0}^{t_1} \frac{V_1}{R_1} \cdot dt \pm V_{\text{offset}_2} + V_{\text{offset-selfadded}} \approx -\frac{1}{C_2} \int_{t_0}^{t_1} \frac{V_1}{R_1} \cdot dt + V_{\text{offset-selfadded}} = -\frac{1}{C_2} \int_{t_0}^{t_1} \frac{1}{R_1 \cdot C_1} [I_{\text{const}} t]_{t_0}^{t_1} \cdot dt + V_{\text{offset-selfadded}}$$

$$= -\frac{1}{R_1} \frac{1}{C_1} \frac{1}{C_2} \int_{t_0}^{t_1} [I_{\text{const}} t]_{t_0}^{t_1} \cdot dt + V_{\text{offset-selfadded}} = -\left[\frac{1}{2} \frac{1}{R_1} \frac{1}{C_1} \frac{1}{C_2} I_{\text{const}} t^2 \right]_{t_0}^{t_1} + V_{\text{offset-selfadded}}$$

$$= -\left[\frac{1}{2} \frac{1}{30 \cdot 10^3} \frac{1}{1 \cdot 10^{-9}} \frac{1}{1 \cdot 10^{-9}} 200 \cdot 10^{-6} t^2 \right]_0^{4 \cdot 10^{-6}} + 0.125 = -0.053 + 0.125 = 0.072V$$

Compare this calculated value with the simulation result (A2), the mismatch is 0.178mV. This small difference will not affect the accuracy of the system. The coming part shows the simulation results of AD8638 with the constant current source.

Constant current source with AD8638

AD8638 has been used as integrator in the readout electronics of the new approach. The performance of using this operational amplifier has been shown in Figure D.2.8.

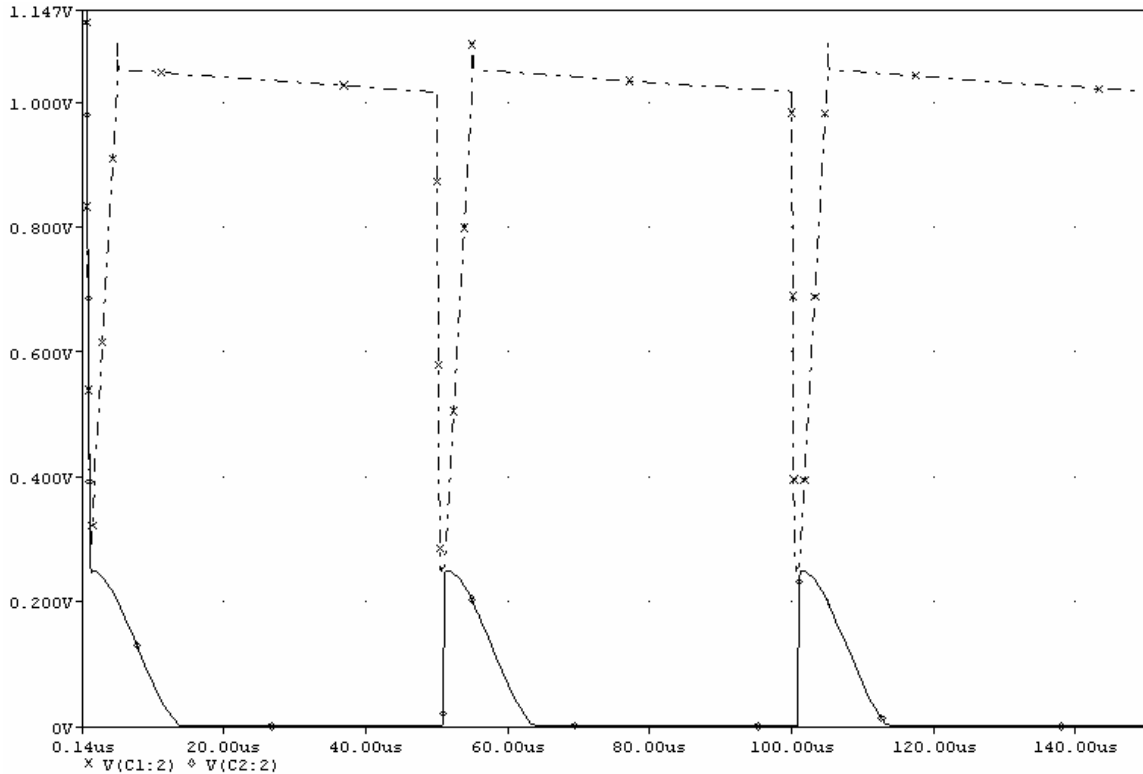


Figure D.2.8: Output voltages of both amplifiers of AD8638 with constant current source

The performance of this operational amplifier looks good. The current can be integrated. Again, the upper (dotted) line is the output voltage of the first integrator, while the lower line is the output voltage of the second integrator. Figure D.2.9 shows a closer view of the results at t around $54\mu\text{s}$.

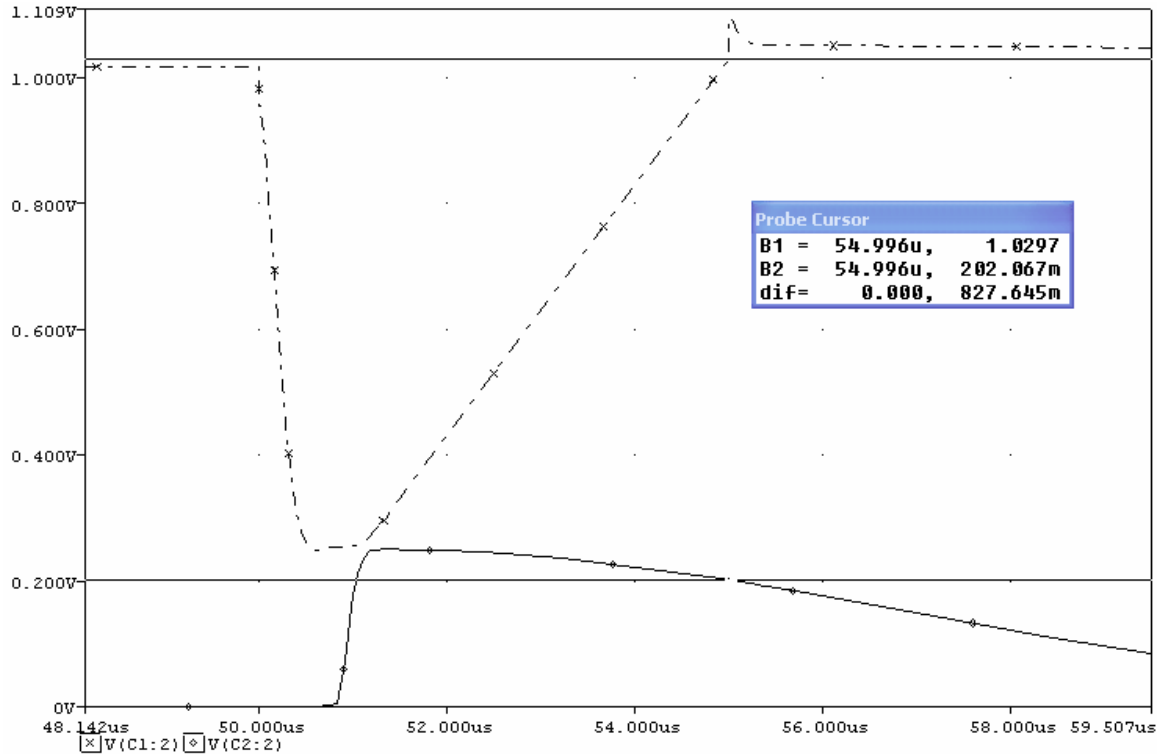


Figure D.2.9: Output voltages of AD8638 with constant current source

Recall the hands-on calculation values of the output voltages.

$$\begin{aligned}
 V_1 &= \frac{1}{C_1} \int_{t_0}^{t_1} I_{\text{photodiode}} dt \pm V_{\text{offset}_1} + V_{\text{offset-selfadded}} = \frac{1}{C_1} \int_{t_0}^{t_1} I_{\text{const}} dt + V_{\text{offset-selfadded}} = \frac{1}{C_1} [I_{\text{const}} t]_{t_0}^{t_1} + V_{\text{offset-selfadded}} \\
 &= \frac{1}{1.0 \cdot 10^{-9}} \left[200 \cdot 10^{-6} t \right]_0^{4 \cdot 10^{-6}} + V_{\text{offset-selfadded}} = 0.8V + 0.25V = 1.05V \\
 V_2 &= -\frac{1}{C_2} \int_{t_0}^{t_1} \frac{V_1}{R_1} dt \pm V_{\text{offset}_2} + V_{\text{offset-selfadded}} \approx -\frac{1}{C_2} \int_{t_0}^{t_1} \frac{V_1}{R_1} dt + V_{\text{offset-selfadded}} = -\frac{1}{C_2} \int_{t_0}^{t_1} \frac{1}{R_1 \cdot C_1} [I_{\text{const}} t]_{t_0}^{t_1} \cdot dt + V_{\text{offset-selfadded}} \\
 &= -\frac{1}{R_1} \frac{1}{C_1} \frac{1}{C_2} \int_{t_0}^{t_1} [I_{\text{const}} t]_{t_0}^{t_1} \cdot dt + V_{\text{offset-selfadded}} = -\left[\frac{1}{2} \frac{1}{R_1} \frac{1}{C_1} \frac{1}{C_2} I_{\text{const}} t^2 \right]_{t_0}^{t_1} + V_{\text{offset-selfadded}} \\
 &= -\left[\frac{1}{2} \frac{1}{30 \cdot 10^3} \frac{1}{1 \cdot 10^{-9}} \frac{1}{1 \cdot 10^{-9}} 200 \cdot 10^{-6} t^2 \right]_0^{4 \cdot 10^{-6}} + 0.25 = -0.053 + 0.25 = 0.197V
 \end{aligned}$$

According to the simulation, the output voltage of the first integrator (B1) is 1.0297V. Compare to the hand calculation, the mismatch is 20.3mV. This mismatch is the largest among all operational amplifiers. The mismatch also can not be disregarded.

Figure D.2.9 shows the output voltage of the second integrator at $t \approx 55\mu\text{s}$ of 202.067mV. The mismatch is 5.067mV. Again, this error is the largest among all operational amplifiers. Compare this mismatch value with the previous one, this amount is smaller, but it can not be disregarded.

D.2.2 Evaluation of the performance for the constant current source

Table D.1 summarises the mismatches and the error using the three operational amplifiers that have been discussed previously.

Table D.1: Evaluations of the obtained results for the constant current source

	OP-262		OPA-355		AD8638	
	V ₁ [V]	V ₂ [mV]	V ₁ [V]	V ₂ [mV]	V ₁ [V]	V ₂ [mV]
<i>Hands-on calculation</i>	1.05V	197	0.925	72	1.05V	197
<i>Simulation results</i>	1.0484	196.271	0.92684	71.722	1.029V	202.067
<i>Mismatch [mV]</i>	1.6	1.729	1.84	1.278	21	5.067
<i>Error [%]</i>	0.152	0.877	0.199	1.775	2	2.5

The largest mismatch is for AD8638. The value exceeds the error margin of the A/D converter. The reference of the A/D converter will be set at $V_{ref} = 1.5V$ with 10bit analogue-to-digital conversion. The first two bits of the A/D converter can be ignored. That means, all mismatch values below $(2 \cdot 1.5/2^{10}) 2.9mV$ can be accepted.

All errors of the tested operational amplifiers are acceptable, except the AD8638. This operational amplifier shows the largest mismatch.

Recall Table 3.1 where the properties of all operational amplifiers are shown. Compare the OP-262 with the AD8638, the OP-262's performance exceeds in slew rate and the noise only. The offset voltage and the bias current of OP-262 are much higher than AD8638, which it is expected that the performance will be worse in terms of accuracy.

Examining the aspects, which is represented in Table 3.1, of the Operational Amplifiers, the bandwidth, the slew rate and the noise level of OPA-355 are better than OP-262. The performance of OPA-355, in terms of accuracy is worse than OP-262. This might be due to the bias current, which is the lowest for OP-262 among the three selected amplifiers. The typical offset voltage does not influence the accuracy much. This can be explained by comparing the value of offset voltage of all three amplifiers. The offset voltage value of OP-262 is larger than AD8638, but in terms of accuracy, OP-262 is more accurate.

However, there is no clear aspect that can show a relationship of the accuracy of the system. This relationship might become more evident once more aspects of the amplifiers are compared and investigated.

The next evaluation will be discussed about the performance of the readout electronics using a linear current source. As discussed earlier in this chapter, this current source has a slow fall-off time. The fall time is set to $5\mu s$ and the pulse width is set back to $1\mu s$.

D.2.3 Simulation results with the constant current source

Linear Current Source with OP-262

Figure D.2.10 shows the results of the OP-262 with the linear current source.

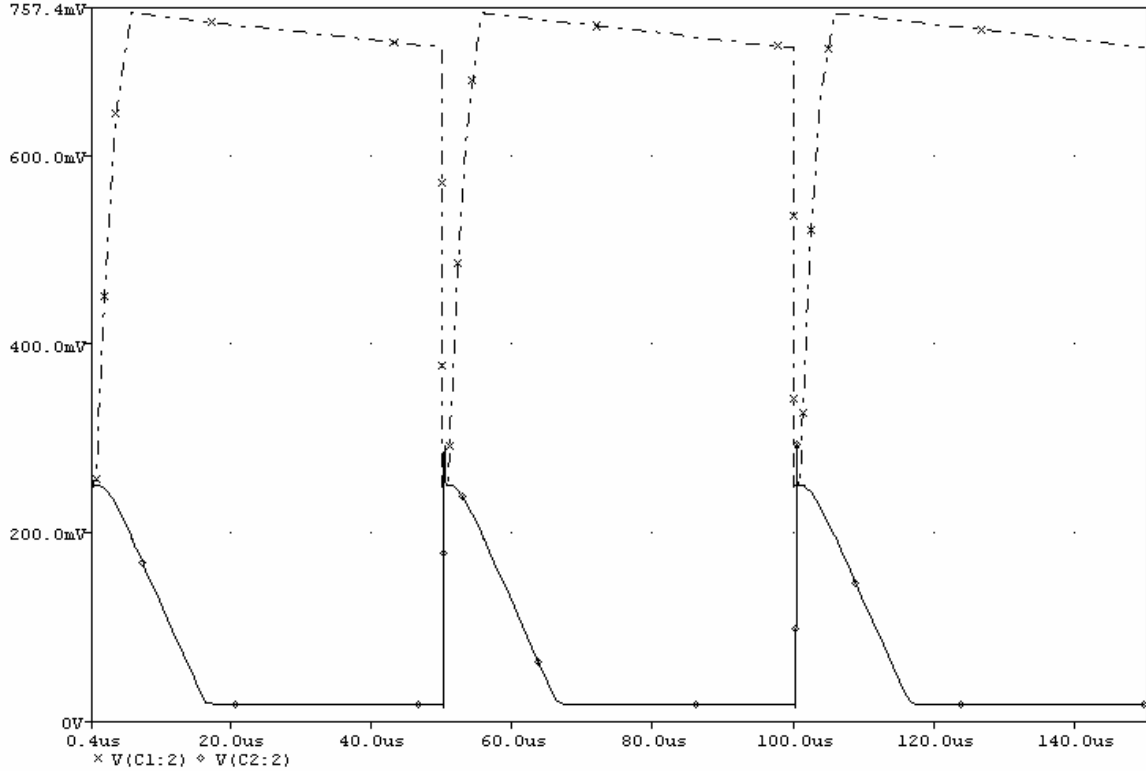


Figure D.2.10: Output voltages of both amplifiers of OP-262 with linear current source

The top dotted line is the output voltage of the first integrator. The line below is the output voltage of the second integrator. Recall the hands-on calculations for the linear current source. In case of the output voltage of the first integrator, we have:

$$\begin{aligned}
 V_1 &= \frac{1}{C_1} \int_{t_0}^{t_1} I_{\text{photodiode}} \cdot dt \pm V_{\text{offset}_1} + V_{\text{offset-selffaded}} = \frac{1}{C_1} \int_{t_0}^{t_1} I_{\text{linear}} \cdot dt + V_{\text{offset-selffaded}} \\
 &= \frac{1}{C_1} \int_{t_0}^{t_1} (200 \cdot 10^{-6} - 40t) \cdot dt + V_{\text{offset-selffaded}} = \frac{1}{C_1} \left[200 \cdot 10^{-6} t - 20t^2 \right]_{t_0}^{t_1} + \text{const} + V_{\text{offset-selffaded}} \\
 &\approx \frac{1}{C_1} \left[200 \cdot 10^{-6} t - 20t^2 \right]_{t_0}^{t_1} + V_{\text{offset-selffaded}} = \frac{1}{1 \cdot 10^{-9}} \left[200 \cdot 10^{-6} t - 20t^2 \right]_0^{5 \cdot 10^{-6}} + V_{\text{offset-selffaded}} \\
 &= 0.5V + 0.25V = 0.75V
 \end{aligned}$$

The hands-on calculation for the output voltage of the second integrator is:

$$\begin{aligned}
 V_2 &= -\frac{1}{C_2} \int_{t_0}^{t_1} \frac{V_1}{R_1} \cdot dt \pm V_{\text{offset}_2} + V_{\text{offset-selffaded}} \approx -\frac{1}{C_2} \int_{t_0}^{t_1} \frac{V_1}{R_1} \cdot dt + V_{\text{offset-selffaded}} = -\frac{1}{C_2} \int_{t_0}^{t_1} \frac{1}{R_1 \cdot C_1} I_{\text{linear}} \cdot dt + V_{\text{offset-selffaded}} \\
 &= -\frac{1}{R_1} \frac{1}{C_1} \frac{1}{C_2} \int_{t_0}^{t_1} (200 \cdot 10^{-6} t - 20t^2 + \text{const}) \cdot dt + V_{\text{offset-selffaded}} = -\frac{1}{R_1} \frac{1}{C_1} \frac{1}{C_2} \left[100 \cdot 10^{-6} t^2 - \frac{20}{3} t^3 \right]_{t_0}^{t_1} + \text{const} + V_{\text{offset-selffaded}} \\
 &\approx -\frac{1}{R_1} \frac{1}{C_1} \frac{1}{C_2} \left[100 \cdot 10^{-6} t^2 - \frac{20}{3} t^3 \right]_{t_0}^{t_1} + V_{\text{offset-selffaded}} = -\frac{1}{30 \cdot 10^3} \frac{1}{1 \cdot 10^{-9}} \frac{1}{1 \cdot 10^{-9}} \left[100 \cdot 10^{-6} t^2 - \frac{20}{3} t^3 \right]_0^{5 \cdot 10^{-6}} + 0.25 \\
 &= -\frac{1}{3 \cdot 10^{-14}} (1.67 \cdot 10^{-15}) + 0.25 = 0.194V
 \end{aligned}$$

Figure D.2.11 shows the results of both output voltages that are zoomed in at t around $54\mu\text{s}$.

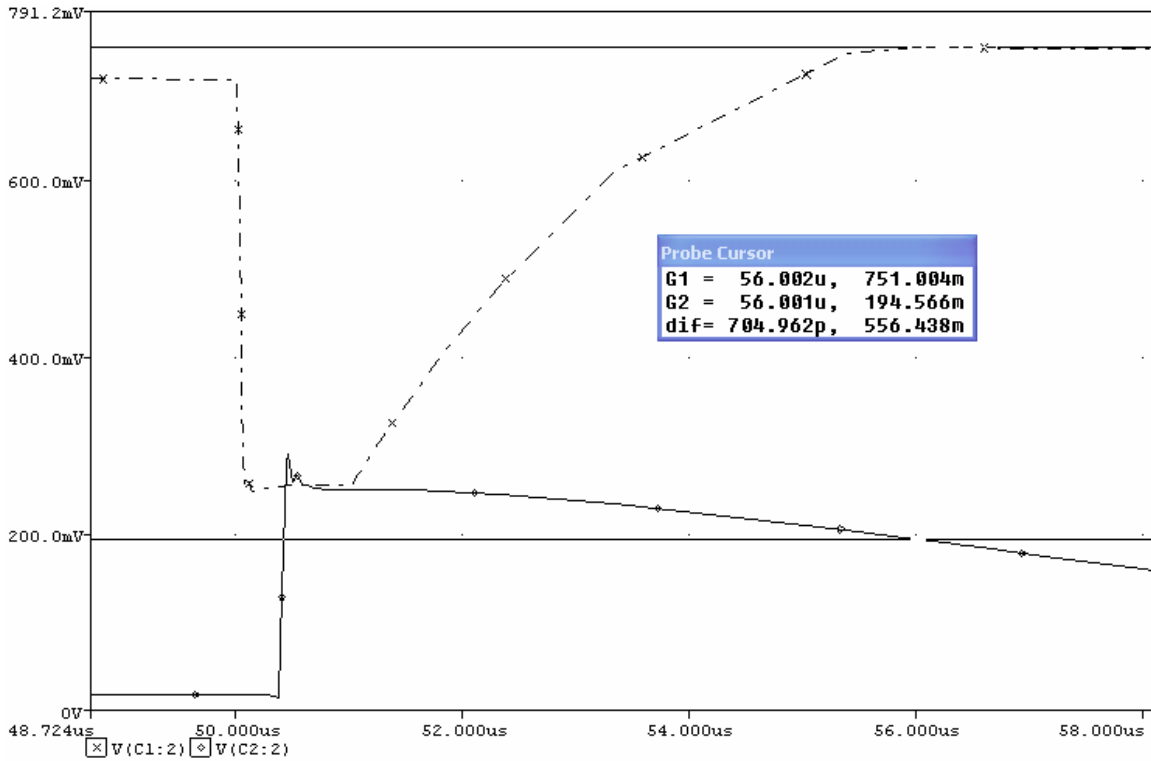


Figure D.2.11: Output voltages of both amplifiers of OP-262 with linear current source zoomed in at t around $54\mu\text{s}$

G1 and G2 indicate the output voltages of the first integrator and the second integrator, respectively. The mismatch of the output voltage of the first integrator is 1.004mV , while the mismatch of the output voltage of the second integrator is 0.566mV . This results an error of 0.13% and 0.29% for the first and the second integrator, respectively. The small difference in the mismatch is ignorable, since it will not affect the accuracy of the measurement.

Linear Current Source with OPA-355

This operational amplifier has been used by TNO in their readout circuits for measuring the oxygen level. Now, the performance of this amplifier has been tested for the new approach with the linear current source. Figure D.2.12 shows the results of the performance of this operational amplifier.

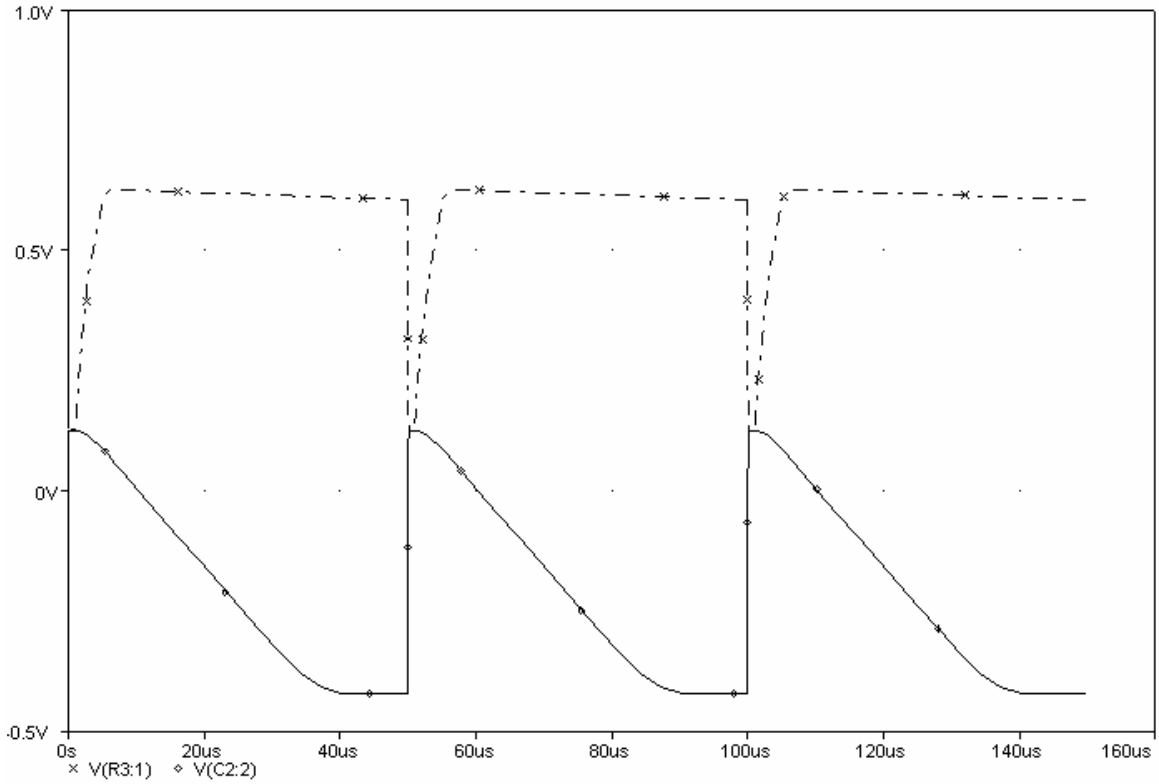


Figure D.2.12: Output voltages of both amplifiers of OPA-355 with linear current source

This operational amplifier is dual supplied ($\pm 2.5V$) to be able to do simulations in PSpice. Therefore, the output voltage of the second integrator can be negative. This output voltage is the bottom line graph. The dotted line is the output of the first integrator.

Figure D.2.13 shows a closer look at the signal.

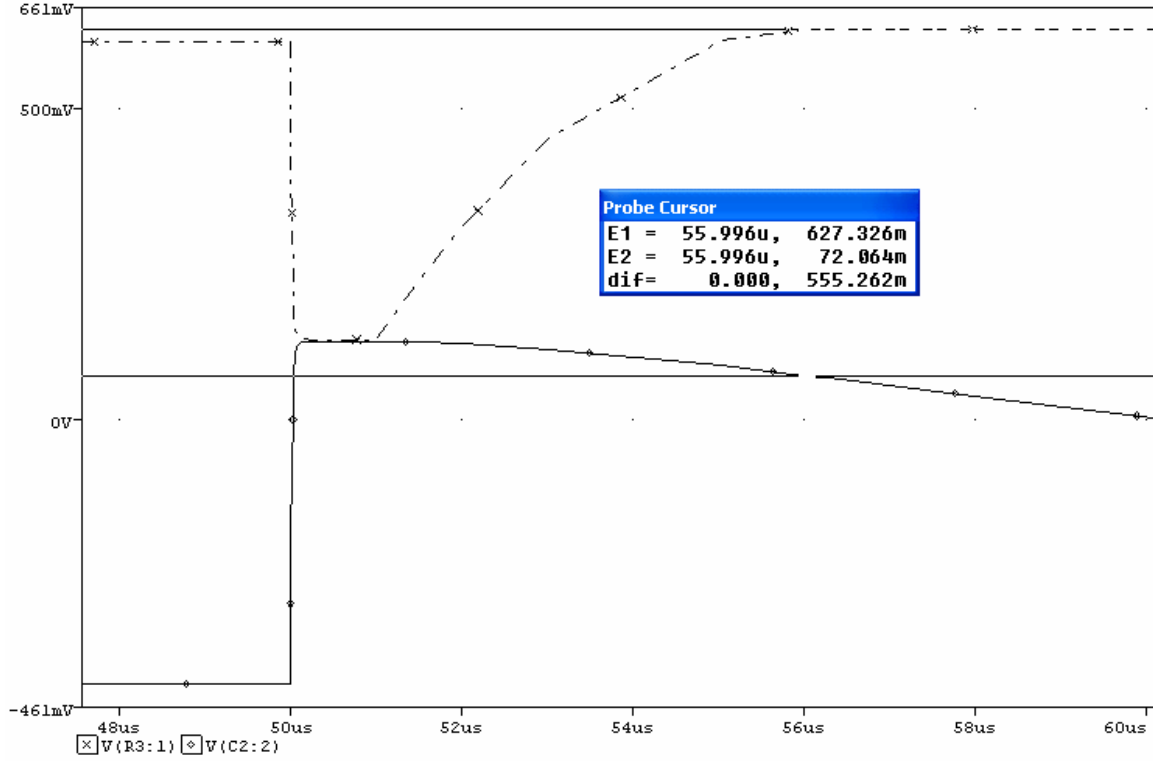


Figure D.2.13: Output voltages of both amplifiers of OPA-355 with linear current source zoomed in at t around $54\mu\text{s}$

Recall the hands-on calculation for both output voltages:

$$\begin{aligned}
 V_1 &= \frac{1}{C_1} \int_{t_0}^{t_1} I_{\text{photodiode}} dt \pm V_{\text{offset}_1} + V_{\text{offset-selffaded}} = \frac{1}{C_1} \int_{t_0}^{t_1} I_{\text{linear}} dt + V_{\text{offset-selffaded}} \\
 &= \frac{1}{C_1} \int_{t_0}^{t_1} (200 \cdot 10^{-6} - 40t) \cdot dt + V_{\text{offset-selffaded}} = \frac{1}{C_1} \left[200 \cdot 10^{-6} t - 20t^2 \right]_{t_0}^{t_1} + \text{const} + V_{\text{offset-selffaded}} \\
 &\approx \frac{1}{C_1} \left[200 \cdot 10^{-6} t - 20t^2 \right]_{t_0}^{t_1} + V_{\text{offset-selffaded}} = \frac{1}{1 \cdot 10^{-9}} \left[200 \cdot 10^{-6} t - 20t^2 \right]_0^{5 \cdot 10^{-6}} + V_{\text{offset-selffaded}} \\
 &= 0.5V + 0.125V = 0.625V
 \end{aligned}$$

$$\begin{aligned}
 V_2 &= -\frac{1}{C_2} \int_{t_0}^{t_1} \frac{V_1}{R_1} dt \pm V_{\text{offset}_2} + V_{\text{offset-selffaded}} \approx -\frac{1}{C_2} \int_{t_0}^{t_1} \frac{V_1}{R_1} dt + V_{\text{offset-selffaded}} = -\frac{1}{C_2} \int_{t_0}^{t_1} \frac{1}{R_1 \cdot C_1} I_{\text{linear}} \cdot dt + V_{\text{offset-selffaded}} \\
 &= -\frac{1}{R_1} \frac{1}{C_1} \frac{1}{C_2} \int_{t_0}^{t_1} (200 \cdot 10^{-6} t - 20t^2 + \text{const}) \cdot dt + V_{\text{offset-selffaded}} = -\frac{1}{R_1} \frac{1}{C_1} \frac{1}{C_2} \left[100 \cdot 10^{-6} t^2 - \frac{20}{3} t^3 \right]_{t_0}^{t_1} + \text{const} + V_{\text{offset-selffaded}} \\
 &\approx -\frac{1}{R_1} \frac{1}{C_1} \frac{1}{C_2} \left[100 \cdot 10^{-6} t^2 - \frac{20}{3} t^3 \right]_{t_0}^{t_1} + V_{\text{offset-selffaded}} = -\frac{1}{30 \cdot 10^3} \frac{1}{1 \cdot 10^{-9}} \frac{1}{1 \cdot 10^{-9}} \left[100 \cdot 10^{-6} t^2 - \frac{20}{3} t^3 \right]_0^{5 \cdot 10^{-6}} + 0.125 \\
 &= -\frac{1}{3 \cdot 10^{-14}} (1.67 \cdot 10^{-15}) + 0.125 = 69.4mV
 \end{aligned}$$

The simulation shows output voltages of V_1 627.326mV and $V_2 = 72.064mV$. The mismatch of the first and the second output voltages are 0.326mV and 2.664mV, respectively. Both

mismatches are significantly more than the previous amplifier. However, both mismatch values can be disregarded.

Linear Current Source with AD8638

This operational amplifier will be used as integrators of the alternative system. Its performance for the constant current source is the worst. Figure D.2.14 shows the performance of this amplifier for the linear current source.

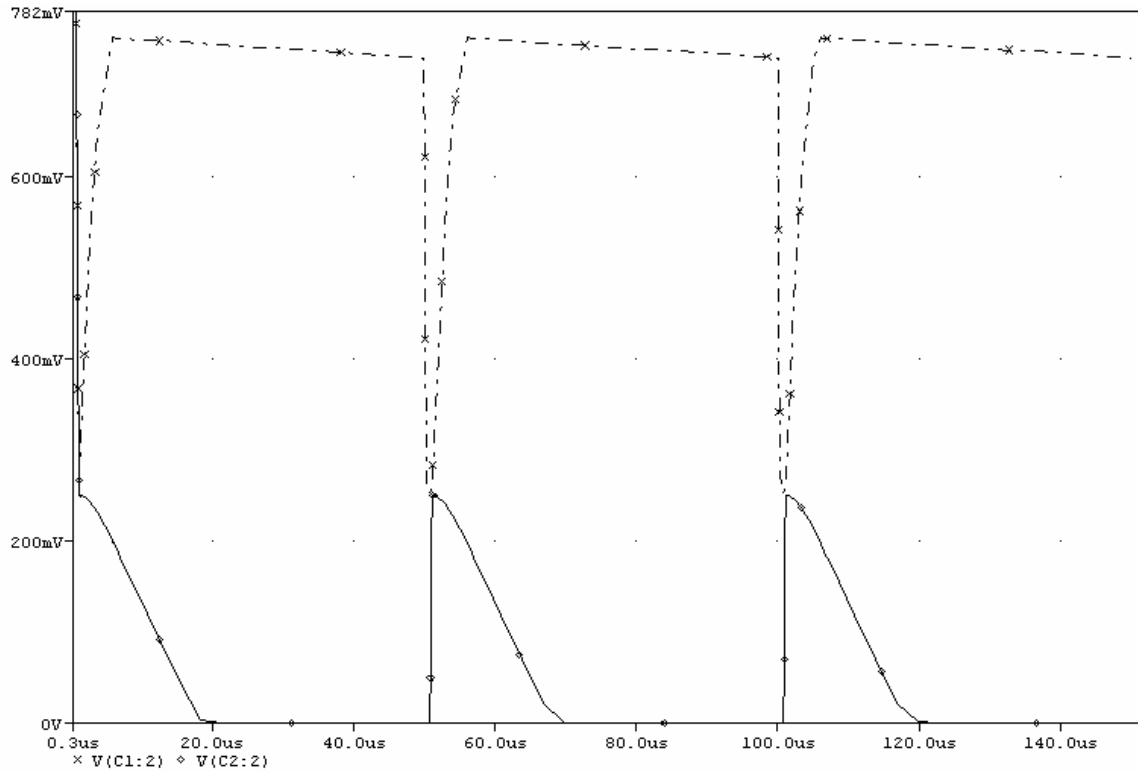


Figure D.2.14: Output voltages of both amplifiers of AD8638 with linear current source

The dotted line that is on top is the output voltage of the first integrator. The straight line that lies on the bottom is the output voltage of the second amplifier. Figure D.2.15 shows a zoomed-in area of the plot.

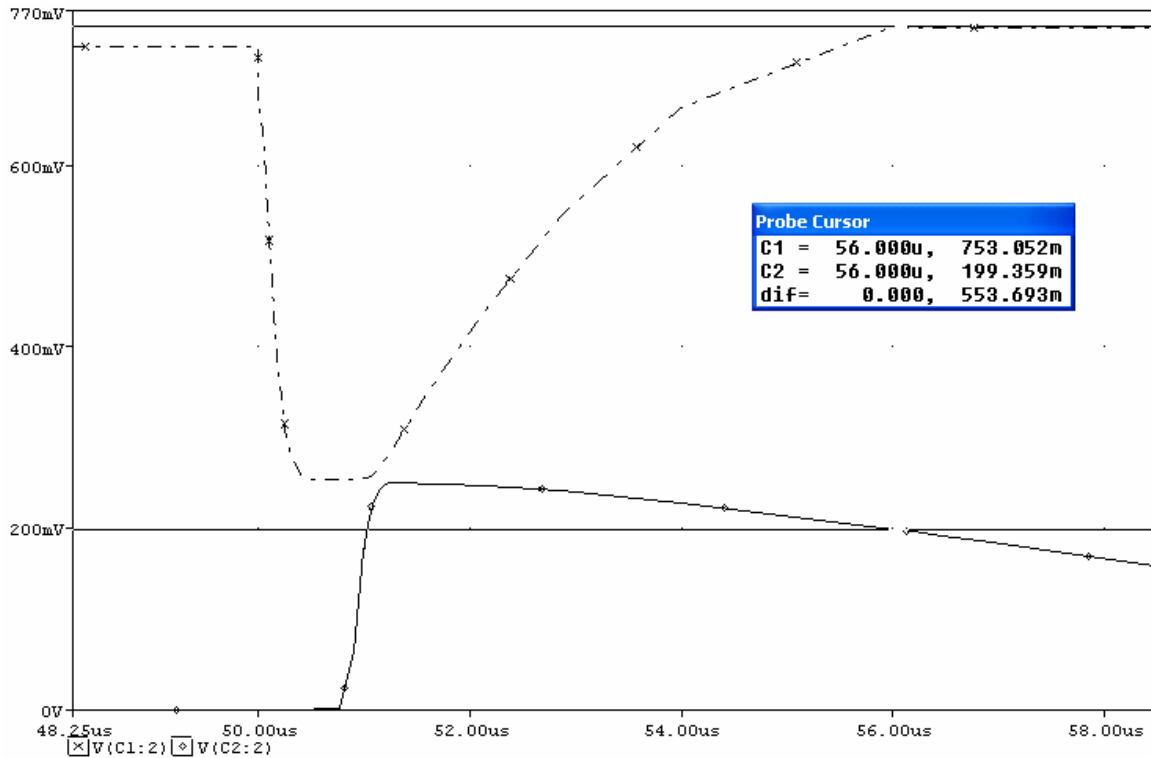


Figure D.2.15: Output voltages of both amplifiers of AD8638 with linear current source zoomed in at t around $54\mu\text{s}$

C1 shows the output voltage of the first integrator, while C2 shows the output voltage of the second integrator. The mismatch values for the first and the second integrator are 3.052mV and 5.359mV , respectively. Both mismatched can not be disregarded, since the mismatches exceed slightly over the error of the A/D converter.

D.2.4 Evaluation of the performance for the linear current source

Table D.2 summarizes performances of all operational amplifiers.

Table D.2: Evaluations of the obtained results for the linear current source

	OP-262		OPA-355		AD8638	
	V_1 [mV]	V_2 [mV]	V_1 [mV]	V_2 [mV]	V_1 [mV]	V_2 [mV]
Hands-on calculation	750	194	625	69.4	750	194
Simulation results	751.004	194.566	627.326	72.064	753.052	199.359
Mismatch [mV]	1.004	0.566	2.326	2.664	3.052	5.359
Error [%]	0.139	0.29	0.372	3.84	0.407	2.76

OP-262 shows the best performance among all amplifiers. Earlier in this section, it also has the best performance in case of the constant current source (see Table D.1). Its error is the smallest and also does the mismatch.

The error is the largest at the output voltage of the second integrator. This also applies for the constant current source as the linear current source. This is due to the relative low output voltage value compare to the output voltage of the first integrator. Thus, a small mismatch gives relatively more error.

AD8638 has the largest mismatch among all amplifiers. However, the error is very close to OPA-355. Compare the performance of AD8638 using the constant current source with the performance of AD8638 using the linear current source, the performance of using the linear current source is much better. It shows less mismatch and the errors of both output voltages are also lower. Although there is no difference in the simulation setup, this decrease in mismatch cannot be fully understood. Notice that the integration time for the linear current is 1 μ s longer than the constant current source. We can see if the integration time can affect the measurement by comparing the hand on calculation with the simulation results in case of a fall off time of 4 μ s.

Recall formula (D.8):

$$\begin{aligned}
 V_1 &= \frac{1}{C_1} \int_{t_0}^{t_1} I_{photodiode} \cdot dt \pm V_{offset_1} + V_{offset-selfadded} = \frac{1}{C_1} \int_{t_0}^{t_1} I_{linear} \cdot dt + V_{offset-selfadded} \\
 &= \frac{1}{C_1} \int_{t_0}^{t_1} (200 \cdot 10^{-6} - 50t) \cdot dt + V_{offset-selfadded} = \frac{1}{C_1} \left[200 \cdot 10^{-6} t - 25t^2 \right]_{t_0}^{t_1} + const + V_{offset-selfadded} \\
 &\approx \frac{1}{C_1} \left[200 \cdot 10^{-6} t - 25t^2 \right]_{t_0}^{t_1} + V_{offset-selfadded} = \frac{1}{1 \cdot 10^{-9}} \left[200 \cdot 10^{-6} t - 25t^2 \right]_0^{4 \cdot 10^{-6}} + 0.25 \\
 &= 0.4 + 0.25 = 0.65V
 \end{aligned}$$

$$\begin{aligned}
 V_2 &= -\frac{1}{C_2} \int_{t_0}^{t_1} \frac{V_1}{R_1} \cdot dt \pm V_{offset_2} + V_{offset-selfadded} \approx -\frac{1}{C_2} \int_{t_0}^{t_1} \frac{V_1}{R_1} \cdot dt + V_{offset-selfadded} = -\frac{1}{C_2} \int_{t_0}^{t_1} \frac{1}{R_1 \cdot C_1} I_{linear} \cdot dt + V_{offset-selfadded} \\
 &= -\frac{1}{R_1} \frac{1}{C_1} \frac{1}{C_2} \int_{t_0}^{t_1} (200 \cdot 10^{-6} t - 25t^2 + const) \cdot dt + V_{offset-selfadded} = -\frac{1}{R_1} \frac{1}{C_1} \frac{1}{C_2} \left[100 \cdot 10^{-6} t^2 - \frac{25}{3} t^3 \right]_{t_0}^{t_1} + const + V_{offset-selfadded} \\
 &\approx -\frac{1}{R_1} \frac{1}{C_1} \frac{1}{C_2} \left[100 \cdot 10^{-6} t^2 - \frac{25}{3} t^3 \right]_{t_0}^{t_1} + V_{offset-selfadded} = -\frac{1}{30 \cdot 10^3} \frac{1}{1 \cdot 10^{-9}} \frac{1}{1 \cdot 10^{-9}} \left[100 \cdot 10^{-6} t^2 - \frac{25}{3} t^3 \right]_0^{4 \cdot 10^{-6}} + 0.25 \\
 &= -0.0356 + 0.25 = 214.4mV
 \end{aligned}$$

The results of the simulations are shown in Figure D.2.16. Again, A1 is the output voltage of the first integrator (the line on the top) and A2 is the output voltage of the second amplifier (the line on the bottom). The mismatches of the first and the second integrator are 3.831mV and 3.551mV.

The mismatch at the output voltage of the second amplifier is significantly lower (\approx 1.8mV improvement) than in case of a longer integration time while the mismatch of the output voltage of the first amplifier is slightly (\approx 0.8mV) larger. This phenomenon cannot be understood. With this simulation result, it can be concluded that the duration of the integration time has influence on the accuracy of the system.

There is something very remarkable issue in the simulations results that are shown in Figure D.2.15 and in Figure D.2.16. During the discharging time (from 50 to 51 μ s), the capacitor of the first integrator is fully discharged, while the capacitor of the second integrator starts discharging after the switch has been turned off. Other operational amplifiers do not show this phenomenon.

AD8638 was chosen form using as integrators, since it has the lowest offset voltage and low bias current. Its bandwidth is much less than OPA-356. The idea of introducing the alternative

read-out system is to prove it well functioning of the complete sensor system using a simple circuit with fewer number of components and less high-end performance components.

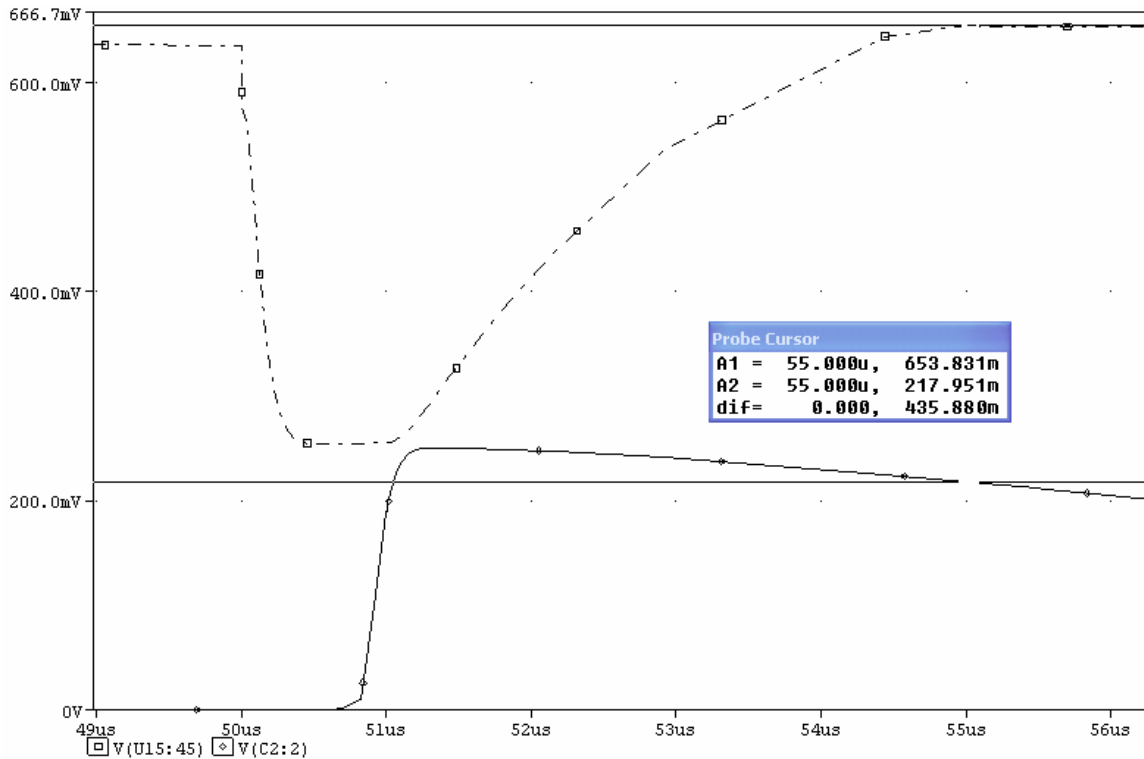


Figure D.2.16: Simulation results of AD8638 with integration of $4\mu\text{s}$ with a linear current source

D.3 Conclusions

Two kinds of current source have been used for testing the performances of the three operational amplifiers: OP-262, OPA-355 and AD8638. The output voltages of both integrators from the simulations in PSpice have been compared with the output voltages that have been calculated by hand. The results show that there is always a mismatch for all amplifiers and for both kinds of current sources.

The mismatch is the smallest for OP-262 while this operational amplifier has the lowest bandwidth. AD8638 shows the largest mismatch in case of the constant current source. However, the mismatch decreases significantly when a linear current has been used. Shortening or extending the integration time will have influence on the mismatches in hand-on calculated values and the simulation results.

The discharge time of the second operational amplifier of AD8638 is absent during $50 - 51\mu\text{s}$. The output voltage at this amplifier shows a significant increase right after $51\mu\text{s}$, which means that the switches are starting to turn off. This might be due to the relative low slew rate compared to other operational amplifiers.

One remarkable note is for OPA-355. Its performance becomes worse in case of using linear current source compared. The mismatch becomes larger. It is decreased by $\approx 0.5 - 1.4\text{mV}$. Examining OP-262, the performance, in terms of mismatch, becomes better in case of using the linear current source. Looking at the examined aspects (see Table 3.1), OP-262 does not have an aspect that out performances other investigated amplifiers. More aspects have to study in order to explain the performance.

For analyzing the performance, the mismatch is more important than the error. Therefore, the absolute difference in the hand-on calculation has a more significant meaning than the relative change.

The alternative read-out system is based on integration of charges during the discharge period of the switches. Compare all output voltages of the first operational amplifiers in case of the constant current source and the ones in case of the linear current source, the change is about 300mV. However, the difference is much smaller, $\approx 3\text{mV}$, when the output voltages of the second operational amplifiers have been compared for both current sources. This small change is due to the relative large resistor value that is in between the both amplifiers. Reduce this resistor value will generate more current through the second amplifier, which means that the change at the second output will become larger. Overall, the alternative system can be used for determining the oxygen level. Due to relatively high mismatch that AD8638 produces, one should do compensation during calculation of the oxygen.

